Processes Controlling the Variability of Sea Surface Temperature in the North Indian Ocean over Decadal Time Scale

A Thesis submitted to Goa University for the award of the Degree of

DOCTOR OF PHILOSOPHY

IN

MARINE SCIENCE

By
JOSHUA ROSARIO D'MELLO

Research Guide
DR. S. PRASANNA KUMAR
Former Acting Director
CSIR- National Institute of Oceanography
Dona Paula- 403004, Ilhas, Goa, India

Goa University,
Taleigão Plateau, Ilhas, Goa
JULY, 2017

Dedicated to my Parents.....

CONTENTS

Chapter 4: Factors Controlling the Inter-Decadal Variability

Statement

As required under the university ordinance 0.19.8 (vi), I hereby state that the present thesis entitled "**Processes controlling the variability of sea surface temperature in the North Indian Ocean over decadal time scale**" is my original contribution and the same has not been submitted on any previous occasion. To the best of my knowledge, the present study is the first comprehensive work of its kind from the area mentioned.

The literature related to the problem investigated has been cited. Due acknowledgements have been made wherever facilities and suggestions have been availed off.

Joshua Rosario D'Mello

CSIR- National Institute of Oceanography

Dona Paula, Ilhas, Goa

Place: Dona Paula

Date:

Certificate

This is to certify that the thesis entitled "**Processes controlling the variability of sea surface temperature in the North Indian Ocean over decadal time scale**" submitted by Mr. Joshua Rosario D'Mello, for the award of the degree of Doctor of Philosophy in Marine Science is based on original studies carried out by her under my supervision.

The thesis or any part of thereof has not been previously submitted for any other degree or diploma in any university or institution.

(Dr. S. Prasanna Kumar)

Research Supervisor

CSIR-National Institute of Oceanography

Dona Paula, Ilhas, Goa

Place: Dona Paula

Date:

ACKNOWLEDGEMENTS

There are a number of persons who have helped me complete my thesis. I would like to express my profound gratitude to my research guide Dr. S. Prasanna Kumar for his excellent, encouraging and patient guidance to me, through the period of my thesis work. I thank him for always making time and being available to me, for giving me many insights, and also the efforts of coming specially to guide me even after his superannuation. I thank his family too whose sacrifices helped make it possible.

I would like to thank the faculty review committee for all the valuable comments and suggestions given to me. I thank the past and present members of the F.R.C., Dr. P. M. Muraleedharan, Vice-Chancellor's nominee, Dr. Y. K. Somayajulu, the previous V.C.'s-nominee; Dr. M. K. Janarthanam, the Dean of the faculty of Life Sciences and the previous deans; Dr. C. U. Rivonker, Head of the Marine Sciences Department and past Heads Dr. H.B. Menon and Dr. G.N. Nayak. I also thank the reviewers, examiner and others who have and will be putting in their efforts and time.

I thank the Council of Scientific and Industrial Research, New Delhi for providing me with a fellowship, in-order to pursue a Ph. D. I would like to thank the present director of the CSIR-National Institute of Oceanography, Dona Paula, Prof. Sunil K. Singh, past directors Dr. Satish Shetye, Dr. Syed Wajih Ahmed Naqvi, Dr. S. Prasanna Kumar, Dr. V.S.N. Murty and the administrative and library and other staff of NIO, for all the facilities and help provided during my research period.

I also thank the past and present Chancellors, Vice-Chancellors and the staff of Goa University, its library staff and the administrative staff of the Department of Marine Sciences Mr. Yeshwant Naik, Mr. Samrat, Mr. Ashok, Mr. Laxmikant, Ms. Sonali Kundaikar, Ms. Sneha, Dr. V. Gopakumar and many others for all the administrative and other help rendered.

I have used a lot of freely available datasets, softwares, model etc. I thank all those who have been responsible, for making it possible for me to use them freely.

As the years went by I was helped and encouraged by a number of well-wishers and friends. I thank Dr. P. Vethamony, Dr. Aftab Can, Dr. Suryanarayana, Dr. M. R. Ramesh Kumar, Dr. S. Upadhyay, Mr. Anselmo Almeida, Mr. R. J. K. Charyulu, Mr. M.S.S. Sarma, Mr. A. K.

Saran, Dr. A. Unnikrishnan, Dr. Lisette D'Souza, Dr. Prabha Devi, Dr. Maria Desa, Dr. Gopalakrishna, Dr. Pratima Kessarkar, late Dr. Pradip Narvekar, Dr. Sushant Naik, and many others for encouraging me through words and smiles all along. I also thank my friends Dr. Jayu Narvekar, Dr. P. J. Vidya, Divya David, P. Byju, Upal Parrikar, Dr. Priyanka Banerjee, K. Navaneeth, M. Kirthan, M. Ashwini, Vrinda Sharma, Preeti, Dr. Lina Mergulhão, Sumesh G., Shyam, Rashmi, Dr. Samiksha, Jyoti, Nidheesh, Charles, Akhil, Keerthi, Sunil, Ashok, Arati, Shweta, Valetta, Dominique, Maria, Nandadeep, Mrunmayee, Muthukumar, Subha Anand, Larissa, Stecy, Conchita, Lalita, Rajat, Suchandan, Govardhan, Jesly, Ruchita, Asha, Samidha, Rheane, Svetlana, Maryanne, Sweety, Shilpa, Dr. Lina Fernandes, Maheshwar, Dinesh, Cheryl, Larsen, Fr. Jude, Br. Onasis, Br. Jollyson, Br. Agnel, Elvira, Ralph, Azzan, Eric, Mahesh, Glen, Vijith, Amol, Selrina, Vinit, Viola, Pravin, Rahul, Chaitanya, Chinnu, Remya, Kranti, Ronnie, and many many others, for the help, nice memories and times.

Through the period of Ph. D., I was helped physically, emotionally, spiritually by my family and many friends and well-wishers. I thank my family, my grand-mothers, Mrs. Clotilda D'Mello and Mrs. Maria Marta Dias, aunties and uncles especially Ms. Elizabeth D'Mello, Mrs. Sumina Dias and late Mr. Mateus Dias, my cousins, my sister Janice, brother-in-law John and their families. I remember my father late Mr. Joslin D'Mello, who was among the first who instilled interest about the Earth in me, through the maps he brought for me in my young days.; and I also profoundly thank my mother Rose for whom words will not be enough, for waiting for me patiently and encouraging and sacrificing a lot for me all these years.

There are many who have helped me through the years to reach this level, my teachers and many others whose names may not feature here. There are many whose help may not be obvious, but their direct or indirect effects felt, just like tele-connections in the environment. My sincere thanks to them all.

Finally I thank the Almighty God for giving me the capability and an opportunity and help in the form of so many people, to help me complete this thesis. To all **DÊU BOREM KORUM**!

ABSTRACT

Climate change is an important topic, with global warming being one of its manifestations and sea-level rise, melting of polar ice-caps, receding glaciers, ocean acidification, being among others. In the study of climate change sea surface temperature (SST) is an important parameter which is strongly related to air-sea interaction processes and hence would depict climate change experienced by any part of the ocean. In the Indian Ocean, most of the studies pertaining to the SST are focused on deciphering the seasonality and the factors responsible for such variability. There are very few studies that examined the variability of the Indian Ocean in the inter-annual to decadal time scales. This was the motivation for the present study entitled "Processes controlling the variability of sea surface temperature in the North Indian Ocean over decadal time scale". The study had three objectives, (1) to decipher inter-decadal variability in SST in the northern Indian Ocean, (2) to identify the factors responsible for the observed variability, and (3) to delineate the role of El Niño-Southern Oscillation (ENSO) and Indian Ocean Dipole (IOD). The study domain was the North Indian Ocean (NIO) spanning from equator to 25^{o}N latitude and from 45^{o}E to 99^{o}E longitude. A suite of ocean and atmospheric data, both in-situ as well as remote sensing data, were used. The data used for the study period was from January 1960 to December 2011.

The Fast Fourier Transformation (FFT) of de-trended (seasonal and annual cycles) 60-month running mean SST in showed three dominant periodicities of 3.7 year, 5year and 10 year at 95% significance level in the north Indian Ocean. The first two were of ENSO periodicity, while the third one was decadal. Thus, the data analysis showed that decadal periodicity was one among the dominant ones. The area-averaged 60-month running mean SST in the north Indian Ocean, the Arabian Sea and the Bay of Bengal, all showed four distinct decadal cycles

which co-varied with the decadal sunspot number cycles. The decadal SST cycles that were identified with the sunspot number cycle were (1) 1964 March to 1975 June, (2) 1975 June to 1985 December, (3) 1985 December to 1995 November and (4) 1995 November to 2008 July. The spatial distribution of the standard deviation of decadal SST showed that in the Arabian Sea standard deviation was lesser than the Bay of Bengal.

The analysis of the linear trend line and slopes of the 60-month running mean SST in the northern Indian Ocean, the Arabian Sea and the Bay of Bengal showed that the slope and the trend changed in all the four decadal cycles. In the 1st decadal cycle slope of the SST trend line in the NIO showed a weak increasing trend with a value of 0.0019°C/year. In the Arabian Sea the slope of the trend line showed a weak decline with a value -0.0011°C/year. In contrast, the trend of SST in the Bay of Bengal showed an increase with a value of 0.0061°C/year. In the 2nd decadal cycle, however, the slope of the mean SST in all the three regions, NIO, Arabian Sea and the Bay of Bengal, showed an increasing trend with a value of 0.0153°C/year, 0.0143°C/year and 0.0170°C/year respectively.

In the 3rd decadal cycle the slope of the mean SST in all the three regions showed a decreasing trend with a value of -0.0049°C/year for the NIO, -0.0041°C/year for the Arabian Sea and -0.0059°C/year for the Bay of Bengal. In contrast, in the 4th decadal cycle the slope of the mean SST in all the 3 regions showed an increasing slope with a value of 0.0124°C/year for the NIO, 0.0141°C/year for the Arabian Sea and 0.0101°C/year for the Bay of Bengal.

The most striking feature and salient characteristics that emerged out of the analysis of the area-averaged 60-month running mean SST from 1960 to 2011 was (1) a linear warming trend, (2) presence of dominant decadal cycle riding over this linear warming trend, and (3)

disruption of the decadal cycle after 1995. The slope of the linear trend line of SST for the pre-1995 period in the Arabian Sea was lesser than that of the post-1995 period indicating an accelerated warming in the Arabian Sea in the later period. In contrast, in the Bay of Bengal the slope of the linear of SST for the period pre-1995 was greater than that of the post-1995 period indicating a slowdown in the rate of warming in the later period.

There were spatially and seasonally differentiated warming pattern in the Arabian Sea which was linked spatially and temporally different ocean-atmospheric processes operating in these regions. The accelerated warming in the post-1995 period in the Arabian Sea was closely linked to the reduced upwelling along the Somali coast which supplies subsurface cooler waters to the upper ocean. The reduced wind speed also contributes to the warming by reducing the evaporative cooling. These processes in tandem with the monotonic increase in the atmospheric CO_2 concentration lead to the observed accelerated warming.

In the Bay of Bengal the slowdown in the warming trend post-1995 was closely linked to the increasing trend in the number of depressions, cyclones and severe cyclones (DCS) in the post-1995 period. These atmospheric systems are capable of transferring large quantities of subsurface cooler waters to the upper ocean during their life-span. This was examined using a PWP-model forced by heat momentum and freshwater fluxes. When the model was forced by cyclonic winds, the model produced deeper mixed layer thickness corroborating the finding that more number of cyclonic systems in the Bay of Bengal will cool the upper ocean due to the mixing with subsurface cooler waters. Though the increase in the DCS causes the SST to fall, this will counteract the CO_2 concentration induced SST rise. As the increase in the DCS cannot completely offset the CO_2 concentration induced rise in SST, the effect was manifested as a slowdown in the observed SST warming.

Based on the Dipole Mode Index (DMI) and the Oceanic Nino Index (ONI), the individual years during the study period were classified into nine combinations of ENSO and IOD states. This was used further to explore the relationship of SST with ENSO and IOD. The most commonly occurred condition was ENSO-neutral and IOD-neutral, while El Nino and IOD negative did not occur at all.

The largest positive SST anomalies were in the El Niño- IOD positive composite years, while the largest negative SST anomalies were in the La Niña- Neutral IOD and La Niña- Negative IOD years for the period 1963 to 1975. The largest positive SST anomalies were in the El Niño- IOD positive year, while the negative SST anomalies of largest magnitudes were seen in the La Niña- Neutral IOD and La Niña- Negative IOD years during the period 1975 to 1986. The largest positive SST anomalies were in the El Niño- IOD neutral years while the largest negative SST anomalies were in the ENSO neutral- IOD negative and in the El Niño- IOD positive years during the period 1986 to 1995. The largest positive SST anomalies were in the El Nino-IOD positive and the largest negative anomalies were in the La Nina-neutral IOD. The analysis showed that the SST anomalies were progressively increasing from the first decadal period (1963-1975) to fourth decadal period (1995-2008) and as the anomalies of SST become more and more positive, the influence of ENSO and IOD becomes weaker.

LIST OF TABLES

LIST OF FIGURES

LIST OF PUBLICATIONS

1. D'Mello, J. R. and S. Prasanna Kumar, Why is the Bay of Bengal experiencing a reduced rate of sea surface warming? International Journal of Climatology, 36, 1539–1548 (2016). doi: 10.1002/joc.4414.

2. D’Mello, J. R. and S. Prasanna Kumar, Processes controlling the accelerated-warming of the Arabian Sea. International Journal of Climatology, 38, 1074–1086 (2018). doi: 10.1002/joc.5198.

CHAPTER 1

INTRODUCTION

1.1 Sea Surface Temperature

Sea Surface Temperature (SST) is the temperature of the water closest to the sea surface. The SST is a measure of energy in the top layer of the ocean, due to the movement of molecules (https://podaac.jpl.nasa.gov/SeaSurfaceTemperature). Based on different definitions and methods used for the measurement of SST, the top layer within which the SST is measured ranges from 10 micrometers to around 20 m below the sea surface.

Some of the methods to measure the SST include bucket thermometer, ship sea-water intake valves, buoys, moorings, satellites etc. (http://oceanworld.tamu.edu/resources/ocng_textbook/chapter06/chapter06_06.htm). Bucket thermometers directly measure the temperature of the sea surface. It is measured by the thermometer, whose mercury expands or contracts proportionally to the rise or fall in temperature. Thermistor is a semi-conductor, whose resistance varies rapidly and proportionally to the temperature. Many instruments use thermistors to measure the SST. The ship injection-temperature is the temperature of the water taken in by the ship to cool its engines. The depth of the intake valve varies between ships. Though convenient and providing a large volume of data in the pre-satellite era, the temperature data obtained are restricted mainly to the sea lanes. They could have issues if the valve of the ship is below a stratified layer of water. Satellite measures temperature through the infrared and microwave radiations released from the ocean. The peak radiation's wavelength, from the ocean, is expected in these wavelength ranges as predicted by the Wien's Displacement Law. The satellites measure the infrared radiations from approximately

the top-most 10 micrometers of the surface, while the microwave radiations are measured approximately from the top-most 1 millimeter of the surface. Satellite measurements help in the global collection of SST data at lesser temporal scales too. However, the presence of clouds leads to the absorption of the mainly infrared radiations by the clouds, causing absence of data (https://podaac.jpl.nasa.gov/SeaSurfaceTemperature). Ocean moorings also measure the SST, besides measuring temperatures at lower depths too. They have instruments placed on them at various depths, measuring the temperatures and giving a time-series at the location. Ocean drifters also give SST values besides measuring the temperature at various depths.

Water has a high specific heat capacity. Oceans play an important role in the climate system, partly due to this property of water. About 3.5 meters of the water column contains as much energy as the entire atmospheric column. The radiative and turbulent heat fluxes transfer this thermal inertia of the ocean to the atmosphere. The energy fluxes depend on many atmospheric parameters including the wind speed, humidity, air temperature, cloudiness etc., but a single oceanic parameter, i.e. SST [*Deser et al.*, 2010]. SST affects the atmosphere above. SST measurements are important as it is a parameter in tropical cyclone formation [*Dare and McBride*, 2011]. The SST is also a parameter affecting the formation of sea-fog [*Tang*, 2012]. The SST also affects wind speeds through changes in SST gradients [*Back and Bretherton*, 2009; *O'Neill*, 2012]. The SST is also important in the formation of El Niño-Southern Oscillation (ENSO) [*Trenberth et al.*, 2007; http://www.cpc.noaa.gov/products/analysis_monitoring/ensostuff/ensofaq.shtml#DIFFER], Indian Ocean dipole (IOD) [*Saji et al.*, 1999; *Webster et al.*, 1999] etc. climate modes. Climate change is manifested through various phenomena and parameters, such as global warming etc. which in turn can be seen identified through some parameters, one of which is SST [see *IPCC Report AR5 SPM, 2013; Xie et al. 2010*]. SST measurements over a long period of time help in understanding the

variability, besides also the rate of SST increase or decrease.

1.2 Global warming and climate changes

Climate change is an important topic, with global warming being one of its manifestations and sea-level rise, melting of polar ice-caps, receding glaciers, ocean acidification, being among others [see *IPCC Report AR5 SPM, 2013*]. The factors that determine the Earth's climate are changes in the Earth's radiation balance. This is primarily regulated through three ways namely changes in the (1) incoming solar radiation, (2) fraction of solar radiation reflected by the Earth and (3) long-wave radiation that is released by the Earth towards space. The solar cyclicities and Milankovitch cycles [*Milankovitch 1920, 1941*] impact the first aspect, while the second could be due to changes in the albedo of the ice cover, snow-cover, vegetation and soil type. The increasing greenhouse gas concentrations impact the third aspect. The climate responds to these changes through various processes, which can result into positive or negative feedback mechanisms [*IPCC Report AR 4*, 2007].

The amount of energy reaching the top of the Earth's atmosphere, when facing the sun during daytime, per second, is 1370 W/m^2. About one-fourth of this energy reaches the Earth’s surface per second. A little less than one-third of the energy, averaged over the entire planet, is reflected. Clouds and aerosols are responsible for a little more than 70 % of the reflected energy, while the remaining energy reflection is contributed to by the ice-cover, snow-cover and deserts. The energy which is not reflected is absorbed by the Earth's surface chiefly and to a lesser extent by the atmosphere. This incoming energy is released as outgoing long-wave radiations [*Kiehl and Trenberth*, 1997] (see Figure 1.1). To release 240 W/m^2, the temperature should be -19 °C, but the average temperature of the Earth is higher at 14°C. This is due to

the greenhouse effect [*IPCC Report AR4*, 2007].

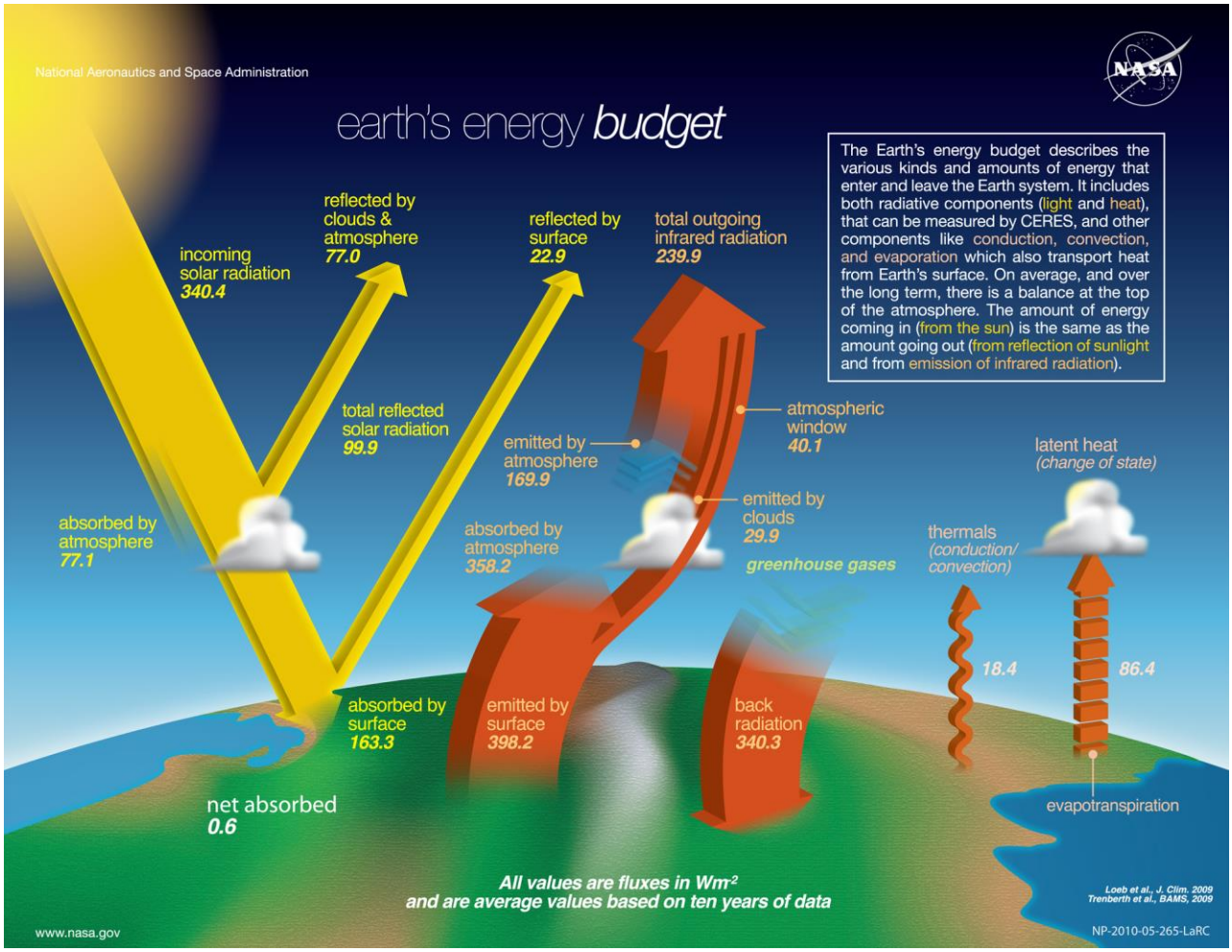

Figure 1.1 Earth's energy budget (https://en.wikipedia.org/wiki/Earth%27s_energy_budget; https://commons.wikimedia.org/w/index.php?curid=32285340, by NASA- http://science-edu.larc.nasa.gov/energy_budget/ quoting Loeb et al., J. Clim 2009 & Trenberth et al, BAMS 2009, Public Domain)

The greenhouse effect is the partial blocking of the long-wave radiations from leaving the Earth's atmosphere. The main constituents of the atmosphere are nitrogen (78.08%) and oxygen (20.95%) and they do not have a greenhouse effect (see Figure 1.2). The minor constituents of the atmosphere such as carbon dioxide (0.036%), methane (0.00017%) and nitrous oxide (00003%) and water vapour (0 to 4%) have greenhouse effect. These minor

constituents of the atmosphere, known as greenhouse gases, allow the incoming shortwave radiation from the Sun to pass through the atmosphere, while they block the long-wave radiation from leaving the atmosphere. Clouds though block outgoing long-wave radiations and cause local heating; they also reflect solar radiation and tend to have a net cooling effect. The concentration of carbon dioxide in the atmosphere is increasing [*Keeling et al*., 2001] (Figure 1.3). As the ability of the long-wave radiations to escape from the atmosphere is dependent on the concentration of green house gases, this increase in carbon dioxide causes the trapping of the long-wave radiations in the earth's atmosphere to a greater extent and thus leads to a warming (Figure 1.4).

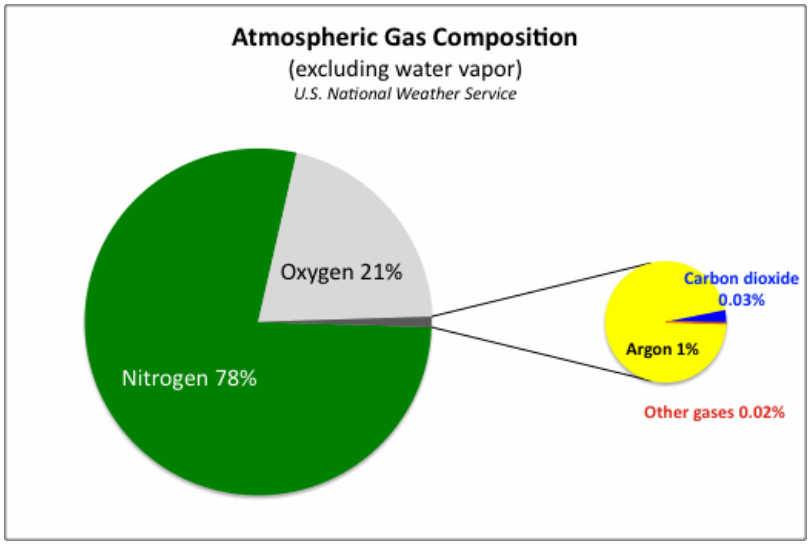

Figure 1.2 Atmospheric gas composition, excluding water vapour.
(http://burnanenergyjournal.com/wp-content/uploads/2011/05/atmospheric.gif)

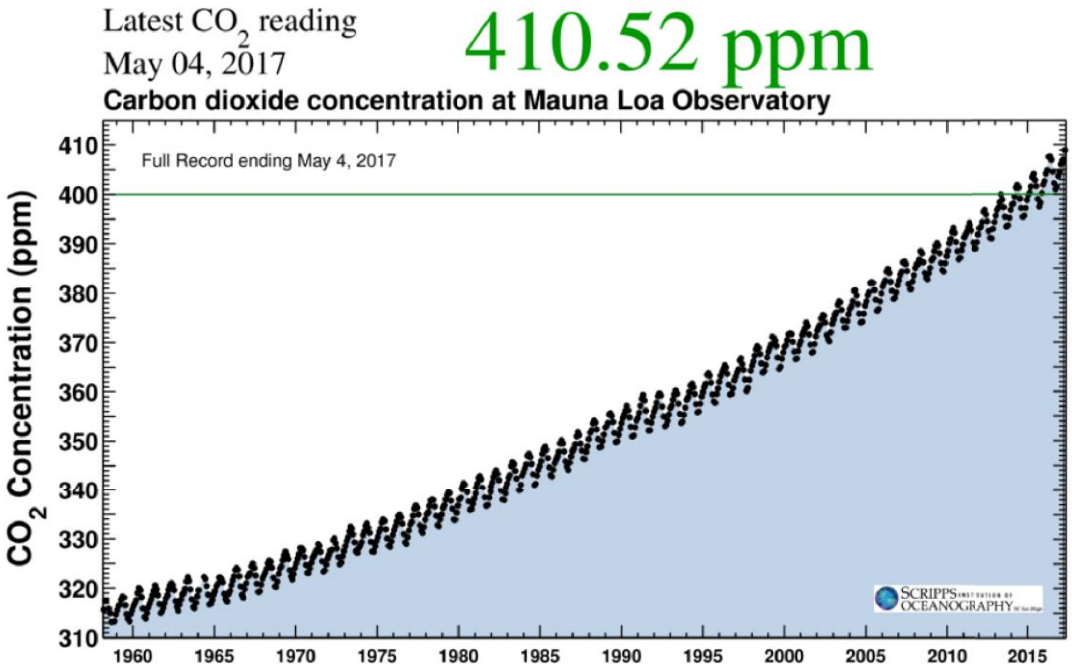

Figure 1.3 Keeling curve showing the atmospheric carbon dioxide concentration at Mauna Loa Observatory. (https://commons.wikimedia.org/w/index.php?curid=58530710, by Scrippsnews, CC BY-SA 4.0)

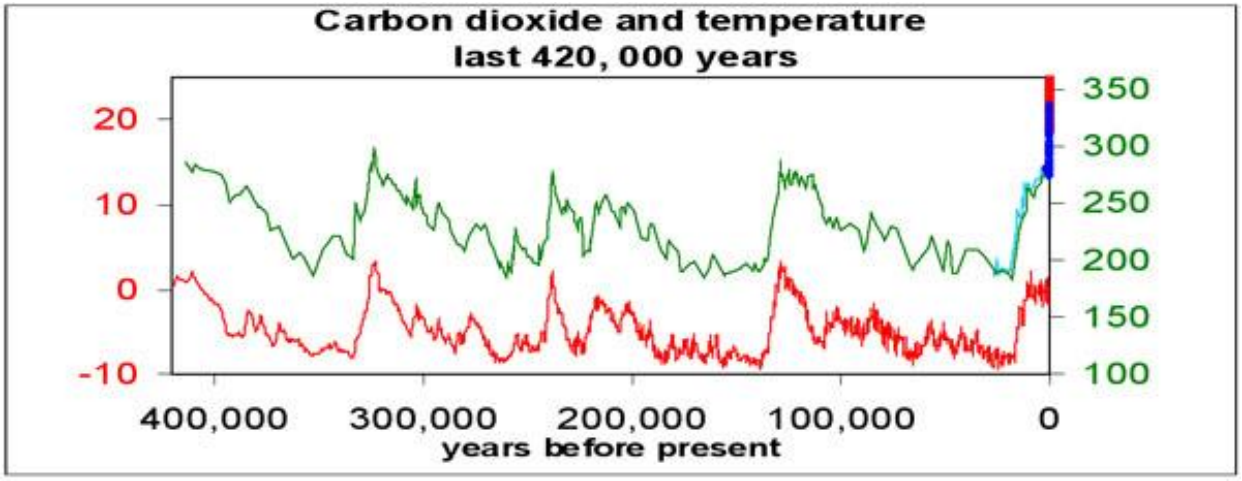

Figure 1.4 Historical temperature (red) and carbon dioxide concentrations (green) as reconstructed from the Vostok ice core, Antarctica, showing the relationship between them. (http://www.climatekelpie.com.au/understand-climate/climate-science/carbon-dioxide-and-temperature-the-relationship)

1.3 Effect of global warming

The warming atmosphere has many effects. The increase in the temperature leads to the melting of ice and associated rise in the sea level. In addition, the thermal expansion of oceanic waters would also lead to the rise in sea level. The resultant seal level rise would flood and submerge low-lying coastal regions and islands, which in turn would impact the human populations. Another effect of the melting ice-cover is a positive feedback mechanism, in which the reduced albedo causes an increase in the absorption of incoming solar radiation by the ocean. This in turn causes further warming of the ocean, leading to an increase in melting of ice, leading to a further reduction of the albedo [*Deser et al*., 2000]. Another impact of warming is that the increase in the temperature can also lead to the melting of the Arctic permafrost and there could be a release of trapped carbon, causing further warming [*Zimov et al*., 2006]. The permafrost melting could lead to increased plant growth which may initially off-set the carbon release to the atmosphere. However, there is a tipping point, beyond which the soil starts acting a source of carbon to the atmosphere, through the melting of the permafrost and release of carbon dioxide and methane to the atmosphere, causing a further greenhouse warming, and further increasing the temperature [*Schuur et al.,* 2009].

The CLAW hypothesis proposes a feedback loop that occurs between the earth's climate system and ocean ecosystems [*Charlson et al*., 1987]. The name CLAW is an acronym from the first letters of the surnames of the proposers of this hypothesis, namely Robert **C**harlson, James **L**ovelock, Meinrat **A**ndreae and Stephen **W**arren [*Andreae et al*., 1995; *Andreae and Crutzen*, 1997]. According to this hypothesis when there is more solar energy available, the growth of phytoplankton increase. This would lead to an increase in the production of dimethylsulfide (DMS) in sea water as some phytoplankton produce di-

methylsulfoniopropionate (DMSP). The DMS enters the atmosphere through air-sea exchange process where it is oxidised into sulphur dioxide. This in turn form sulfate aerosols which act as a cloud condensation nuclei (CCN). This causes an increase in the cloud droplet number and thus consequently increasing the liquid water content of the clouds, finally leading to an increase in the cloud area. This in turn increases the cloud albedo, causing more reflection of the incident solar radiation, thus decreasing the forcing which caused an initiation of the process. The CLAW hypothesis can operate in the opposite direction too, in which a reduced incident solar radiation, leads to a decreased cloud cover and thus to an increase in the amount of solar radiation reaching the Earth's surface.

The anti-CLAW hypothesis proposes that with increasing solar radiation, there will be a greater stratification of the ocean, leading to a lesser amount of nutrients being present in the euphotic zone. This leads to lesser DMS production and consequently a lesser amount of cloud cover. This will lead to an increase in the incident solar radiation, further stratifying the ocean [*Lovelock*, 2007].

1.4 Evidence of global warming

The warming of the Earth is unequivocal, according to the fourth assessment report of the Inter-governmental Panel for Climate Change (IPCC) [*IPCC AR4, Solomon et al*., 2007]. The surface temperatures of both the land and the ocean have risen at the rate of 0.85 °C during the period from 1880 to 2012 [*Hartmann et al.*, 2013]. Similarly, the globally integrated upper ocean heat content, between 0 to 700 m depths, also show an increase from 1971 to 2010 [*Rhein et al*., 2013]. The effects of global warming and increasing temperatures, to a larger extent, are seen in the Polar Regions, than else-where, due to polar amplification

[*Manabe and Wetherald*, 1975; *Lee*, 2014], for example, the amplification of Arctic warming [*Cohen et al.*, 2014; *Acosta Navarro et al.*, 2016]. However, this warming is not uniform. Similarly, the annual mean sea-ice extent also shows regional differences in the different regions of Arctic and Antarctica. Though there is receding annual mean sea-ice extent in the Arctic, the annual mean sea-ice extent in the Antarctic is increasing, but only at a rate which is one-third to that of the Arctic [*IPCC Report AR5 SPM*, 2013].

1.5 Sea surface temperature (SST) as a proxy of climate variability

The sea surface temperature (SST) is an important parameter in oceanography which is strongly related to air-sea interaction processes. It can provide useful indices for various ocean-atmosphere processes including climate phenomena. While traditionally the surface temperature of the ocean has been measured using bucket thermometers, with the advent of space-based satellite observations since 1970s, SSTs have been determined using radiometers onboard satellites.

There have been studies in the past that examined the response of SST in different regions of the world ocean in the context of know climate variability. Natural modes of climate variability have been studied extensively in the Pacific and Atlantic Oceans [*Han et al*., 2014], primarily due to the availability of longer time-series data. In the Pacific Ocean the first report of climate change by way of strong anomalous winter in 1976-1977 was by *Nitta and Yamada* [1989] and *Trenberth* [1990] who noticed a "step-like" shift in the winter-time sea level pressure in the North Pacific. Subsequently, *Miller et al*. [1994] termed it as "regime shift" while describing the climate change event. Later, *Francis and Hare* [1994 and 1997] and *Hare and Francis* [1995] through a series of papers brought out the link between

production of Alaska salmon and inter-decadal changes in the North Pacific climate. The Pacific Ocean Decadal Oscillation (PDO) [*Mantua et al*., 1997] has warm and cool phases. During warm PDO phases SSTs tend to be anomalously cool in the central North Pacific and anomalously warm SSTs along west cost of America.

In the Atlantic Ocean, the Atlantic multidecadal oscillations (AMO) occurs at periods of 60 to 80 years [*Schlesinger and Ramankutty*, 1994], which has impacts on the Sahel drought [*Rowell et al*., 1995]. The AMO also has been shown to influence the number of storms and hurricanes forming in the tropical Atlantic and in the Caribbean Sea [*Goldenberg et al*., 2001; *Molinari and Mestas-Nuñez*, 2003]. The AMO index reveals a warm period from the years 1930 to 1970 and a cooler period from 1970 to 1994 [*Trenberth and Shea*, 2006]. The effects of rainfall and dust on SST were studied by *Wang et al*. [2012]. According to *Wang et al.* [2012] the SSTs were cold from the late 1960s to the early 1990s. This was a period of less rainfall over Sahel and there was consequently a high amount of dust over the North Atlantic. This blocked the solar radiation further cooling the SSTs. The number of aerosols also affects the amount of low clouds through the formation of condensation nuclei and also by reducing the cloud droplet size [*Kaufman et al*., 2005]. The aerosol induced change in the cloud cover can affect the SST in the North Atlantic by changing the amount of heat flux into the ocean. The opposite mechanism occurred in the period before the late 1960s and after the early 1990s. Warmer SSTs lead to more rain over the Sahel, causing lesser dust. Consequently there is a reduced blockage of insolation by aerosols leading to a further warming in the SSTs [*Wang et al*., 2012].

In the Indian Ocean, most of the studies pertaining to the SST are focused on deciphering the seasonality and the factors responsible for such variability. For example, *Yu et al*. [2007] obtained a correlation of greater than 0.9 between SST and net heat flux (Q_{net}) in the central

equatorial region and in the region south of 15°S highlighting the important role of net heat flux in the seasonal evolution of the SSTs in these regions. On the other hand, evolution of SSTs in the Western Arabian Sea, Eastern Equatorial Indian Ocean near Sumatra and thermocline ridge between 5 °S to 12 °S in the central southern basin [*Wyrtki*, 1971], are mainly controlled by oceanic processes [*Yu et al.*, 2007]. More specifically, the SSTs in the western Arabian Sea and in the thermocline ridge region are controlled by the Ekman suction induced thermocline depth variations [*McCreary et al.*, 1993] in association with the westward propagation of the wind-induced Rossby waves [*Yu and Rienecker*, 1999; *Feng and Meyers*, 2003].

There are few studies that examined the variability of the Indian Ocean in the inter-annual to decadal time scales. Till recently, the focus of research was in the tropical Pacific due to the El Niño-Southern Oscillation phenomenon. Only recently was the Indian Ocean Dipole (IOD) [*Saji et al.*, 1999] or the Indian Ocean Zonal Mode (IOZM) [*Webster et al.*, 1999] identified. IOD is sustained on inter-annual time-scales through positive feedback between the equatorial winds and zonal SST gradients, and reaches peak amplitudes in the boreal fall (September to November). Positive IOD have warm SST anomalies (SSTAs) in the tropical west Indian Ocean and cold SSTAs in the tropical east Indian Ocean. Negative IOD phase is vice-versa. Two other modes of Indian Ocean inter-annual SST variability have also been identified; viz. the Indian Ocean basin mode and the subtropical SST mode. There is a basin-wide warming or cooling over the Indian Ocean, during the Indian Ocean basin mode. This is ENSO-induced cloud cover pattern change, which in turn affects the shortwave radiation [*Klein et al.*, 1999]. Indian Ocean air-sea interaction and ocean dynamics maintain this mode beyond ENSO termination [*Du et al.*, 2009]. The subtopical SST dipole mode is characterised by warm SSTA in the south-west Indian Ocean, to the south of Madagascar, and cold SSTAs in the eastern Indian Ocean off Australia, in its positive phase. It varies inter-annual, with a

peak development in the austral (southern hemisphere) summer [*Behera and Yamagata*, 2001; *Suzuki et al.*, 2004]. The Antarctic Circumpolar Wave [*White and Peterson*, 1996] and air-sea interaction in the tropical Indo-Pacific may contribute to the generation of the subtropical SST dipole mode [*Morioka et al.*, 2012, 2013]. Though there are a few studies in the Indian Ocean, these are much lesser than the better studied Pacific Ocean and Atlantic Ocean. *Keerthi et al.* [2013] studied the interannual variaibility of the mixed layer depth in the tropical Indian Ocean. *Han and Webster* [2002] using a 4 and a half layer model and *Somayajulu et al.* [2003] using Topex/ poseidon altimetry data of SSHA analysed the inter-annual variability in the circulation. Subsequently, *Rao et al.* [2010] studied the inter-annual variability of the Kelvin wave propagation in the coastal Bay of Bengal, equatorial Indian Ocean and in the south-east Arabian Sea. In the decadal time scale, *Mandke and Bhide* [2003] reported an epochal decrease in the Bay of Bengal storm frequency, while *Cole et al.* [2000] suggested the decadal variability in the western Indian Ocean proxy records related to the tropical Pacific Ocean decadal variation.

Rupa Kumar et al. [2002] was the first to examine the long-term variability of SST in the Indian Ocean, suggesting a rate of increase of 0.5°C and 0.4 °C per 100 years, in the Arabian Sea and in the Bay of Bengal respectively, in the period from 1902 to 1994. *Goes et al.* [2005], based on 8 years (1997 to 2004) of data, argued that a winter and spring reduction in the Eurasian snow-cover is consistent with a mid-latitude continental warming trend in the Northern Hemisphere; and that these create conditions favourable in the western Arabian Sea, for stronger May to July winds causing lower SSTs, besides an increase in the phytoplankton production. With the help of more comprehensive data set, *Levitus et al.* [2005] showed that the Indian Ocean warmed over the past 50 years except at the base of the mixed layer at the equator and in the south-equatorial current. Based on 1960 to 1999 thermal data from Indian Ocean, *Alory et al.* [2007] showed a warming of around 1°C over large regions in the AS.

Using three different data sets for the period 1960 to 2006, *Prasanna Kumar et al.* [2009] found a disruption in the natural decadal cycle in the Arabian Sea SST after 1995 and a linear rise in the SSTs. A comprehensive review of the variability in the SST ranging from inter-annual to multi-decadal time scales in all the 3 oceans along with probable mechanisms were reviewed by *Deser et al.* [2010]. Han et al. [2014] inferred from Hadley Centre Sea Ice and SST data that the tropical Indian Ocean regions warmed faster than most of the tropical Pacific and Atlantic, since the 1950s. *Roxy et al.* [2014] showed that the western tropical Indian Ocean is warming faster than the rest of the tropical oceans, while *Dinesh Kumar et al.* [2016] reported an increasing SST of 0.12°C/decade in the AS for the period from 1960 to 2009.

There have been some studies on the effects of the El Niño-Southern Oscillation (ENSO) and the Indian Ocean Dipole (IOD) on the SSTs. ENSO dominates the inter-annual climate variability of the North Indian Ocean [*Tourre and White*, 1995; *Tourre and White*, 1997]. *Klein et al.* [1999] studied that the SSTs in the tropical Indian Ocean rise 3 to 6 months after the El Niño. With the progress of the El Niño, changes in the surface heat flux causes the tropical Indian Ocean to warm. The IOD, identified by studies of *Saji et al.* [1999] and *Webster et al.* [1999], is characterised by the occurrence of warm SST anomalies in the western tropical Indian Ocean and of cool SST anomalies in the Eastern Indian Ocean. Zonal wind anomalies blowing from the cool to the warm regions occur with the SST anomalies. The simplest index is the east-west difference of the tropical SST. *Krishnamurthy and Kirtman* [2003] studying the Indian Ocean response to El Niño said that it depends on the phase of El Niño with respect to the monsoons. This is due to the seasonal monsoon affecting the western tropical Indian Ocean SST, which in turn affects the local air-sea feedbacks. Besides this there is Madden Julian Oscillation (MJO) which begins in the Indian Ocean and propagates eastward into the Pacific Ocean. They provide westerly wind bursts affecting the

onset of El Niño in the western Pacific. MJO has a periodicity of 30 to 60 days [*Madden and Julian*, 1994].

IOD may not be completely independent of ENSO and it can be excited by ENSO [*Krishnamurthy and Kirtman*, 2003; *Zhong et al.*, 2005]. Within the Indian Ocean, the local response to El Niño can be affected by the feedbacks between the ocean and atmosphere [*Zhong et al.*, 2005]. There is a high correlation between ENSO and dipole mode during 1960 to 1983 and from 1993 onwards, but not in the intervening period [*Clark et al.*, 2003]. The relationship between ENSO and IOD has changed over time and the dipole could be excited by other modes of climate variability [*Annamalai et al.*, 2005; *Ihara et al.*, 2008]. *Drbohlav et al.* [2007] analysed the wind patterns and SSTs during IOD events, in the El Niño and non-El Niño years. In the IOD years, there is a higher pressure over the eastern Indian Ocean. There are stronger easterly winds in the north-west Indian Ocean, causing the advection of warmer water from the central to the western Indian Ocean. In the eastern Indian Ocean, the stronger south-easterlies, cause more meridional and vertical advection of cold sub-surface waters. Hence, the north-western Indian Ocean warms in El Niño years while the south-eastern Indian Ocean cools. In non-El Niño years, the stronger westerlies in the north-west Indian Ocean and stronger easterlies in the south-east Indian Ocean cause more advection of cold waters in these regions. Besides in the south-east Indian Ocean there is cooling due to the latent heat and sensible heat loss, leading to a cooling in the eastern Indian Ocean, in non-El Niño years.

1.6 Motivation

It is amply evident from the above discussion that in the Indian Ocean seasonal cycle being

dominant variability it has been studied extensively. Though there are some studies on the inter-annual variability of SST and still fewer studies on the decadal SST variability, present understanding on how different regions within the Indian Ocean is responding to climate variability and change is far from adequate. The rim of the Indian Ocean has some of the most populous countries in the world, which are highly vulnerable to climate variability and change [*Han et al.*, 2014]. There is a strong demand for improving our understanding of the long-term climate change, especially in the inter-annual to decadal [*Milne et al.*, 2009; *Church et al.*, 2011] and multi-decadal time scale in this region. This is the motivation for my study. The present study attempts to understand the nature and characteristics of the SST variability in the northern Indian Ocean, considering two basins, the Arabian Sea and the Bay of Bengal separately.

1.7 Objectives

The objectives of the present study, i.e. "Processes controlling the variability of sea surface temperature in the North Indian Ocean over decadal time scale", are as follows:

1. To decipher inter-decadal variability in SST in the northern Indian Ocean.

2. To identify the factors responsible for the observed variability.

3. To delineate the role of El Niño-Southern Oscillation (ENSO) and Indian Ocean Dipole (IOD)

1.8 Organization of the thesis

The first chapter of the thesis is the present chapter, i.e. the introduction. This chapter

explains the sea surface temperature and the ways to measure it, climate change and the various parameters showing it, effects of climate change and SST as a proxy of climate variability. The motivation of the study and the objectives of the study are also given in this chapter.

The second chapter is on the data and methodology. The third chapter is on the inter-decadal variability of SST in the North Indian Ocean, while the fourth chapter is on the parameters affecting the inter-decadal SSTs. The fifth chapter is on the El Niño Southern Oscillation (ENSO) and Indian Ocean Dipole (IOD) roles in the SST variability. The sixth chapter is the summary and conclusions.

CHAPTER 2

DATA AND METHODOLOGY

2.1 Introduction

A number of data sets were used to achieve the objectives of the thesis. Data were downloaded and analysed in the study period from 1960 January to 2011 December, whenever available. The region of the study is the North Indian Ocean, extending from the Equator to 25°N and from 45°E to 99°E (Figure 2.1).

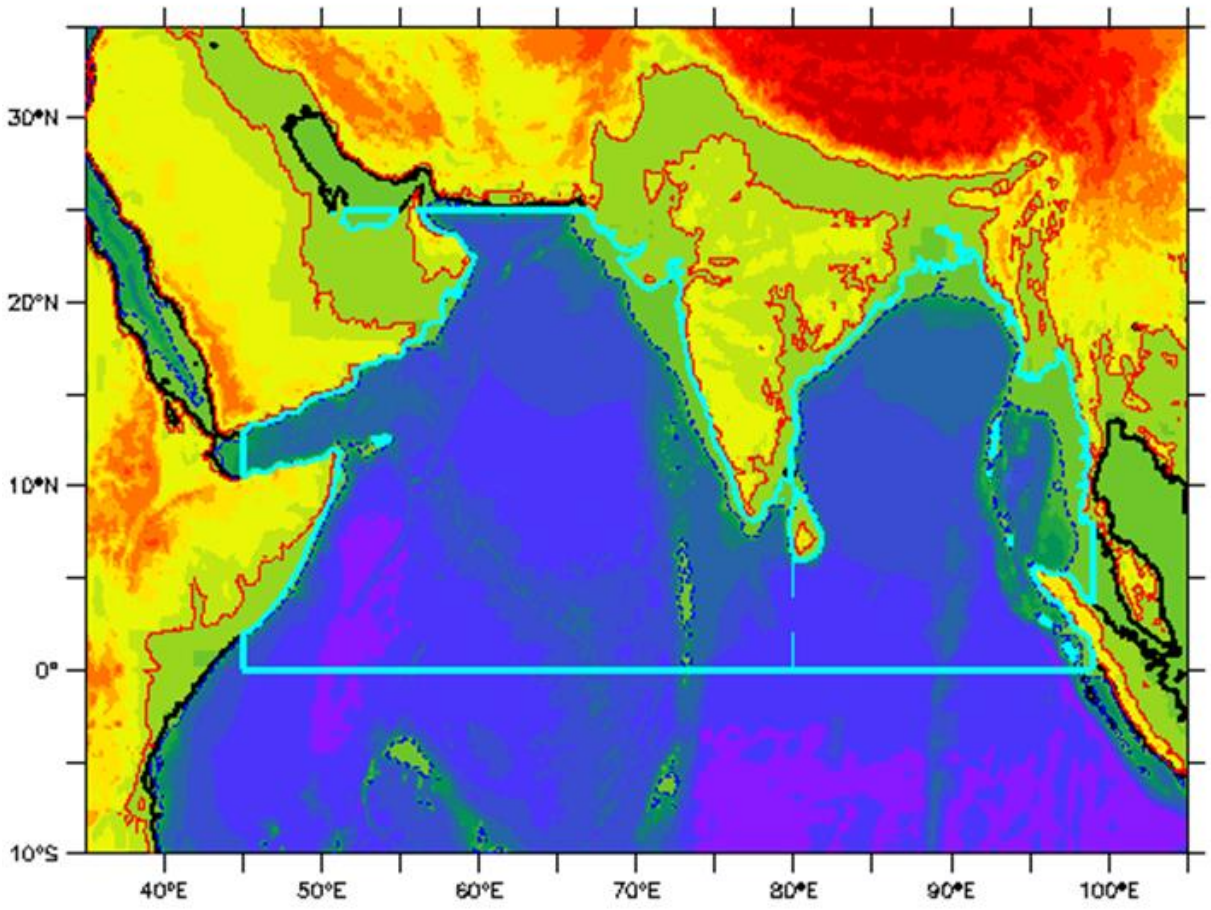

Figure 2.1 Region of study, the North Indian Ocean (Eq.- 25°N, 45°E- 99°E), is indicated in the map by the area enclosed in the light blue solid line

2.2 Data sets used

2.2.1 International Comprehensive Ocean Atmosphere Data Set (ICOADS)

The International Comprehensive Ocean Atmosphere Data Set (ICOADS) was used to obtain SST data, besides also the zonal and meridional components of wind, air temperature, specific humidity and sea level pressure [*Woodruff et al.*, 2005]. The data was downloaded from www.esrl.noaa.gov/psd/data/gridded/data.coads.1deg.html, globally and in the period from 1960 January to 2011 December. The data set used was monthly and had a spatial resolution of 1° by 1°.

2.2.2 Solar Influence Data Centre (SIDC) Data Set

The international sunspot number data were obtained from the solar influence data centre (SIDC) webpage, ftp://ftp.ngdc.noaa.gov/STP/SOLAR_DATA/SUNSPOT_NUMBERS/INTERNATIONAL/monthly/MONTHLY. The data is now available at http://sidc.oma.be/sunspot-data/. The data set used was monthly, available from 1749 January onwards, and having an internationally averaged value. The dataset used was for the period from 1960 January to 2011 December. The sunspot number was used as a proxy for the solar irradiance [*Willson and Hudson*, 1988], as the latter was available only from 1975.

2.2.3 Atmospheric Carbon dioxide Concentration Data Set

The atmospheric carbon dioxide concentration data set was obtained by merging the data at Mauna Loa, from 1958 March to 1979 December, (ftp://ftp.cmdl.noaa.gov/ccg/co2/trends/co2_mm_mlo.txt), with the averaged global data from 1980 January to 2011 December

(ftp://ftp.cmdl.noaa.gov/ccg/co2/trends/co2_mm_gl.txt) [*Keeling et al.,* 2001]. The atmospheric carbon dioxide concentration data is monthly.

2.2.4 Objectively Analysed Air-Sea Fluxes (OA Flux) Data Set

The evaporation data was obtained from the Objectively Analysed Air-Sea Fluxes (OA Flux) Data Set (http://dss.ucar.edu/datasets/ds260.1/) [*Yu et al.,* 2008]. The data was at every 1° by 1° global and monthly from 1958 January to 2011 December. The units were in cm/year.

2.2.5 Climate Diagnostic Centre (CDC) derived National Centres for Environmental Prediction (NCEP) reanalysis products

The precipitation rate data was obtained from the Climate Diagnostic Centre (CDC) derived National Centres for Environmental Prediction (NCEP) reanalysis products (http://www.esrl.noaa.gov/psd/cgi-bin/db_search/). The precipitation rate data was a monthly mean, from 1948 January to 2014 September, and had values globally, on the land and over the ocean too. The data was gridded roughly every 1.875° by 1.875°. The longitudes had 192 points in the east to west direction, while the latitudes had 94 points in the north to south direction. The data used was in the period from 1960 January to 2011 December.

The precipitation rate data was filtered to include values only over the ocean, by masking the land values. The precipitation rate units were also converted from kg/(m^2s) to cm/year, by the following relationship.

$$\text{Precipitation (cm/year)} = \text{Precipitation (kg/(m}^2\text{s))} * 60 * 60 * 24 * 365.25 / 10$$

2.2.6 National Centres for Environmental Prediction/National Centre for Atmospheric Research (NCEP/NCAR) Reanalysis Monthly Means and Other Derived Variables Data Set

The monthly gridded values of net shortwave radiation (SWR), net longwave radiation (LWR), latent heat flux (LHF) and sensible heat flux (SHF) were obtained from the National Centres for Environmental Prediction/National Centre for Atmospheric Research (NCEP/NCAR) Reanalysis Monthly Means and Other Derived Variables data set [*Kalnay et al.,* 1996]. The website used to obtain the data was http://www.esrl.noaa.gov/psd/data/gridded/ data.ncep.reanalysis.derived.surfaceflux.html.

The variables downloaded were monthly values, which was analysed in the period from 1960 January to 2011 December. The values were global, over both land and the ocean. To obtain oceanic values the variables were masked over the land, and all the variables were considered positive downwards, i.e. positive into the ocean. So in general the values of SWR were positive, while those of LWR, LHF and SHF, were generally negative. The net heat flux (NHF), which was also considered positive downwards, into the ocean, was calculated as follows.

$$\text{Net Heat Flux} = \text{SWR} + \text{LWR} + \text{LHF} + \text{SHF}$$

2.2.7 India Meteorological Department (IMD) e-atlas data

The data on the number of depressions, cyclones and severe cyclonic storms (DCS) were taken from the e-atlas of India Meteorological Department (IMD), available at http://www.rmcchennaieatlas.tn.nic.in/login.aspx?ReturnUrl=%2f. The data was over the Bay

of Bengal. The DCS informations were subsequently compiled and made into a number for each month and analysed in the period from 1960 January to 2011 December.

2.3 Price-Weller-Pinkel (PWP) Model

The Price–Weller–Pinkel (PWP) model [*Price et al.,* 1986] is a mixed-layer model that is similar to the dynamic instability model of Price et al. (1978), but is modified to include mixing in the stratified fluid, below the mixed-layer. The model takes into account mixing processes namely (1) free convection arising due to surface heat loss, (2) mixed-layer entrainment by relaxation and (3) shear flow instability driven mixing. Generally, mixing due to free convection in the Bay of Bengal is very shallow and mostly confined to the upper few tens of centimetres of the water column. In contrast, the last two are the dominant processes that determine the depth of the mixed-layer and are related to momentum flux by the wind through the Richardson number.

Since the vertical mixing of the water is caused by changes in the density due to the changes in the net heat and fresh water fluxes and momentum flux they were calculated from zonal and meridional wind stress components, shortwave and longwave radiations, latent and sensible heat fluxes, evaporation, precipitation and riverine discharge, riverine runoff and catchment area data. The model was initialized with the climatological temperature and salinity profiles and the daily fluxes were used to force the model. The model was run for 730 days (2 years), with a time step of 86400 seconds (1 day) and with a vertical grid interval of 1 m.

The daily wind stress components were obtained from http://apdrc.soest.hawaii.edu/dods/public_data/satellite_product/ifremer/daily_flux, while the daily evaporation data was obtained from

ftp://ftp.whoi.edu/pub/science/oaflux/data_v3/daily/ evaporation/. The daily rainfall data was obtained from http://apdrc.soest.hawaii.edu/dchart/index.html?dset= a2c287de3ad7cab9999e50371916fe. The daily riverine discharge, run-off and catchment area data for the rivers Sittang, Irrawaddy, Chindwin, Brahmaputra, Ganges, Damodar, Subarnarekha, Godavari, Krishna, Penner and Cauvery were obtained from http://www.compositerunoff.sr.unh.edu [*Fekete et al.*, 2000]. Similarly, for the rivers Mahanadi, Ponnaiyar, Vaigai, Mahaveli Ganga and Gin Ganga the riverine discharge, riverine runoff and catchment area data were obtained from http://www.sage.wisc.edu/riverdata/scripts/ station_table.php?qual=32&filenum=1114. The fore-mentioned website gave data for the riverine discharge and runoff data of the river Brahmani, but the catchment area was taken from *Vaithiyanathan et al.* [1988].

The daily downward solar radiation flux and upward long wave radiation flux were obtained from http://www.esrl.noaa.gov/psd/data/gridded/data.ncep.reanalysis.derived. otherflux.html , while the daily latent heat flux and sensible heat flux data were obtained from http://oaflux.whoi.edu . Temperature [*Locarnini et al.*, 2010] and salinity [*Antonov et al.*, 2010] profile data were taken from World Ocean Atlas 2009 available at http://www.nodc.noaa.gov/OC5/WOA09/ netcdf_data.html. For comparing the model MLD, the data on the mixed-layer depths were taken from *Holte et al.* [2010] (http://mixedlayer.ucsd.edu/data/monthlyclim.nc) and *Keerthi et al.* [2013] (http://www.ifremer.fr/cerweb/deboyer/mld/Surface_Mixed_Layer_ Depth.php). In *Holte et al.* [2010] the MLD climatology was computed using Argo profiles and a hybrid method [*Holte and Talley, 2009*], while in *Keerthi et al.* [2013] the monthly MLD data for the Indian Ocean, during 1969 to 2009 was based on temperature and salinity profiles taken from different sources namely National Oceanographic Data Centre (NODC) World Ocean Database 2009 (WOD 09), World Ocean Circulation Experiment (WOCE) global dataset

version 3.0, and Argo profile data. Using this data monthly mean climatology (1969-2009) was computed for comparing with PWP model output.

The PWP model output is the mixed layer depth (MLD). The model is forced with actual and cyclonic wind speeds and the output MLD obtained is compared to other MLD data, and the influence of cyclonic winds deduced.

CHAPTER 3

INTER-DECADAL VARIABILITY OF SEA SURFACE TEMPERATURE IN THE NORTHERN INDIAN OCEAN

3.1 Introduction

The variability of the SST in the North Indian Ocean over decadal time-scales is less studied compared to shorter time-scales, as seen from the previous chapter. In this chapter, first the various periodicities existing in the SST monthly data, during the study period, were examined by subjecting the 12-month running mean SST data to FFT analysis. For this a 12-month running mean was used for eliminating seasonal and annual cycles, whose amplitudes are much larger than the longer period SST cycles and is not the focus of the present study. To decipher the decadal variability over the study region, 60-month running-mean SSTs are analysed. The 60-month running mean removes variability in SST that is shorter than 5-years. Further, to delineate the basin-scale signatures, SST was averaged over the two basins, the Arabian Sea and the Bay of Bengal, separately and also over the entire North Indian Ocean. Each of the decadal cycle periods from the study period were identified by examining SST with sunspot number cycle. Finally, the averages, standard deviation and slopes of the trendline of SST 60-month running mean were computed and plotted.

3.2 FFT of 12-month running-mean de-trended SST

The FFT of 12-month running-mean de-trended SST for the North Indian Ocean showed 5 distinct peaks which are significant at 95 % level (Figure 3.1). The dominant among them was 43.7 (~3 years 8 months) followed by 61.2 (~5 years) and 122.4 (~10 years). The next dominant peaks at 204 (~17 years) and 29.1 (~2 years 5 months) had similar amplitude.

Based on the amplitude, the first two dominant periods, i.e., 43.7 and 61.2 months, are typical of ENSO, whose periodicity ranges from 3 to 7 years, indicating the influence of ENSO in regulating SST variability in the NIO. The next dominant period, i.e., 122.4 months, affecting the SST is the decadal variability due to the sunspot cycle. Of the next dominant periods, i.e., 29.1 and 204 months, the former is the quasi-biennial oscillation which also impacts the SST.

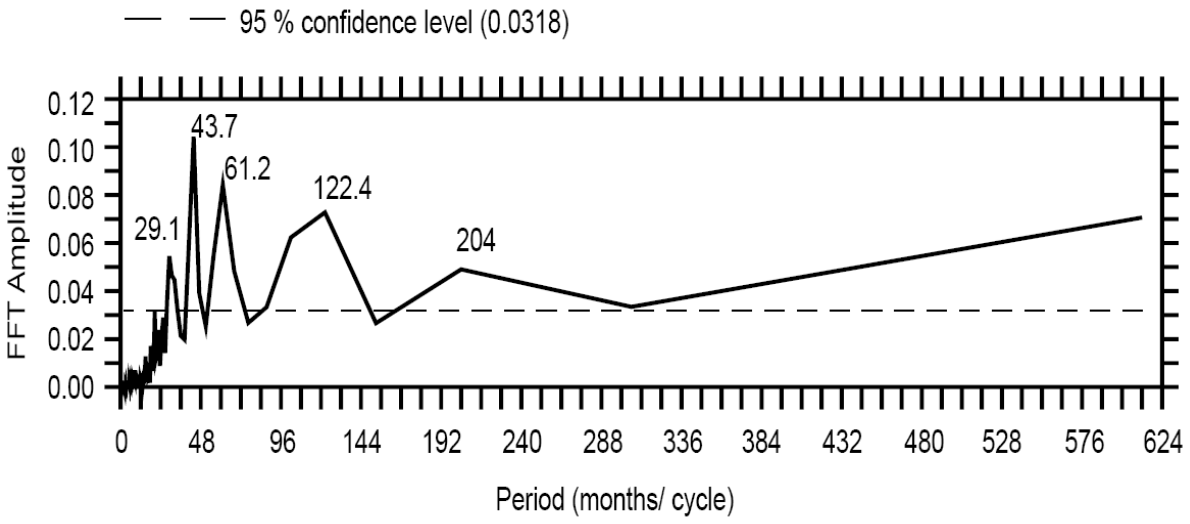

Figure 3.1 FFT amplitude spectrum of the North Indian Ocean (Eq.- 25°N, 45°E- 99°E) obtained by basin-averaged de-trended 12-month running mean of the SST averaged in the period from 1960 January to 2011 December. The 95% Significance level is 0.0318, marked by dashed horizontal line and significant peaks are marked by its period.

Similar computations were carried out for the Arabian Sea and the Bay of Bengal which are presented below.

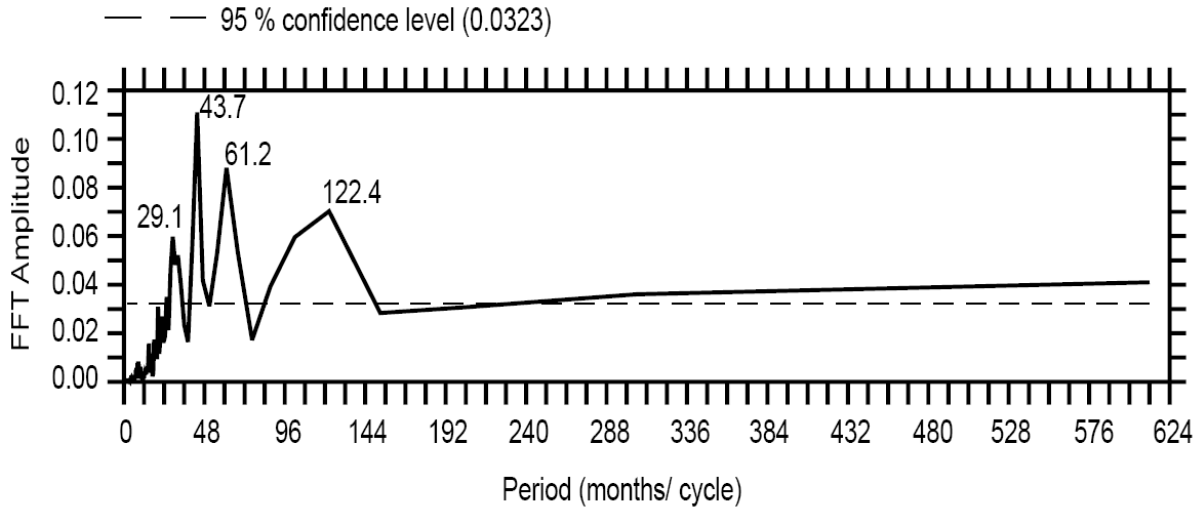

Figure 3.2 FFT amplitude spectrum of the Arabian Sea (Eq.- 25°N, 45°E- 80°E) obtained by basin-averaged de-trended 12-month running mean of the SST averaged in the period from 1960 January to 2011 December. The 95% Significance level is 0.0323, marked by dashed horizontal line and significant peaks are marked by its period.

In the Arabian Sea the dominant periods are 43.7 (~3 years 8 months) followed by 61.2 (~5 years), 122.4 (~10 years) and 29.1 (2 years 5 months) (Figure 3.2). All the peaks are significant at 95 %. Here again, the ENSO periodicities (43.7 and 61.2 months) are the most dominant ones followed by the decadal periodicity (122.4 months) as that of NIO. Note that except 204 months (17 years) all the significant periodicities seen in the NIO were present in the Arabian Sea as well.

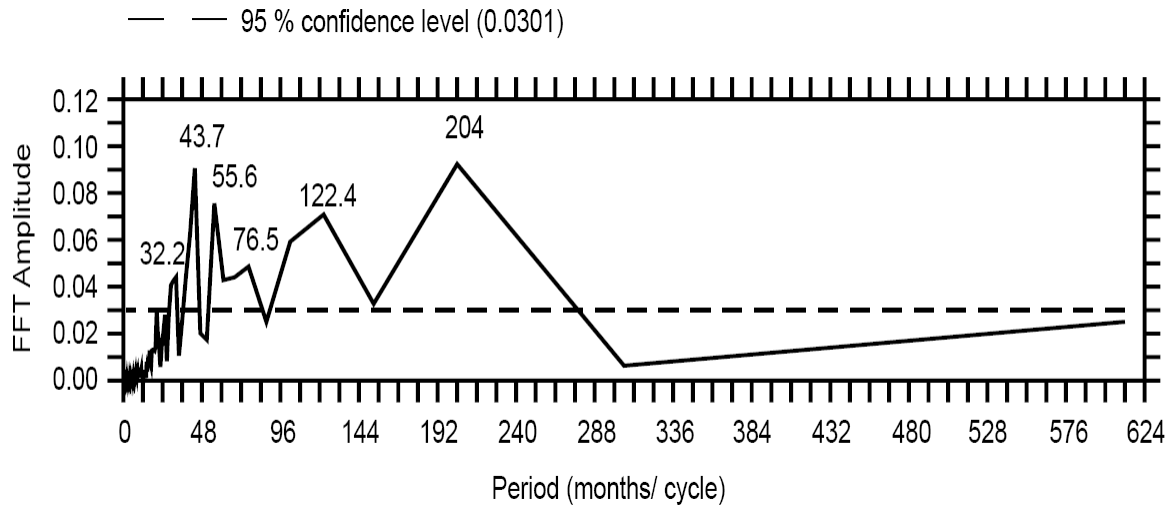

Figure 3.3 FFT amplitude spectrum of the Bay of Bengal (Eq.- 25°N, 80°E- 99°E) obtained by basin-averaged de-trended 12-month running mean of the SST averaged in the period from 1960 January to 2011 December. The 95% Significance level is 0.0301, marked by dashed horizontal line and significant peaks are marked by its period.

In the Bay of Bengal the dominant peaks are seen at 43.7 months (3 years 8 months), followed by 204 months (17 years), 55.6 months (4 years 7 months), 122.4 (10 years 2 months), 76.5 (6 years 4 months) and 32.2 (2 years 8 months) (Figure 3.3). All the periods are significant at 95 % level. Here again, like NIO and Arabian Sea, the 43.7 months (3 years 8 months) period is dominant. However, unlike in the NIO and Arabian Sea, the 204 months (17 years) periodicity co-dominates with the 43.7 months (3 years 8 months) periodicity in the Bay of Bengal.

In summary, for all the 3 domains within the study area, namely NIO, Arabian Sea and Bay of Bengal, the most dominant periodicity seen in the de-trended 60-month running mean of SST using FFT were the ENSO and decadal cycles. Hence, in each of the above domains the decadal cycle was examined.

3.3 Area averaged 60-month running mean SST

The 60-month running-mean area-averaged SST shows a decadal cycle riding over a long-term warming trend in the North Indian Ocean (Figure 3.4). The average temperature in the North Indian Ocean for the period from 1960 January to 2011 December is 28.16 °C. There is an increasing trend of 0.011 °C/year, with a decadal cycle riding on it.

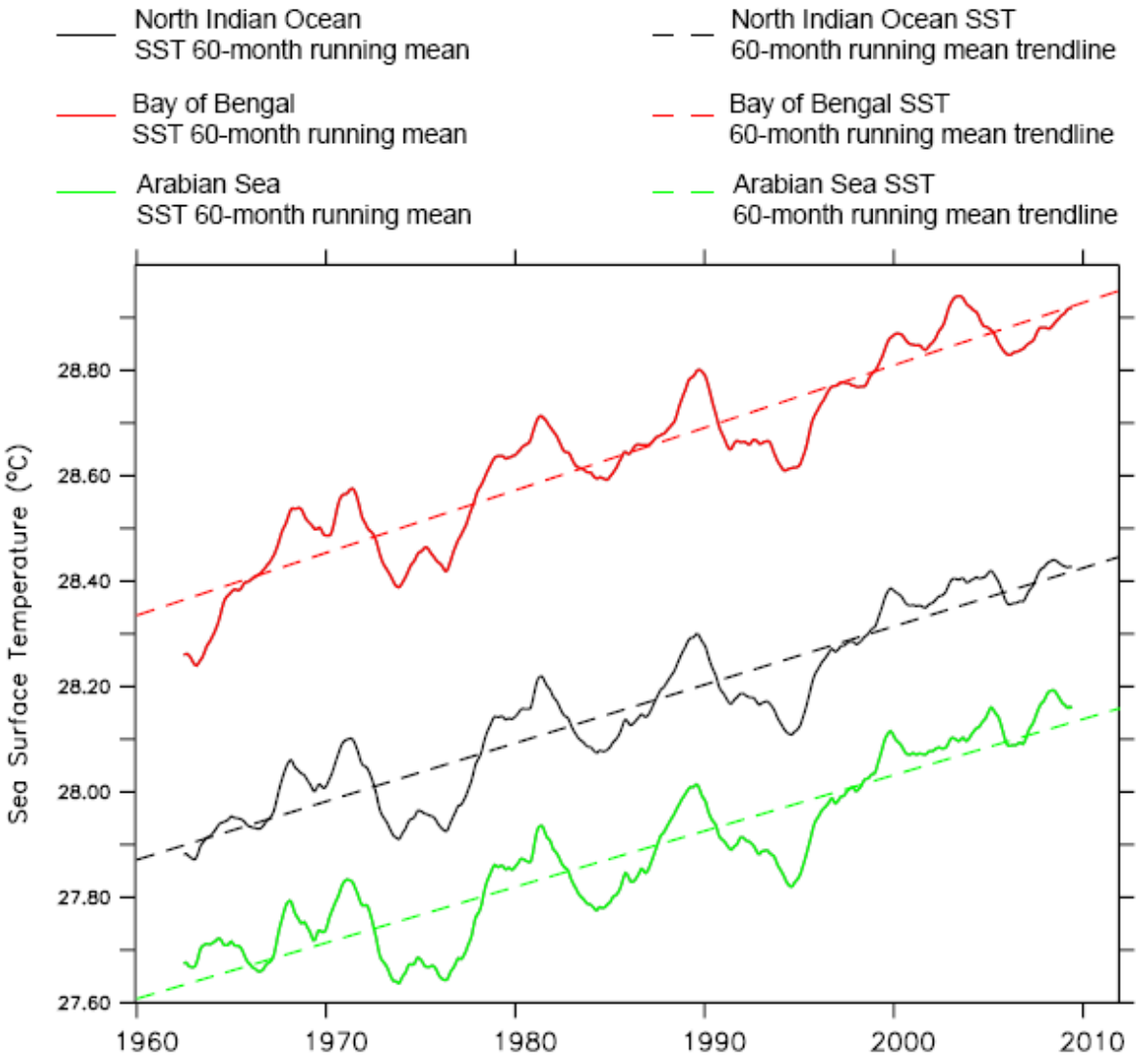

Figure 3.4 Area-averaged 60-month running mean SST (°C) (solid line) and its trendlines (°C/year) (dashed line), from 1960 January to 2011 December, in the North Indian Ocean (Eq.- 25 °N, 45 °E- 99 °E) (black), Arabian Sea (Eq.- 25 °N, 45 °E- 80 °E) (green) and Bay of Bengal (Eq.- 25 °N, 80 °E- 99 °E) (red).

A similar pattern and trend were also seen in the case of the Arabian Sea and the Bay of Bengal. However, the latter is warmer than the former, with the average temperature in the Bay of Bengal being 28.64 °C, while that in the Arabian Sea is 27.88 °C for the period from 1960 January to 2011 December. Though both the basins showed increasing trends in their basin-averaged SSTs, the warming trend in the Bay of Bengal was 0.012 °C/year, which was higher than the Arabian Sea having a value of 0.010 °C/year. Note that the area-averaged 60-month running mean SST, in all the 3 regions, showed a disruption in the decadal cycle in the post-1995 period. Thus, during the study period, 3 distinct decadal cycles were discernible in all the 3 regions prior to 1995.

In order to identify the sunspot number cycle corresponding to each of the decadal cycles of SST, the 60-month running mean of the sunspot number was superimposed on the SST (Figure 3.5). The minima of the sunspot numbers are taken as the beginning/ end of the decadal sunspot number cycle periods. The periods of the sunspot number decadal cycle are (1) 1964 March to 1975 June, (2) 1975 June to 1985 December, (3) 1985 December to 1995 November and (4) 1995 November to 2008 July. Accordingly, the above decadal cycle has been designated as 1^{st}, 2^{nd}, 3^{rd} and 4^{th} respectively.

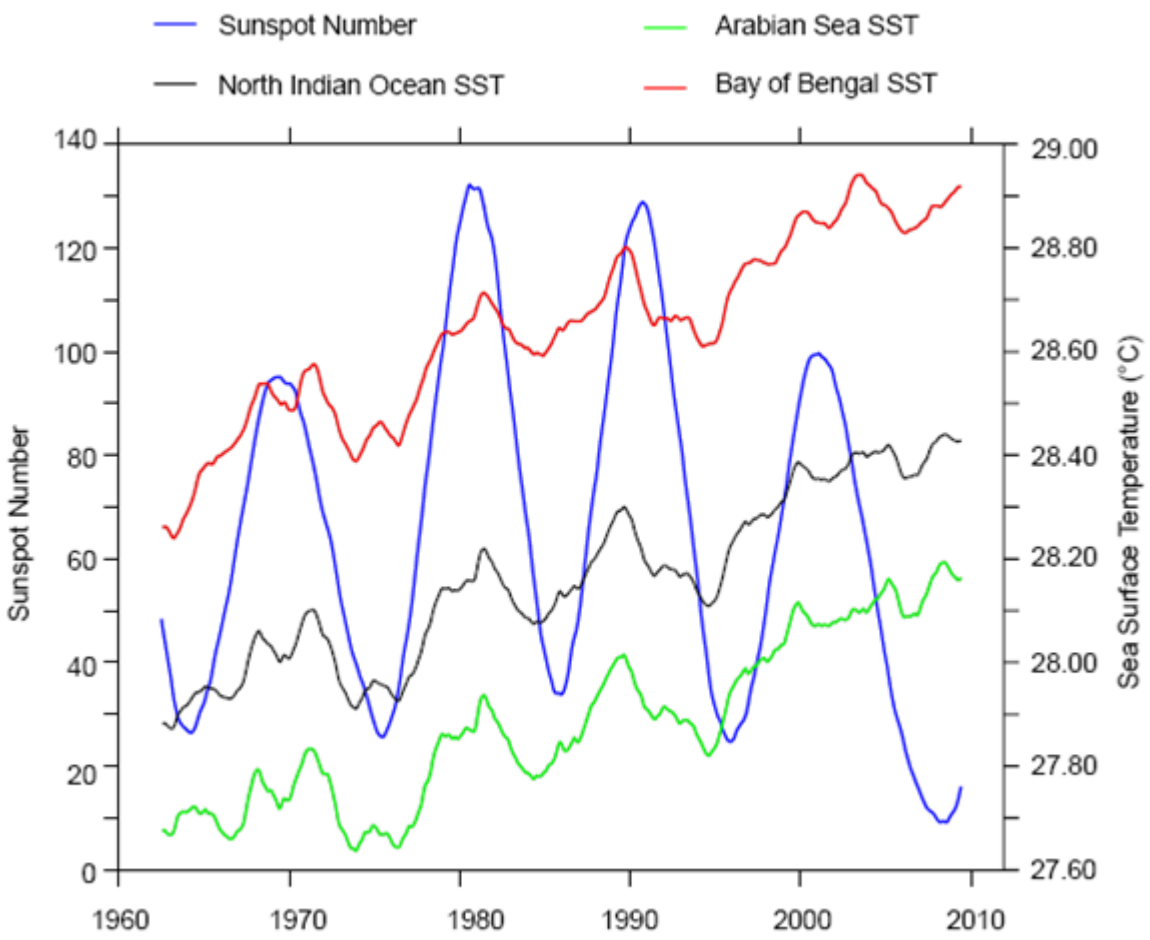

Figure 3.5 The 60-month running mean of the Sunspot number (blue line) and the basin-averaged SST (°C) in the North Indian Ocean (Eq.- 25 °N, 45 °E- 99 °E) (black), Arabian Sea (Eq.- 25 °N, 45 °E- 80 °E) (green) and Bay of Bengal (Eq.- 25 °N, 80 °E- 99 °E) (red), in the period from 1960 January to 2011 December.

Having delineated the area-averaged SST decadal cycle in the entire NIO, Arabian Sea and Bay of Bengal and its corresponding sunspot number cycle, the next step is to examine the characteristics of the mean spatial distribution pattern of 60-month running mean SST for each of the decadal cycle, its standard deviation and slope of the trendline in the study domain, which is detailed in the following sections.

3.4 Spatial distribution of decadal mean SST

The average value of the 60-month running mean SST for the 1st decadal cycle (from 1964 March to 1975 June) was 28.5 °C which was seen in the south-eastern part of the Arabian Sea and most parts of the Bay of Bengal (Figure 3.6a). The north-western Arabian Sea, region encompassing the southern peninsular India and Sri Lanka, and northern Bay of Bengal was colder. The coldest regions were seen off Somalia, Arabia and Indo-Sri Lanka which are known for seasonal upwelling during summer (southwest) monsoon. Though the pattern remained similar in the period of 2nd decadal cycle (from 1975 June to 1985 December) also, the region of 28.5 °C has expanded northwards in the Bay of Bengal and the cold water region in the Indo-Sri Lankan upwelling region had shrunk (Figure 3.6b). In the 3rd decadal cycle (from 1985 December to 1995 November) an intensification of warming was discernible within the region of 28.5 °C SST, by way of the appearance of region of 29 °C SST in the equatorial regions (Figure 3.6c). Note also that the region of 28.5 °C has further expanded northwards in the Bay of Bengal, while the cold water region in the Indo-Sri Lankan upwelling region had further shrunk. In the 4th decadal cycle SST in almost entire Bay of Bengal, equatorial region and the eastern Arabian Sea showed an increase (Figure 3.6d). The area occupied by the Indo-Sri Lanka upwelling region shrunk to the least of the 4 decades. Similarly, the Somali upwelling which had the coldest SST during the 1st decadal cycle showed warmest SST in the 4th decadal cycle. In contrast, the Oman upwelling did not show changes as large as the rest of the upwelling regions.

The range of decadal average 60-month running mean SST in the 1st to 4th sunspot number cycle were 24.43°C to 30.58°C, 24.81°C to 31.16°C, 24.04°C to 30.41°C and 24.26°C to 30.50°C respectively.

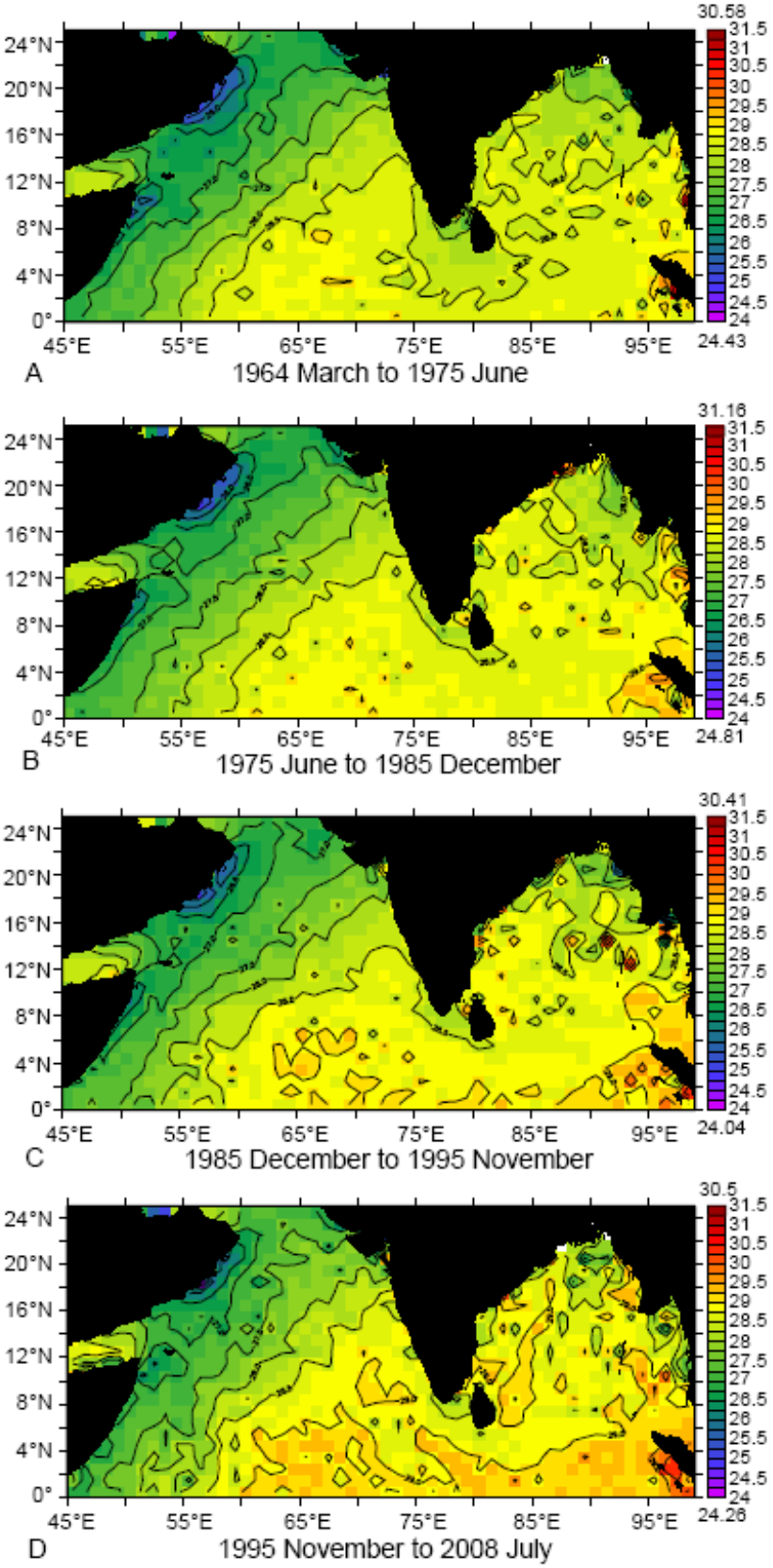

Figure 3.6 North Indian Ocean (Eq.- 25 °N, 45 °E- 99 °E) SST 60-month running mean average (°C), in the periods from 1964 March to 1975 June (figure 3.6 a), 1975 June to 1985 December (figure 3.6 b), 1985 December to 1995 November (figure 3.6 c) and 1995 November to 2008 July (figure 3.6 d).

In order to bring out the progressive changes in the SST over the region of large SST variability, the relative changes in the isotherm over regions of upwelling, such as Somalia, Arabia and Indo-Sri Lanka, have been examined closely. The area bounded by the isotherm 26.5 °C (indicator isotherm of Somalia upwelling), which encompasses areas of temperature lesser than 26.5 °C, off Somalia showed a progressive reduction from 1st decadal cycle to 4th decadal cycle. However, the maximum reduction in the aerial extent of 26.5 °C occurred during the period from 1st to 2nd and 3rd decadal cycles. In the 4th decadal cycle, which corresponds to the period of rapid warming, the 26.5 °C completely disappeared from Somali upwelling region. A similar reduction in the aerial extent of upwelling region of Indo-Sri Lanka was discernible from the area bounded by the 28.5 °C isotherm (indicator isotherm for Indo-Sri Lanka upwelling). However, unlike the Somalia upwelling region, the indicator isotherm did not completely disappear from Indo-Sri Lanka upwelling region. In complete contrast, the 26.5 °C isotherm off Oman (indicator isotherm of Oman upwelling) showed the least change in terms of the aerial extent. However, during the 4th decadal cycle when the entire study domain experienced enhanced warming, the Oman upwelling also underwent a reduction in the upwelling area.

Another area which showed distinct warming is the Sumatra region which is located in the Indo-Pacific warm pool region and bounded by the 29 °C isotherm. In the 1st decadal cycle the area bounded by the 29 °C isotherm was very small, which expands rapidly up to the 4th decadal cycle. The aerial extend grows rapidly both northward and westward in the 3rd and 4th decadal cycles. In the 4th decadal cycle it extends well into the eastern Bay of Bengal up to 12 °N and westward along the equator into the Arabian Sea up to 60 °E.

3.5 Spatial distribution of decadal standard deviation of 60-month running mean SST

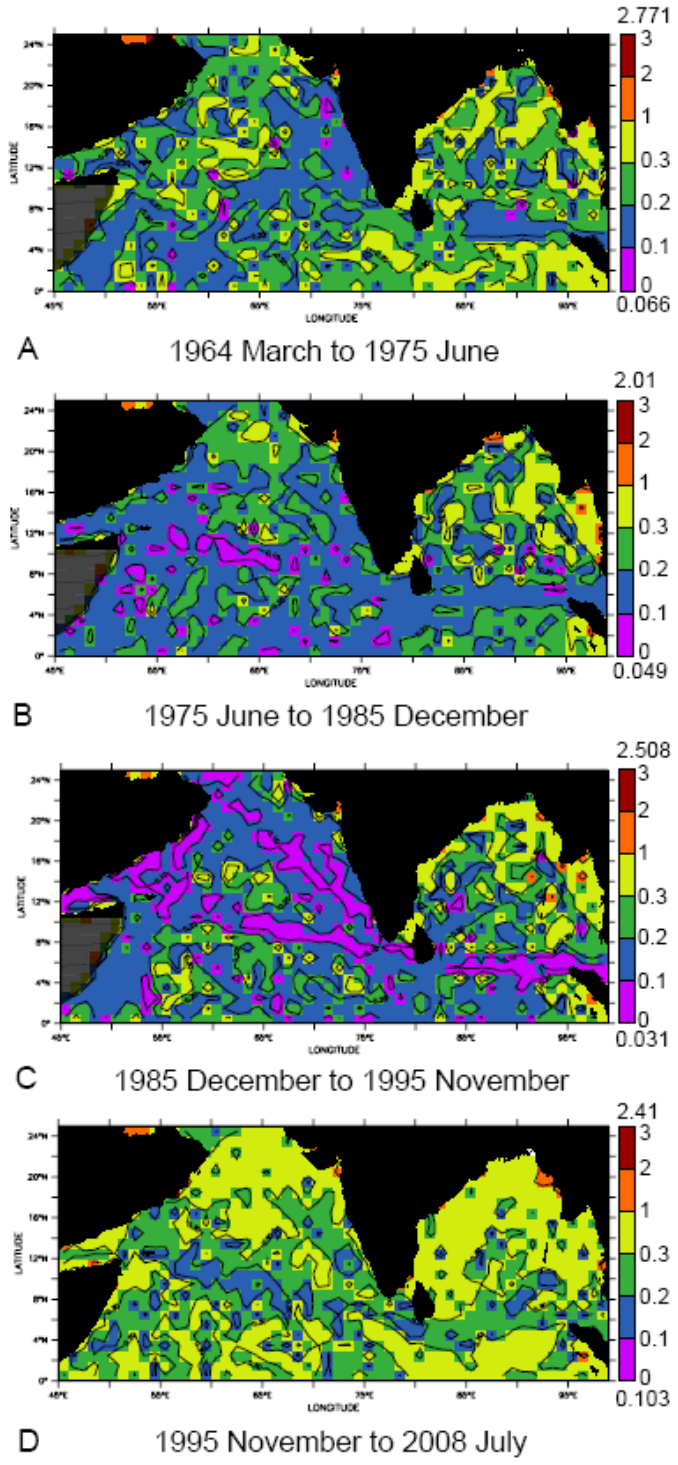

Figure 3.7 The 60-month running mean standard deviation of SST (°C) in the northern Indian Ocean, in the periods from 1964 March to 1975 June (figure 3.7a), 1975 June to 1985 December (figure 3.7b), 1985 December to 1995 November (figure 3.7c) and 1995 November to 2008 July (figure 3.7d).

The standard deviation of the 60-month running mean SST, in general, showed less spatial variability over the study domain in all the decadal cycle considered for the study (Figure 3.7 a–d).

In general, the Arabian Sea showed lesser standard deviation values than the Bay of Bengal. In the 1st decadal cycle the standard deviation was lesser along the Somali coast, southern parts of the Arabian Sea, western coast of India, and central and southern Bay of Bengal. The area of low standard deviations increases in the Arabian Sea in the 2nd and 3rd decadal cycle, while the area of higher standard deviation seen along the coastal Bay of Bengal also expands. The standard deviation in the 4th decadal cycle in the entire study domain showed high values except in a zonal band in a north-west to south-east direction from the tip of Somalia toward Indo-Sri Lanka region and into the Bay of Bengal (Figure 3.7d).

3.6 Spatial distribution of 60-month running mean SST slopes

The slopes of the 60-month running mean of SST in the 1st decadal cycle were negative in a band oriented in a north-west south-east direction in the Arabian Sea encompassing the region up to south of Sri Lanka and several patches in the Bay of Bengal (Figure 3.8a). Rest of the regions had positive slope. In the 2nd decadal cycle positive slope replaces the band of negative slope seen during the 1st decadal cycle, except in the northern parts of the Arabian Sea (Figure 3.8b). The small patches of positive slope in the Bay of Bengal seen during the 1st decadal cycle showed spatial expansion during the 2nd decadal cycle. Once again, during the 3rd decadal cycle major parts of the Arabian Sea and the Bay of Bengal showed a negative trend (Figure 3.8c). Along the western Bay of Bengal a band of positive slope is seen hugging the coast.

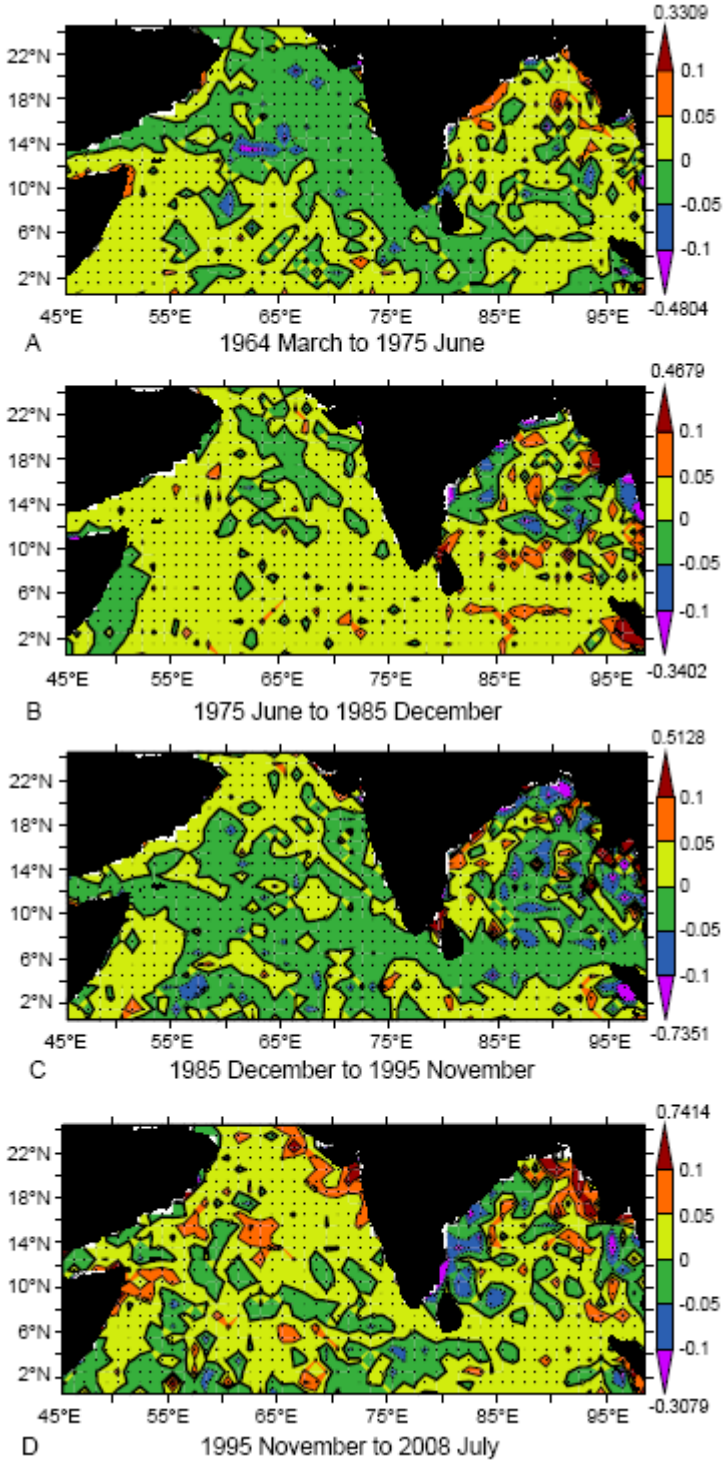

Figure 3.8 The slopes of the 60-month running mean SST (°C/year), in the periods from 1964 March to 1975 June (figure 3.8 a), 1975 June to 1985 December (figure 3.8 b), 1985 December to 1995 November (figure 3.8 c) and 1995 November to 2008 July (figure 3.8 d).

In the 4th decadal cycle, the slope showed a band of positive values hugging the western boundary of the Bay of Bengal, a reverse trend as that of 3rd decadal cycle (Figure 3.8d). Except this region the rest of the study domain showed positive slope.

Thus, dominant alternating positive and negative slopes occur in the eastern Arabian Sea and in the western Bay of Bengal. There are smaller and less distinct oscillating patterns off Sumatra, off Somalia and in the southern Bay of Bengal.

Having delineated the decadal mean spatial patterns of the 60-month running mean SST, its standard deviation and the slopes of the trendline, it is important to examine the area-averaged 60-month running mean SST trendlines during each of the four decadal cycles in the Northern Indian Ocean, Arabian Sea and the Bay of Bengal which is detailed below.

3.7 Area-averaged 60-month running mean SST, trend and slopes in each of the decadal cycle periods

The area-averaged 60-month running mean SST slopes in the North Indian Ocean (NIO), Arabian Sea and Bay of Bengal are computed for each of the decadal cycle and presented in figure 3.9 a–c. The salient feature of the SST trendlines in the NIO, Arabian Sea and the Bay of Bengal during the period of study was (1) a linear warming trend, (2) presence of dominant decadal cycle riding over this linear warming trend, and (3) disruption of the decadal cycle after 1995. Though the area-averaged 60-month running mean SST in all the 3 regions showed a linear increasing trend from 1960 January to 2011 December, the trend in the individual decadal cycle are quite different for NIO, Arabian Sea and the Bay of Bengal. In the NIO the area-averaged 60-month running mean SST showed an increase at the rate of 0.0110°C/year (coefficient of determination, R^2= 0.87), while that in the Arabian Sea and in

the Bay of Bengal were 0.0106°C/year (R^2= 0.84) and 0.0118°C/year (R^2= 0.87) respectively.

Note that the rate of SST rise was higher in the Bay of Bengal than in the Arabian Sea.

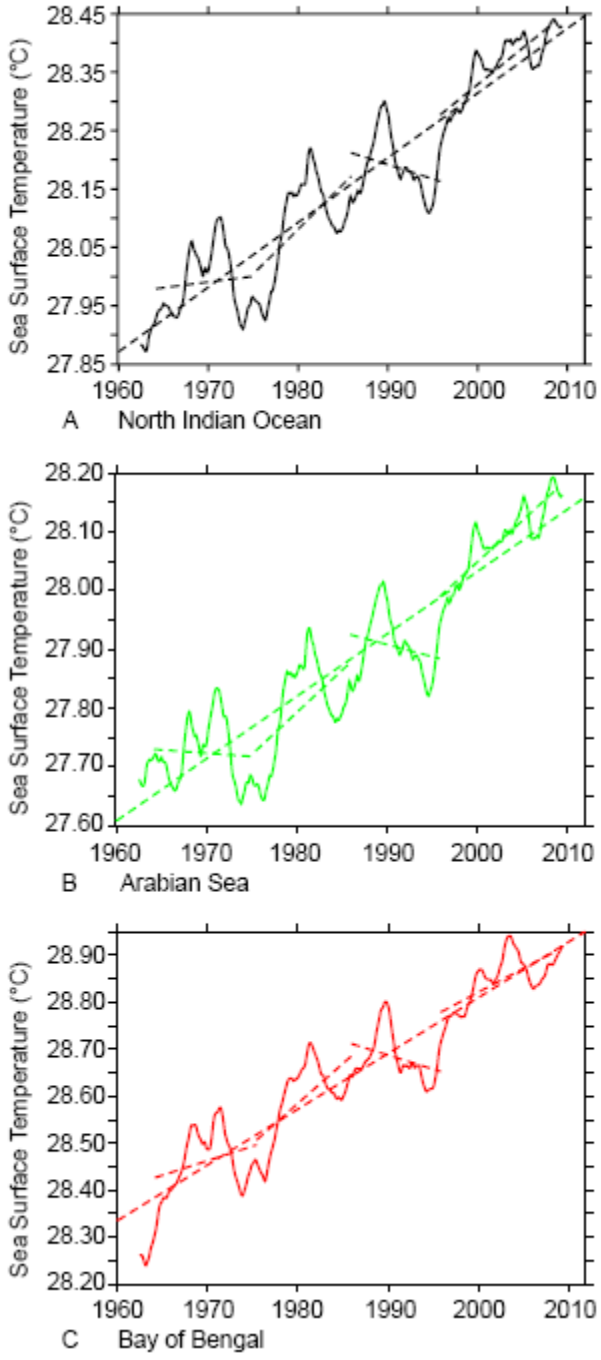

Figure 3.9 The area-averaged 60-month running mean SST (°C) (solid line) and trendlines (°C/year) (dashed line), from 1960 January to 2011 December and in the sunspot number cycle periods viz. 1964 March to 1975 June, 1975 June to 1985 December, 1985 December to 1995 November and 1995 November to 2008 July, in the North Indian Ocean (Eq.- 25 °N, 45 °E- 99 °E) (black) (Figure 3.9a), Arabian Sea (Eq.- 25 °N, 45 °E- 80 °E) (green) (Figure 3.9b) and Bay of Bengal (Eq.- 25 °N, 80 °E- 99 °E) (red) (Figure 3.9c).

In the 1st decadal cycle slope of the SST trend line in the NIO showed a weak increasing trend with a value of 0.0019°C/year (R^2=0.01). In the Arabian Sea the slope of the trend line showed a weak decline with a value -0.0011°C/year (R^2=0.00). In contrast, the trend of SST in the Bay of Bengal showed an increase with a value of 0.0061°C/year (R^2=0.10). The magnitude of the slope in the Arabian Sea was the least.

In the 2nd decadal cycle, the slope of the area-averaged 60-month running mean SST in the NIO showed an increasing trend of 0.0153°C/year (R^2= 0.34). Contrary to the 1st decadal cycle, both the Arabian Sea and the Bay of Bengal showed an increasing trend during 2nd decadal cycle. However, the rise in the Bay of Bengal, 0.0170°C/year (R^2=0.42) was much higher than the rise in the Arabian Sea i.e. 0.0143°C/year (R^2=0.29).

In the 3rd decadal cycle the slope of the area averaged 60-month running mean SST in the NIO showed a decreasing trend of -0.0049°C/year (R^2=0.07). Both the Arabian Sea and the Bay of Bengal showed a decreasing trend with a slope of -0.0041°C/year (R^2=0.05) and -0.0059°C/year (R^2=0.11) respectively.

In the 4th decadal cycle the slope of the area-averaged 60-month running mean SST in the NIO showed an increasing trendline slope of 0.0124°C/year (R^2=0.72). The basin-averaged slope of the SST trendline in the Arabian Sea was 0.0141°C/year (R^2=0.786) and in the Bay of Bengal it was 0.0101°C/year (R^2=0.479).

3.8 Disruption of the decadal cycle and changes in SST trends in the post-1995 period

One of the characteristic features of the area-averaged 60-month running mean SST that emerged from the previous section was the disruption of decadal cycle after 1995. As it is well known that natural decadal cycle is driven by solar activity [*White* et al., 1997] the sunspot number, which is a proxy for the solar irradiance [*Wilson and Hudson*, 1988], was plotted along with SST to see the correspondence between the two in the Arabian Sea (Figure 3.10) and the Bay of Bengal (Figure 3.11). It is also pertinent to examine the slope of the trend line before and after 1995, which are also given in above mentioned figures. Note that the figure also includes the 60-month running mean carbon dioxide concentration, which will be discussed in the next chapter, while dealing with the factors responsible for the observed variability.

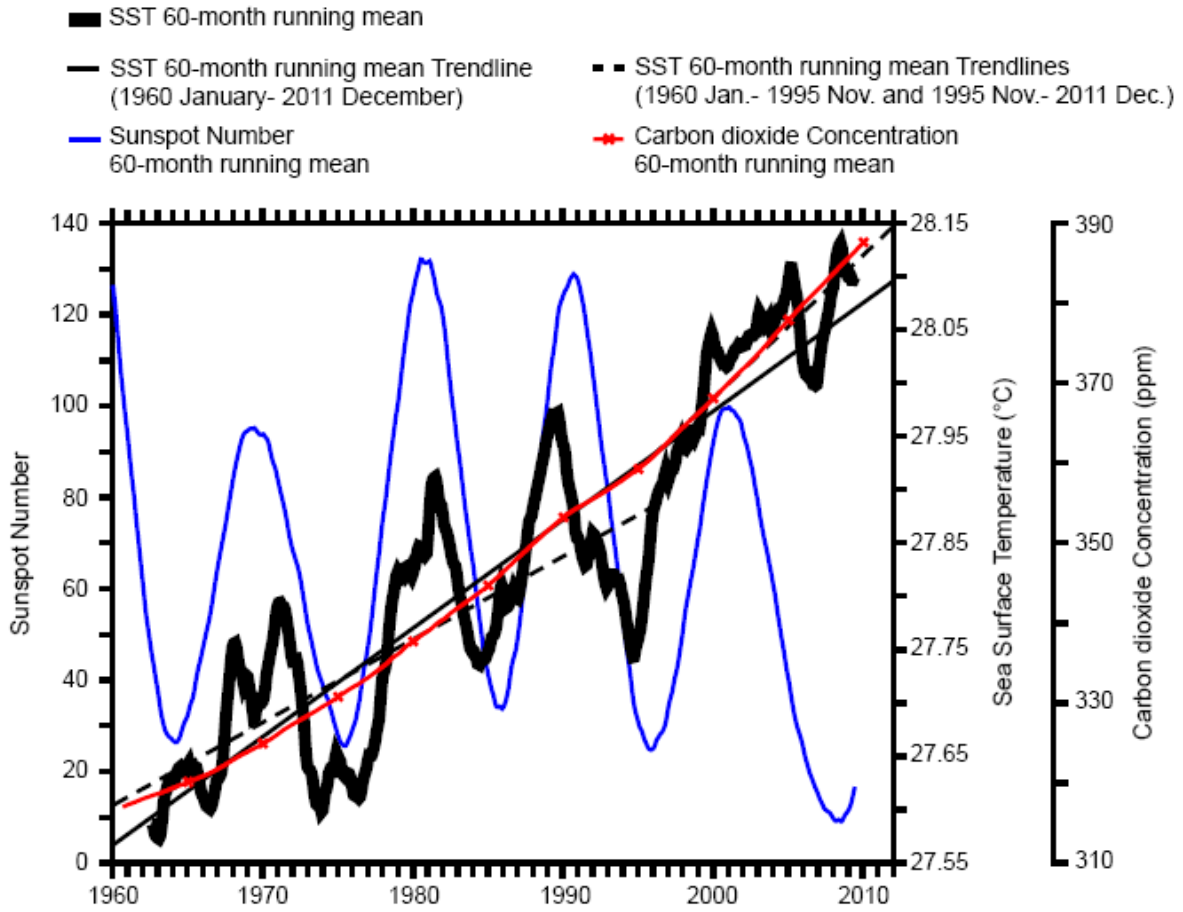

Figure 3.10 The 60-month running mean SST (^{o}C) (thick black line) in the Arabian Sea from 1960 January to 2011 December, with trendlines for the entire period (thin black line) and in the pre and post 1995 November periods (thin black dashed lines). The 60-month running means of sunspot number (thin blue line) and carbon dioxide concentration (thin red line with cross marks) [*D'Mello and Prasanna Kumar*, 2017].

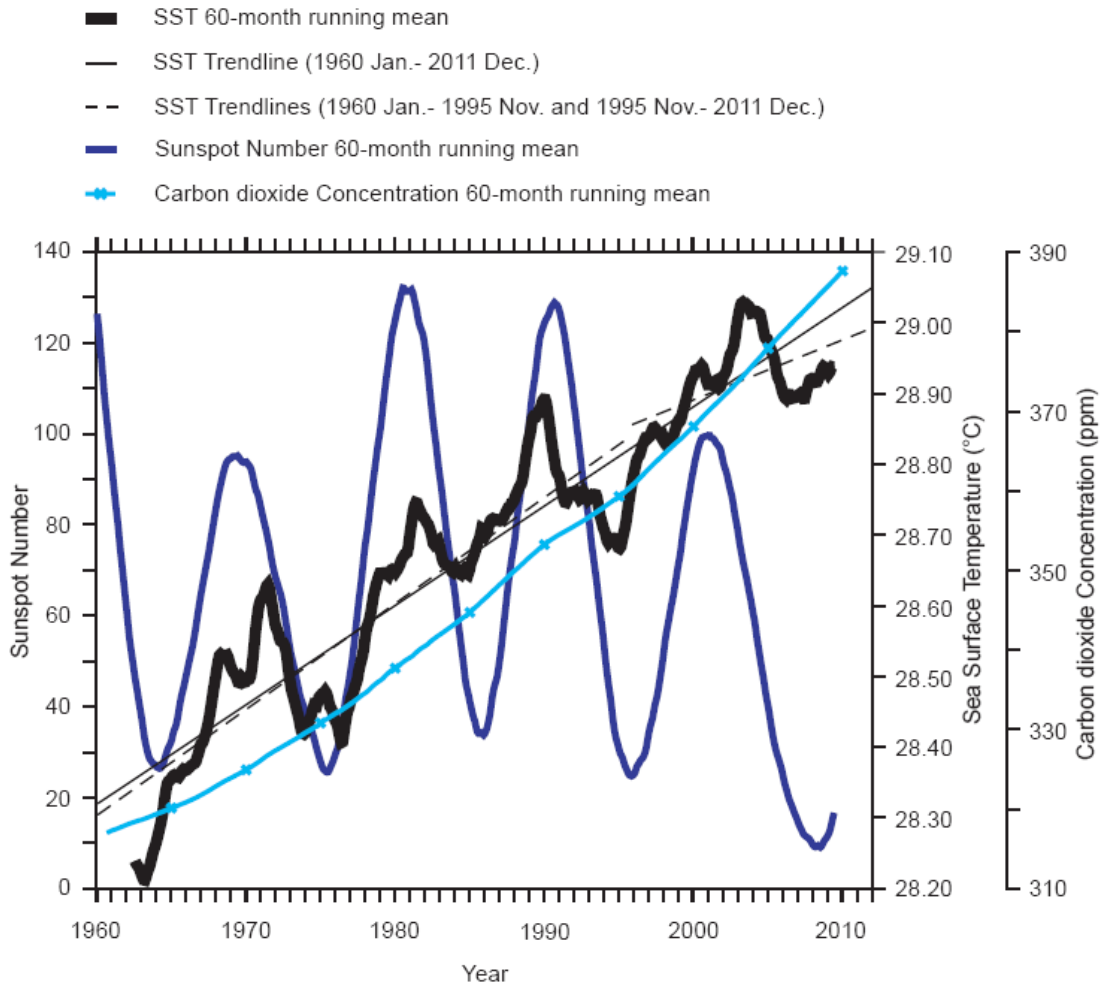

Figure 3.11 Basin-averaged 60-month running mean SST (thickest line, black) in the Bay of Bengal (Eq. to 25 °N, 80 °E to 99 °E), sunspot number (thick line, blue) and carbon dioxide concentration (thick line with cross-marks, light-blue) for the period 1960 January to 2011 December. SST trendline for the entire period of study (thin line, black) and pre-1995 and post-1995 SST trendlines (thin dashed lines, black) are also shown [*D'Mello and Prasanna Kumar*, 2016].

In the Arabian Sea as well as in the Bay of Bengal, the SST, in general, showed a covariance with sunspot number from 1960 to 1995 indicating that the SST decadal cycle was primarily driven by the solar activity. However, after 1995, the link between the SST and the sunspot number seems to have disconnected. The linear warming trend for the Arabian Sea and the Bay of Bengal from 1960 to 2011 showed that the Bay of Bengal was warming faster

(0.0140^{o}C/year) than the Arabian Sea (0.0102^{o}C/year) (Table 3.1). Similar was the pattern of warming in the pre-1995 period for both the seas. In the post-1995 period the Arabian Sea showed an accelerated warming compared to pre-1995 period. In contrast, the Bay of Bengal showed a slowdown in the rate of warming during post-1995 period compared the pre-1995 period. The reasons for the observed difference in the rate of warming during pre and post-1995 periods will be dealt with in the next chapter.

Table 3.1 Slopes of the linear trend line of 60-month running mean SST in the Arabian Sea and the Bay of Bengal for different periods.

Serial Number	**Period**	**Slope of the SST linear trend line (°C/year)**	
		Arabian Sea	**Bay of Bengal**
1	1960-2011	0.0102	0.0140
2	1960-1995	0.0078	0.0149
3.	1995-2011	0.0136	0.0084

CHAPTER 4

FACTORS CONTROLLING THE INTER-DECADAL VARIBAILITY

4.1 Introduction

In the previous chapter inter-decadal variability of the northern Indian Ocean comprising of the Arabian Sea and the Bay of Bengal has been examined. In this chapter the potential factors that are responsible for the inferred inter-decadal variability has been examined in sections 4.2 to 4.5. In order to decipher the factors, at first the variability in each of the sunspot number cycle periods are analysed with respect to various parameters namely the wind speed, evaporation minus precipitation (E-P) and net heat flux (NHF). The slopes of each of the above parameters and correlation coefficients were computed to identify those regions where the correlation coefficient had a significance level above 95%. Table 4.1 provides number of points used for calculation and the details pertaining to colour scheme used for shading of significance level of 95 % and 99 % correlation coefficients, while Table 4.2 contains number of point and T-values of slopes for significance level greater than or equal to 95%.

Further, factors responsible for the post 1995 break in the decadal cycle along with the reasons for the changes in the linear warming trend in the Arabian Sea and the Bay of Bengal were examined in section 4.6.

Table 4.1 Values of correlation coefficient ≥ 95% and ≥ 99% significance levels in various sunspot number cycle periods, and the colour scheme used for shading the figures till section 4.5.4.

Sunspot Number Cycle Period	**Number of points**	**Correlation Coefficient**	
		≥ 95 % Significance level **Light red/blue positive /negative**	**≥ 99 % Significance level** **Dark red /blue positive /negative**
1964 March to 1975 June	136	+/-0.168	+/-0.220
1975 June to 1985 December	127	+/-0.174	+/-0.228
1985 December to 1995 November	120	+/-0.179	+/-0.234
1995 November to 2008 July	153	+/-0.159	+/-0.208

Table 4.2 T-values of slopes for significance level greater than or equal to 95% in various sunspot number cycle periods, used for slope figures till section 4.5.4.

Sunspot Number Cycle Period	**Number of points**	**T-values of slopes for significance level ≥ 95%**
1964 March to 1975 June	136	+/-1.978
1975 June to 1985 December	127	+/-1.979
1985 December to 1995 November	120	+/-1.980
1995 November to 2008 July	153	+/-1.976

4.2 Factors controlling the SST variability during the sunspot number cycle period from 1964 to 1975

In this sunspot number cycle based on the slopes of wind speed, net heat flux (positive into the ocean), E-P (evaporation minus precipitation) and their correlation with SST (Figure 4.1), two regions were identified (Figure 4.2) which could explain the distribution of the SST linear trendline slope.

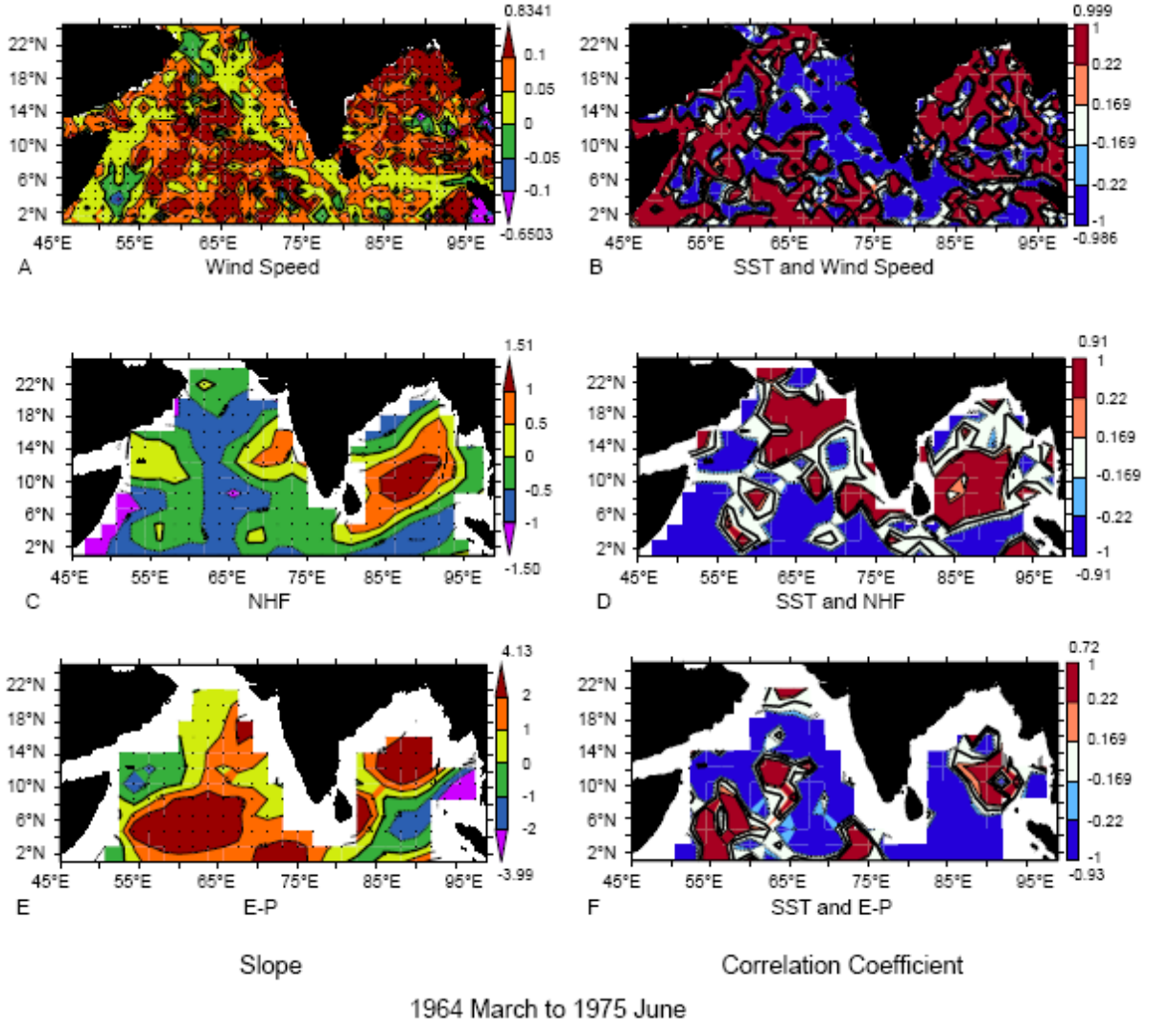

Figure 4.1 60-month running mean slopes (left) of wind speed ((m/s)/year), net heat flux ((W/m^2)/year) and E-P ((cm/year)/year) and their correlation coefficients (right) with SST, in the period from 1964 March to 1975 June. Slope regions above 95 % significance levels are shaded. 2-tailed t-statistic $\geq$ |1.978|, N=136. Regions above 95 % significance levels of correlation coefficients are shaded. r = +/- 0.169, significance level= 95 %; r = +/- 0.22, significance level= 99 %, N= 136. N is the number of points.

These 2 regions are eastern Arabian Sea and southwest Bay of Bengal, which are represented approximately by solid circles/ellipses in Figure 4.2.

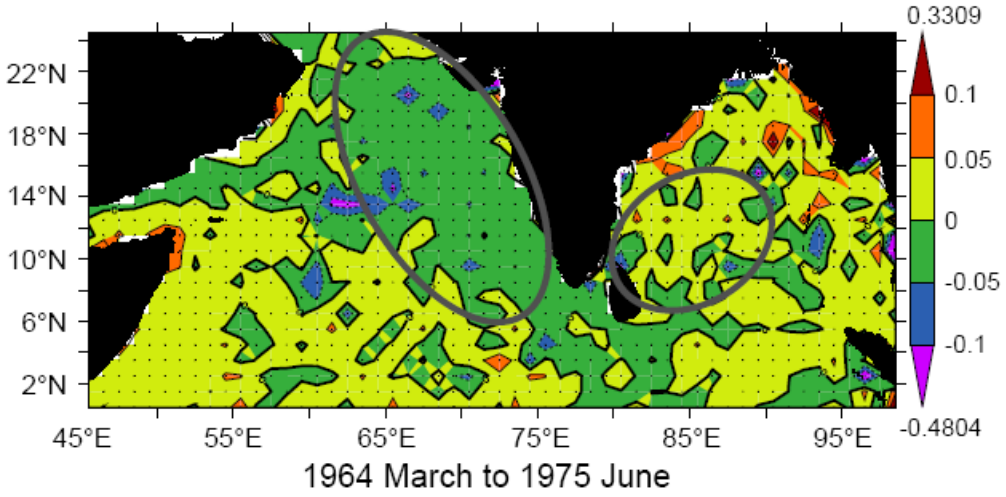

Figure 4.2 Regions studied SST variability demarcated by solid circles/ellipses in the sunspot number cycle period from 1964 March to 195 June. Shading is for the slope of the 60-month running mean SST trend line.

4.2.1 Eastern Arabian Sea

The SST slopes in the north Indian Ocean generally showed a decreasing trend (Figure 4.2) in the eastern Arabian Sea, in the sunspot number cycle period from 1964 to 1975. The wind speed and SST have an inverse relationship (Figure 4.1A and B)). Stronger winds can cause lesser SSTs through enhanced cooling, due to higher evaporation and/ or wind-mixing with the generally cooler subsurface waters. The opposite process of weaker wind speeds, leading to lesser evaporative cooling and also lesser mixing with the generally cooler subsurface waters results in warmer surface temperatures. A similar relationship and leading to above mentioned process explains the observed decreasing trend in SST in the waters to the south of Sri Lanka.

The net heat flux showed a decreasing trend (Figure 4.1C) and positive correlation with SST (Figure 4.1D), everywhere in the eastern Arabian Sea except along a small patch in the central west coast. This implies that the observed decreasing trend in SST was also impacted by the deceasing trend of the net heat flux into the ocean.

The evaporation minus precipitation (E-P) showed an increasing trend along the eastern Arabian Sea (Figure 4.1E) with a negative correlation with SST (Figure 4.1F). This condition would warrant either an increase in evaporation or a decrease in precipitation. In the former case it would lead to a decrease in SST.

In fact, in the eastern Arabian Sea, the observed decreasing trend in SST during this decadal cycle was contributed by increasing wind speed, decreasing net heat flux and increasing E-P.

4.2.2 Southern Bay of Bengal

In the southern Bay of Bengal, the SST showed an increasing trend (Figure 4.2), in general, with small patches showing decreasing trend. The increase observed in the trend of wind speed (Figure 4.1A), cannot support the observed general warming trend in this region. Similarly, the E-P (Figure 4.1 E and F), which showed an increasing trend would also not help in explaining the warming trend. The net heat flux (Figure 4.1C and D), however, could explain the observed warming trend in the south-western Bay of Bengal as it showed a positive trend indicating input of heat into the ocean.

4.3 Factors controlling the SST variability during the sunspot number cycle period from 1975 to 1985

In this sunspot number cycle based on the slopes of wind speed, net heat flux and the E-P and their correlation with SST (Figure 4.3) eight regions were identified (Figure 4.4) which could explain the distribution of the SST linear trendline slope.

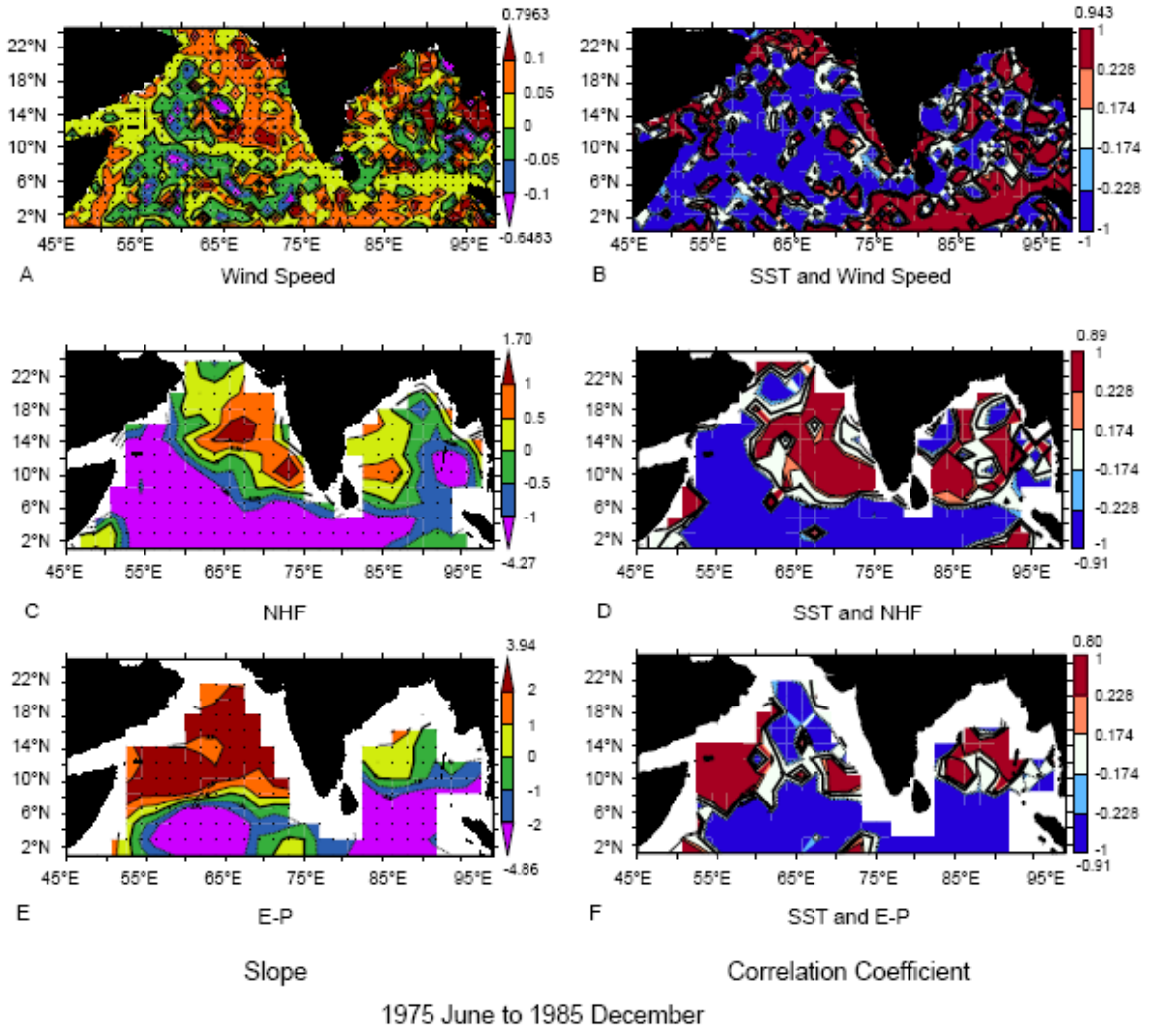

Figure 4.3 60-month running mean slopes (left) of wind speed ((m/s)/year), net heat flux ((W/m^2)/year) and E-P ((cm/year)/year) and their correlation coefficients (right) with SST, in the period from 1975 June to 1985 December. Slope regions above 95 % significance levels are shaded. 2-tailed t-statistic ≥ |1.979|, N=127. Regions above 95 % significance levels of correlation coefficients are shaded. r = +/- 0.174, significance level= 95 %; r = +/- 0.228, significance level= 99 %, N= 127. N is the number of points.

These 8 regions are equatorial Arabian Sea, equatorial Bay of Bengal, north-eastern Arabian Sea, south-western Bay of Bengal, south-eastern Arabian Sea, north-western Bay of Bengal, western Arabian Sea and off Somali coast which are represented approximately by solid circles/ellipses in Figure 4.4.

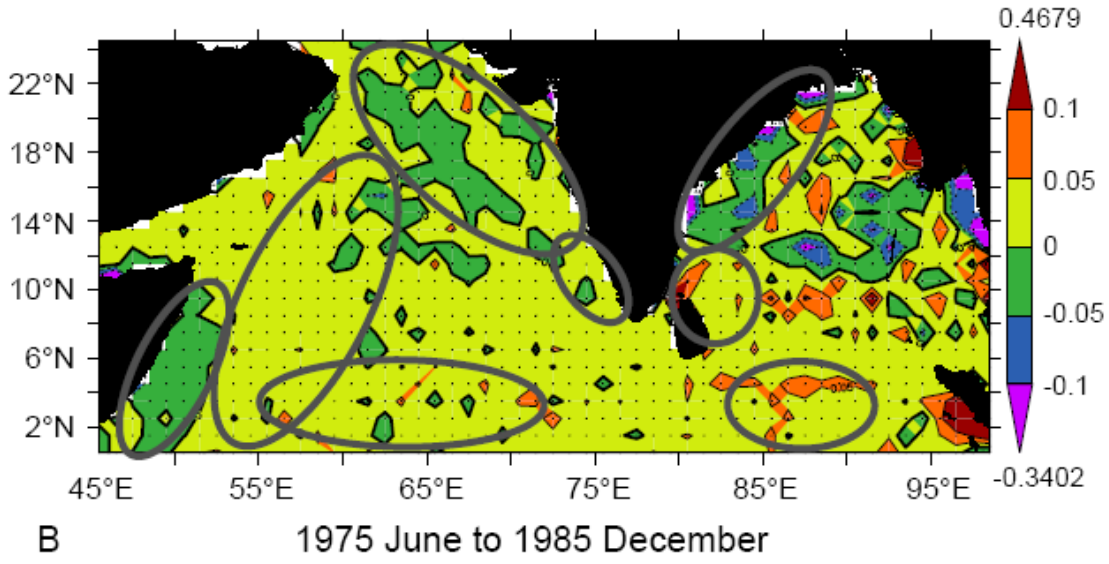

Figure 4.4 Map showing the regions of study of the SST variability demarcated by solid circles/ellipses in the sunspot number cycle period from 1975 June to 1985 December. Shading is for the slope of the 60-month running mean SST trend line.

4.3.1 Equatorial Arabian Sea and Equatorial Bay of Bengal

In the sunspot number cycle period from 1975 to 1985, the regions of the equatorial Arabian Sea and the equatorial Bay of Bengal showed increasing trend in the SSTs (Figure 4.4). The wind speed showed a decreasing trend in the equatorial Arabian Sea with negative correlation, while it showed an increasing trend with positive correlation in the equatorial Bay of Bengal (Figure 4.3A and B). The net heat flux in both the regions showed a decreasing trend with negative correlation (Figure 4.3C and D), which were unfavourable for the observed increasing trend in the SST. The E-P showed a decreasing trend in both regions with a negative correlation (Figure 4.3E and F) implying a decreased evaporation or

increased precipitation which is favourable to the observed increasing trend of SST. In the equatorial Arabian Sea both decreasing wind speed and decreasing E-P leads to the increase in the SST trend. On the other hand, in the equatorial Bay of Bengal it is only the reduced E-P that would cause the observed increase in the SST trend.

4.3.2 South-Eastern Arabian Sea and South-Western Bay of Bengal

In the sunspot number cycle period from 1975 to 1985 the south-eastern Arabian Sea and the south-western Bay of Bengal showed increasing trends in the SSTs (Figure 4.4). The wind speed in both the regions showed increasing trend with negative correlation (Figure 4.3 A and B). This condition is not favourable for the observed increase in the SST. The net heat flux also showed an increasing trend into the ocean but with a positive correlation (Figure 4.3 C and D), which were favourable for the observed increasing SST trend. There was a large gap in the E-P data in the south-eastern Arabian Sea, but in the south-western Bay of Bengal it showed both negative (southern part of the region) and positive (northern part of the region) slopes with correlation also showing negative (southern part of the region) and positive (northern part of the region) values. In the southern part of the south-western Bay of Bengal the decreasing E-P trend favours the increasing SST trend. Thus, the increasing net heat flux into the ocean is the only forcing that favoured the increased SST trend in the south-eastern Arabian Sea, while in the south-western Bay of Bengal the net heat flux and to some extent the E-P contributed towards the observed increasing SST trend.

4.3.3 North-Eastern Arabian Sea and North-Western Bay of Bengal

In the sunspot number cycle period from 1975 to 1985, the north-eastern Arabian Sea and north-western Bay of Bengal showed a predominant decreasing trend in SSTs (Figure 4.4). The wind speed showed an increasing trend with negative correlation with SST (Figure 4.3 A and B). This condition is favourable for the observed SST trend. In contrast, the net heat flux in both the regions showed an increasing trend, but the correlation with SST was positive in the north-eastern Arabian Sea and negative in the north-western Bay of Bengal (Figure 4.3 C and D). The slopes of the heat flux trend were not favourable for the SST decreasing trend in both the regions. The increased E-P trend along with negative correlation with SST (Figure 4.3 E and F) in the north-eastern Arabian Sea implies that the increased evaporation supports decreasing trend in SST. In the north-western Bay of Bengal, due to large data gap it was not possible to infer any relation meaningfully. Thus, in the north eastern Arabian Sea increased wind speed along with increased E-P lead to the decreasing trend in SST, while in the north-western Bay of Bengal increasing SST trend was driven by winds alone.

4.3.4 Western Arabian Sea

The western Arabian Sea showed a predominantly increasing trend in SSTs (Figure 4.4). The wind speed showed a decreasing trend with negative correlation with SST (Figure 4.3 A and B), which supports the observed SST trend in this region. The net heat flux showed an increasing trend in the northern part of the western Arabian Sea, while in the southern part the trend was negative (Figure 4.3C). The correlation of net heat flux with SST was, in general, negative (Figure 4.3D). Since the correlation was negative, the net heat flux was not responsible for the observed warming in the western Arabian Sea. Similarly, the E-P showed

an increasing trend in the northern part, while it was decreasing in the southern part (Figure 4.3 E). The correlation, however, was negative throughout the region. Hence, in the southern part E-P was favourable for the warming of SST. Thus, in the western Arabian Sea, wind speed and to some extent the E-P supported the observed warming trend in SST.

4.3.5 Off Somali Coast

The SSTs off Somali coast showed a decreasing trend (Figure 4.4). The wind speed showed a predominantly increasing trend with negative correlation (Figure 4.3A and B), which favoured the observed decreasing SST trend. In contrast, the net heat flux which showed a decreasing trend and a negative correlation with SST (Figure 4.3 C and D), which was not favourable for the observed SST trend. The large data gaps in E-P inhibited any meaningful inference on its role in contributing to the observed trend in SST. Thus, off Somali coast the observed decreasing trends of the SST were driven by the increasing wind speed trends.

4.4 Factors controlling the SST variability during the sunspot number cycle period from 1985 to 1995

In this sunspot number cycle based on the slopes of wind speed, net heat flux, E-P and their correlation with SST (Figure 4.5), four regions were identified (Figure 4.6) which could explain the distribution of the SST linear trendline slope.

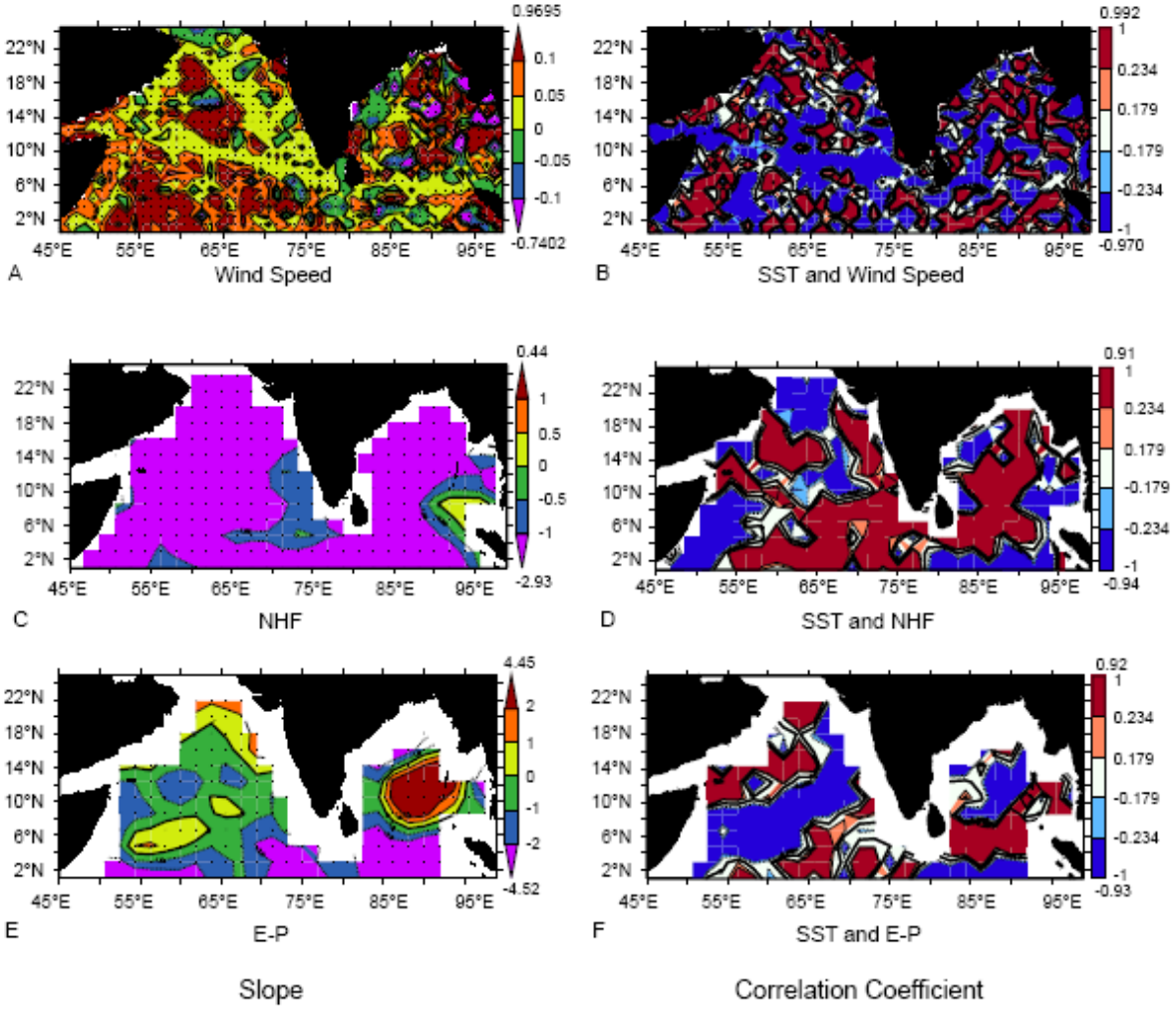

Figure 4.5 60-month running mean slopes (left) of wind speed ((m/s)/year), net heat flux ((W/m^2)/year) and E-P ((cm/year)/year) and their correlation coefficients (right) with SST, in the period from 1985 December to 1995 November. Slope regions above 95 % significance levels are shaded. 2-tailed t-statistic $\geq$ |1.980|, N=120. Regions above 95 % significance levels of correlation coefficients are shaded. r = +/- 0.179, significance level= 95 %; r = +/- 0.234, significance level= 99 %, N= 120. N is the number of points.

These four regions are central Bay of Bengal, equatorial Arabian Sea, eastern Arabian Sea and north-western Bay of Bengal which are represented approximately by solid circles/ellipses in Figure 4.6

.

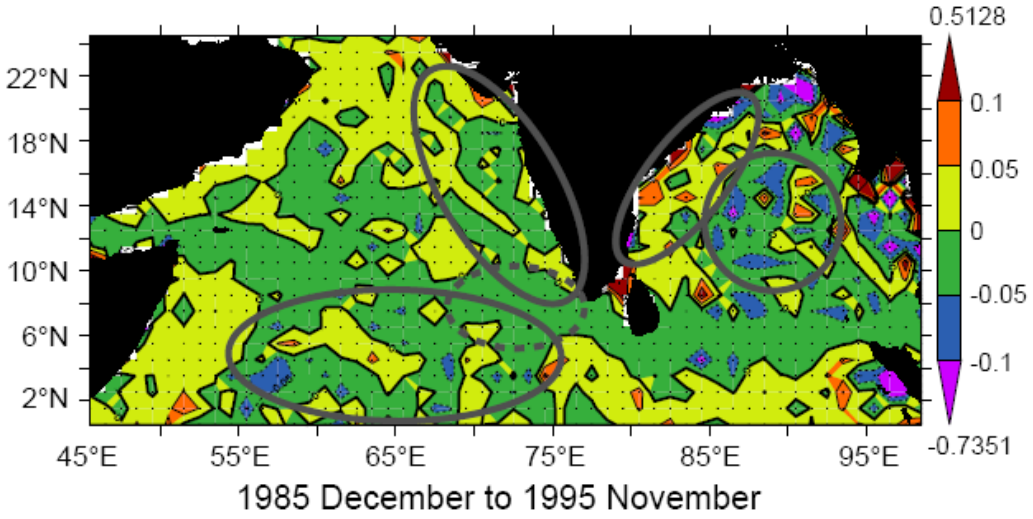

Figure 4.6 Map showing the regions of study of the SST variability demarcated by solid circles/ellipses in the sunspot number cycle period from 1985 December to 1995 November. Shading is for the slope of the 60-month running mean SST trend line.

4.4.1 Central Bay of Bengal

In the central Bay of Bengal, there was a decreasing trend in the SST (Figure 4.6). The predominantly increasing trend of the wind speed and its generally negative correlation with SST was favourable to the observed decreasing SST trend (Figure 4.5 A and B). The net heat flux showed a decreasing trend with positive correlation coefficients with SST (Figure 4.5 C and D). This was also favourable for a decreasing SST trend which was observed. The E-P also showed an increasing trend with negative correlation with SST (Figure 4.5 E and F)., which also was favourable for decreasing trend in SST. Thus, in the central Arabian Sea, the decreasing trends in the SST were driven by the combination of increasing wind speed and E-P trends and decreasing NHF trends.

4.4.2 Equatorial Arabian Sea and Eastern Arabian Sea

In the sunspot number cycle period from 1985 to 1995, there was a decreasing trend of SST in the equatorial Arabian Sea and also in the eastern Arabian Sea (Figure 4.6). The increasing trend in wind speed and its predominantly negative correlation coefficient with the SST (Figure 4.5 A and B) was favourable for the observed decreasing trend in SST, in both the regions. The net heat flux showed a decreasing trend with positive correlation coefficients with SST (Figure 4.5 C and D). This was also favourable for the observed predominantly decreasing SST trends in the equatorial Arabian Sea and in the eastern Arabian Sea. The E-P shows a decreasing trend in the equatorial Arabian Sea and in the eastern Arabian Sea. The correlation coefficients between E-P and SST in the equatorial Arabian Sea was negative and so also for the region of eastern Arabian Sea (Figure 4.5 E and F). Note that the E-P has large data gaps in the eastern Arabian Sea regions, which has to be dealt with caution while interpreting the results. However, the decrease in the E-P trends discernible from figure was not favourable to explain the observed decreasing SST trends. Thus, in the equatorial Arabian Sea and in the eastern Arabian Sea, the decreasing trends in the SST were due to increasing trends in the wind speeds and decreasing trend in the net heat flux.

4.4.3 North-Western Bay of Bengal

In the sunspot number cycle period from 1985 to 1995, the North-west Bay of Bengal SST showed a significant increasing trend predominantly (Figure 4.6). The decreasing trend in wind speed and its negative correlation with SST in general (Figure 4.5 A and B), indicate conditions which were favourable for the warming of SST. The net heat flux showed a decreasing trend into the ocean and its correlation coefficients with SST were negative

(Figure 4.5 C and D). These conditions were not favourable for the observed warming trend. The large data gaps in E-P inhibited any meaningful inference on its role in contributing to the observed trend in SST (Figure 4.5 E and F). Thus in the waters of the north-western Bay of Bengal, the observed increasing trends of the SST were driven by the decreasing wind speed trends.

4.5 Factors controlling the SST variability during the sunspot number cycle 1995 to 2008

In this sunspot number cycle period based on the slopes of wind speed, net heat flux and the E-P and their correlation with SST (Figure 4.7), six regions were identified (Figure 4.8) which could explain the distribution of the SST linear trendline slope. These six regions are northern Arabian Sea, western Arabian Sea, eastern Arabian Sea, southern Arabian Sea, north-eastern Bay of Bengal and north-western Bay of Bengal which are represented approximately by solid ellipses in Figure 4.8.

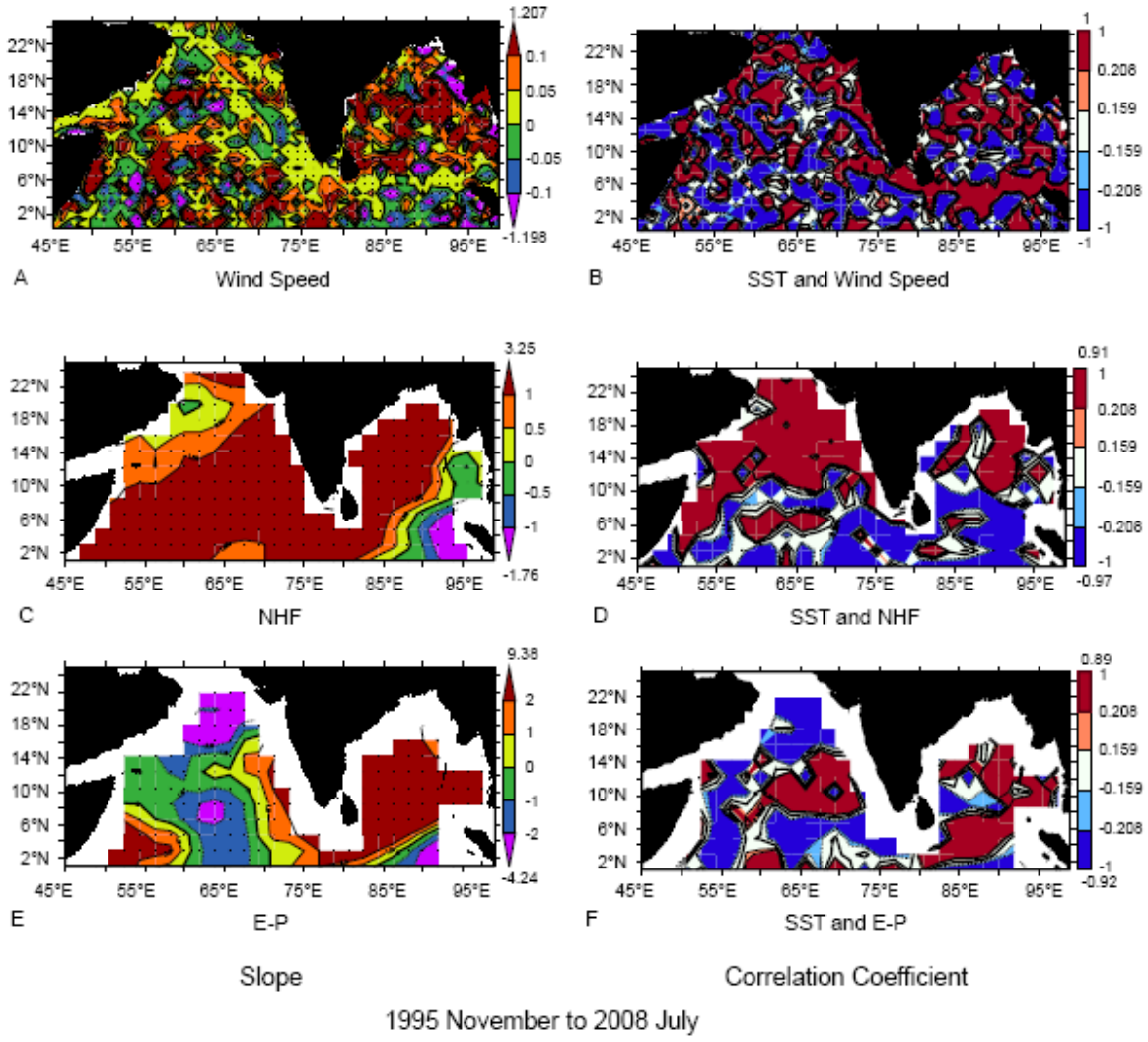

Figure 4.7 60-month running mean slopes (left) of wind speed ((m/s)/year), net heat flux ((W/m^2)/year) and E-P ((cm/year)/year) and their correlation coefficients (right) with SST, in the period from 1995 November to 2008 July. Slope regions above 95 % significance levels are shaded. 2-tailed t-statistic ≥ |1.976|, N=153. Regions above 95 % significance levels of correlation coefficients are shaded. r = +/- 0.159, significance level= 95 %; r = +/- 0.208, significance level= 99 %, N= 153. N is the number of points.

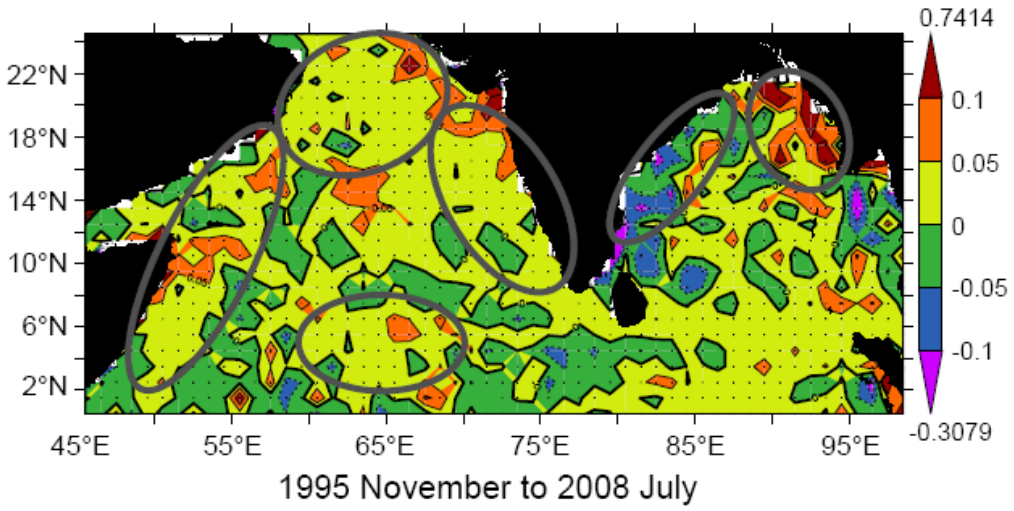

Figure 4.8 Map showing the regions of study of the SST variability demarcated by solid ellipses in the sunspot number cycle period from 1995 November to 2008 July. Shading is for the slope of the 60-month running mean SST trend line.

4.5.1 Southern Arabian Sea

In the sunspot number cycle period from 1995 to 2008, the SSTs in the southern Arabian Sea showed an increasing trend (Figure 4.8). The wind speed trends were a mixture of both positive and negative and correlation coefficients were largely negative (Figure 4.7 A and B). The net heat flux had positive trends into the ocean and positive correlation coefficients between 6 °N to 8 °N latitudes in the region considered (Figure 4.7 C and D). This was favourable for the observed SST trend. The E-P had a decreasing trend and a negative correlation coefficient with SST (Figure 4.7 E and F). This also was favourable for the increasing SST trend. Thus, in the southern Arabian Sea the decreasing trend in the E-P drives the observed increasing SST trend, besides contributions from the increasing net heat flux.

4.5.2 Northern Arabian Sea, Western Arabian Sea and Eastern Arabian Sea

The SST showed an increasing trend predominantly, in the northern, western and eastern Arabian Sea regions (Figure 4.8). The wind speed showed a predominantly increasing trend in the northern Arabian Sea and in the eastern Arabian Sea and a mixture of positive and negative correlation coefficients (Figure 4.7 A and B). This was not favourable to the generally increasing SST trends of the northern Arabian Sea and eastern Arabian Sea. However, in the western Arabian Sea the wind speed showed a decreasing trend (Figure 4.7 A) and the correlation of wind speed with SST was predominantly negative (Figure 4.7 B). This was favourable to the observed increasing SST trends in the western Arabian Sea. The net heat flux showed an increasing trend and positive correlation coefficients in all the three regions (Figure 4.7 C and D). This was favourable for the observed SST rise in the northern, western and eastern Arabian Sea. The E-P showed a decreasing trend in part of the western Arabian Sea and in the northern Arabian Sea (Figure 4.7 E). Due to large data gap in the eastern regions it is not possible to infer anything meaningful for that region. The correlation coefficients were negative in the western Arabian Sea and northern Arabian Sea (Figure 4.7 F), which points to its favourable conditions for the SST warming trend. Thus, the increasing SST trends were driven by the increasing NHF into the ocean in the western, northern and eastern Arabian Sea; decreasing trend in E-P in the western and northern Arabian Sea and decreasing wind speeds in the western Arabian Sea.

4.5.3 North-Eastern Bay of Bengal

The SST showed an increasing trend in the north-eastern Bay of Bengal (Figure 4.8). There were predominantly increasing wind speed trends in most of the region (Figure 4.7 A) and

positive correlation with SST (Figure 4.7 B), which was not congenial for the observed increasing trend in SST. The NHF showed an increasing trend into the ocean (Figure 4.7 C) and a positive correlation coefficient with SST (Figure 4.7 D). This was favourable for the observed rising trend in SST. The E-P, which had a large data gap, showed a small region with increasing trend (Figure 4.7 E) and a positive correlation coefficient with SST (Figure 4.7 F). However, this was not favourable to explain the observed increasing SST trend. Thus, in the north-eastern Arabian Sea, the increasing trend in SST was driven by the increasing NHF into the ocean.

4.5.4 North-Western Bay of Bengal

The north-western Bay of Bengal showed a decreasing trend in SST (Figure 4.8). There were some areas in the north-western Bay of Bengal, where the wind speeds showed an increasing trend and its correlation coefficients with SST was negative (Figure 4.7 A and B). In these areas the wind speed was favourable to the observed SST decreasing trend. The NHF showed an increasing trend into the ocean with regions of both positive and negative correlation coefficients (Figure 4.7 C and D). However, the trends and the negative correlation coefficients were not favourable to explain the observed decreasing SST trend. The E-P data was available only for a very small portion of the region, where E-P showed an increasing trend with positive correlation (Figure 4.7 E and F). However, this was not favourable to explain the observed SST decreasing trend. Thus, in the north-western Bay of Bengal, the decreasing trend in SST could be explained only with the help of increasing trend in wind speed.

The factors affecting the SST trends in 4 different sunspot number cycle periods and in different spatial regions within the northern Indian Ocean discussed in sections 4.2 to 4.5 are summarised in Table 4.3 below.

Table 4.3 Factors controlling the SST trend in different sunspot number cycles in the northern Indian Ocean

Period	**Region**	**SST trend**	**Factors controlling the SST trend**		
			Wind Speed	**NHF**	**E-P**
1964 to 1975	Eastern Arabian Sea	Decreasing	Yes	Yes	Yes
	Southern Bay of Bengal	Increasing	No	Yes	No
1975 to 1985	Equatorial Arabian Sea	Increasing	Yes	No	Yes
	Equatorial Bay of Bengal	Increasing	No	No	Yes
	South-eastern Arabian Sea	Increasing	No	Yes	No
	South-western Bay of Bengal	Increasing	No	Yes	Yes*
	North-eastern Arabian Sea	Decreasing	Yes	No	Yes
	North-western Bay of Bengal	Decreasing	Yes	No	No
	Western Arabian Sea	Increasing	Yes	No	Yes*
	Off Somali Coast	Decreasing	Yes	No	No
1985 to 1995	Central Bay of Bengal	Decreasing	Yes	Yes	Yes
	Equatorial Arabian Sea	Decreasing	Yes	Yes	No
	Eastern Arabian Sea	Decreasing	Yes	Yes	No
	North-western Bay of Bengal	Increasing	Yes	No	No
1995 to 2008	Southern Arabian Sea	Increasing	No	Yes*	Yes
	Northern Arabian Sea	Increasing	No	Yes	Yes
	Western Arabian Sea	Increasing	Yes	Yes	Yes

	Eastern Arabian Sea	Increasing	No	Yes	No
	North-eastern Bay of Bengal	Increasing	No	Yes	No
	North-western Bay of Bengal	Decreasing	Yes*	No	No
* symbol indicates a part of the region's SST is impacted by a factor					

4.6 Factors responsible for the disruption of the decadal cycle and changes in SST trends in the post-1995 period

In the previous chapter, while examining the basin-averaged SST variability in the Arabian Sea and the Bay of Bengal, it was noted that in both the basins the SST showed a dominant decadal cycle which was riding over an overall warming trend during the study period (Figure 3.10 and 3.11). These decadal cycles showed a disruption in mid-nineties in both the basins with different slopes during pre and post-1995 periods (Table 3.1). The Arabian Sea showed an accelerated post-1995 warming trend in comparison to pre-1995 period. In contrast, the Bay of Bengal showed a slow-down in the post-1995 warming rate in comparison to pre-1995 period. In this section the reasons for such difference were examined in the context of prevailing regional ocean-atmospheric processes. In the case of the Arabian Sea the spatial distribution of the SST trend during pre and post 1995 were examined to identify the factors responsible for the post-1995 accelerated warming, while in the case of the Bay of Bengal the basin-averaged trend in SST was analyzed to decipher the reasons for the slow-down in the post 1995 rate of warming.

4.6.1 Arabian Sea

4.6.1.1 Regions and Seasons causing the accelerated SST warming

In order to understand the reasons for accelerated warming in the Arabian Sea post-1995 period, the spatial map of the difference in SST slopes between post and pre-1995 period was prepared (Figure 4.9a). Further, the season-wise differences in slopes were given in Figure 4.9 b-e. The seasons considered are the following:

1.	Late winter	January and February	(Figure 4.9b)
2.	Spring	March to May	(Figure 4.9c)
3.	Summer	June to September	(Figure 4.9d)
4.	Fall	October and November	(Figure 4.9e)

It was evident from the Figure 4.9a that the accelerated warming over the Arabian Sea is not uniform everywhere. The highest accelerated-warming of the SST occurred along the north-eastern Arabian Sea (off the Konkan, Saurashtra, Kutch and Makran coasts), off Oman, off northern Somalia, central AS and parts of the southern AS.

The highest seasonal accelerated-warming occurred in the late-winter in the north-eastern Arabian Sea (Figure 4.9b), in spring-season in the central and north-eastern Arabian Sea (Figure 4.9c), in summer along the western-boundary of the Arabian Sea (Figure 4.9d) and in fall in the central Arabian Sea (Figure 4.9e).

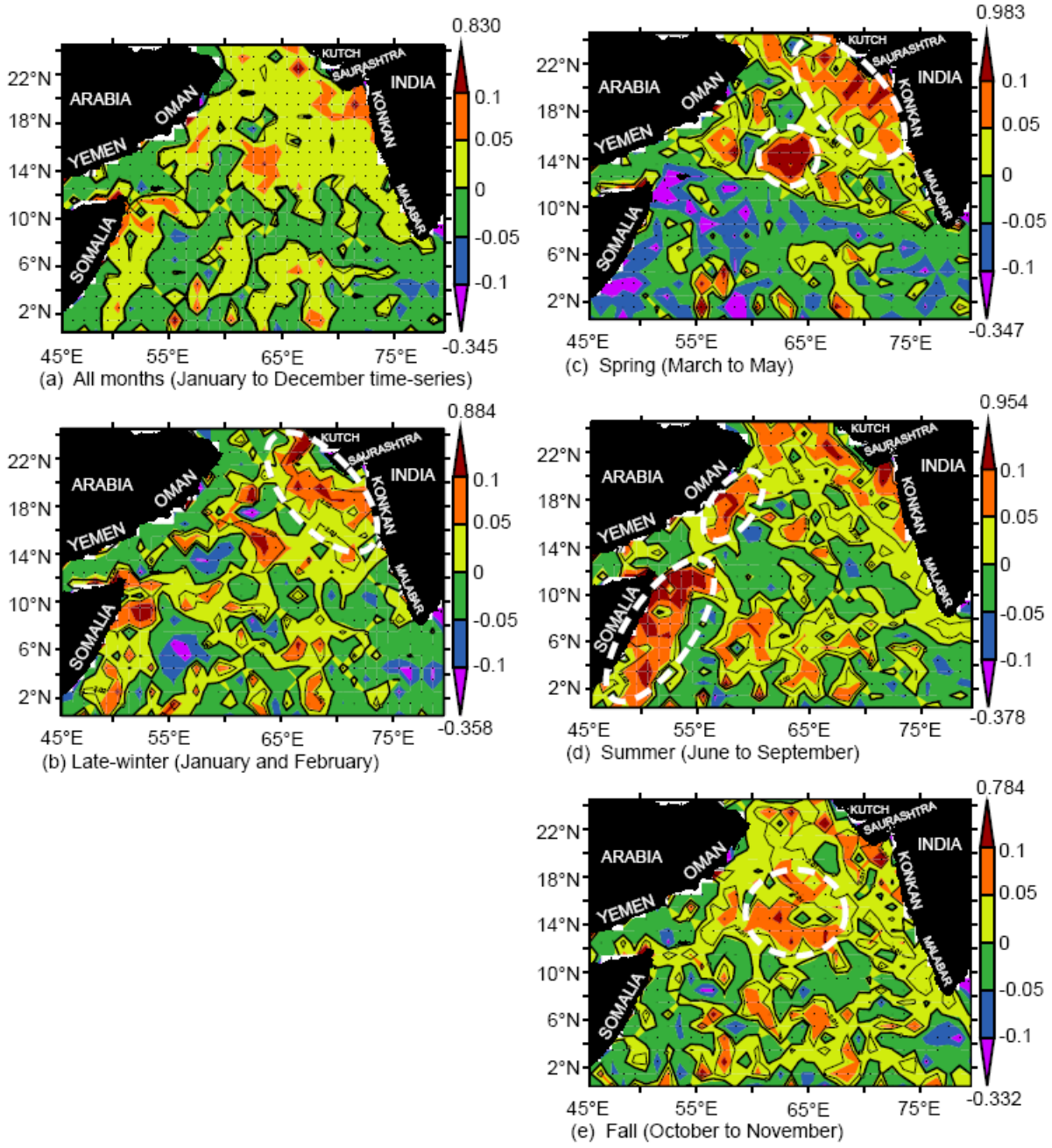

Figure 4.9 Arabian Sea slope difference (°C/year) between the periods from 1995 November to 2011 December and 1960 January to 1995 November, of SST 60-month running mean (Panel a) and of SST 5-year running means in late-winter (January to February) (Panel b), spring season (March to May) (Panel c), summer (June to September) (Panel d) and fall season (October to November) (Panel e). The regions are shaded (dotted) if significant at the 95 % level. The regions are shaded above and contoured at |t-value| > 1.964, number of points (N) = 560 (Panel a); |t-value| > 2.015, N = 44 (Figs. 2b-2d) and |t-value| > 2.014, N= 45 (Panel e). The approximate regions of highest SST warming are indicated by a dashed ellipse/ circle [*D'Mello and Prasanna Kumar*, 2017].

In order to understand the causative factors, various parameters' slopes and their correlation with SST were analysed in each season, in the post-1995 period. This allowed the identification of the parameters which are favourable for the accelerated rise of SST, in the season and region considered.

4.6.1.2 Late-winter season in the North-Eastern Arabian Sea

In the late-winter season, the north-eastern Arabian Sea showed an accelerated rise. The correlation of NHF with SST was significant and positive in the north-eastern Arabian Sea (Figure 4.10a). The NHF trends were also positive into the ocean (Figure 4.10b). These conditions were favourable for the rise of SST. The correlation coefficient of E-P with SST was also negative and significant in the north-east Arabian Sea (Figure 4.10c). The slopes of E-P showed a significant decreasing trend (Figure 4.10d). This was also favourable for the SST increasing trend in this region.

The Latent Heat Flux (LHF) was then analysed. The LHF and SST correlation coefficient was significant and positive in the north-east Arabian Sea (Figure 4.10e). The LHF into the ocean also showed a significant increasing trend (Figure 4.10f). This condition was also favourable for the increased SST. The correlation coefficient of evaporation with SST was negative and significant in the north-east Arabian Sea (Figure 4.10g). The slopes of evaporation showed a significant decreasing trend (Figure 4.10h). This was also favourable for the SST increasing trend in the north-east Arabian Sea region.

The correlation coefficient between specific humidity and SST was positive in the north-east Arabian Sea (Figure 4.10i). The specific humidity showed an increasing trend (Figure 4.10j). The accelerated warming, in the post-1995 period, in the north-eastern Arabian Sea in late-

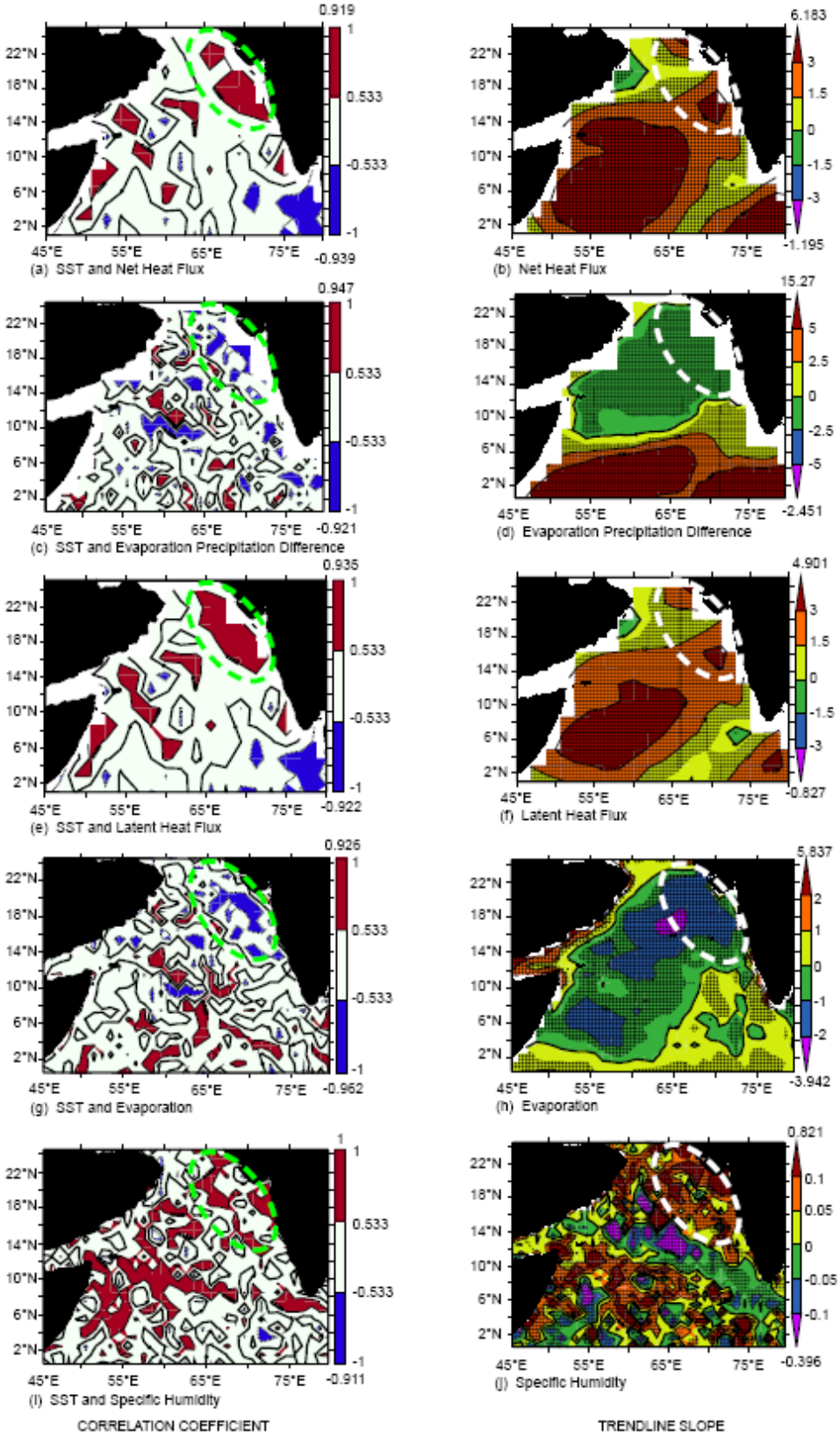

Figure 4.10 Arabian Sea late-winter season (January to February) averaged, correlation coefficients of SST with net heat flux (NHF) (Panel a), evaporation precipitation difference (E-P) (Panel c), latent heat flux (LHF) (Panel e), evaporation (Panel g) and specific humidity (Panel i), coloured for regions having 95 % and above significance level (r>|+/-0.5325|, N=14). Late-winter season averaged slopes of NHF ((W/m^2)/year) (Panel b), E-P ((cm/year)/year) (Panel d), LHF ((W/m^2)/year) (Panel f), evaporation ((cm/year)/year) (Panel h) and specific humidity ((g/kg)/year) (Panel j), are shaded for regions having 95 % and above significance level (2-tailed t-statistic ≥ |+/-2.18|, N=14). Both NHF and LHF are considered positive into the ocean. The approximate region of highest accelerated SST warming is indicated by a dashed ellipse [*D'Mello and Prasanna Kumar*, 2017].

winter was due to the reduced evaporation, due to an increasing trend in the specific humidity (Figure 4.10).

4.6.1.3 Spring season in the North-Eastern Arabian Sea and Central Arabian Sea

The spring season showed an accelerated rise in the north-eastern and central Arabian Sea. The correlation coefficient of E-P with SST was also negative and significant in the north-eastern and central Arabian Sea (Figure 4.11a). The slopes of E-P showed a significant decreasing trend (Figure 4.11b). This was also favourable for the SST increasing trend in the regions.

The correlation of NHF with SST was significant and positive in the north-east Arabian Sea and central Arabian Sea (Figure 4.11c). The NHF trends were also positive into the ocean (Figure 4.11d). These conditions were also favourable for the rise of SST in both the regions.

The correlation coefficient of evaporation with SST was negative and significant in the north-eastern and central Arabian Sea regions (Figure 4.11e). The slopes of evaporation showed a significant decreasing trend (Figure 4.11f). This was also favourable for the SST increasing trend in the north-eastern and central Arabian Sea regions.

The Latent Heat Flux (LHF) was then analysed. The LHF and SST correlation coefficient was significant and positive in the north-east Arabian Sea (Figure 4.12a). The LHF into the ocean also showed significant increasing trends in both the regions (Figure 4.12b). These conditions were also favourable for the increased SST.

The correlation coefficient of the wind speed and SST was significant and negative in the central Arabian Sea (Figure 4.12c). The wind speed trend was also decreasing (Figure 4.12 d), implying a favourable contribution for an increasing SST trend.

The correlation coefficient between specific humidity and SST was positive in the north-eastern and central Arabian Sea (Figure 4.12e). The specific humidity showed an increasing trend (Figure 4.12f).

The continued accelerated-warming trend in the north-eastern Arabian Sea, into spring season, was due to the reducing-trends in the latent heat flux release to the atmosphere, due to an increasing trend in specific humidity. The central Arabian Sea spring accelerated-warming, was due to reducing trends in the evaporation and the latent heat flux release to the atmosphere. Both were caused by reducing trends in wind speeds (Figures 4.11 and 4.12).

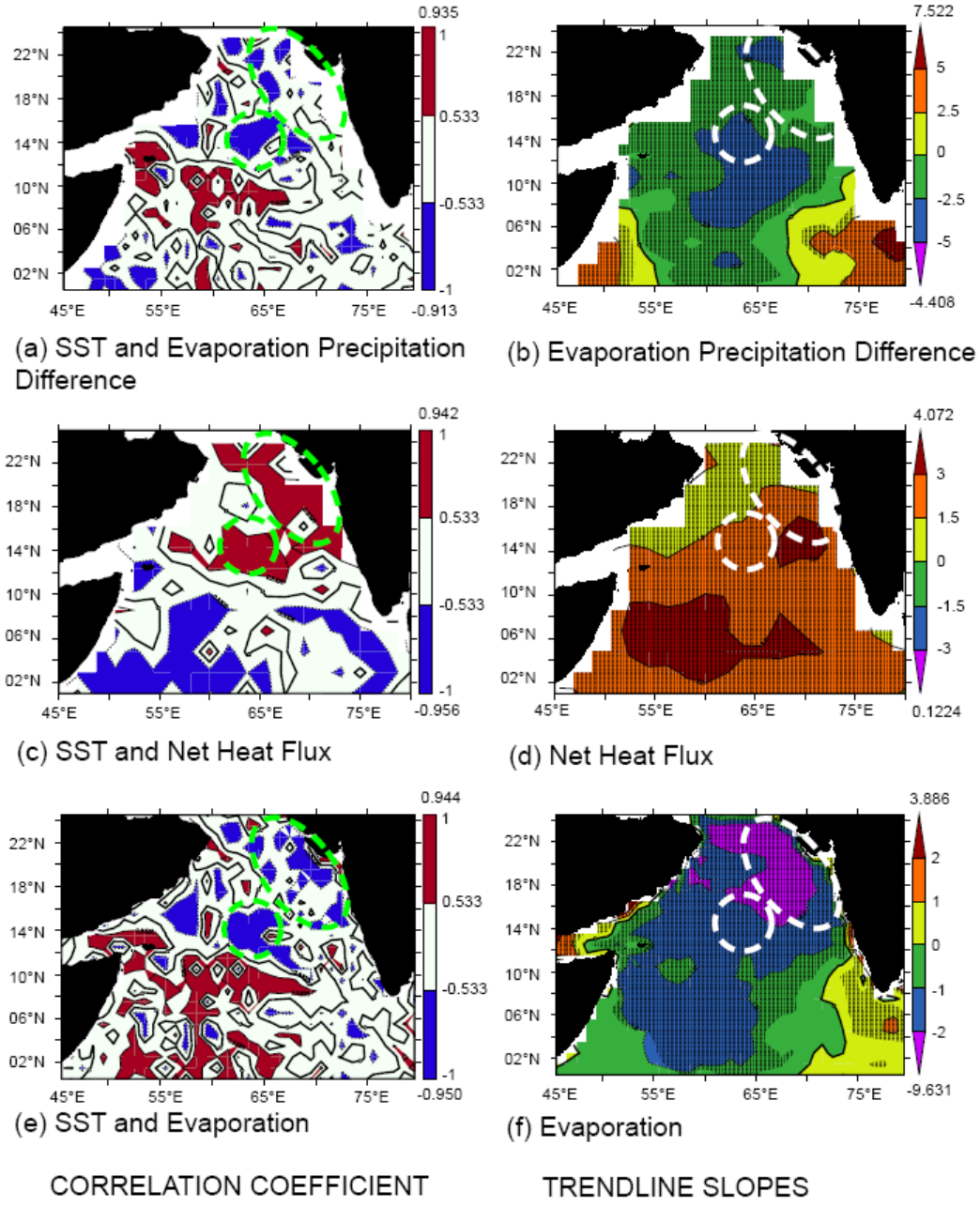

Figure 4.11 Arabian Sea spring season (March to May) averaged, correlation coefficients of SST with evaporation precipitation difference (E-P) (Panel a), net heat flux (NHF) (Panel c) and evaporation (Panel e), coloured for regions having 95 % and above significance level (r>|+/-0.5325|, N=14). Spring season averaged slopes of E-P ((cm/year)/year) (Panel b), NHF ((W/m^2)/year) (Panel d) and evaporation ((cm/year)/year) (Panel f), are shaded (cross-hatching) for regions having 95 % and above significance level (2-tailed t-statistic ≥ |+/-2.18|, N=14). NHF is considered positive into the ocean. The approximate regions of highest accelerated SST warming are indicated by a dashed ellipse/ circle [*D'Mello and Prasanna Kumar*, 2017].

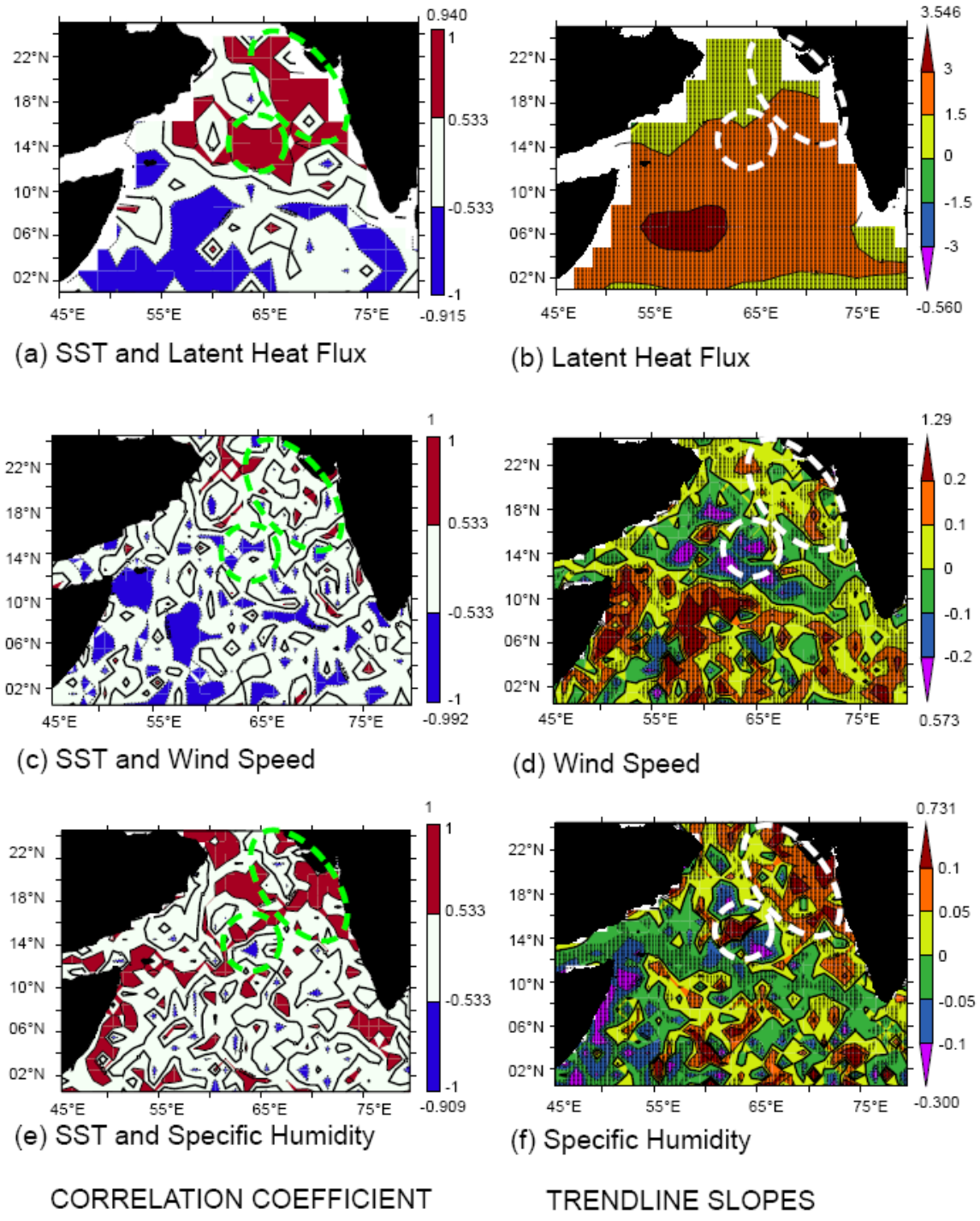

Figure 4.12 Arabian Sea spring season (March to May) averaged, correlation coefficients of SST with latent heat flux (LHF) (Panel a), wind speed (Panel c) and specific humidity (Panel e), coloured for regions having 95% and above significance level (r>|+/-0.5325|, N=14). Spring season averaged slopes of LHF ((W/m^2)/year) (Panel b), wind speed ((m/s)/year) (Panel d) and specific humidity ((g/kg)/year) (Panel f), are shaded (cross-hatching) for regions having 95 % and above significance level (2-tailed t-statistic ≥ |+/-2.18|, N=14). LHF is considered positive into the ocean. The approximate regions of highest accelerated SST warming are indicated by a dashed ellipse/ circle [*D'Mello and Prasanna Kumar*, 2017].

4.6.1.4 Summer season in the Somalia and Arabia coasts

In the summer season the regions of highest accelerated warming were located off the Arabian Peninsula and off Somalia. The spatial patterns of the isotherms (Figure 4.13a) in the pre-1995 period (black) and post-1995 period (red) showed a decrease in the area bounded by the cooler isotherms in the post-1995 period. The vertical distribution of temperature averaged over equator to 12^{o}N (Figure 4.13b) showed that the surfacing of isotherms, in the post-1995 period, were more towards the west, indicating a lesser extend of upwelling. The wind speed showed a decreasing trend and had a significant negative correlation with SST (Figure 4.14a) off Somalia (Figure 4.14b), indicating that these factors were favouring a reduction in upwelling.

The correlation coefficient between wind speed and SST was significantly negative off the Arabian Peninsula as well (Figure 4.14a). A reducing trend in wind speed was also seen here (Figure 4.14b). Besides this the E-P and evaporation also showed significant negative correlation coefficients with SST (Figure 4.14 c and e) and a decreasing trend, off the Arabian Peninsula (Figure 4.14 d and f). Thus, the reducing wind speed was favourable for a reduction in evaporation, which in turn increased the observed SST warming.

In the summer season, the reducing trend in the wind-speed caused lesser upwelling along the Somali coast (Figure 4.13), in contrast along the Arabia coast the reducing wind speed trend resulted in a reduction in the evaporation (Figure 4.14), which lead to accelerated warming of the SSTs, in these regions.

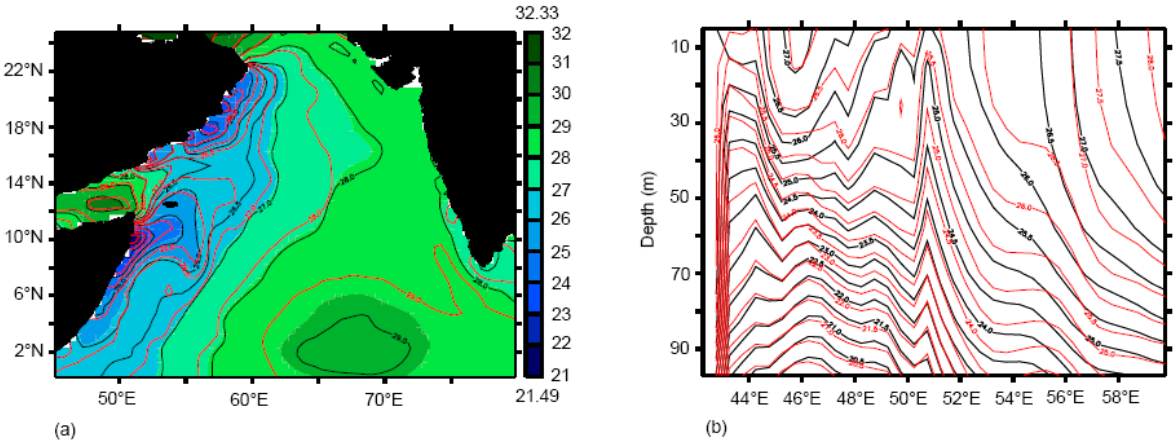

Figure 4.13 Arabian Sea averaged June to September, Simple Ocean Data Assimilation (SODA): a) surface temperature (°C), at 5 m depth, shaded in the period averaged from 1960 January to 2011 December, contoured in the period from 1960 January to 1995 November (black) and from 1995 November to 2011 December (red); and b) temperature (°C) section up to 100 m depth, averaged off the Somali coast (Eq. to 12 °N) in the period from 1960 January to 1995 November (black) and 1995 November to 2011 December (red) [*D'Mello and Prasanna Kumar*, 2017].

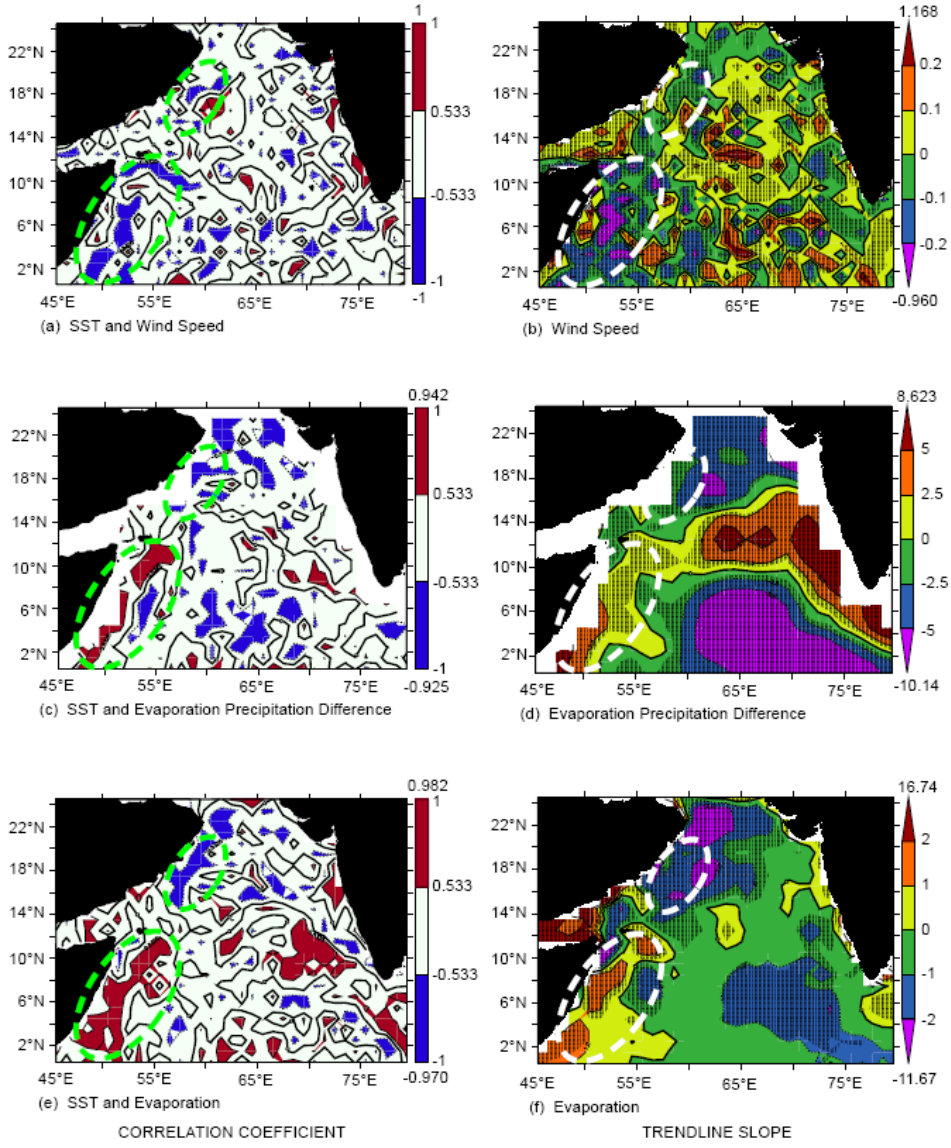

Figure 4.14 Arabian Sea summer season (June to September) averaged, correlation coefficients of SST with wind speed (Panel a), evaporation precipitation difference (E-P) (Panel c) and evaporation (Panel e), coloured for regions having 95 % and above significance level (r>|+/-0.5325|, N=14). Summer season averaged slopes of wind speed ((m/s)/year) (Panel b), E-P ((cm/year)/year) (Panel d) and evaporation ((cm/year)/year) (Panel f) are shaded (cross-hatching) for regions having 95 % and above significance level (2-tailed t-statistic ≥ |+/-2.18|, N=14|). The approximate regions of highest accelerated SST warming are indicated by dashed ellipses [*D'Mello and Prasanna Kumar*, 2017].

4.6.1.5 Fall season in the Central Arabian Sea

The fall season showed an accelerated rise in the central Arabian Sea. The correlation of NHF with SST was significant and positive in the central Arabian Sea (Figure 4.15a). The NHF trends were also positive into the ocean (Figure 4.15b). These conditions were favourable for the rise of SST in the region.

The correlation coefficient of E-P with SST was negative and significant in the central Arabian Sea (Figure 4.15c). The slopes of E-P showed a significant decreasing trend (Figure 4.15d). This was also favourable for the SST increasing trend in the region.

The Latent Heat Flux (LHF) was then analysed. The LHF and SST correlation coefficient was significant and positive in the central Arabian Sea (Figure 4.15e). The LHF into the ocean also showed significant increasing trends in the central Arabian Sea (Figure 4.15f). This condition was also favourable for the increased SST.

The correlation coefficient between specific humidity and SST was positive in central Arabian Sea (Figure 4.16a). The specific humidity showed an increasing trend in the upper part of the region shown (Figure 4.16b).

The Longwave Radiation (LWR) and SST correlation coefficient was significant and positive in the central Arabian Sea (Figure 4.16c). The LWR into the ocean also showed significant increasing trends in the central Arabian Sea (Figure 4.16d), indicating a favourable condition for the increased SST in the central Arabian Sea.

The correlation coefficient of evaporation with SST was negative and significant in the central Arabian Sea regions (Figure 4.16e). The slopes of evaporation showed a significant decreasing trend (Figure 4.16f). This was also favourable for the SST increasing trend in the central Arabian Sea region.

Thus, in fall, the accelerated warming of SST in the central Arabian Sea ws due to the increasing trend of net heat flux into the ocean, due to reducing trends in the latent heat flux (Figure 4.15) and longwave radiation release to the atmosphere. The reducing trend of evaporation also contributes to the accelerated SST warming, in some parts of the central Arabian Sea (Figure 4.16) [*D'Mello and Prasanna Kumar,* 2017].

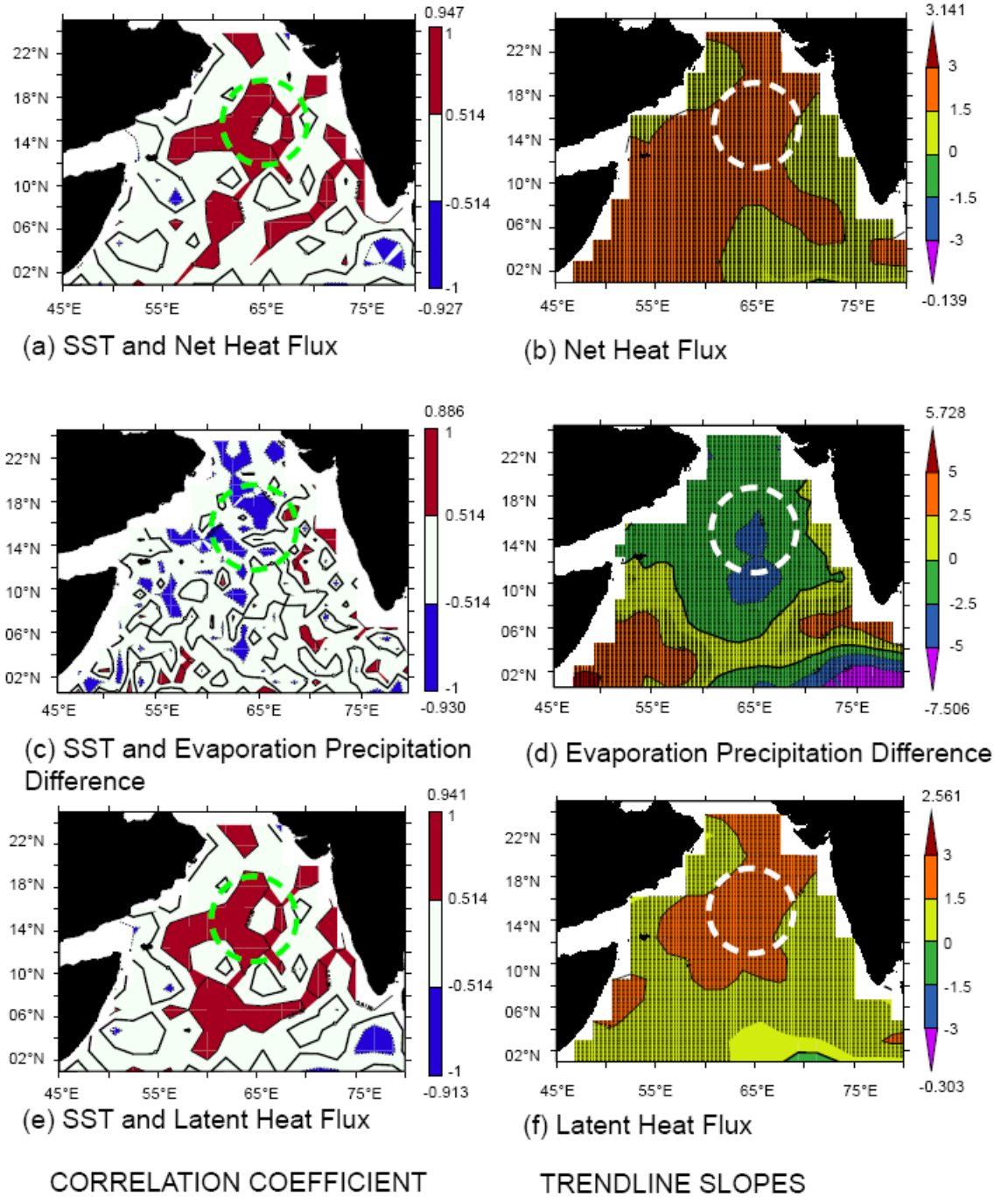

Figure 4.15 Arabian Sea fall season (October to November) averaged, correlation coefficients of SST with net heat flux (NHF) (Panel a), evaporation precipitation difference (E-P) (Panel c) and latent heat flux (LHF) (Panel e), coloured for regions having 95% and above significance level ($r>|+/-0.514|$, N=15). Spring season averaged slopes of NHF ((W/m^2)/year) (Panel b), E-P ((cm/year)/year) (Panel d) and LHF ((W/m^2)/year) (Panel f), are shaded (cross-hatching) for regions having 95 % and above significance level (2-tailed t-statistic $\geq |+/-2.160|$, N=15). NHF and LHF are considered positive into the ocean. The approximate region of highest accelerated SST warming is indicated by a dashed circle [*D'Mello and Prasanna Kumar,* 2017].

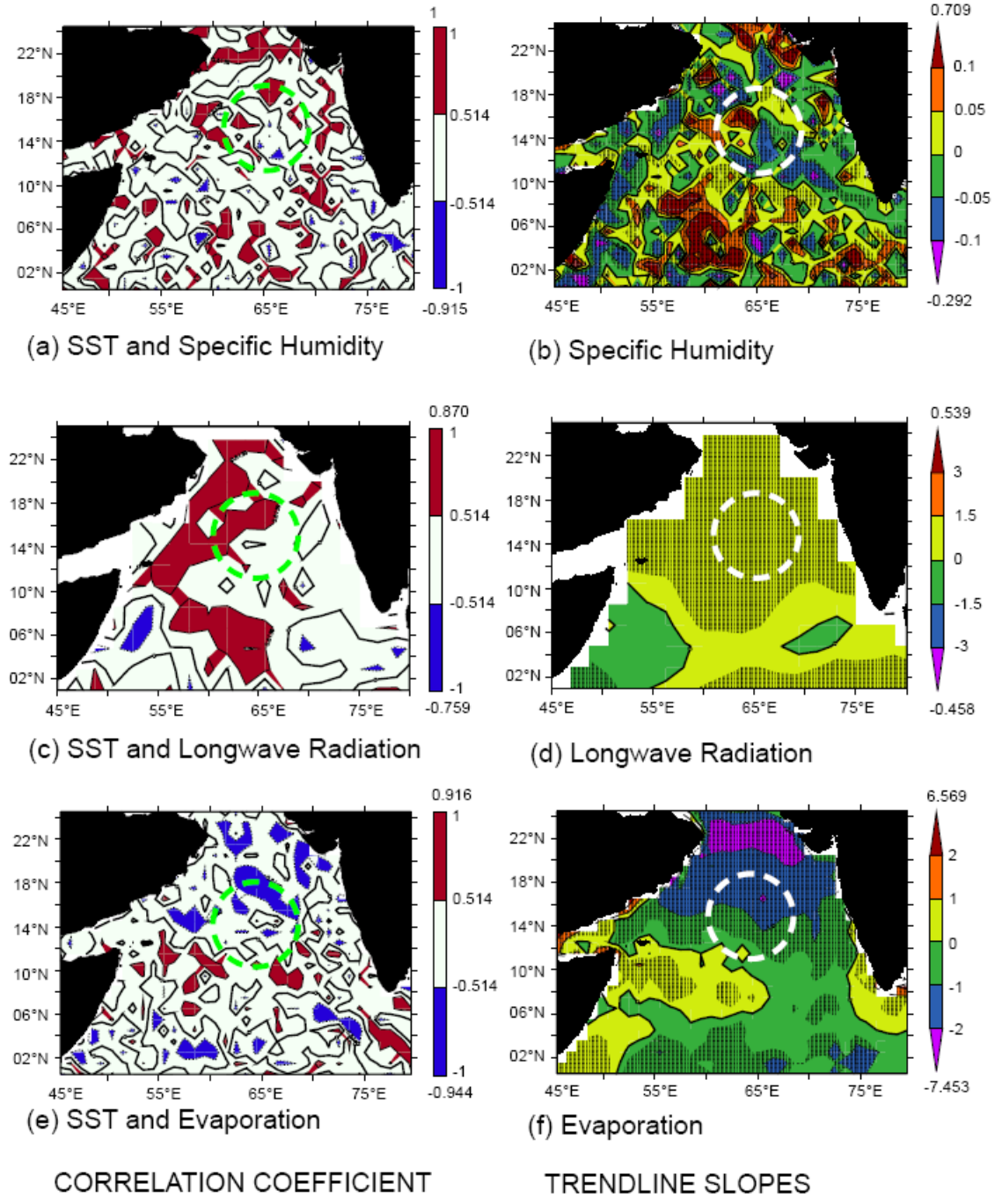

Figure 4.16 Arabian Sea fall season (October to November) averaged, correlation coefficients of SST with specific humidity (Panel a), longwave radiation (LWR) (Panel c) and evaporation (Panel e), coloured for regions having 95% and above significance level (r>|+/-0.514|, N=15). Spring season averaged slopes of specific humidity ((g/kg)/year) (Panel b), LWR ((W/m^2)/year) (Panel d) and evaporation ((cm/year)/year) (Panel f), are shaded (cross-hatching) for regions having 95 % and above significance level (2-tailed t-statistic ≥ |+/-2.160|, N=15). LWR is considered positive into the ocean. The approximate region of highest accelerated SST warming is indicated by a dashed circle [*D'Mello and Prasanna Kumar*, 2017].

4.6.2 Bay of Bengal

4.6.2.1 Trends of SST and number of depressions, cyclones and severe cyclones

Recall from the previous chapter that the 60-month running mean SST in the Bay of Bengal showed a decadal cyclicity in the period from 1960 January to 1995 November, riding over a warming trend (see Figure 3.11). The pre-1995 SST trendline slope of 0.015°C/year (R^2=0.79) showed a reduction in the post-1995 period to 0.008°C/year (R^2=0.35), indicating the slowdown in the SST rise (Table 3.1).

The monotonic increase in the carbon dioxide concentration during the study period would support the accelerated warming in the Bay of Bengal even during post-1995 period, which was not the case. A reduction in the rate of warming can be brought about by any process that would cool the upper ocean by supplying the subsurface cool waters. This could be accomplished by the process of either upwelling or tropical cyclones. Since Bay of Bengal is not known to have strong upwelling region, but known for the occurrence depressions and tropical cyclones every year, the number of depressions, cyclones and severe cyclones (DCS) were examined during the study period and presented in Figure 4.17.

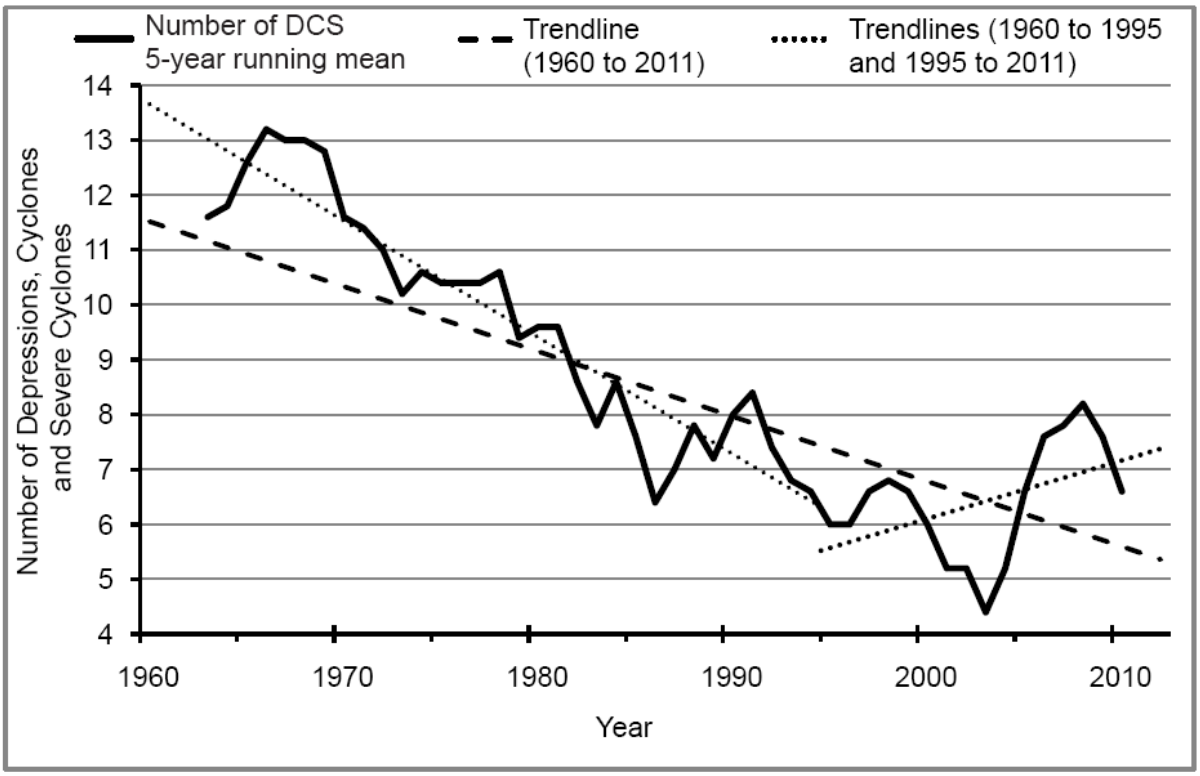

Figure 4.17 Five-year running mean of the total number of DCS in the Bay of Bengal (Eq. to 25 °N, 80 °E to 99 °E) (thick line, black) for the period from 1960 to 2011. Trendlines for the entire period of study (dashed line, black) and in the pre-1995 and post-1995 periods (dotted lines, black) are also shown [*D'Mello and Prasanna Kumar,* 2016].

The number of depressions, cyclones and severe cyclones showed a decline during pre-1995 and an increase in post-1995 period. In order to further understand the factors responsible for the slow-down in warming a partial correlation was carried out for all the parameters and provided in Table 4.4.

Table 4.4. Bay of Bengal (BoB) partial correlation coefficients (*r*) and significance levels, between the 60-month running mean of SST and 60-month running mean of the international sunspot number, 60-month running mean of the global CO_2 concentration and 60-month running mean of the BoB number of DCS, in different periods [*D'Mello and Prasanna Kumar*, 2016].

Partial correlation	**Period**	**Sunspot number**		**CO_2 concentration**		**Number of DCS**	
		r	Significance level (%)	r	Significance level (%)	r	Significance level (%)
SST	1960-2011	**0.74**	**> 99.99**	**0.88**	**> 99.99**	**-0.18**	**> 99.99**
	1960-1995	**0.76**	**> 99.99**	**0.47**	**> 99.99**	**-0.26**	**> 99.99**
	1995-2011	0.2	99.03	**0.82**	**> 99.99**	**-0.43**	**> 99.99**
Both partial correlation and significance level values are in bold face, when significance level is greater than 99.99%							

The partial correlation between sunspot number and SST reduces from 0.76 (significance level > 99.99%) in the pre-1995 period to 0.2 (significance level= 99.03%) in the post-1995 period. This indicates the weakening of the SST link with sunspot number in the post-1995 period. This weakening link causes the disruption of the SST decadal cycle after-1995.

In contrast, the partial correlation coefficient between the SST and the CO_2 concentration increases in the post-1995 period. The correlation coefficient increases from 0.47 (significance level> 99.99%) in the pre-1995 period to 0.82 (significance level> 99.99%) in the post-1995 period. Similarly, the partial correlation coefficient between the SST and the DCS increases from -0.26 (significance level> 99.99%) in the pre-1995 period to -0.43

(significance level> 99.99%), in the post-1995 period. This shows the link between SST and DCS in the post-1995 period is stronger.

4.6.2.2 Price-Weller-Pinkel Model Simulation

The cyclonic systems such as depression, cyclone and severe cyclones are expected to cool the surface waters through mechanical mixing with the generally cooler sub-surface waters. In order to examine this cooling, a Price-Weller-Pinkel model was used. As mentioned earlier in chapter 2, the PWP model is a mixed-layer model, similar to a dynamic instability model of Price et al. (1978). The model takes into account mixing processes namely (1) free convection arising due to surface heat loss, (2) mixed-layer entrainment by relaxation and (3) shear flow instability driven mixing. Generally, mixing due to free convection in the BoB is very shallow and mostly confined to the upper few tens of centimetres of the water column. In contrast, the last two are the dominant processes that determine the depth of the mixed-layer and are related to momentum flux by the wind through the Richardson number. Since the vertical mixing of the water is caused by changes in the density due to the changes in the net heat and fresh water fluxes and momentum flux they were calculated from zonal and meridional wind stress components, shortwave and longwave radiations, latent and sensible heat fluxes, evaporation, precipitation and riverine discharge, riverine runoff and catchment area data [*D'Mello and Prasanna Kumar*, 2016].

The model was initialized with the climatological temperature and salinity profiles and the daily fluxes were used to force the model. The model was run for 730 days (2 years), with a time step of 86400 seconds (1 day) and with a vertical grid interval of 1 m.

The model was forced with increasing winds in a stepped manner from 10th October so as to attain peak value of 63 km/hr (run 1, Panel b in Figure 4.18) and 87 km/hr (run 2, Panel c in Figure 4.18) on 12th October and 120 km/hr (run 3, Panel d in Figure 4.18) on 13th October. The model MLDs were found to be 38 m (run 1), 44 m (run 2) and 62 m (run 3) respectively, while it was 30m when forced with actual winds of 13 km/hr (Panel a in Figure 4.18). The above shows that the increasing wind speeds associated with the cyclones increases the mixed layer depth. As the mixed layer depths and the Ekman Depths are similar (Figure 4.18), the MLD deepening which occurred with the forcing of cyclonic wind speeds, occurs through wind-mixing. The sub-surface waters are generally cooler than the surface waters. This causes a reduction of the mixed-layer temperatures and consequently the SST. A deepening trend of the mixed layer depths was seen in the post-1995 period (Figure 4.19) [*D'Mello and Prasanna Kumar,* 2016].

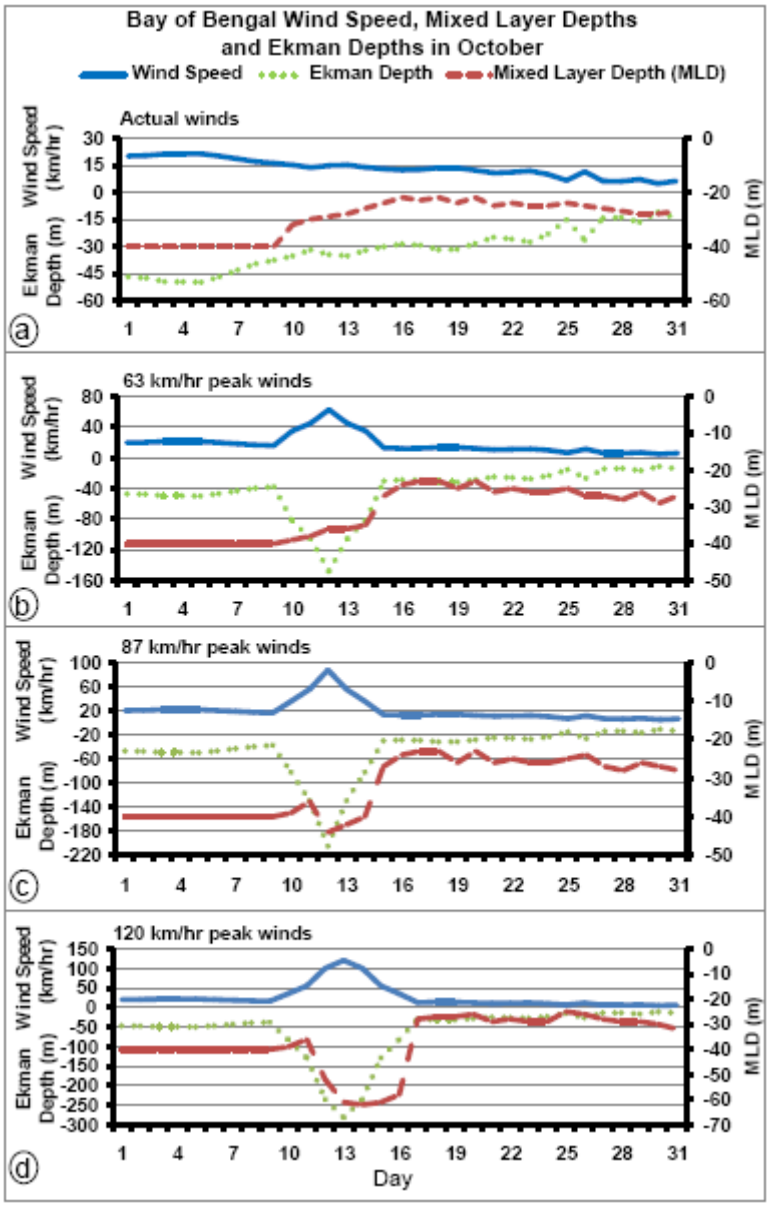

Figure 4.18 Bay of Bengal wind speeds (km/hr; blue solid line), Ekman depths (m; green dotted line) and mixed-layer depths (m, red dashed lines) for actual wind speeds (Panel a), model wind speeds peaking to 63 km/hr (Panel b), model wind speeds peaking to 87 km/hr (Panel c) and model wind speeds peaking to 120 km/hr (Panel d), all in the month of October [*D'Mello and Prasanna Kumar*, 2016].

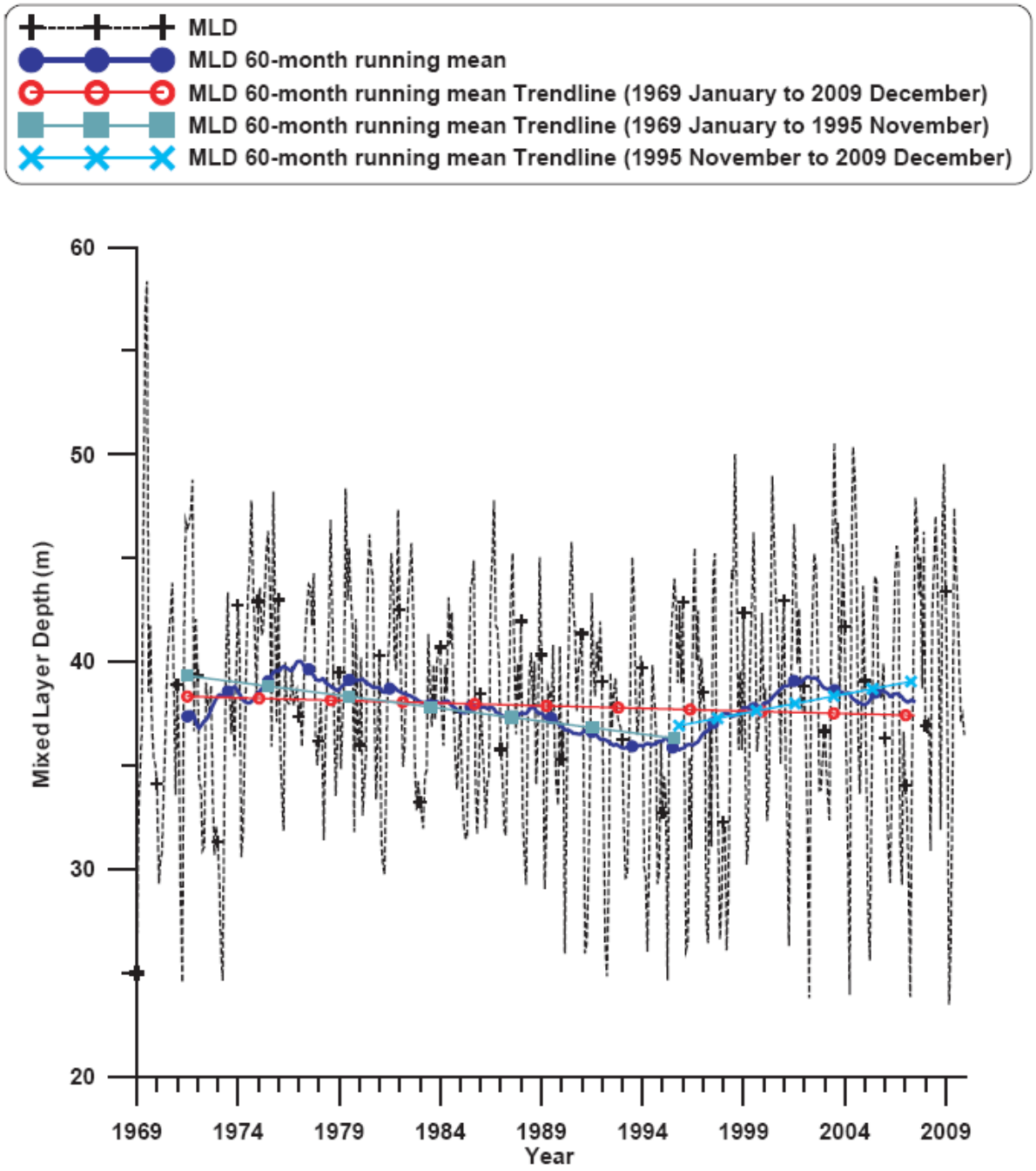

Figure 4.19 Bay of Bengal (Eq.- 25 °N, 80 °E- 99 °E) basin-averaged mixed layer depth (MLD) in metres. Data plotted is monthly (dashed line with "+" symbols), 60-month running mean (line with filled circles), and trendlines of the 60-month running mean, in the periods from 1969 January to 2009 December (line with open circles) and from 1969 January to 1995 November (line with filled squares) and from 1995 November to 2009 December (line with "X" symbols) [*D'Mello and Prasanna Kumar*, 2016].

Thus, the increase in the DCS causes the SST to fall. This is opposite to the CO_2 concentration induced SST rise. Both these processes oppose each other. As the increase in the DCS cannot completely offset the CO_2 concentration induced rise, the effect is manifested as a slowdown in the observed SST warming [*D'Mello and Prasanna Kumar*, 2016].

CHAPTER 5

RELATIONSHIP OF SST WITH ENSO AND IOD

5.1 Introduction

The El Niño-Southern Oscillation (ENSO) [*Trenberth,* 1997] and the Indian Ocean Dipole (IOD) [*Saji et al*., 1999] are the two dominant climate modes that could potentially influence the northern Indian Ocean on inter-annual time-scales. The ENSO is a tropical Pacific ocean-atmosphere coupled phenomenon, while IOD is an ENSO equivalent phenomenon in the tropical Indian Ocean. Very often ENSO and IOD was seen working in tandem and complementing each other in bringing about changes in the ocean and atmosphere in a coupled mode [*Meyers et al*., 2007]. For example, an anomalous cooling of the SST over the tropical Indian Ocean along with suppression of convection activity takes place during the positive phase of ENSO (warmer than normal SST in the eastern equatorial Pacific) and IOD (colder than normal SST in the eastern tropical Indian Ocean). Reverse is the case during a negative phase of ENSO (colder than normal SST in the eastern equatorial Pacific) and IOD (warmer than normal SST in the eastern tropical Indian Ocean). In this chapter the relationship of northern Indian Ocean SST with the ENSO and the IOD is analysed.

The ENSO strength is computed using the Oceanic Niño Index (ONI), while the IOD strength is computed using the Dipole Mode Index (DMI). The calculations of the ONI and DMI are given in detail in chapter 2. Various composite cases of the SST are analysed in periods nearly corresponding to the sunspot number cycle periods. For this analysis a 13-month running mean SST was used in order to retain the effect of ENSO and IOD, but to remove the annual variability.

5.2 ENSO and IOD indices

The ONI and the DMI were plotted in Figure 5.1 and Figure 5.2 respectively.

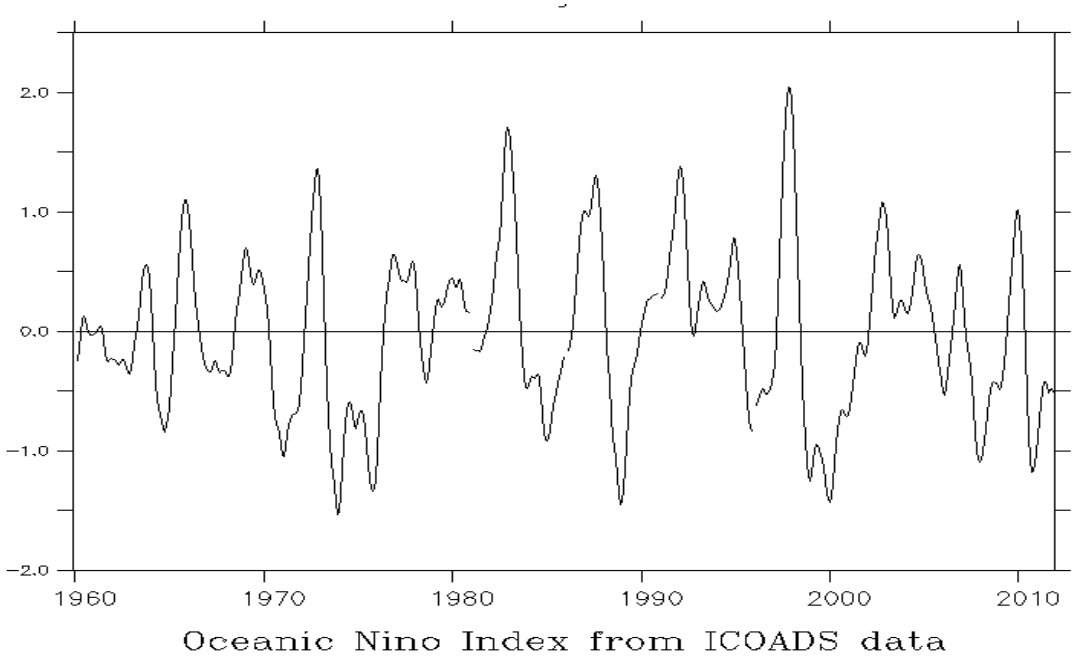

Figure 5.1 Oceanic Niño Index (ONI) for the period from 1960 to 2011 calculated using ICOADS data.

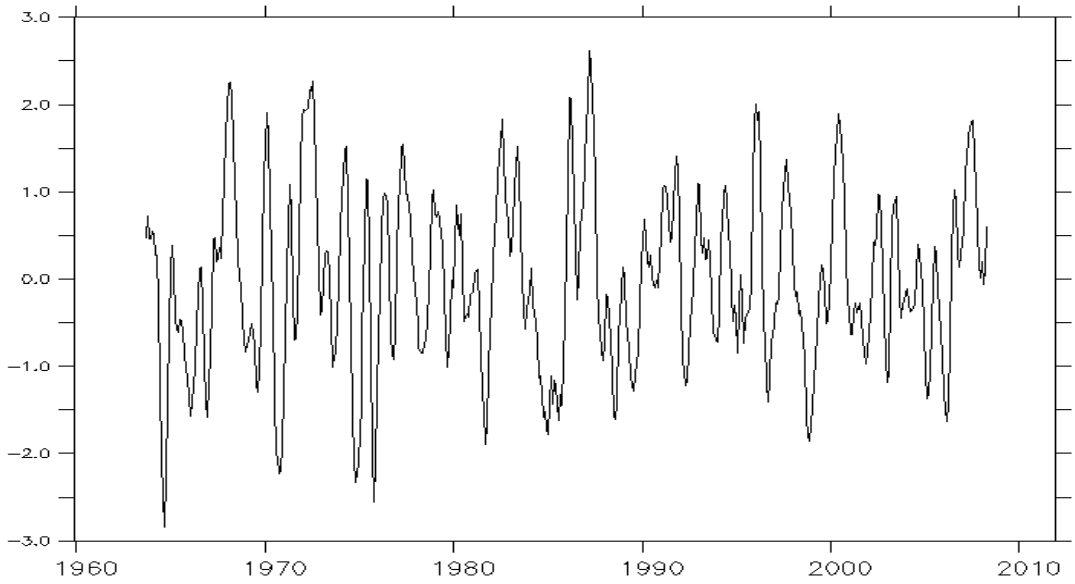

Figure 5.2 Dipole Mode Index (DMI) for the period from 1960 to 2011

ENSO was considered as an El Niño, if the ONI for 5-consecutive months is above 0.5 °C; La Niña, if lesser than 0.5 °C and neutral otherwise. The DMI is considered as IOD positive, if the value exceeds 1 standard deviation; as IOD negative, if the value is lesser than -1 standard deviation and neutral in other cases.

The combinations of ENSO and IOD strengths gave nine cases for the composites, in which one case does not occur at all. Based on the ONI, the ENSO strengths were classified as El Niño, neutral ENSO and La Niña; while based on the DMI averaged from the June to November, the IOD strengths were classified as positive IOD, neutral IOD and negative IOD. The years of each case begins in June and ends in May of the following year. The composite year list is given in Table 5.1.

Table 5.1 Years of El Niño, Neutral ENSO and La Niña with IOD positive, IOD neutral and IOD negative years, in the period from 1960 to 2011

YEARS	El Niño	ENSO Neutral	La Niña
IOD Positive	1972-73, 1977-78, 1982-83, 1991-92, 1994-95, 1997-98	1961-62, 1963-64, 2006-07	2000-01, 2007-08
IOD Neutral	1965-66, 1968-69, 1976-77, 1986-87, 1987-88, 2002-03, 2004-05, 2009-10	1960-61, 1962-63, 1966-67, 1967-68, 1969-70, 1978-79, 1979-80, 1980-81, 1983-84, 1990-91, 1992-93, 1993-94, 2001-02, 2003-04, 2005-06, 2008-09	1971-72, 1973-74, 1974-75, 1975-76, 1995-96, 1999-00, 2010-11
IOD Negative	NIL	1981-82, 1985-86, 1989-90	1964-65, 1970-71, 1984-85, 1988-89, 1996-97, 1998-99

The most common combination of the ENSO-IOD states is of the years having the ENSO neutral-IOD neutral combination. It is clear from the table 5.1 that El Niño and IOD negative years combination is absent in the period of analysis from 1960 to 2011.

The period considered for the ENSO and IOD effect were from 1963 June to 1975 May, 1975 June to 1986 May, 1986 June to 1995 May and 1995 June to 2008 May. The tables showing the correlation coefficients at 95% and 99 % levels, for the various composites, in the various sunspot number cycle periods are presented in Table 5.2 to Table 5.5.

Table 5.2 Table showing the values of 95 % and 99 % significance levels used for correlation coefficients in the periods from 1963 June to 1975 May.

1963 June to 1975 May	**Significance Level**	**El Niño**	**ENSO Neutral**	**La Niña**
IOD Positive	95 %	+/- 0.5760	+/- 0.5760	—
	99 %	+/- 0.7079	+/- 0.7079	—
IOD Neutral	95 %	+/- 0.4044	+/- 0.3291	+/- 0.3291
	99 %	+/- 0.5151	+/- 0.4238	+/- 0.4238
IOD Negative	95 %	—	—	+/- 0.4044
	99 %	—	—	+/- 0.5151

Table 5.3 Table showing the values of 95 % and 99 % significance levels used for correlation coefficients in the periods from 1975 June to 1986 May.

1975 June to 1986 May	**Significance Level**	**El Niño**	**ENSO Neutral**	**La Niña**
IOD Positive	95 %	+/- 0.4044	—	—
	99 %	+/- 0.5151	—	—
IOD Neutral	95 %	+/- 0.5760	+/- 0.2845	+/- 0.5760
	99 %	+/- 0.7079	+/- 0.3683	+/- 0.7079
IOD Negative	95 %	—	+/- 0.4044	+/- 0.5760
	99 %	—	+/- 0.5151	+/- 0.7079

Table 5.4 Table showing the values of 95 % and 99 % significance levels used for correlation coefficients in the periods from 1986 June to 1995 May.

1986 June to 1995 May	**Significance Level**	**El Niño**	**ENSO Neutral**	**La Niña**
IOD Positive	95 %	+/- 0.4044	—	—
	99 %	+/- 0.5151	—	—
IOD Neutral	95 %	+/- 0.4044	+/- 0.3291	—
	99 %	+/- 0.5151	+/- 0.4238	—
IOD Negative	95 %	—	+/- 0.576	+/- 0.5760
	99 %	—	+/- 0.7079	+/- 0.7079

Table 5.5 Table showing the values of 95 % and 99 % significance levels used for correlation coefficients in the periods from 1995 June to 2008 May.

1995 June to 2008 May	Significance Level	El Niño	ENSO Neutral	La Niña
IOD Positive	95 %	+/- 0.5760	+/- 0.5760	+/- 0.4044
	99 %	+/- 0.7079	+/- 0.7079	+/- 0.5151
IOD Neutral	95 %	+/- 0.4044	+/- 0.3291	+/- 0.4044
	99 %	+/- 0.5151	+/- 0.4238	+/- 0.5151
IOD Negative	95 %	—	—	+/- 0.4044
	99 %	—	—	+/- 0.5151

5.3 Analysis for the ENSO and IOD Composites during 1963 June to 1975 May

5.3.1 Composite of SST anomalies

The 13-month running mean composite SST anomalies (SSTA) were plotted in the period from 1963 June to 1975 May in Figure 5.3. This period is close to the sunspot number cycle period from 1964 March to 1975 June. In this period El Niño and IOD positive, ENSO neutral and IOD positive, El Niño and IOD neutral, ENSO neutral and IOD neutral, La Niña and IOD neutral, La Niña and IOD negative year composites are present. The base period is the entire period from 1960 January to 2011 December.

5.3.1.1 El Niño and IOD positive years

The El Niño and IOD positive years showed positive SSTAs in the entire North Indian Ocean, with the exception being a part of the north Arabian Sea (Figure 5.3A). The largest positive anomalies were seen in the regions off the coast of Somalia and in the western equatorial region.

5.3.1.2 ENSO neutral and IOD positive years

The ENSO neutral and IOD positive years showed a negative SSTAs in the entire north Indian Ocean, with the exception of a small region in the central Arabian Sea extending up to the south-eastern Arabian Sea, where the SSTA was positive (Figure 5.3B).

5.3.1.3 El Niño and IOD neutral years

The El Niño and IOD neutral years showed negative SSTAs in the north Indian Ocean, with small regions of positive anomaly in the Arabian Sea and parts of Bay of Bengal (Figure 5.3D).

5.3.1.4 ENSO neutral and IOD neutral years

The ENSO neutral and IOD neutral composite showed general negative SSTAs in the northern Indian Ocean, except in a large region in the Arabian Sea along the west coast extending up to the central Arabian Sea (Figure 5.3 E).

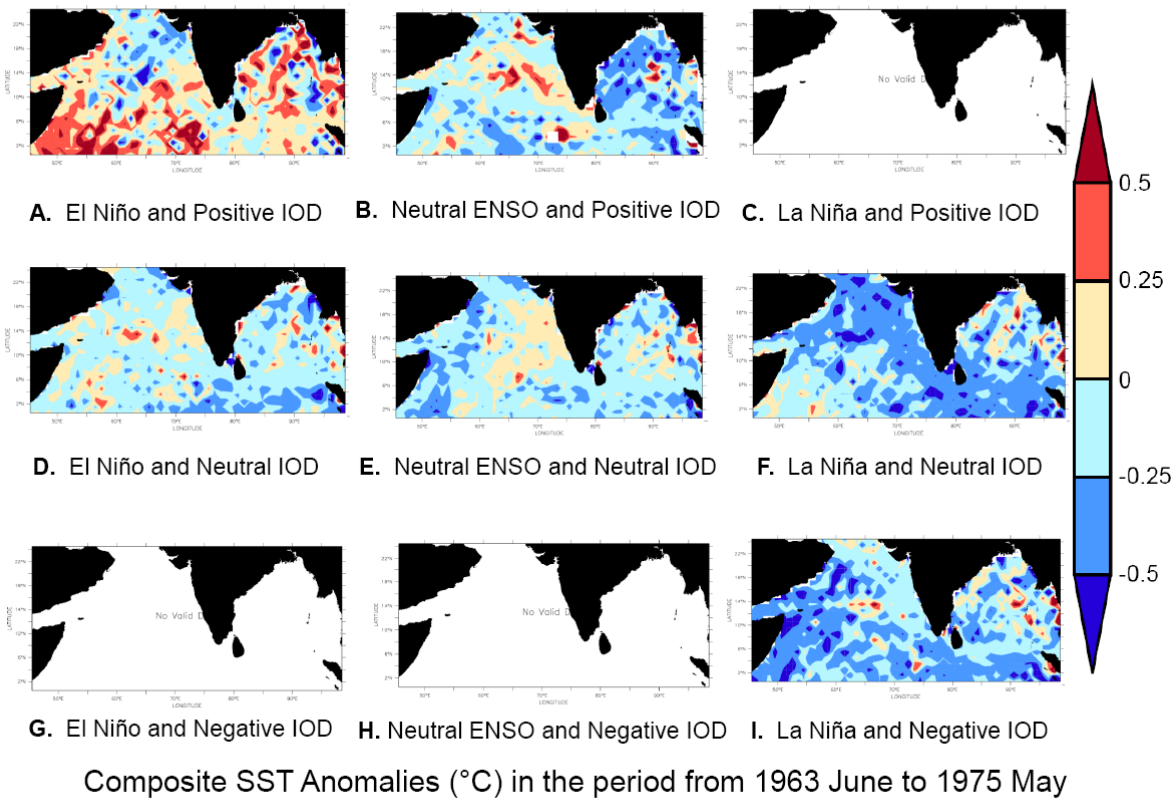

Figure 5.3 The 13-month running mean composite SST anomalies in the period from 1963 June to 1975 May

5.3.1.5 La Niña and IOD neutral years

The La Niña and IOD neutral composite showed more negative SSTAs throughout the northern Indian Ocean (Figure 5.3F). Note the small patches of positive SSTAs in the Bay of Bengal in the central and eastern regions.

5.3.1.6 La Niña and IOD negative years

The La Niña and IOD negative composite Also showed negative SSTAs throughout the north Indian Ocean with few small patches of positive SSTAs in the Arabian Sea and the Bay of Bengal (Figure 5.3I).

5.3.2 Impacts of fluxes in generating the observed SSTs

The composites of the correlation coefficient of fluxes of momentum (wind speed), freshwater (E-P) and net heat (NHF) with SST and their respective anomalies were examined to decipher the role of these fluxes in generating the observed SST.

The composites of momentum flux (wind speed) (Figures 5.4 and 5.5), freshwater flux (E-P) (Figures 5.6 and 5.7) and net heat flux (NHF) (Figures 5.8 and 5.9) were analysed in the context of the anomalies and correlation coefficients with respect to SST in order to see their effects on the SST in the various composites and periods considered, especially on the larger regions of increasing or decreasing significant trends.

The period from 1963 June to 1975 May had a decreasing SST trend in the eastern Arabian Sea and in the southern Bay of Bengal (Figure 3.8). The decreasing trend in the some parts of the eastern Arabian Sea was affected by the quicker wind speeds which occurred in the La Niña- IOD neutral composite (Figures 5.4F and 5.5F). The E-P positive anomalies also affect the SSTs in the some regions of the East Arabian Sea in the El Niño-IOD neutral and La Niña- IOD neutral composites (Figures 5.6F and 5.7F).

In the northern Arabian Sea, the decreasing SST trend was contributed by the lesser NHF into the ocean. This occurred in the La Niña- IOD neutral and in the La Niña- IOD negative

composites (Figures 5.8F, 5.8I, 5.9F and 5.9I). These two composites make up 5 years of the period from 1963 June to 1975 May.

In the central Bay of Bengal the SST increasing trend was due to the higher NHF into the ocean. This was seen in the La Niña- IOD neutral composite (Figures 5.8 and 5.9).

The largest positive SSTAs were in the El Niño- IOD positive composite years, while the largest negative SSTAs were in the La Niña- Neutral IOD and La Niña- Negative IOD composites (Figure 5.3A, 5.3F and 5.3I).

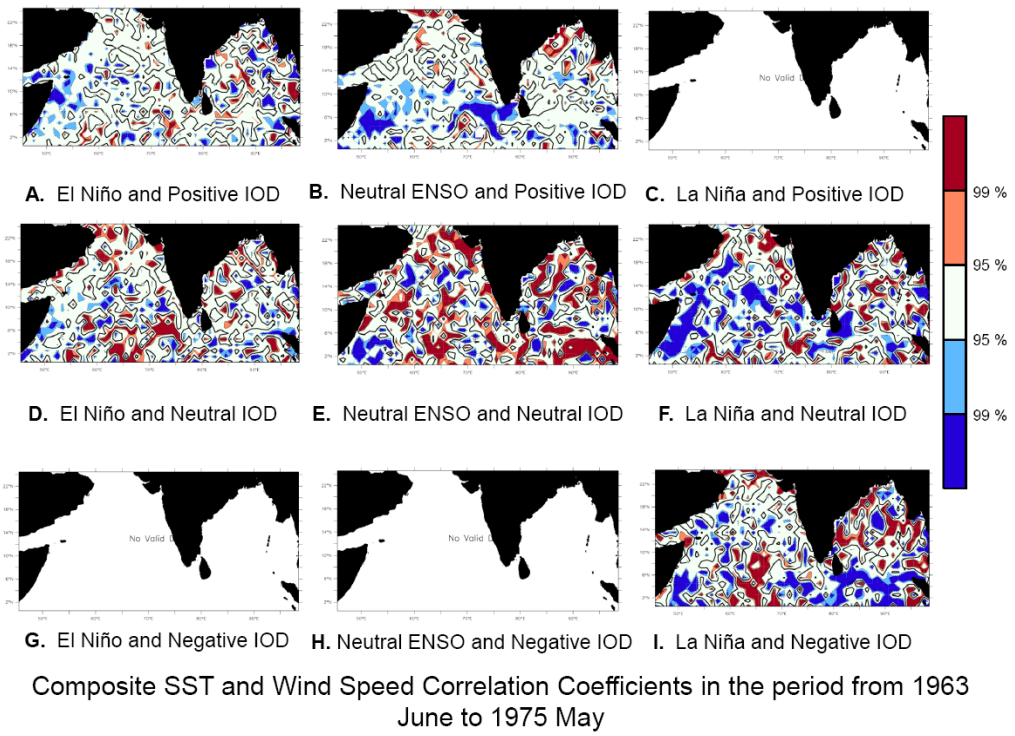

Figure 5.4 Correlation coefficients of 13-month running mean composites of SST and Wind Speed in the period from 1963 June to 1975 May

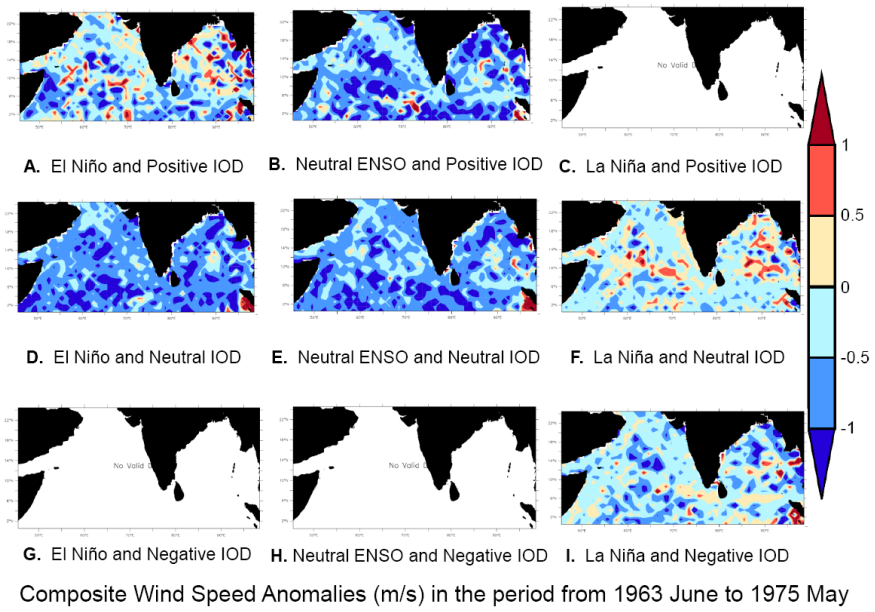

Figure 5.5 Composite Wind Speed 13-month running mean anomalies in the period from 1963 June to 1975 May

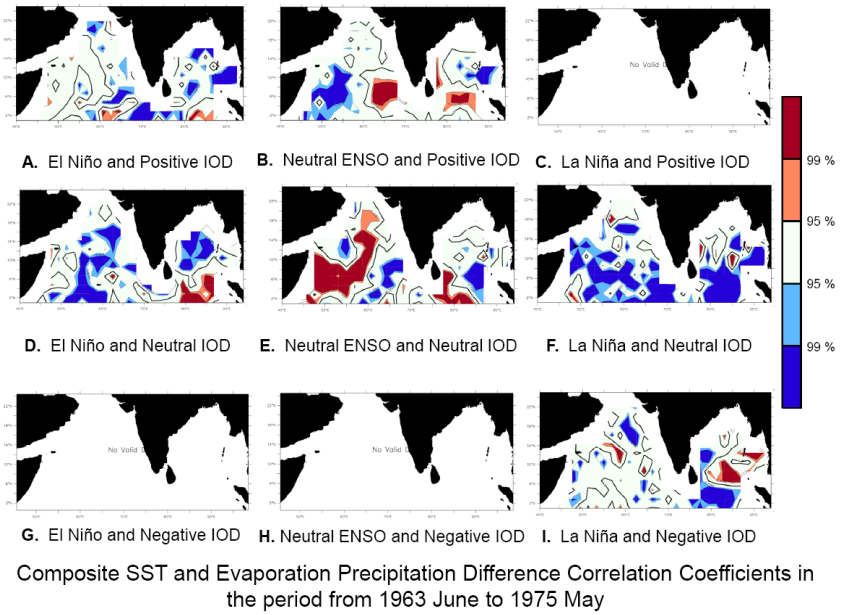

Figure 5.6 Correlation coefficients of 13-month running mean composites of SST and Evaporation Precipitation Difference in the period from 1963 June to 1975 May

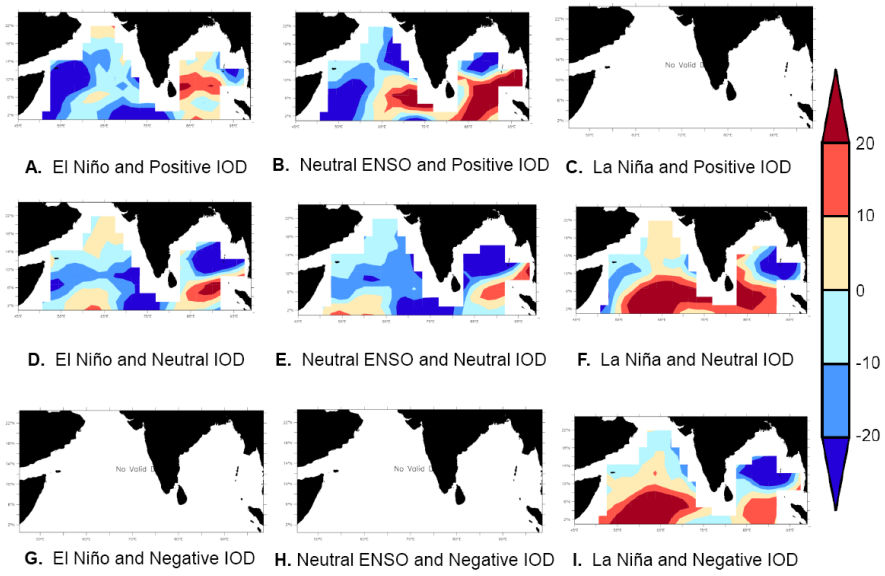

Figure 5.7 Composite Evaporation Precipitation Difference 13-month running mean anomalies in the period from 1963 June to 1975 May

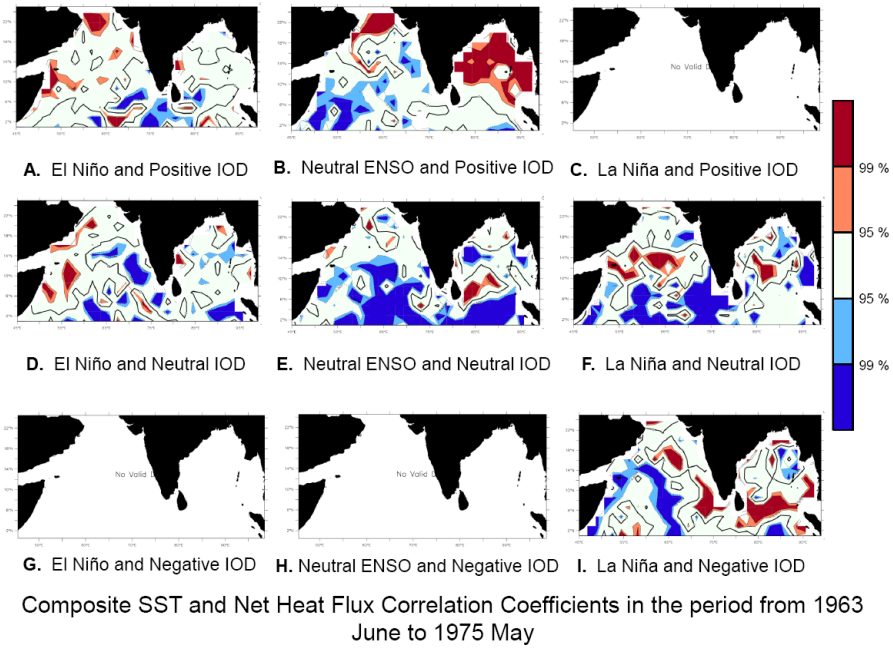

Figure 5.8 Correlation coefficients of 13-month running mean composites of SST and Net Heat Flux in the period from 1963 June to 1975 May

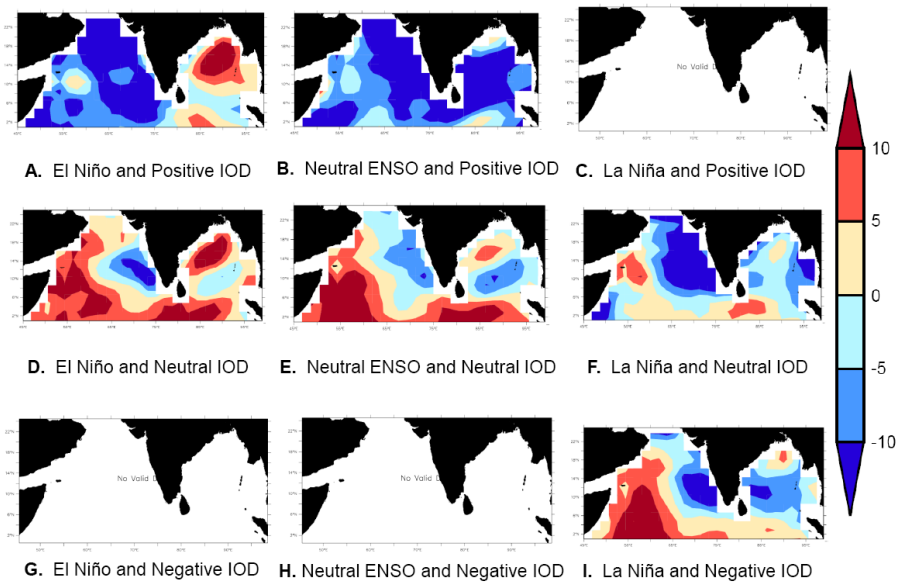

Figure 5.9 Composite Net Heat Flux 13-month running mean anomalies in the period from 1963 June to 1975 May

5.4 Analysis for the ENSO and IOD Composites during 1975 June to 1986 May

5.4.1 Composite SST anomalies

The composite of 13-month running mean SST anomalies were plotted in the period from 1975 June to 1986 May (Figure 5.10). This period was similar to the sunspot number cycle period from 1975 June to 1985 December. In this sunspot number cycle period El Niño and IOD positive, El Niño and IOD neutral, ENSO neutral and IOD neutral, La Niña and IOD neutral, ENSO neutral and IOD negative and La Niña and IOD negative year composites were present.

5.4.1.1 El Niño and IOD positive years

The composite of the El Niño and IOD positive years for SSTAs were generally positive throughout the north Indian Ocean. The SSTAs in the east Arabian Sea and in the north-eastern Bay of Bengal were negative (Figure 5.10A).

5.4.1.2 El Niño and IOD neutral years

The 13-month running mean SSTA composite of the El Niño and IOD positive years showed a generally negative values in most of the region under study. However, positive SSTAs were also seen in the central Arabian Sea and regions scattered across the Bay of Bengal (Figure 5.10D).

5.4.1.3 ENSO neutral and IOD neutral years

In the ENSO neutral and IOD neutral composite, the SSTAs were generally negative in the Arabian Sea and eastern Bay of Bengal, but positive in the west Bay of Bengal. This composite combination occurred four times in the sunspot number cycle period (Figure 5.10E).

5.4.1.4 La Niña and IOD neutral years

In the La Niña and IOD neutral composite, the SSTAs were almost negative throughout the study domain. The region off eastern Bay of Bengal had some positive values (Figure 5.10F).

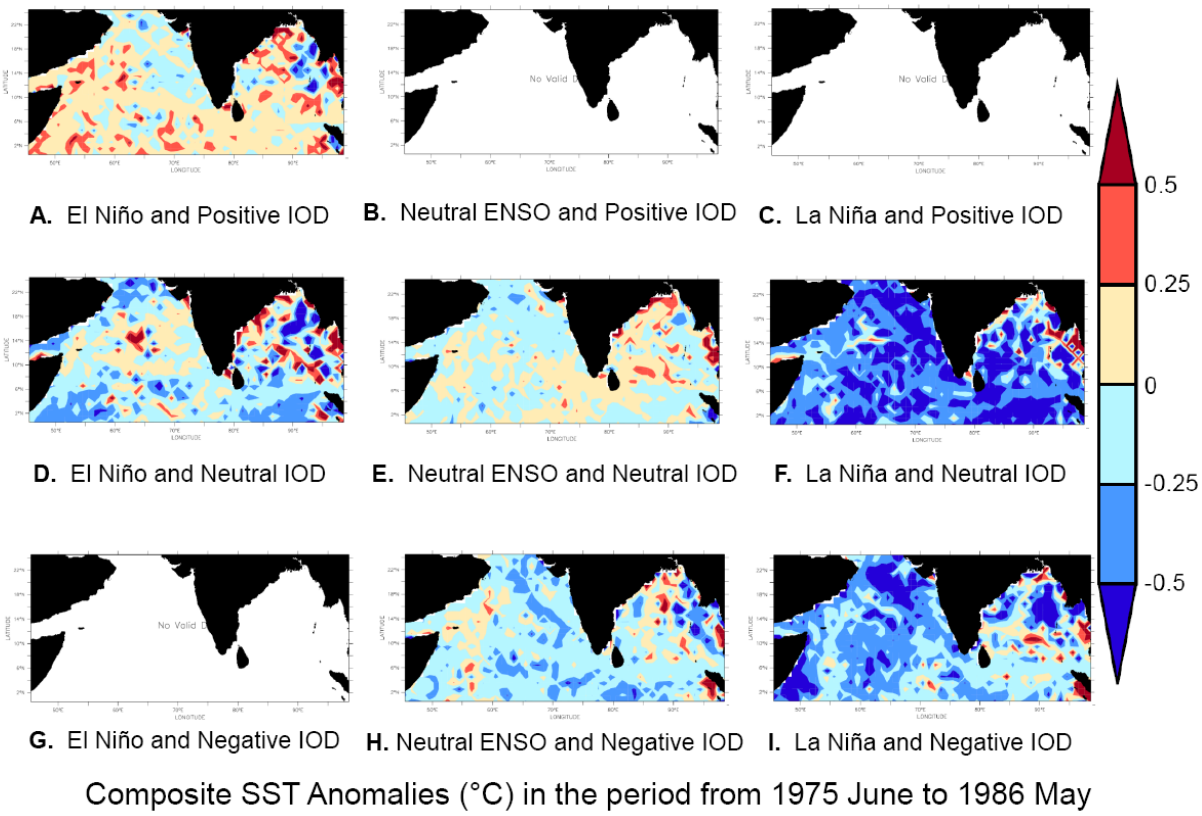

Figure 5.10 The 13-month running mean composite of SST anomalies in the period from 1975 June to 1986 May

5.4.1.5 ENSO neutral and IOD negative years

In the ENSO neutral and IOD negative composite, the SSTAs were generally negative, with larger negative anomalies found in the north-eastern Arabian Sea. Some positive SSTAs were found in the West Arabian Sea and in the head and central Bay of Bengal regions (Figure 5.10H).

5.4.1.6 La Niña and IOD negative years

In the La Niña and IOD negative composite, the SSTAs were generally negative in the North Indian Ocean. The largest negative SSTAs were in the north-eastern Arabian Sea, off Somalia and parts of the central Bay of Bengal. The positive SSTAs were seen in the some parts of the south-central and eastern Bay of Bengal (Figure 5.10I).

5.4.2 Impacts of fluxes in generating the observed SSTs

In the period from 1975 June to 1985 May, the SST rise in the equatorial Arabian Sea and equatorial Bay of Bengal and the decreasing SST trends in the north-east Arabian Sea (Figure 3.8) were seen in the context of the effect the fluxes on them.

The equatorial Arabian Sea and the equatorial Bay of Bengal regions showed an increasing trend caused by the lesser evaporation precipitation difference. This was seen in the El Niño-IOD positive composite (Figures 5.10A, 5.13A and 5.14A).

In some of the parts of the North-East Arabian Sea the SST decreasing trend was due to the higher difference between the evaporation and precipitation. This was seen in the La Niña-IOD neutral (Figure 5.10F, 5.13F and 5.14F) and in the La Niña- IOD negative composites (Figure 5.10I, 5.13I and 5.14I).

The largest positive SSTAs were in the El Niño- IOD positive composite while the negative SSTAs of largest magnitudes were seen in the La Niña- Neutral IOD and La Niña- Negative IOD composites (Figure 5.10A, 5.10F and 5.10I).

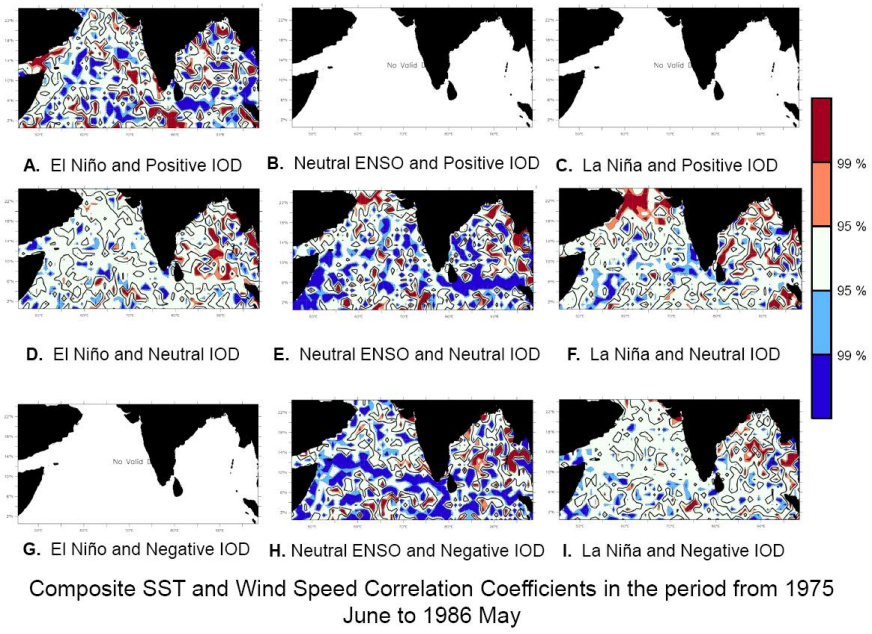

Figure 5.11 Correlation coefficients of 13-month running mean composites of SST and Wind Speed in the period from 1975 June to 1986 May

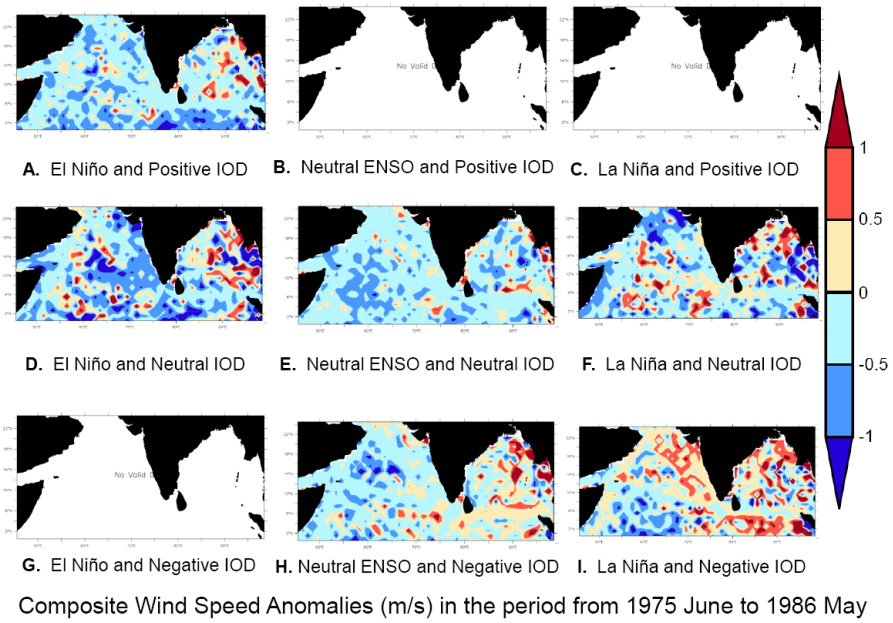

Figure 5.12 Composite Wind Speed 13-month running mean anomalies in the period from 1975 June to 1986 May

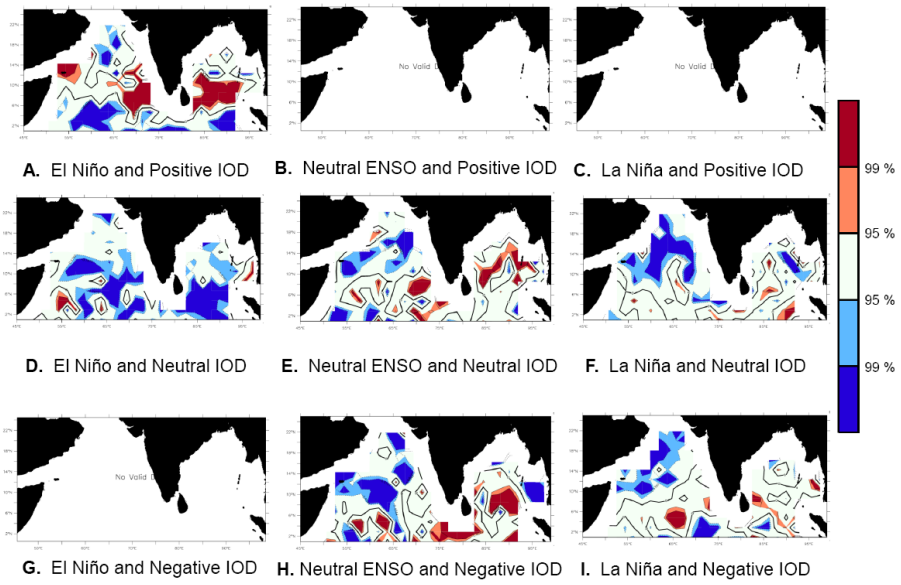

Figure 5.13 Correlation coefficients of 13-month running mean composites of SST and Evaporation Precipitation Difference in the period from 1975 June to 1986 May

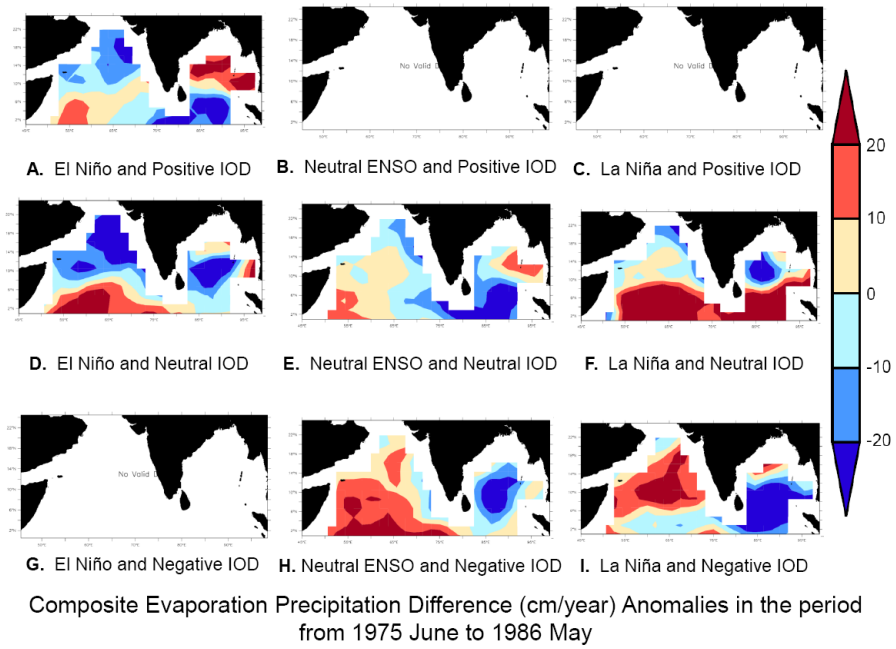

Figure 5.14 Composite Evaporation Precipitation Difference 13-month running mean anomalies in the period from 1975 June to 1986 May

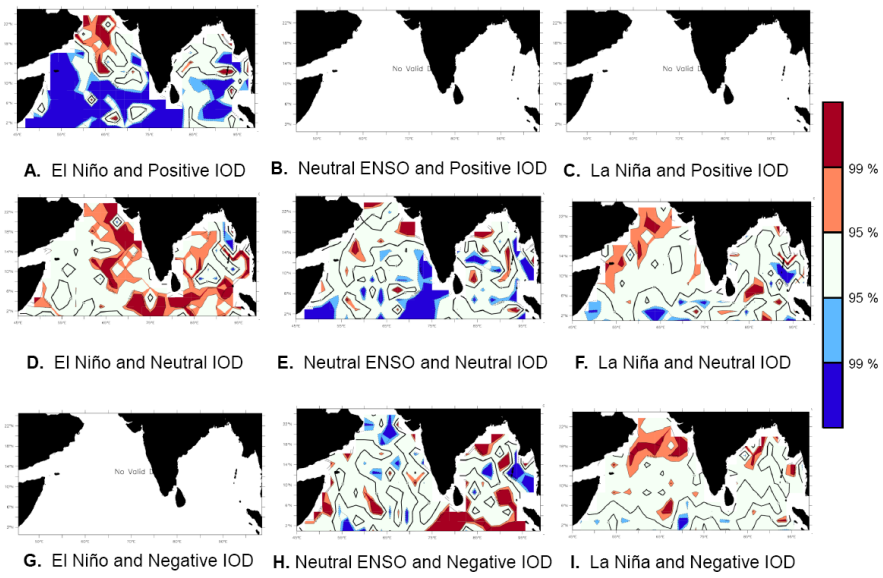

Figure 5.15 Correlation coefficients of 13-month running mean composites of SST and Net Heat Flux in the period from 1975 June to 1986 May

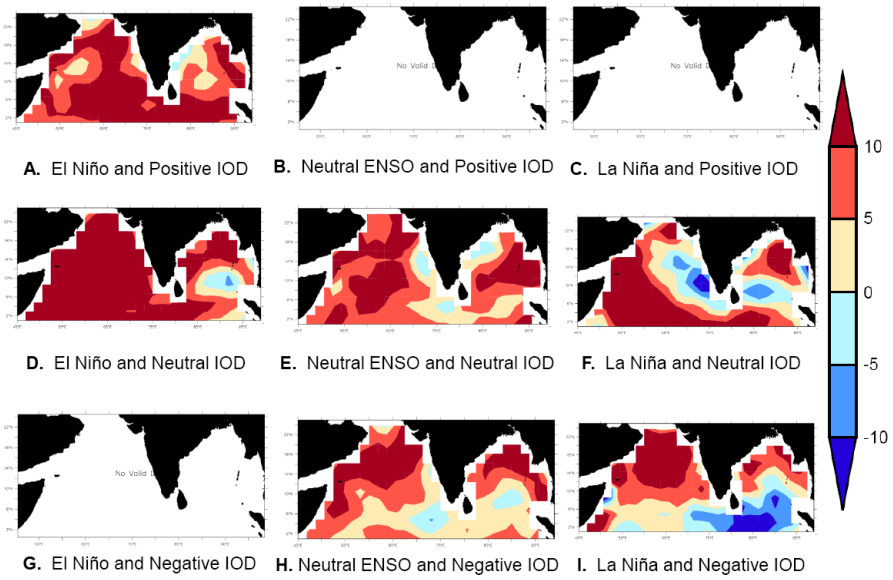

Figure 5.16 Composite Net Heat Flux 13-month running mean anomalies in the period from 1975 June to 1986 May

5.5 Analysis for the ENSO and IOD Composites during 1986 June to 1995 May

5.5.1 Composite SST anomalies

The composite of 13-month running mean SST anomalies were plotted in the period from 1986 June to 1995 May (Figure 5.17), which was close to the sunspot number cycle period from 1985 December to 1995 November. In this period El Niño and IOD positive, El Niño and IOD neutral, ENSO neutral and IOD neutral, ENSO neutral and IOD negative and La Niña and IOD negative year composites were present.

5.5.1.1 El Niño and IOD positive years

In the El Niño and IOD positive composite, in the period from 1986 June to 1995 May, the 13-month running mean SSTAs were negative in the entire Arabian Sea, except in the equatorial region. In the equatorial regions the Arabian Sea as well as the Bay of Bengal and eastern and western parts of the Bay of Bengal showed positive values of SSTAs (Figure 5.17A).

5.5.1.2 El Niño and IOD neutral years

In the El Niño and IOD neutral composite there were positive SST anomalies in most of the study domain, except off Somalia and northern part of the Arabia (Figure 5.17D).

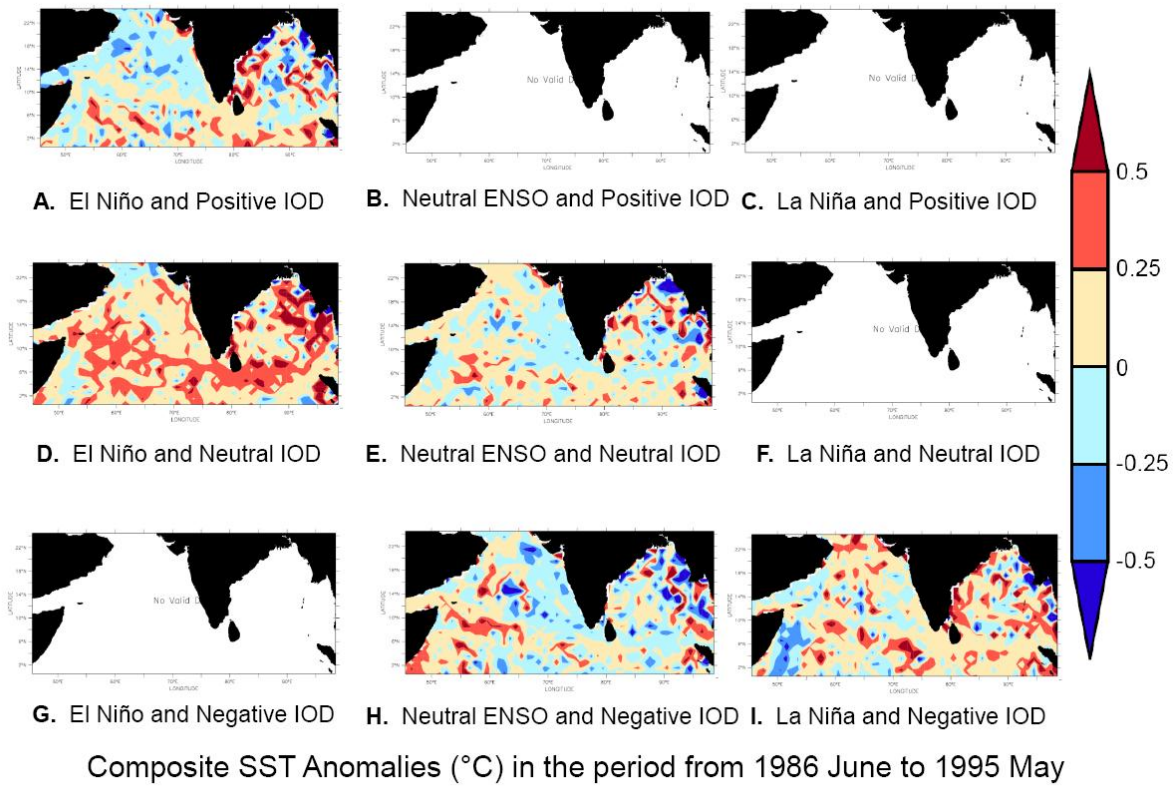

Figure 5.17 Composite SST 13-month running mean anomalies in the period from 1986 June to 1995 May

5.5.1.3 ENSO neutral and IOD neutral years

In the ENSO neutral and IOD neutral composite there were both positive and negative SSTAs. Most parts of the Arabian Sea had positive SSTAs, while regions off the west coast of India showed negative anomalies. Similarly, most part of the Bay of Bengal had positive SSTAs, while parts of the central Bay of Bengal showed negative anomalies (Figure 5.17E).

5.5.1.4 ENSO neutral and IOD negative years

In the ENSO neutral and IOD neutral composite, negative SSTAs were seen in the eastern Arabian Sea, while positive anomalies were seen in the rest of the regions. In the Bay of Bengal, however, most of the regions had negative anomalies. In the eastern Bay of Bengal both strong positive and negative anomalies were noticed (Figure 5.17H).

5.5.1.5 La Niña and IOD negative years

In the La Niña and IOD negative composite, most of the study regions showed positive SST anomalies. The exceptions were near the part of the eastern Arabian Sea, Somalia and Arabia regions, and some parts of the central Bay of Bengal (Figure 5.17I).

5.5.2 Impacts of fluxes in generating the observed SSTs

In the period from 1985 June to 1995 May, the SST decreasing trends in the equatorial Arabian Sea and in the eastern Arabian Sea (Figure 3.8) were seen with respect to the effect of the fluxes.

Some parts of the equatorial Arabian Sea region showed negative SSTAs (Figure 5.17). The evaporation precipitation difference showed higher values in the El Niño- IOD positive composite (Figures 5.20A and 5.21A). Besides this the lesser NHF into the ocean also during the El Niño- IOD positive composite aids in the decreasing SST trend too (Figures 5.22A and 5.23A).

A decreasing SST trend in the eastern Arabian Sea correlates well with the higher evaporation precipitation difference seen in the ENSO neutral- IOD negative composite (Figure 5.20H and 5.21H). This is reflected in the significant negative correlation coefficient between the SST and evaporation precipitation difference in some regions of the eastern Arabian Sea, in the ENSO neutral- IOD negative composite (Figure 5.20H and 5.21H).

The largest positive SSTAs were in the El Niño- IOD neutral composite (Figure 5.17D) while the largest negative SSTAs in magnitude were in the ENSO neutral- IOD negative (Figure 5.17H) and in the El Niño- IOD positive composites (Figure 5.17A).

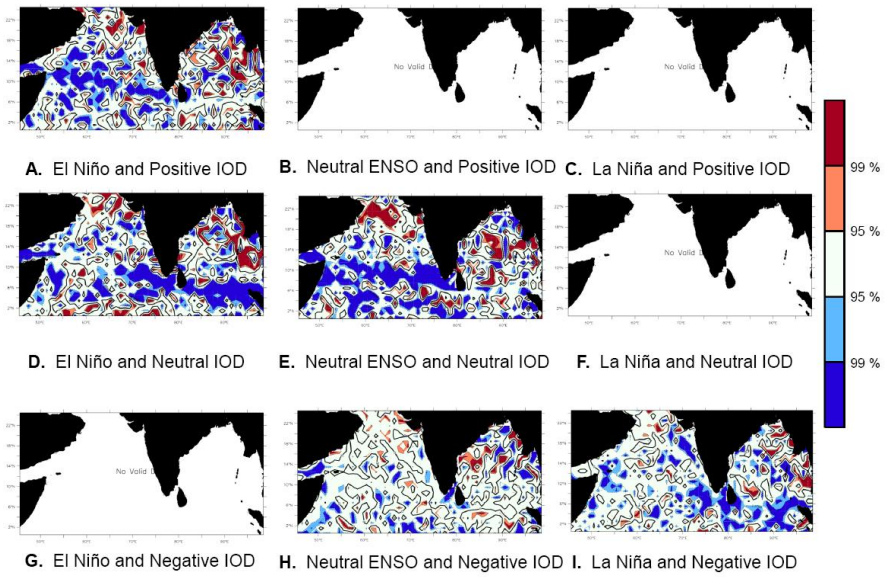

Figure 5.18 Correlation coefficients of 13-month running mean composites of SST and Wind Speed in the period from 1986 June to 1995 May

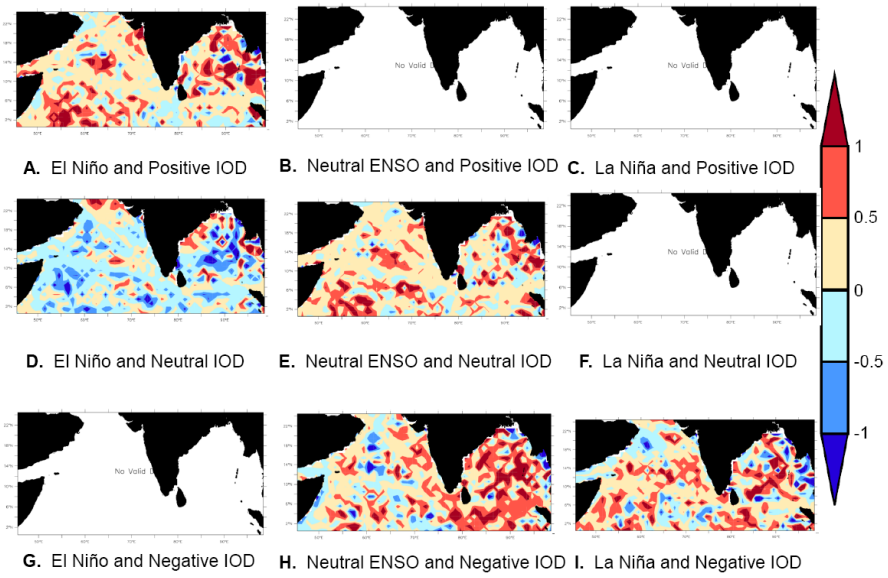

Figure 5.19 Composite Wind Speed 13-month running mean anomalies in the period from 1986 June to 1995 May

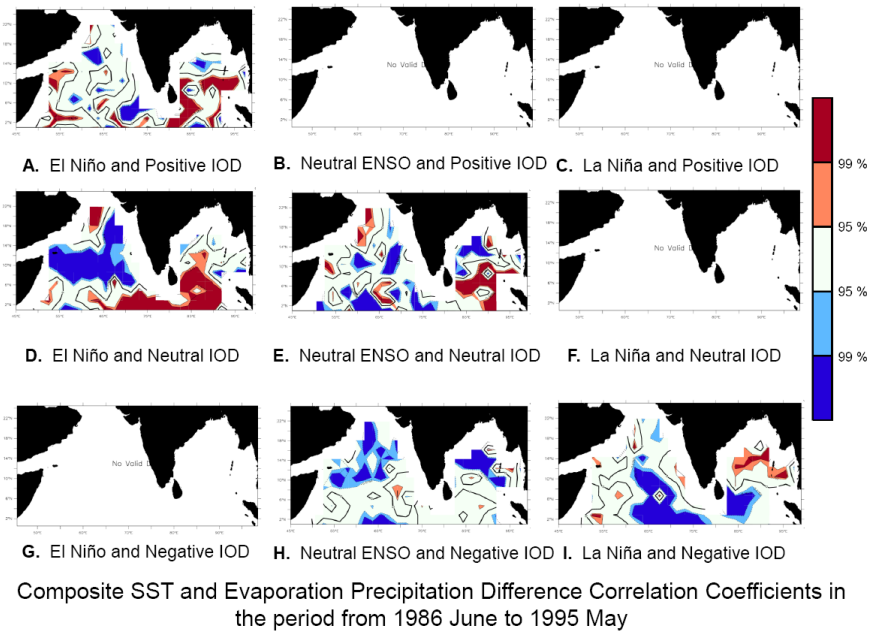

Figure 5.20 Correlation coefficients of 13-month running mean composites of SST and Evaporation Precipitation Difference in the period from 1986 June to 1995 May

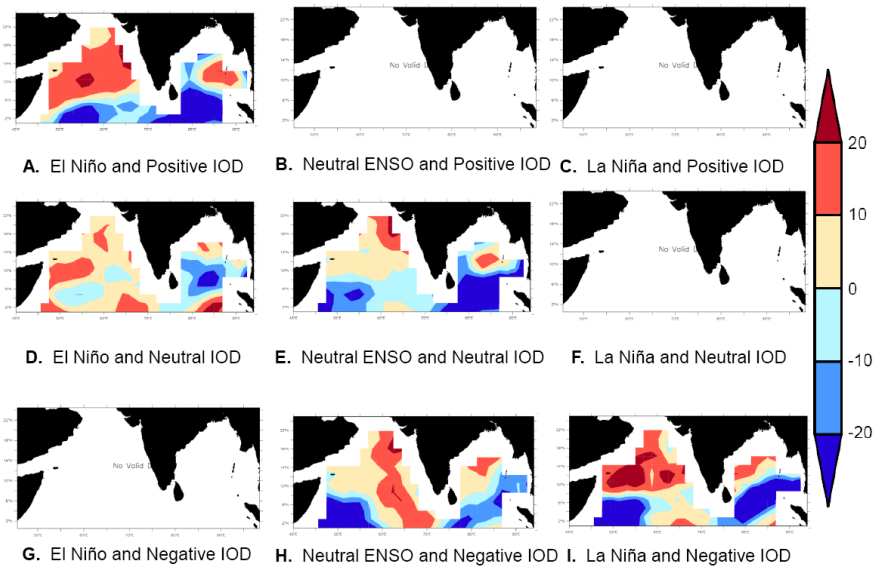

Figure 5.21 Composite Evaporation Precipitation Difference 13-month running mean anomalies in the period from 1986 June to 1995 May

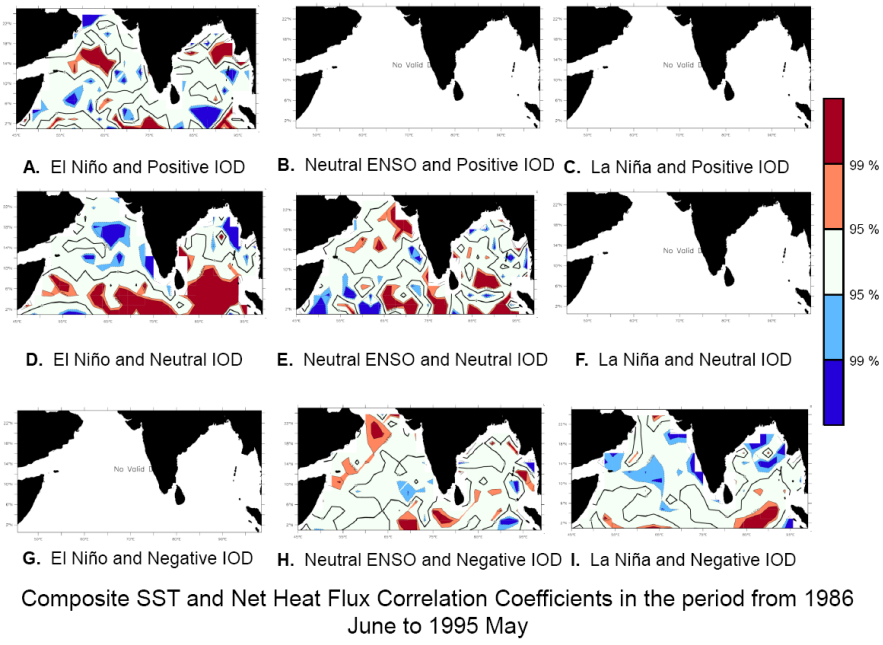

Figure 5.22 Correlation coefficients of 13-month running mean composites of SST and Net Heat Flux in the period from 1986 June to 1995 May

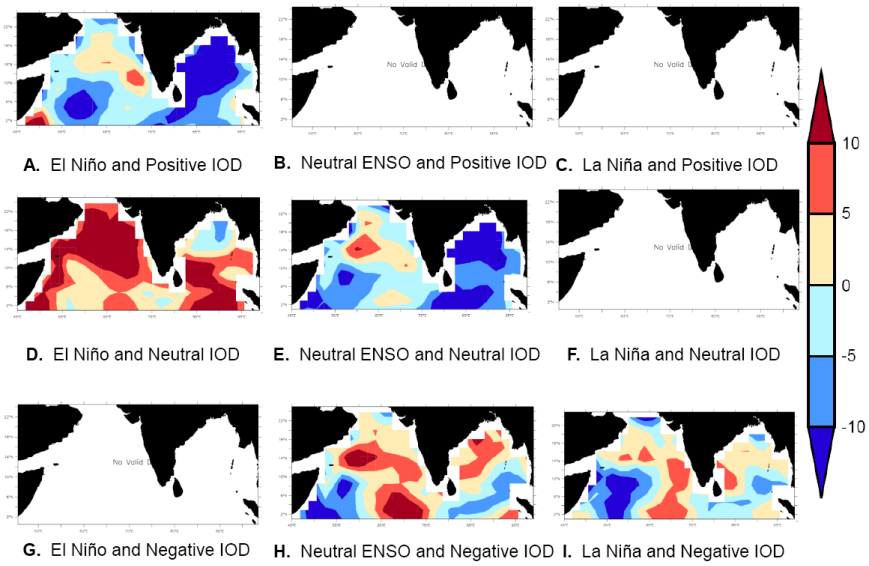

Figure 5.23 Composite Net Heat Flux 13-month running mean anomalies in the period from 1986 June to 1995 May

5.6 Analysis for the ENSO and IOD Composites during 1995 June to 2008 May

5.6.1 Composite SST anomalies

The composite 13-month running mean SST anomalies were plotted in the period from 1995 June to 2008 May (Figure 5.24), which was close to the sunspot number cycle period from 1995 November to 2008 July. In this period El Niño and IOD positive, ENSO neutral and IOD positive, La Niña and IOD positive, El Niño and IOD neutral, ENSO neutral and IOD neutral, La Niña and IOD neutral and La Niña and IOD negative year composites were present.

5.6.1.1 El Niño and IOD positive years

In the El Niño and IOD positive composite, in the period from 1995 June to 2008 May, the 13-month running mean SSTAs positive over almost the entire Arabian Sea and the Bay of Bengal with high values (Figure 5.24A).

5.6.1.2 ENSO neutral and IOD positive years

In the ENSO neutral and IOD positive composite, the SSTAs were positive in most parts of the study domain, similar to the previous composite, except some regions in the central parts of the Bay of Bengal and regions close to the equatorial Arabian (Figure 5.24B).

5.6.1.3 La Niña and IOD positive years

In the La Niña and IOD positive composite, the SSTAs were largely negative along the eastern and western Bay of Bengal, parts of the north-western Arabian Sea and in a zonal band oriented in north-east-south-west direction in the Arabian Sea. The rest of the regions had positive anomalies of SST (Figure 5.24C).

5.6.1.4 El Niño and IOD neutral years

In the El Niño and IOD neutral composite, the SSTAs were positive over most of the Arabian Sea and the Bay of Bengal. The region off southern part of Somalia and central eastern part of the Bay of Bengal had negative SSTAs (Figure 5.24D).

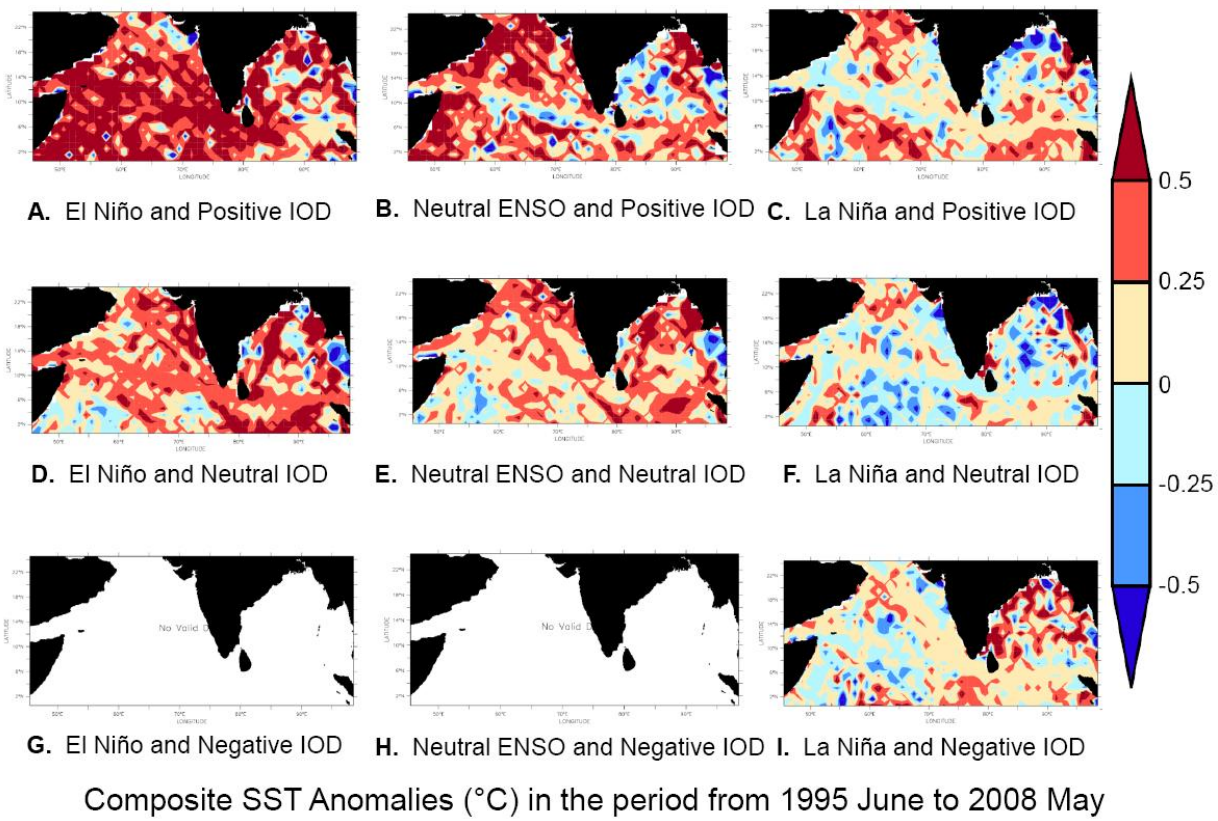

Figure 5.24 Composite SST 13-month running mean anomalies in the period from 1995 June to 2008 May

5.6.1.5 ENSO neutral and IOD neutral years

In the ENSO neutral and IOD neutral composite the patter of SST anomalies were similar to that of the previous composites, with positive anomalies dominating most parts of the study domain (Figure 5.24E).

5.6.1.6 La Niña and IOD neutral years

In the La Niña and IOD neutral composite, the positive SSTAs were seen only at few places in the Arabian Sea and the Bay of Bengal. Most of the study domain was seen with negative SSTAs (Figure 5.24F).

5.6.1.7 La Niña and IOD negative years

In the La Niña and IOD negative composite, the Arabian Sea had both positive and negative SST anomalies, almost equal in areas. In the Bay of Bengal, however, positive anomalies were dominantly seen (Figure 5.24I).

5.6.2 Impacts of fluxes in generating the observed SSTs

In the period from 1995 June to 2008 May, the SST showed an increasing trends in most parts of the Arabian Sea (Figure 3.8), however, the wind speed did not show any corresponding influence. The increasing SST trend in the northern Arabian Sea (Figures 3.8 and 5.24) was aided by a decreasing trend in the difference between evaporation and precipitation. The correlation between SST and E-P was negative in part of the northern Arabian Sea (Figures 5.27B and 5.28B), which was seen in the ENSO neutral- IOD positive composite.

The increasing trend of SST in the Southern Arabian Sea (Figure 3.8) appeared to be mediated by a reduction in the E-P in the El Niño- IOD positive composite period. The SST

and E-P showed significant negative correlation coefficients in this composite, in part of the southern Arabian Sea (Figures 5.27A and 5.28A).

The increasing SST trends in the northern Arabian Sea, appeared to be aided by the increasing NHF into the ocean. There were significant positive correlation coefficients between SST and NHF in parts of the northern Arabian Sea (Figure 5.29A and 5.30A in the El Niño- IOD positive composite.

The increasing SST trends of the western Arabian Sea were also favoured by the decrease of E-P. There were regions in the western Arabian Sea which showed significant negative correlation coefficients between SST and E-P, in the El Niño- Neutral IOD composite (Figures 5.27D and 5.28D).

The increasing SST trend of the eastern Arabian Sea, were favoured by the increased NHF into the ocean. There were significant positive correlation coefficients between SST and NHF in parts of the eastern Arabian Sea (Figures 5.29E and 5.30E) in the ENSO neutral- IOD neutral composites.

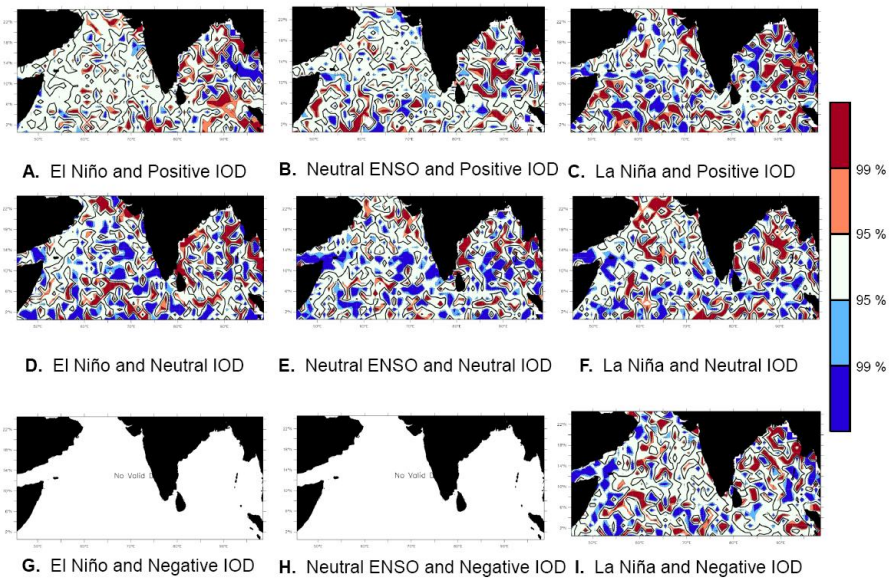

Figure 5.25 Correlation coefficients of 13-month running mean composites of SST and Wind Speed in the period from 1995 June to 2008 May

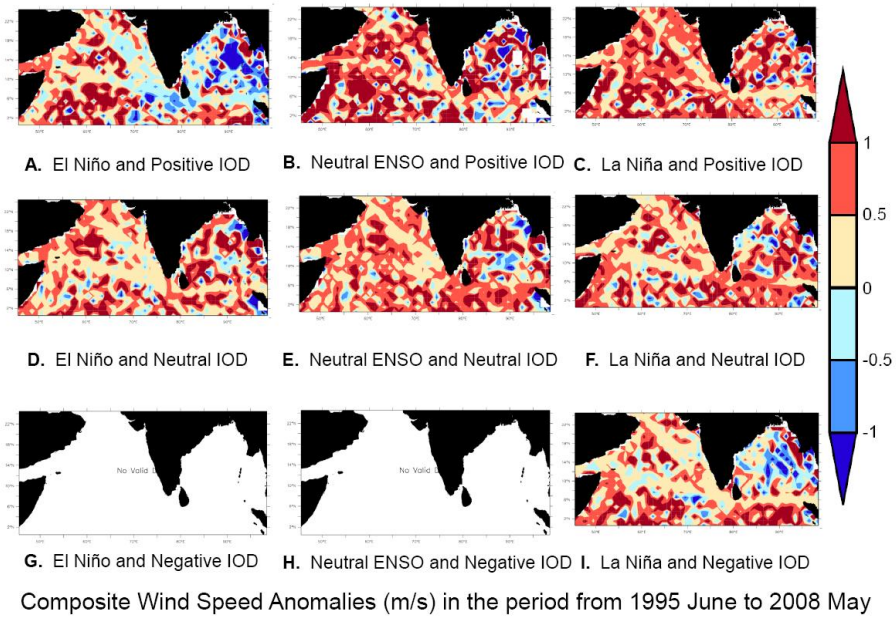

Figure 5.26 Composite Wind Speed 13-month running mean anomalies in the period from 1995 June to 2008 May

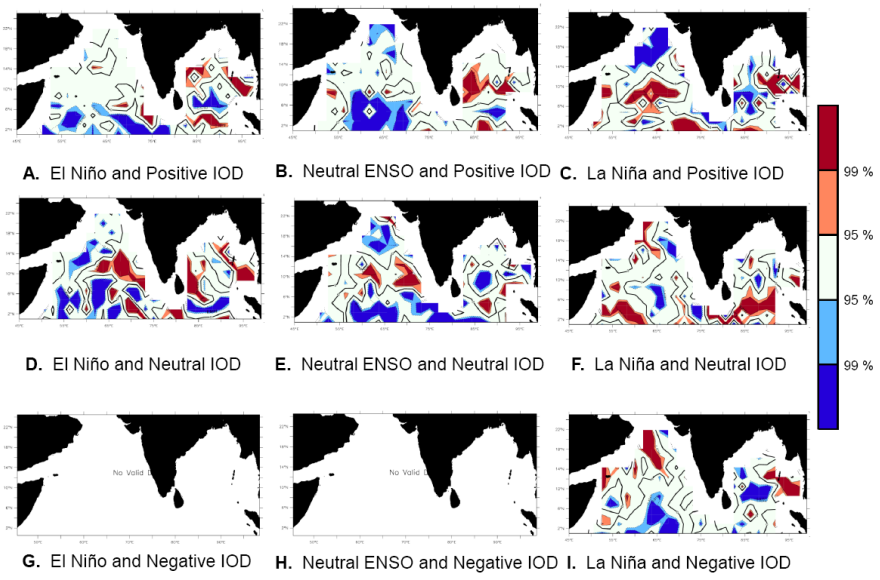

Figure 5.27 Correlation coefficients of 13-month running mean composites of SST and Evaporation Precipitation Difference in the period from 1995 June to 2008 May

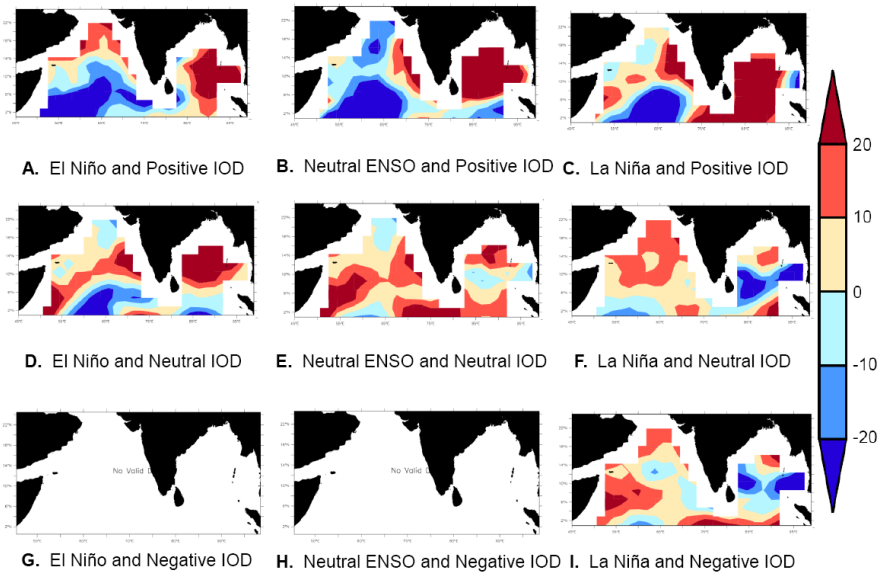

Figure 5.28 Composite Evaporation Precipitation Difference 13-month running mean anomalies in the period from 1995 June to 2008 May

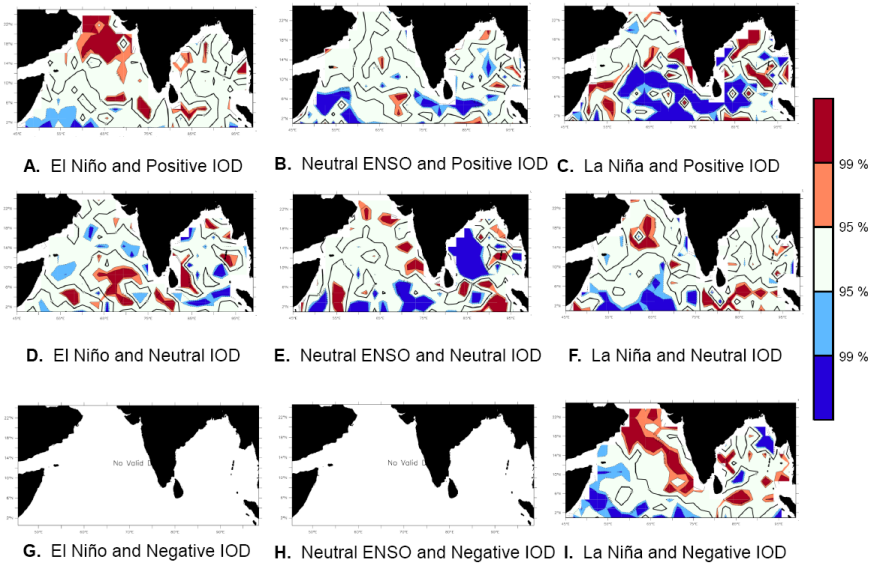

Figure 5.29 Correlation coefficients of 13-month running mean composites of SST and Net Heat Flux in the period from 1995 June to 2008 May

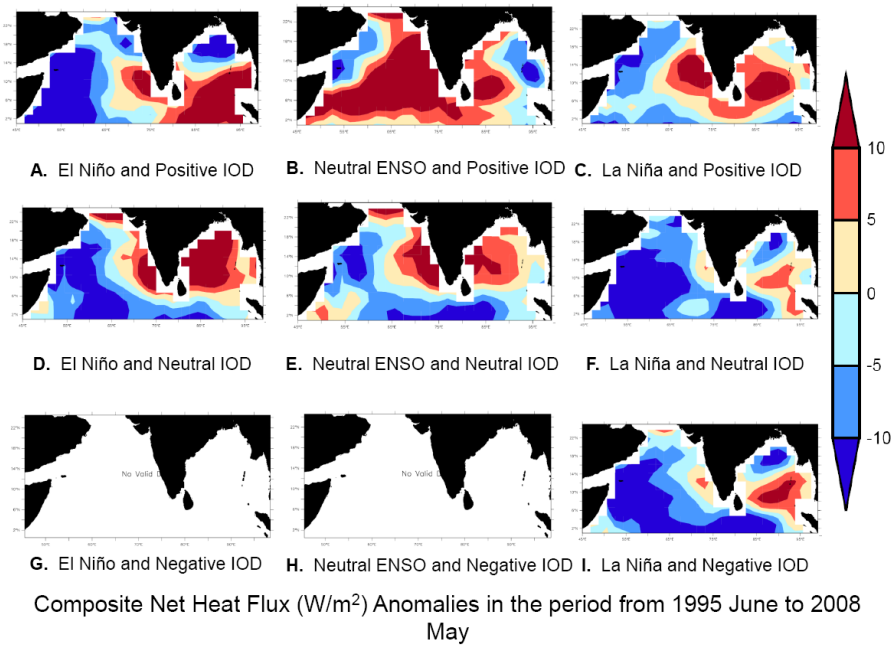

Figure 5.30 Composite Net Heat Flux 13-month running mean anomalies in the period from 1995 June to 2008 May

In summary, it was inferred from the above results that the SST anomalies were progressively increasing from the first decadal period (1963-1975) to fourth decadal period (1995-2008) that was studied. As the anomalies of SST become more and more positive, the influence of ENSO and IOD becomes weaker.

CHAPTER 6

SUMMARY AND CONCLUSION

Climate change is an important topic, with global warming being one of its manifestations and sea-level rise, melting of polar ice-caps, receding glaciers, ocean acidification, being among others. The factors that determine the Earth's climate are changes in the Earth's radiation balance. The warming of the Earth is unequivocal; however, this warming is not uniform. The increase in the temperature leads to the melting of ice and associated rise in the sea level. In addition, the thermal expansion of oceanic waters would also lead to the rise in sea level. The resultant sea level rise would flood and submerge low-lying coastal regions and islands, which in turn would impact the human populations.

The sea surface temperature (SST) is an important parameter in oceanography which is strongly related to air-sea interaction processes. It can provide useful indices for various ocean-atmosphere processes including climate phenomena. In the Indian Ocean, most of the studies pertaining to the SST are focused on deciphering the seasonality and the factors responsible for such variability. There are very few studies that examined the variability of the Indian Ocean in the inter-annual to decadal time scales. This was the motivation for the present study and the thesis entitled “Processes controlling the variability of sea surface temperature in the North Indian Ocean over decadal time scale”.

The study had following three objectives:

1. To decipher inter-decadal variability in SST in the northern Indian Ocean.
2. To identify the factors responsible for the observed variability.

3. To delineate the role of El Niño-Southern Oscillation (ENSO) and Indian Ocean Dipole (IOD).

The thesis has been organized in six chapters with the first chapter dealing with introduction, giving background information about the importance of global warming and climate change and the urgency in understanding it in the northern Indian Ocean comprising of the Arabian Sea and the Bay of Bengal. A brief literature review was provided to bring out the need for the present study and subsequently the objectives were set. The second chapter deals with the study domain, various types of data and model that has been used in the study. The study domain was the North Indian Ocean (NIO) spanning from the equator to 25^{o}N latitude and from 45^{o}E to 99^{o}E longitude. A suite of ocean and atmospheric data, both in-situ as well as remote sensing data, were used. The data used for the study period was from January 1960 to December 2011. This chapter also provided elaborate information on the type of data, its source, and its spatial and temporal resolutions. The methodology followed for various computations and the Price-Weller-Pinkel (PWP) model set up and its forcing were also elaborated.

The third chapter deals with the first objective, the inter-decadal variability of the SST in the north Indian Ocean. The Fast Fourier Transformation (FFT) of de-trended (seasonal and annual cycles) 12-month running mean SST showed three dominant periodicities of 3.7 years, 5 years and 10 years at 95% significance level in the north Indian Ocean. The first two were of ENSO periodicity, while the third one was decadal. Thus, the data analysis showed that decadal periodicity was one among the dominant ones. The area-averaged 60-month running mean SST in the north Indian Ocean, the Arabian Sea and the Bay of Bengal, all

showed four distinct decadal cycles which co-varied with the decadal sunspot number cycles. The decadal SST cycles that were identified with the sunspot number cycle were (1) 1964 March to 1975 June, (2) 1975 June to 1985 December, (3) 1985 December to 1995 November and (4) 1995 November to 2008 July. Accordingly, the above decadal cycle has been designated as 1st, 2nd, 3rd and 4th respectively. The temperature range of the spatial distribution of the decadal average 60-month running mean SST in the 1st to 4th sunspot number cycle were 24.43°C to 30.58°C, 24.81°C to 31.16°C, 24.04°C to 30.41°C and 24.26°C to 30.50°C respectively. The spatial distribution of the standard deviation of decadal SST showed that in the Arabian Sea standard deviation was lesser than the Bay of Bengal.

The analysis of the linear trend line and slopes of the 60-month running mean SST in the northern Indian Ocean, the Arabian Sea and the Bay of Bengal showed that the slope and the trend changed in all the four decadal cycles. In the 1st decadal cycle slope of the SST trend line in the NIO showed a weak increasing trend with a value of 0.0019°C/year. In the Arabian Sea the slope of the trend line showed a weak decline with a value -0.0011°C/year. In contrast, the trend of SST in the Bay of Bengal showed an increase with a value of 0.0061°C/year. In the 2nd decadal cycle, however, the slope of the mean SST in all the three regions, NIO, Arabian Sea and the Bay of Bengal, showed an increasing trend with a value of 0.0153°C/year, 0.0143°C/year and 0.0170°C/year respectively.

In the 3rd decadal cycle the slope of the mean SST in all the three regions showed a decreasing trend with a value of -0.0049°C/year for the NIO, -0.0041°C/year for the Arabian Sea and -0.0059°C/year for the Bay of Bengal. In contrast, in the 4th decadal cycle the slope of the mean SST in all the 3 regions showed an increasing slope with a value of 0.0124°C/year for the NIO, 0.0141°C/year for the Arabian Sea and 0.0101°C/year for the Bay of Bengal.

The most striking feature and salient characteristics that emerged out of the analysis of the area-averaged 60-month running mean SST from 1960 to 2011 was (1) a linear warming trend, (2) presence of dominant decadal cycle riding over this linear warming trend, and (3) disruption of the decadal cycle after 1995. The slope of the linear trend line of SST for the pre-1995 period in the Arabian Sea was lesser than that of the post-1995 period indicating an accelerated warming in the Arabian Sea in the later period. In contrast, in the Bay of Bengal the slope of the linear of SST for the period pre-1995 was greater than that of the post-1995 period indicating a slowdown in the rate of warming in the later period.

The factors that are responsible for the inter-decadal variability of SST form the content of the fourth chapter, which was the second objective of the thesis. The factors affecting the SST trends in 4 different sunspot number cycle periods and in different spatial regions within the northern Indian Ocean are summarised in a tabular form below.

Period	**Region**	**SST trend**	**Factors controlling the SST trend**		
			Wind Speed	**NHF**	**E-P**
1964 to 1975	Eastern Arabian Sea	Decreasing	Yes	Yes	Yes
	Southern Bay of Bengal	Increasing	No	Yes	No
1975 to 1985	Equatorial Arabian Sea	Increasing	Yes	No	Yes
	Equatorial Bay of Bengal	Increasing	No	No	Yes
	South-eastern Arabian Sea	Increasing	No	Yes	No
	South-western Bay of Bengal	Increasing	No	Yes	Yes*
	North-eastern Arabian Sea	Decreasing	Yes	No	Yes

	North-western Bay of Bengal	Decreasing	Yes	No	No
	Western Arabian Sea	Increasing	Yes	No	Yes*
	Off Somali Coast	Decreasing	Yes	No	No
1985 to 1995	Central Bay of Bengal	Decreasing	Yes	Yes	Yes
	Equatorial Arabian Sea	Decreasing	Yes	Yes	No
	Eastern Arabian Sea	Decreasing	Yes	Yes	No
	North-western Bay of Bengal	Increasing	Yes	No	No
1995 to 2008	Southern Arabian Sea	Increasing	No	Yes*	Yes
	Northern Arabian Sea	Increasing	No	Yes	Yes
	Western Arabian Sea	Increasing	Yes	Yes	Yes
	Eastern Arabian Sea	Increasing	No	Yes	No
	North-eastern Bay of Bengal	Increasing	No	Yes	No
	North-western Bay of Bengal	Decreasing	Yes*	No	No
* symbol indicates a part of the region's SST is impacted by a factor					

There are spatially and seasonally differentiated warming pattern in the Arabian Sea which was linked spatially and temporally different ocean-atmospheric processes operating in these regions. The accelerated warming in the post-1995 period in the Arabian Sea was closely linked to the reduced upwelling along the Somali coast which supplies subsurface cooler waters to the upper ocean. The reduced wind speed also contributes to the warming by reducing the evaporative cooling. These processes in tandem with the monotonic increase in the atmospheric CO_2 concentration lead to the observed accelerated warming.

In the Bay of Bengal the slowdown in the warming trend post-1995 was closely linked to the increasing trend in the number of depressions, cyclones and severe cyclones (DCS) in the post-1995 period. These atmospheric systems are capable of transferring large quantities of

subsurface cooler waters to the upper ocean during their life-span. This was examined using a PWP-model forced by heat momentum and freshwater fluxes. When the model was forced by cyclonic winds, the model produced deeper mixed layer thickness corroborating the finding that more number of cyclonic systems in the Bay of Bengal will cool the upper ocean due to the mixing with subsurface cooler waters. Though the increase in the DCS causes the SST to fall, this will counteract the CO_2 concentration induced SST rise. As the increase in the DCS cannot completely offset the CO_2 concentration induced rise in SST, the effect was manifested as a slowdown in the observed SST warming.

The relationship of SST with ENSO and IOD, which was the third objective, formed the content of the fifth chapter. Based on the Dipole Mode Index (DMI) and the Oceanic Nino Index (ONI), the individual years during the study period were classified into nine combinations of ENSO and IOD states which is detailed in the table below.

YEARS	**El Niño**	**ENSO Neutral**	**La Niña**
IOD Positive	1972-73, 1977-78, 1982-83, 1991-92, 1994-95, 1997-98	1961-62, 1963-64, 2006-07	2000-01, 2007-08
IOD Neutral	1965-66, 1968-69, 1976-77, 1986-87, 1987-88, 2002-03, 2004-05, 2009-10	1960-61, 1962-63, 1966-67, 1967-68, 1969-70, 1978-79, 1979-80, 1980-81, 1983-84, 1990-91, 1992-93, 1993-94, 2001-02, 2003-04, 2005-06, 2008-09	1971-72, 1973-74, 1974-75, 1975-76, 1995-96, 1999-00, 2010-11

IOD Negative	NIL	1981-82, 1985-86, 1989-90	1964-65, 1970-71, 1984-85, 1988-89, 1996-97, 1998-99

The most commonly occurred condition was ENSO-neutral and IOD-neutral, while El Nino and IOD negative did not occur at all.

The largest positive SST anomalies were in the El Niño- IOD positive composite years, while the largest negative SST anomalies were in the La Niña- Neutral IOD and La Niña- Negative IOD years for the period 1963 to 1975. The largest positive SST anomalies were in the El Niño- IOD positive year, while the negative SST anomalies of largest magnitudes were seen in the La Niña- Neutral IOD and La Niña- Negative IOD years during the period 1975 to 1986. The largest positive SST anomalies were in the El Niño- IOD neutral years while the largest negative SST anomalies were in the ENSO neutral- IOD negative and in the El Niño- IOD positive years during the period 1986 to 1995. The largest positive SST anomalies were in the El Nino-IOD positive and the largest negative anomalies were in the La Nina-neutral IOD. The analysis showed that the SST anomalies were progressively increasing from the first decadal period (1963-1975) to fourth decadal period (1995-2008) and as the anomalies of SST become more and more positive, the influence of ENSO and IOD becomes weaker.

FUTURE WORK

The work carried out in the present thesis is based purely on the statistical analysis of several kinds of ocean and atmospheric data sets. A simple mixed layer model, PWP, was utilized to explore the mixed layer deepening under the influence of cyclonic wind conditions in the Bay of Bengal for explaining the observed slow down in warming trend.

The future work must utilize climate models to simulate the warming scenarios in the Indian Ocean and ocean-atmosphere coupled model to explore and understand the various oceanic and atmospheric processes in tandem that could explain the response of the Indian Ocean to the future warming.

REFERENCES

Acosta Navarro, J. C., V. Varma, I. Riipinen, Ø. Seland, A. Kirkevåg, H. Struthers, T. Iversen, H.-C. Hansson and A. M. L. Ekman. Amplification of Arctic warming by past air pollution reductions in Europe. *Nature Geoscience,* **9,** 277–281 (2016). doi:10.1038/ngeo2673.

Alory, G., S. Wijffels and G. Meyers. Observed temperature trends in the Indian Ocean over 1960–1999 and associated mechanisms. *Geophysical Research Letters,* **34,** L02606 (2007). doi:10.1029/2006GL028044.

Andreae, M. O. and P. J. Crutzen. Atmospheric Aerosols: Biogeochemical Sources and Role in Atmospheric Chemistry. *Science,* **276,** 1052–1058 (1997). doi: 10.1126/science.276.5315.1052.

Andreae, M. O., W. Elbert and S. J. de Mora. Biogenic sulphur emissions and aerosols over the tropical South Atlantic. 3. Atmospheric dimethylsulfide, aerosols and cloud condensation nuclei. *Journal of Geophysical Research,* **100,** 11335–11356 (1995). doi: 10.1029/94JD02828.

Annamalai, H., S. P. Xie, J. P. McCreary and R. Murtugudde. Impact of the Indian Ocean SST on developing El Niño. *Journal of Climate,* **18,** 302–319 (2005).

Antonov, J. I., D. Seidov, T. P. Boyer, R. A. Locarnini, A. V. Mishonov, H. E. Garcia, O. K. Baranova, M. M. Zweng and D. R. Johnson. World Ocean Atlas 2009, Volume 2: Salinity, in: Levitus S, *NOAA Atlas NESDIS 69*. U.S. Government Printing Office: Washington, D.C., U.S.A. (2010).

Back, L.E. and C. S. Bretherton. On the Relationship between SST Gradients, Boundary Layer Winds, and Convergence over the Tropical Oceans. *Journal of Climate,* **22,** 4182–4196 (2009). doi: 10.1175/2009JCLI2392.1.

Behera, S. K. and T. Yamagata. Subtropical SST dipole events in the southern Indian Ocean. *Geophysical Research Letters*, **28**, 327–330 (2001). doi: 10.1029/2000GL011451.

Charlson, R. J., J. E. Lovelock, M. O. Andreae and S. G. Warren. Oceanic phytoplankton, atmospheric sulphur, cloud albedo and climate. *Nature*, **326,** 655–661 (1987). doi: 10.1038/326655a0.

Church, J. A., J. M. Gregory, N. J. White, S. M. Platten and J. X. Mitrovica. Understanding and projecting sea level change. *Oceanography*, **24**, 130–143 (2011), doi: 10.5670/oceanog.2011.33.

Clark, C. O., P. J. Webster and J. E. Cole. Inter-decadal variability of the relationship between Indian Ocean zonal mode and East African coastal rainfall anomalies. *Journal of Climate*, **16,** 548–554 (2003).

Cohen, J., J. A. Screen, J. C. Furtado, M. Barlow, D. Whittleston, D. Coumou, J. Francis, K. Dethloff, D. Entekhabi, J. Overland and J. Jones. Recent Arctic Amplification and extreme mid-latitude weather. *Nature Geoscience*, **7,** 627–637 (2016). doi: 10.1038/ngeo2234.

Cole, J. E., R. B. Dunbar, T. R. McClanahan and N. A. Muthinga. Tropical Pacific Forcing of Decadal SST Variability in the Western Indian Ocean over the Past Two Centuries. *Science,* **287,** 617–619 (2000). doi: 10.1126/science.287.5453.617.

D'Mello, J.R. and S. Prasanna Kumar. Why the Bay of Bengal is experiencing a reduced rate of sea surface warming? *International Journal of Climatology,* **36,** 1539– 1548 (2016). doi: 10.1002/joc.4414

D'Mello, J. R. and S. Prasanna Kumar. Processes controlling the accelerated-warming of the Arabian Sea. *International Journal of Climatology,* **38,** 1074–1086 (2018, accepted in 2017). doi: 10.1002/joc.5198

Dare, R. A. and J. L. McBride. The Threshold Sea Surface Temperature Condition for Tropical Cyclogenesis. *Journal of Climate,* **24**, 4570–4576 (2011). doi: http://dx.doi.org/10.1175/JCLI-D-10-05006.1.

Deser, C., M. A. Alexander, S.-P. Xie and A. S. Phillips. Sea Surface Temperature Variability: Patterns and Mechanisms. *Annual Review of Marine Science,* **2,** 115–143 (2010). doi: 10.1146/annurev-marine-120408-151453.

Deser, C. A., J. E. Walsh and M. S. Timlin. Arctic Sea Ice Variability in the Context of Recent Atmospheric Circulation Trends. *Journal of Climate,* **13,** 617–633 (2000). doi: http://dx.doi.org/10.1175/1520-0442(2000)013<0617:ASIVIT>2.0.CO;2.

Dinesh Kumar, P. K., Y. Steeven Paul, K. R. Muraleedharan, V. S. N. Murthy, P. R. Preenu. Comparision of the long-term variability of Sea Surface Temperature in the Arabian Sea and Bay of Bengal. *Regional Studies in Marine Science,* **3,** 67–75 (2016). doi:http://dx.doi.org/10.1016/j.rsma.2015.05.004.

Drbohlav, H.-K. L., S. Gualdi and A. Navarra. A Diagnostic Study of the Indian Ocean Dipole Mode in El Niño and Non-El Niño Years. *Journal of Climate,* **20,** 2961–2977 (2007). doi: 10.1175/JCLI4153.1.

Du, Y., S.-P. Xie, G. Huang and K. Hu. Role of air–sea interaction in the long persistence of El Niño–induced north Indian Ocean warming. *Journal of Climate,* **22**, 2023–2038 (2009). doi: 10.1175/2008JCLI2590.1.

Fekete, B. M., C. J. Vorosmarty and W. Grabs. Global Composite Runoff Fields based on observed river discharge and simulated water balances. Global Runoff Data Centre, Koblenz, Germany (2000).

Feng, M. and G. Meyers. Inter-annual variability in the tropical Indian Ocean. A two year time scale of IOD. *Deep-Sea Research,* **11,** 2263–2284 (2003).

Francis, R. C. and S. R. Hare. Decadal-scale regime shifts in the large marine ecosystems of the Northeast Pacific: a case for historical science. *Fisheries Oceanography,* **3,** 279–291 (1994). doi: 10.1111/j.1365-2419.1994.tb00105.x.

Francis, R. C., S. R. Hare, A. B. Hollowed and W. S. Wooster. Effects of interdecadal climate variability on the oceanic ecosystems of the NE Pacific. *Fisheries Oceanography,* **7,** 1–21 (1997). doi: 10.1046/j.1365-2419.1998.00052.x.

Goes, J. I., P. G. Thoppil, H. do Rosario Gomes and J. T. Fasullo. Warming of the Eurasian Landmass is making the Arabian Sea more Productive. *Science,* **308,** 545–547 (2005).

Goldenberg, S. B., C. Landsea, A. M. Mestas-Nuñez, and W. M. Gray. The recent increase in Atlantic hurricane activity. *Science,* **293,** 474–479 (2001).

Han, W., J. Vialard, M. J. McPhaden, T. Lee, Y. Masumoto, M. Feng, and W. P. M. de Ruijter. Indian Ocean Decadal Variability: A Review. *Bulletin of the American Meteorological Society,* **95,** 1679–1703 (2014). doi: http://dx.doi.org/10.1175/BAMS-D-13-00028.1.

Han, W. and P. J. Webster. Forcing Mechanisms of Sea Level Interannual Variability in the Bay of Bengal. *Journal of Physical Oceanography,* **32,** 216–239 (2002).

Hare, S. R. and R. C. Francis. Climate change and salmon production in the Northeast Pacific Ocean. In R. J. Beamish, *Canadian Special Publication of Fisheries and Aquatic Sciences,* **121,** 357–372 (1995).

Hartmann, D. L., A. M. G. Klein Tank, M. Rusticucci, L. V. Alexander, S. Brönnimann, Y. Charabi, F. J. Dentener, E. J. Dlugokencky, D. R. Easterling, A. Kaplan, B. J. Soden, P.W. Thorne, M. Wild and P. M. Zhai, 2013: Observations: Atmosphere and Surface. In: Climate Change 2013: The Physical Science Basis. Contribution of Working Group I to the Fifth Assessment Report of the Intergovernmental Panel on Climate Change [Stocker, T. F., D. Qin, G.-K. Plattner, M. Tignor, S. K. Allen, J. Boschung, A. Nauels, Y. Xia, V. Bex and P. M. Midgley (eds.)]. Cambridge University Press, Cambridge, United Kingdom and New York, NY, USA.

Holte, J., J. Gilson, L. Talley and D. Roemmich. Argo Mixed Layers, Scripps Institution of Oceanography/UCSD (2010). http://mixedlayer.ucsd.edu, accessed 15th October, 2014.

Holte, J. and L. Talley. A New Algorithm for Finding Mixed Layer Depths with Applications to Argo Data and Subantarctic Mode Water Formation. *Journal of Atmospheric and Oceanic Technology,* **26,** 1920–1939 (2009). doi:10.1175/2009JTECHO543.1.

Ihara, C., Y. Kushnir and M. A. Cane. Warming trend of the Indian Ocean SST and Indian Ocean dipole from 1880 to 2004. *Journal of Climate,* **21,** 2035–2046 (2008).

IPCC, 2007: Climate Change 2007: The Physical Science Basis. Contribution of Working Group I to the Fourth Assessment Report of the Intergovernmental Panel on Climate Change

[Solomon, S., D. Qin, M. Manning, Z. Chen, M. Marquis, K.B. Averyt, M. Tignor and H.L. Miller (eds.)]. Cambridge University Press, Cambridge, United Kingdom and New York, NY, USA, 996 pp.

IPCC, 2013: Summary for Policymakers. In: Climate Change 2013: The Physical Science Basis. Contribution of Working Group I to the Fifth Assessment Report of the Intergovernmental Panel on Climate Change [Stocker, T. F., D. Qin, G.-K. Plattner, M. Tignor, S. K. Allen, J. Boschung, A. Nauels, Y. Xia, V. Bex and P. M. Midgley (eds.)]. Cambridge University Press, Cambridge, United Kingdom and New York, NY, USA.

Kalnay, E., M. Kanamitsu, R. Kistler, W. Collins, D. Deaven, L. Gandin, M. Iredell, S. Saha, G. White, J. Woollen, Y. Zhu, A. Leetmaa, R. Reynolds, M. Chelliah, W. Ebisuzaki, W. Higgins, J. Janowiak, K. C. Mo, C. Ropelewski, J. Wang, R. Jenne and D. Joseph. The NCEP/NCAR 40-year reanalysis project. *Bulletin of the American Meteorological Society*, **77,** 437–470 (1996). doi: http://dx.doi.org/10.1175/1520-0477(1996)077<0437:TNYRP>2.0.CO;2.

Kaufman,Y. J., I. Koren, L. A. Remer, D. Rosenfeld and Y. Rudich. The effect of smoke, dust, and pollution aerosol on shallow cloud development over the Atlantic Ocean. *Proceedings of the National Academy of Sciences of the United States of America,* **102,** 11207–11212 (2005). doi: 10.1073/pnas.0505191102.

Keeling, C.D., S. C. Piper, R. B. Bacastow, M. Wahlen, T. P. Whorf, M. Heimann and H. A. Meijer. Exchanges of atmospheric CO_2 and $^{13}CO_2$ with the terrestrial biosphere and oceans from 1978 to 2000. I. Global aspects, SIO Reference Series, No. 01-06, Scripps Institution of Oceanography, San Diego, 88 pages (2001).

Keerthi, M. G., M. Lengaigne, J. Vialard, C. de Boyer Montégut and P. M. Muraleedharan. Interannual variability of the Tropical Indian Ocean mixed layer depth. *Climate Dynamics,* **40,** 743–759 (2013). doi: 10.1007/s00382-012-1295-2.

Kiehl, J. T. and K. E. Trenberth. Earth's Annual Global Mean Energy Budget. *Bulletin of the American Meteorological Society,* **78,** 197–208 (1997). doi: http://dx.doi.org/10.1175/1520-0477(1997)078<0197:EAGMEB>2.0.CO;2.

Klein, S. A., B. J. Soden and N. C. Lau. Remote Sea Surface Temperature variations during ENSO: Evidence for a tropical atmospheric bridge. *Journal of Climate,* **12,** 917–932 (1999). doi:10.1175/1520-0442(1999)0122.0.CO;2.

Krishnamurthy, V. and B. P. Kirtman. Variability of the Indian Ocean: relation to monsoon and ENSO. *Quarternary Journal of the Royal Meteorological Society,* **129,** 1623–1646 (2003).

Lee, S. A theory for polar amplification from a general circulation perspective. *Asia-Pacific Journal of Atmospheric Sciences*, **50,** 31–43 (2014). doi: 10.1007/s13143-014-0024-7.

Levitus, S., J. I. Antonov and T. P. Bayer. Warming of the World Ocean, 1955-3003. *Geophysical Research Letters,* **32,** L2604, doi: 10.1029/2004GL021592 (2005).

Locarnini, R. A., A. V. Mishonov, J. I. Antonov, T. P. Boyer, H. E. Garcia, O. K. Baranova, M. M. Zweng and D. R. Johnson. World Ocean Atlas 2009, Volume 1: Temperature, in: Levitus, S., *NOAA Atlas NESDIS 68*. U.S. Government Printing Office: Washington, D.C. (2010).

Loeb, N. G., B. A. Wielicki, D. R. Doelling, G. L. Smith, D. F. Keyes, S. Kato, N. Manalo-Smith and T. Wong. Toward Optimal Closure of the Earth's Top-of-Atmosphere Radiation

Budget. *Journal of Climate,* **22,** 748–766 (2009). doi: https://doi.org/10.1175/2008JCLI2637.1

Lovelock, J. E., 2007. The Revenge of Gaia. Penguin, ISBN 0-14-102597-2.

Madden, R. and P. Julian. Observations of the 40-50 day tropical oscillation: A review. *Monthly Weather Review,* **112,** 814–837 (1994).

Manabe, S. and R. T. Wetherald. The effect of doubling the CO_2 concentration on the climate of a general circulation model. *Journal of the Atmospheric Sciences,* **32,** 3–15 (1975). doi: http://dx.doi.org/10.1175/1520-0469(1975)032<0003:TEODTC>2.0.CO;2.

Mandke, S. K. and U. V. Bhide. A study of decreasing storm frequency over Bay of Bengal. *Journal of Indian Geophysical Union,* **7,** 53–58 (2003).

Mantua, N. J., S. R. Hare, Y. Zhang, J. M. Wallace and R. C. Francis. A Pacific decadal climate oscillation with impacts on salmon. *Bulletin of the American Meteorological Society,* **78,** 1069–1079 (1997).

McCreary, J. P., P. K. Kundu and R. L. Molinari. A numerical investigation of dynamics, thermodynamics and mixed-layer processes in the Indian Ocean. *Progress in Oceanography,* **21**, 181–244 (1993).

Meyers, G., P. McIntosh, L. Pigot and M. Pook. The years of El Niño, La Niña, and Interactions with the Tropical Indian Ocean. *Journal of Climate,* **20,** 2872–2880 (2007). doi: https://doi.org/10.1175/JCLI4152.1

Milankovitch, M., 1941. Kanon der Erdbestrahlung, Royal Serbian Academy Special Publication. 132, Sect. Math. Nat. Sci., 33. (Canon of insolation and the ice-age problem, English translation by Israel Program for Scientific Translations, Jerusalem, 1969.)

Milankovitch, M. M., 1920. Théorie Mathématique des Phénomènes Thermiques Produits par la Radiation Solaire. Academie Yougoslave des Sciences et des Arts de Zagreb, Gauthier-Villars, Paris.

Miller, A. J., D. R. Cayan, T. P. Barnett, N. E. Graham and J. M. Oberhuber. The 1976–77 Climate Shift of the Pacific Ocean. *Oceanography*, **7,** 21–26 (1994).

Milne, G. A., W. Roland Gehrels, C. W. Hughes and M. E. Tamisiea. Identifying the causes of sea level change. *Nature Geoscience*, **2**, 471–478 (2009). doi: 10.1038/ngeo544.

Molinari, R. L. and A. M. Mestas-Nuñez. North Atlantic decadal variability and the formation of tropical storms and hurricanes. *Geophysical Research Letters*, **30,** 1541, (2003). doi: 10.1029/2002GL016462.

Morioka, Y., T. Tozuka, S. Masson, P. Terray, J.-J. Luo and T. Yamagata. Subtropical dipole modes simulated in a coupled general circulation model. *Journal of Climate*, **25**, 4029–4047 (2012). doi: 10.1175/JCLI-D-11-00396.1.

Morioka, Y., T. Tozuka and T. Yamagata. How is the Indian Ocean subtropical dipole excited? *Climate Dynamics*, **41**, 1955–1968 (2013). doi: 10.1007/s00382-012-1584-9.

Nitta, T. and S. Yamada. Recent Warming of Tropical Sea Surface Temperature and its Relationship to the Northern Hemisphere Circulation. *Journal of the Meteorological Society of Japan*, **67,** 375–383 (1989).

O'Neill, L. W. Wind Speed and Stability Effects on Coupling between Surface Wind Stress and SST Observed from Buoys and Satellite. *Journal of Climate,* **25,** 1544–1569 (2012). doi: http://dx.doi.org/10.1175/JCLI-D-11-00121.1.

Prasanna Kumar, S., R. P. Roshin, J. Narvekar, P. K. Dinesh Kumar and E. Vivekanandan. Response of the Arabian Sea to global warming and associated regional climate shift. *Marine Environmental Research,* **68,** 217–222 (2009).

Price, J. F., C. N. K. Mooers and L. C. van Leer. Observation and simulation of storm-induced mixed-layer deepening. *Journal of Physical Oceanography,* **8**, 582–599 (1978). doi: http://dx.doi.org/10.1175/1520-0485(1978)008<0582:OASOSI>2.0.CO;2.

Price J. F., R. A. Weller and R. Pinkel. Diurnal cycling: observations and models of the upper ocean response to diurnal heating, cooling, and wind mixing. *Journal of Geophysical Research,* **91**, 8411–8427 (1986). doi: 10.1029/JC091iC07p08411.

Rao, R. R., M. S. Girish Kumar, M. Ravichandran, A. R. Rao, V. V. Gopalakrishna and P. Thadathil. Interannual variability of Kelvin wave propagation in the wave guides of the equatorial Indian Ocean, the coastal Bay of Bengal and the southeastern Arabian Sea during 1993-2006. *Deep-Sea Research I,* **57,** 1–13 (2010).

Rhein, M., S. R. Rintoul, S. Aoki, E. Campos, D. Chambers, R. A. Feely, S. Gulev, G. C. Johnson, S. A. Josey, A. Kostianoy, C. Mauritzen, D. Roemmich, L. D. Talley and F. Wang, 2013: Observations: Ocean. In: Climate Change 2013: The Physical Science Basis. Contribution of Working Group I to the Fifth Assessment Report of the Intergovernmental Panel on Climate Change [Stocker, T. F., D. Qin, G.-K. Plattner, M. Tignor, S. K. Allen, J. Boschung, A. Nauels, Y. Xia, V. Bex and P. M. Midgley (eds.)]. Cambridge University Press, Cambridge, United Kingdom and NewYork, NY, USA.

Rowell, D. P., C. K. Folland, K. Maskell and M. N. Ward. Variability of summer rainfall over tropical North-Africa (1906–92) observations and modelling. *Quarterly Journal of the Royal Meteorological Society,* **121,** 669–704 (1995).

Roxy, M. K., K. Ritika, P. Terray and S. Masson. The Curious Case of Indian Ocean Warming. *Journal of Climate,* **27,** 8501–8509, (2014). doi:http://dx.doi.org/10.1175/JCLI-D-14-00471.1.

Rupa Kumar, S., K. Krishna Kumar, R. G. Ashrit, S. K. Patwardhan and G. B. Pant. Climate Change in India: observations and model projections. In: P. R. Shukla, S. K. Sharma, P. Venkata Ramana (Eds.), Climate Change and India: Issues concerns and oppurtunities. Tata McGraw-Hill Publishing Company Limited, New Delhi (2002).

Saji, N. H., B. N. Goswami, P. N. Vinayachandran and T. Yamagata. A dipole mode in the tropical Indian Ocean. *Nature,* **401,** 360–363 (1999). doi:10.1038/43854.

Schlesinger, M. E. and N. Ramankutty. An oscillation in the global climate system of period 65–70 years. *Nature,* **367,** 723–726 (1994).

Schuur, E. A. G., J. G. Vogel, K. G. Crummer, H. Lee, J. O. Sickman and T. E. Osternkamp. The effect of permafrost thaw on old carbon release and net carbon exchange from tundra. *Nature,* **459,** 556–559 (2009). doi: 10.1038/nature08031.

Somayajulu, Y. K., V. S. N. Murty and Y. V. B. Sarma. Seasonal and inter-annual variability of surface circulation in the Bay of Bengal from TOPEX/Poseidon altimetry. *Deep-Sea Research II,* **50,** 867–880 (2003).

Suzuki, R., S. K. Behera, S. Iizuka and T. Yamagata. Indian Ocean subtropical dipole simulated using a coupled general circulation model. *Journal of Geophysical Research,* **109**, C09001 (2004). doi: 10.1029/2003JC001974.

Tang, Y. The Effect of variable Sea Surface Temperature on Forecasting Sea Fog and Sea Breezes: A case study. *Journal of Applied Meteorology and Climatology,* **51,** 986–990 (2012). doi: http://dx.doi.org/10.1175/JAMC-D-11-0253.1.

Tourre, Y. M. and W. B. White. ENSO Signals in the global upper-ocean temperature. *Journal of Physical Oceanography*, **25,** 1317–1332 (1995).

Tourre, Y. M. and W. B. White. Evolution of the ENSO signal over the Indo-Pacific domain. *Journal of Physical Oceanography*, **27,** 683–696 (1997).

Trenberth, K. E. Recent observed inter-decadal climate changes in the northern hemisphere. *Bulletin of the American Meteorological Society*, **71,** 988–993 (1990).

Trenberth, K. E., J. T. Fasullo and J. Kiehl. Earth's Global Energy Budget. *Bulletin of the American Meteorological Society,* **90,** 311–323 (2009). doi: https://doi.org/10.1175/2008BAMS2634.1

Trenberth, K. E. and T. J. Hoar. El Niño and climate change. *Geophysical Research Letters,* **24,** 3057–3060 (1997). doi: 10.1029/97GL03092

Trenberth, K. E., P. D. Jones, P. Ambenje, R. Bojariu, D. Easterling, A. Klein Tank, D. Parker, F. Rahimzadeh, J. A. Renwick, M. Rusticucci, B. Soden and P. Zhai, 2007: Observations: Surface and Atmospheric Climate Change. In: Climate Change 2007: The Physical Science Basis. Contribution of Working Group I to the Fourth Assessment Report of the Intergovernmental Panel on Climate Change [Solomon, S., D. Qin, M. Manning, Z. Chen,

M. Marquis, K.B. Averyt, M. Tignor and H.L. Miller (eds.)]. Cambridge University Press, Cambridge, United Kingdom and New York, NY, USA.

Trenberth, K. E. and D. J. Shea. Atlantic hurricanes and natural variability in 2005. *Geophysical Reserach Letters,* **33,** L12704 (2006). doi:10.1029/2006GL026894.

Vaithiyanathan, P., A. L. Ramanathan and V. Subramanian. Erosion, Transport and Deposition of sediments by the tropical rivers of India. *Sediment Budgets,* **174,** 561–574 (1988).

Wang, C., S. Dong, A. T. Evan, G. R. Foltz and S.-K. Lee. Multidecadal Covariability of North Atlantic Sea Surface Temperature SST, African Dust, Sahel Rainfall and Atlantic Hurricanes. *Journal of Climate,* **25,** 5404–5415 (2012). doi: http://dx.doi.org/10.1175/JCLI-D-11-00413.1.

Webster, P. J., A. M. Moore, J. P. Loschnigg and R. P. Leben. Coupled ocean-atmosphere dynamics in the Indian Ocean during 1997–98. *Nature,* **401,** 356–360 (1999). doi:10.1038/43848.

White, W. B., J. Lean, D. R. Cayan and M. D. Dettinger. Response of global upper ocean temperature to changing solar irradiance. *Journal of Geophysical Research,* **102,** 3255–3266 (1997). doi: 10.1029/96JC03549.

White, W. B. and R. G. Peterson. An Antarctic circumpolar wave in surface pressure, wind, temperature, and sea-ice extent. *Nature,* **380**, 699–702 (1996). doi: 10.1038/380699a0.

Willson, R. C. and H. S. Hudson. Solar luminosity variations in solar cycle 21. *Nature,* **332,** 810–812 (1988). doi: 10.1038/332810a0.

Woodruff, S. D., S. J. Worley, S. J. Lubker, Z. Ji, J. E. Freeman, D. I. Berry, P. Brohan, E. C. Kent, R. W. Reynolds, S. R. Smith and C. Wilkinson. ICOADS Release 2.5: Extensions and enhancements to the surface marine meteorological archive. *International Journal of Climatology* (CLIMAR-III Special Issue), **31,** 951–967 (2011). doi: 10.1002/joc.2103.

Wyrtki, K. Oceanographic Atlas of the International Indian Ocean Expedition. *National Science Foundation Publication/* ***NSF*** **86-00-01,** pp. 531 (1971).

Xie, S.-P., C. Deser, G. A. Vecchi, J. Ma, H. Teng and A. T. Wittenburg. Global Warming Pattern Formation: Sea Surface Temperature and Rainfall. *Journal of Climate,* **23,** 966–986 (2010). doi: http://dx.doi.org/10.1175/2009JCLI3329.1.

Yu, L. and M. M. Rienecker. Mechanism of the Indian Ocean warming during the 1997-98 El Niño. *Geophysical Research Letters,* **26,** 735–738 (1999).

Yu, L., X. Jin and R. P. Weller. Annual, Seasonal and Inter-annual variability of Air-Sea Heat Fluxes in the Indian Ocean. *Journal of Climate,* **20,** 3190–3209 (2007).

Yu, L., X. Jin and R. A. Weller. Multidecade Global Flux Datasets from the Objectively Analyzed Air-sea Fluxes (OAFlux) Project: Latent and sensible heat fluxes, ocean evaporation, and related surface meteorological variables. Woods Hole Oceanographic Institution, OAFlux Project Technical Report. OA-2008-01, 64pp. Woods Hole. Massachusetts (2008).

Zhong, A., H. H. Hendon and O. Alves. Indian Ocean variability and its association with ENSO in a global coupled model. *Journal of Climate,* **18,** 3634–3649 (2005).

Zimov, S. A., E. A. G. Schuur and F. S. Chapin III. Permafrost and the Global Ocean Budget. *Science,* 312, 1612–1613 (2006). doi: 10.1126/science.1128908.

http://apdrc.soest.hawaii.edu/dchart/ index.html?dset=a2c287de3ad7cab9999e50371916fe

http://apdrc.soest.hawaii.edu/dods/public_data/satellite_product/ifremer/daily_flux

http://burnanenergyjournal.com/wp-content/uploads/2011/05/atmospheric.gif

http://www.climatekelpie.com.au/understand-climate/climate-science/carbon-dioxide-and-temperature-the-relationship

ftp://ftp.cmdl.noaa.gov/ccg/co2/trends/co2_mm_gl.txt

ftp://ftp.cmdl.noaa.gov/ccg/co2/trends/co2_mm_mlo.txt

https://commons.wikimedia.org/w/index.php?curid=32285340

https://commons.wikimedia.org/w/index.php?curid=58530710

http://www.compositerunoff.sr.unh.edu

http://www.cpc.noaa.gov/products/analysis_monitoring/ensostuff/ensofaq.shtml#DIFFER

http://dss.ucar.edu/datasets/ds260.1/

https://en.wikipedia.org/wiki/Earth%27s_energy_budget

http://www.esrl.noaa.gov/psd/cgi-bin/db_search/

www.esrl.noaa.gov/psd/data/gridded/data.coads.1deg.html

http://www.esrl.noaa.gov/psd/data/gridded/data.ncep.reanalysis.derived.surfaceflux.html

http://www.esrl.noaa.gov/psd/data/gridded/data.ncep.reanalysis.derived. otherflux.html

http://www.ifremer.fr/cerweb/deboyer/mld/Surface_Mixed_Layer_ Depth.php

http://mixedlayer.ucsd.edu/data/monthlyclim.nc

ftp://ftp.ngdc.noaa.gov/STP/SOLAR_DATA/SUNSPOT_NUMBERS/INTERNATIONAL/monthly/MONTHLY

http://www.nodc.noaa.gov/OC5/WOA09/ netcdf_data.html

http://oaflux.whoi.edu

http://oceanworld.tamu.edu/resources/ocng_textbook/chapter06/chapter06_06.htm

https://podaac.jpl.nasa.gov/SeaSurfaceTemperature

http://www.rmcchennaieatlas.tn.nic.in/login.aspx?ReturnUrl=%2f

http://www.sage.wisc.edu/riverdata/scripts/ station_table.php?qual=32&filenum=1114

http://science-edu.larc.nasa.gov/energy_budget/

http://sidc.oma.be/sunspot-data/

ftp://ftp.whoi.edu/pub/science/oaflux/data_v3/daily/ evaporation/

INTERNATIONAL JOURNAL OF CLIMATOLOGY
Int. J. Climatol. **36**: 1539–1548 (2016)
Published online 6 August 2015 in Wiley Online Library
(wileyonlinelibrary.com) DOI: 10.1002/joc.4414

RMetS
Royal Meteorological Society

Short Communication

Why is the Bay of Bengal experiencing a reduced rate of sea surface warming?

Joshua Rosario D'Mello and S. Prasanna Kumar*

CSIR-National Institute of Oceanography, Dona Paula, India

ABSTRACT: The sea surface temperature (SST) in the Bay of Bengal (BoB) during the period 1960–1995 showed a decadal cycle, riding over a warming trend. The disruption of the decadal cycle was noticed post-1995 and was followed by a slowdown in the sea surface warming. The cause for the disruption of the SST decadal cycle was the weakening of the link between SST and sunspot number. The rising trend in the SST is due to the increasing atmospheric CO_2 concentration. The post-1995 SST slowdown was due to the increasing influence of the number of depressions, cyclones and severe cyclones in the BoB, the occurrence of which showed an upward trend. Using Price–Weller–Pinkel model we show that cyclonic systems deepen the mixed-layer through enhanced mechanical-mixing with cooler sub-surface waters, thereby reducing the mixed-layer temperature and consequently the SST. This process opposes the SST rise due to increasing atmospheric CO_2 concentration. The net effect of the wind-mixing caused by the increased number of depressions, cyclones and severe cyclones and the increased CO_2 concentration is a SST slowdown in the BoB. This mechanism differs from the SST slowdown mechanisms suggested for the Atlantic and the Pacific.

KEY WORDS SST slowdown; decadal cycle; Bay of Bengal; wind-mixing; Ekman-pumping; regional climate change; sea surface temperature

Received 4 December 2014; Revised 15 May 2015; Accepted 21 May 2015

1. Introduction

The Bay of Bengal (BoB), located in the eastern part of the northern Indian Ocean, has unique geographic and climatic setting. Being bound to its north (~23°N) by the Asian landmass, the basin's water has no link to the polar waters. Besides, the basin's waters experience seasonal wind reversal associated with Asian monsoons, having south-westerly winds during summer monsoon (June to September) and north-easterly winds during winter monsoon (November to February). The south-westerly winds are generally warm and moist, while the north-easterly winds are cold and dry (Prasanna Kumar and Narvekar, 2005). In response to this reversal in wind direction the surface current also reverses in the basin. The BoB has one of the lowest surface salinities of the world oceans, which arises due to (1) excess evaporation over precipitation (~2 m year^{-1}) (Prasad, 1997) and (2) fresh water influx from adjoining rivers (1.625×10^{12} m^3 year^{-1}) (Subramanian, 1993).

Seasonality being the dominant mode of variability in the BoB, seasonal cycle of hydrography and circulation is well researched and documented (see for e.g., Potemra *et al.*, 1991; McCreary *et al.*, 1993; Shetye *et al.*, 1996; Rao and Sivakumar, 2000, 2003; Schott and McCreary, 2001, Shankar *et al.*, 2002; Varkey *et al.*, 1996 and references therein). However, the slower modes such as multi-annual and especially the decadal variability are less explored, making our understanding of the long-term variability of the Indian Ocean, in the context of climate change, rudimentary. In contrast there had been some studies pertaining to the slowdown in the sea surface temperature (SST) warming in the Pacific and the Atlantic (Kosaka and Xie, 2013; Trenberth and Fasullo, 2013; Chen and Tung, 2014; McGregor *et al.,* 2014; Trenberth *et al.*, 2014) oceans. Rupa Kumar *et al.* (2002) was the first to show that the Indian Ocean was warming at the rate of 0.5 °C per 100 years, based on the analysis of SST data during 1904–1994. Subsequently, Prasanna Kumar *et al.* (2009) showed that the Arabian Sea is experiencing a secular warming and a regional climate shift after mid-1990 based on analysis of SST data during 1960–2005. However, no such studies on long-term variability are available in the case of the BoB. It is in this context that in the present study, using 52 years of SST data, we (1) examine the long-term SST trend, (2) decipher the recent change in the rate of warming, and finally (3) identify the factors responsible for the observed changes.

* Correspondence to: S. Prasanna Kumar, CSIR-National Institute of Oceanography (CSIR-NIO), Dona Paula 403 004, Goa, India. E-mail: prasanna@nio.org

2. Materials and methods

2.1. Data

The BoB (0° to 25°N and 80°E to 99°E) SST, u-wind and v-wind components data were extracted from the International Comprehensive Ocean-Atmosphere Data Set (ICOADS) (Woodruff *et al.*, 2005; www.esrl.noaa.gov/psd/data/gridded/data.coads.1deg.html) for the period 1960–2011, having monthly mean values on a 1° by 1° spatial grid. Using the monthly mean SST data, a 60-month running mean was computed for further analysis. We used sunspot number as a proxy for the solar irradiance (Willson and Hudson, 1988) as the latter is available only from 1975. The monthly values of the international sunspot number (Solar Influences Data analysis Centre (SIDC) team, 2012), now available at http://sidc.oma.be/sunspot-data/, were obtained from ftp://ftp.ngdc.noaa.gov/STP/SOLAR_DATA/SUNSPOT_NUMBERS/INTERNATIONAL/monthly/MONTHLY. The annual mean global carbon dioxide concentration data were obtained by merging the carbon dioxide concentration at Mauna Loa from 1958 March to 1979 December (ftp://ftp.cmdl.noaa.gov/ccg/co2/trends/co2_mm_mlo.txt) with the global carbon dioxide concentration data from 1980 January to 2011 December (ftp://ftp.cmdl.noaa.gov/ccg/co2/trends/co2_mm_gl.txt) (Keeling *et al.*, 2001). Data on the number of depressions, cyclones and severe cyclonic storms (DCS) in the BoB was taken from e-atlas of India Meteorological Department available at http://www.rmcchennaieatlas.tn.nic.in/login.aspx?ReturnUrl=%2f for the period 1960–2011.

The evaporation rate was taken from Objectively Analyzed Air-Sea Fluxes (OAFlux; http://dss.ucar.edu/datasets/ds260.1/; Yu *et al.*, 2008), while the precipitation rate was from the climate diagnostic centre (CDC) derived NCEP reanalysis products (http://www.esrl.noaa.gov/psd/cgi-bin/db_search/). The monthly gridded data of the short wave radiation, long wave radiation, latent heat flux and sensible heat flux were from the National Centres for Environmental Prediction/National Centre for Atmospheric Research (NCEP/NCAR) Reanalysis Monthly Means and Other Derived Variables data (Kalnay *et al.*, 1996) and were obtained from (http://www.esrl.noaa.gov/psd/data/gridded/data.ncep.reanalysis.derived.surfaceflux.html).

For comparing the model mixed layer depth (MLD), the data on the MLDs were taken from Holte *et al.* (2010; (http://mixedlayer.ucsd.edu/data/monthlyclim.nc) and Keerthi *et al.* (2013; www.ifremer.fr/cerweb/deboyer/mld/Surface_Mixed_Layer_Depth.php). In Holte *et al.* (2010) the MLD climatology was computed using Argo profiles and a hybrid method (Holte and Talley, 2009), while in Keerthi *et al.* (2013) the monthly MLD data for the Indian Ocean, during 1969–2009 was based on temperature and salinity profiles taken from different sources namely National Oceanographic Data Centre (NODC) World Ocean Database 2009 (WOD 09), World Ocean Circulation Experiment (WOCE) global dataset version 3.0, Argo profile data and Tropical Atmosphere Ocean project Research moored Array for the African-Asian-Australian Monsoon Analysis and prediction (TAO RAMA) buoy daily data. Using this data monthly mean climatology (1969–2009) was computed for comparing with PWP model output.

Data used for plotting the schematic on SST cooling associated with the passage of cyclone Nargis during 27 April to 3 May 2008 is as follows. The SST data is for 2 May 2008 from NOAA daily Optimum Interpolation SST (OISST) obtained from http://www.ncdc.noaa.gov/sst/griddata.php (Reynolds *et al.*, 2007). The vertical temperature data along the 90°E (5-day average centred at 2 May) and 1.5°S (5-day average centred at 3 May) sections (http://www.pmel.noaa.gov/tao/disdel/frames/main.html) are from Research moored Array for African-Asian-Australian Monsoon Analysis and prediction (RAMA) moorings. Daily RAMA mooring data is also used to calculate the cooling by Cyclone Nargis, at the (15°N, 90°E) location. The cyclone track data is from http://weather.unisys.com/hurricane/n_indian/2008H/NARGIS/track.dat.

2.2. Model: Price–Weller–Pinkel model

The Price–Weller–Pinkel (PWP) model (Price *et al.*, 1986) is a mixed-layer model similar to the dynamic instability model of Price *et al.* (1978), but modified to include mixing in the stratified fluid, below the mixed-layer. The model takes into account mixing processes namely (1) free convection arising due to surface heat loss, (2) mixed-layer entrainment by relaxation and (3) shear flow instability driven mixing. More details about the model and the data used to run it are given in the Appendix S1, Supporting Information.

3. Results and discussion

The basin-averaged SST variability is examined to study the dominant variability during the study period from 1960 January to 2011 December. Then the role of the sunspot number and atmospheric CO_2 concentrations, are studied in the mediation of the observed changes. Finally, the PWP model helped to show the mixed-layer deepening and cooling by cyclonic systems, to explain the reason for SST slowdown.

3.1. Decadal cycle and SST warming

The salient feature, of the basin-averaged 60-month running mean monthly SST in the BoB, was a dominant decadal cycle riding over a secular warming trend of 0.014 °C per year (coefficient of determination, $R^2 = 0.88$) during the period 1960–2011 (Figure 1).

The second important feature was the disruption in the decadal cycle as well as the change in the warming trend after 1995. Note that 1995 November is the minimum of the 60-month running mean of the sunspot number cycles, occurring closest to the start of the disrupted SST cycle. Hence it has been chosen as the year for dividing the period

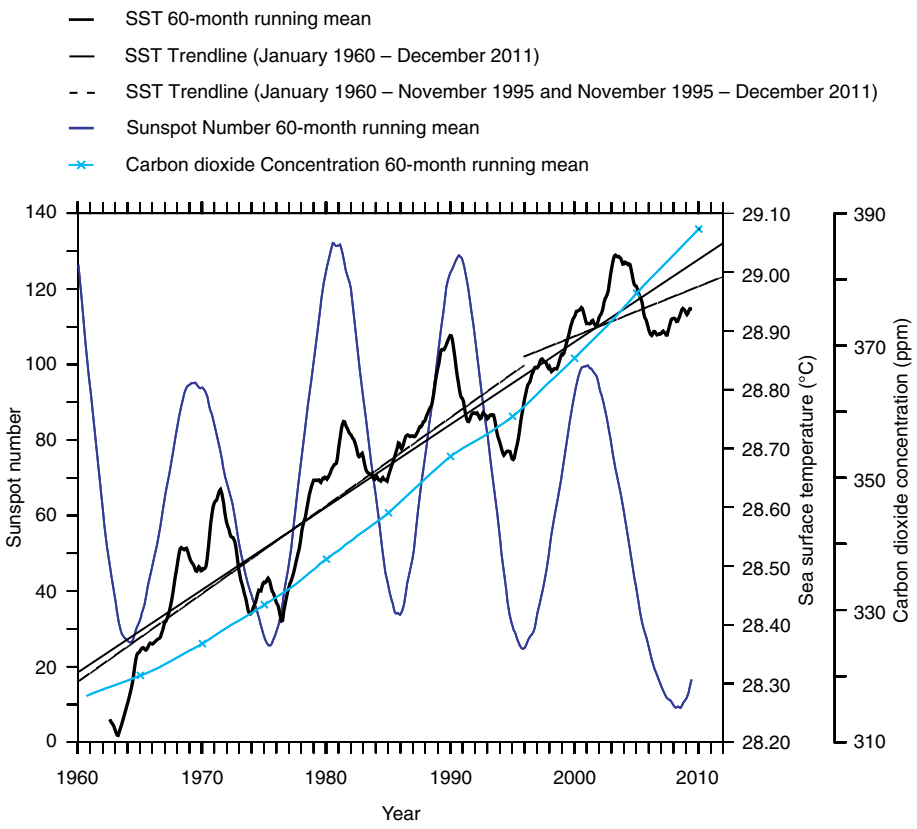

Figure 1. Basin-averaged 60-month running means of Bay of Bengal (Eq. to 25°N, 80–99°E) SST (thickest line), international sunspot number (thick line) and carbon dioxide concentration (thick line with cross marks) for the period 1960 January to 2011 December. SST trend line for the entire period of study (thin line) and pre-1995 and post-1995 SST trend lines (thin dashed lines) are also shown.

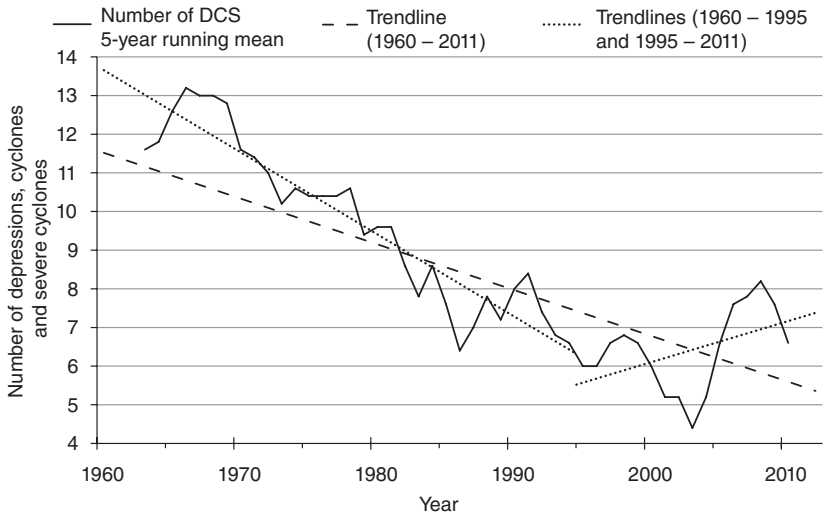

Figure 2. Five-year running mean of the total number of DCS in the Bay of Bengal (Eq. to 25°N, 80–99°E) (solid line) for the period from 1960 to 2011. Trend lines for the entire period of study (dashed line) and in the pre-1995 and post-1995 periods (dotted lines) are also shown.

of study in order to infer the warming trend. Thus, prior to 1995, the trend line of SST showed a warming with a slope of 0.015 °C per year ($R^2 = 0.79$), which slowed down to 0.008 °C per year ($R^2 = 0.35$), after 1995. All the three SST slopes have p-values lesser than 0.05 indicating a significance level of greater than 95%. The difference of the pre-1995 and post-1995 SST slopes also showed a similar p-value.

It has been shown that the natural decadal cycle is closely related to the solar activity (White *et al.*, 1997). An examination of the sunspot number revealed a smooth decadal cycle that co-varied with SST until 1995 (Figure 1). After 1995, though the sunspot number cycle continued its decadal cycle without any disruption, the SST did not show a commensurate decrease with the decreasing sunspot number. In fact, SST continued to increase even

Table 1. Bay of Bengal partial correlation coefficients (r) and significance levels, between the 60-month running mean of SST and the 60-month running mean of the various parameters, viz. the net heat flux (NHF), wind speed (i.e. momentum flux), difference between evaporation and precipitation (E – P) (i.e. freshwater flux) and the number of DCS, in different periods.

Partial correlation	Period	NHF		Wind speed		Number of DCS		E – P	
		r	Significance level (%)	r	Significance level (%)	r	Significance level (%)	r	Significance level (%)
SST	1960–2011	**0.53**	**>99.99**	**0.56**	**>99.99**	**−0.26**	**>99.99**	−0.10	97.62
	1960–1995	**0.60**	**>99.99**	**0.47**	**>99.99**	−0.14	99.44	**−0.59**	**>99.99**
	1995–2011	0.29	99.98	0.17	99.13	**−0.59**	**>99.99**	0.25	99.89

Both partial correlation and significance levels values are in bold face, when significance level is greater than 99.99%.

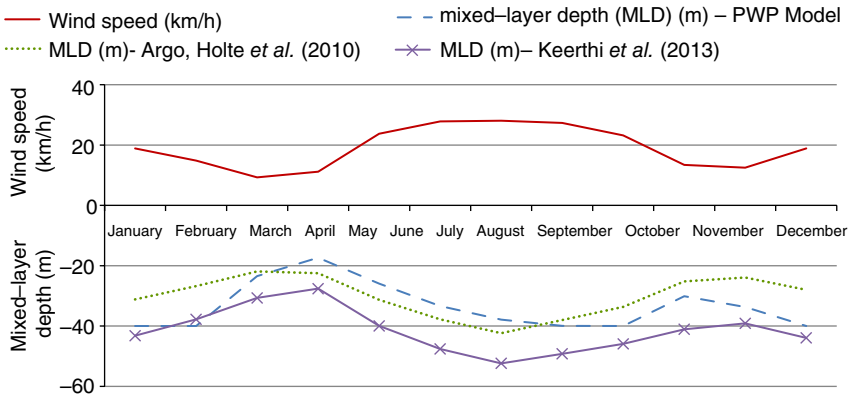

Figure 3. Seasonal cycle of wind speed ($m\,s^{-1}$) (solid line) and mixed-layer depths (m) in the Bay of Bengal from PWP model (dashed line), Holte *et al.* (2010) (dotted line) and Keerthi *et al.* (2013) (line with cross marks).

when the sunspot number cycle started decreasing after 2000. A brief period of decrease in SST was noticed during 2004–2006, before the beginning of the next decadal cycle. Thus, we see a strong link between the decadal cycles of the SST and sunspot number until 1995. This link not only weakens after 1995, a slowdown of SST warming was also observed.

3.2. Correlation of SST with sunspot number and CO_2 concentration

We explored the probable reasons for the observed disruption of decadal cycle and decline in the rate of warming in the BoB after 1995. The solar activity being the primary driver of the decadal variability in the ocean, we examined the correlation coefficient of SST with sunspot number cycle.

The correlation coefficient (r) of the 60-month running means of sunspot number and SST in the various pre-1995 sunspot number cycle periods are high, with $r = 0.66$, 0.63 and 0.78 (all significant at >99.99%), for the periods centred from March 1964 to June 1975, June 1975 to December 1985 and December 1985 to November 1995, respectively. During 1960–1995, when the SST showed an increase, the correlation coefficient with sunspot cycle was 0.58 (significance level >99.99%) and after 1995 it reduced to 0.24 (significance level = 99.82%). Similarly, the correlation coefficient of SST with CO_2 was 0.88 (significance level >99.99%) during 1960–1995 period, which also declined to 0.54 (significance level >99.99%) for the period from 1995 to 2011. Thus, the reduced warming despite the increase in the CO_2 concentration after 1995 indicated that this could be due to reasons other than the CO_2 forcing. We now address the reasons for the reduced warming and identify the processes responsible for it.

3.3. Processes linked to the slowdown in warming

The processes that could reduce the SST in the ocean are (1) upwelling, (2) evaporative cooling, (3) wind-driven/convective mixing and (4) Ekman-pumping. The BoB is not known for the prevalence of strong upwelling except for very localized regions close to the south-western boundary (Shetye *et al.*, 1991) and south of Sri Lanka (Vinayachandran and Yamagata, 1998), during summer monsoon. Evaporative cooling is a process which reduces the surface temperature consequent to the release of latent heat flux to the atmosphere. This could occur either due to an increase in wind speed, which is normally encountered during summer monsoon or with the prevalence of dry air blowing over the ocean as it occurs during winter monsoon (Prasanna Kumar and Narvekar, 2005). The wind-driven mixing, on the other hand, can cool the surface temperature of the ocean by mixing the warm upper ocean water with cold sub-surface water through mechanical-mixing and deepening of mixed layer. This process could potentially lower the SST in the BoB during summer monsoon when the basin-wide wind speeds are the highest. However, though a basin-wide lowering of SST was noticed during summer monsoon the mixed-layer was not very deep, especially in the northern

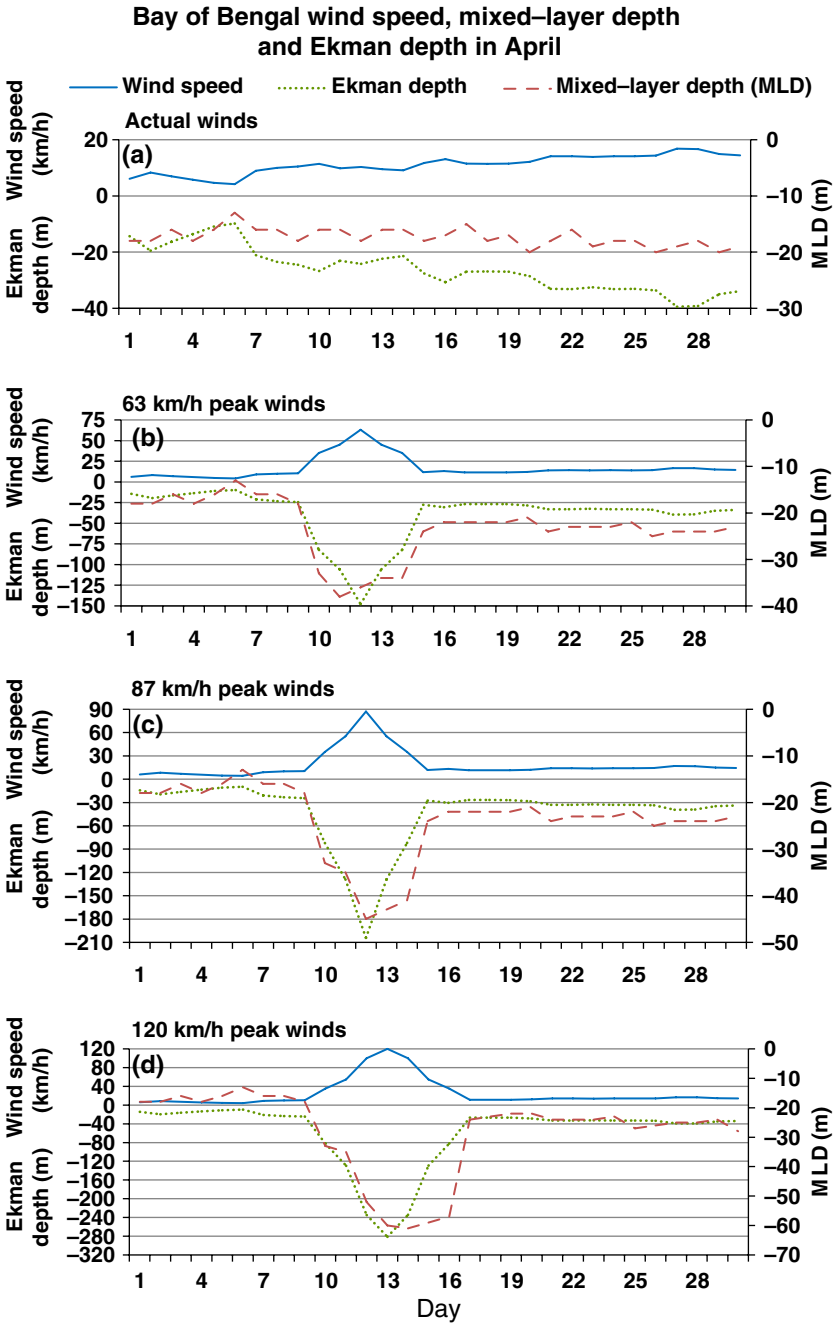

Figure 4. Bay of Bengal wind speeds (km h^{-1}; solid line), Ekman depths (m; dotted line) and mixed-layer depths (m, dashed lines) for actual wind speeds (a), model wind speeds peaking to 63 km h^{-1} (b), model wind speeds peaking to 87 km h^{-1} (c) and model wind speeds peaking to 120 km h^{-1} (d), all in the month of April.

Bay, indicating the role of stratification in curtailing the wind-mixing (Narvekar and Prasanna Kumar, 2014). This points to the overriding role of wind in cooling the surface waters of the BoB through the latent heat loss. Convective mixing is a dominant mechanism of cooling of SST in the northern Arabian Sea, located in the western part of the northern Indian Ocean, during winter (Prasanna Kumar and Prasad, 1996). However, a similar process does not take place in the BoB due to the perennial presence of fresh water in the northern Bay.

Ekman-pumping is yet another process that is capable of bringing down the temperature of the upper ocean through cyclonic winds. The BoB is known for tropical cyclone activity which occurs regularly during spring–summer (April–June) and fall–winter (October–December) transitions. Tropical cyclones induce intense cooling by both enhanced evaporation and vertical mixing under strong winds. Studies by Webster *et al.* (2005) showed that in the northern Indian Ocean categories 4 and 5 cyclones have increased over the years, while Prasanna Kumar *et al.* (2009) based on the data from 1970 to 2007 in the Arabian Sea have showed a fivefold increase in the occurrence and intensity of the most intense cyclone (wind speed exceeded 100 km h^{-1}).

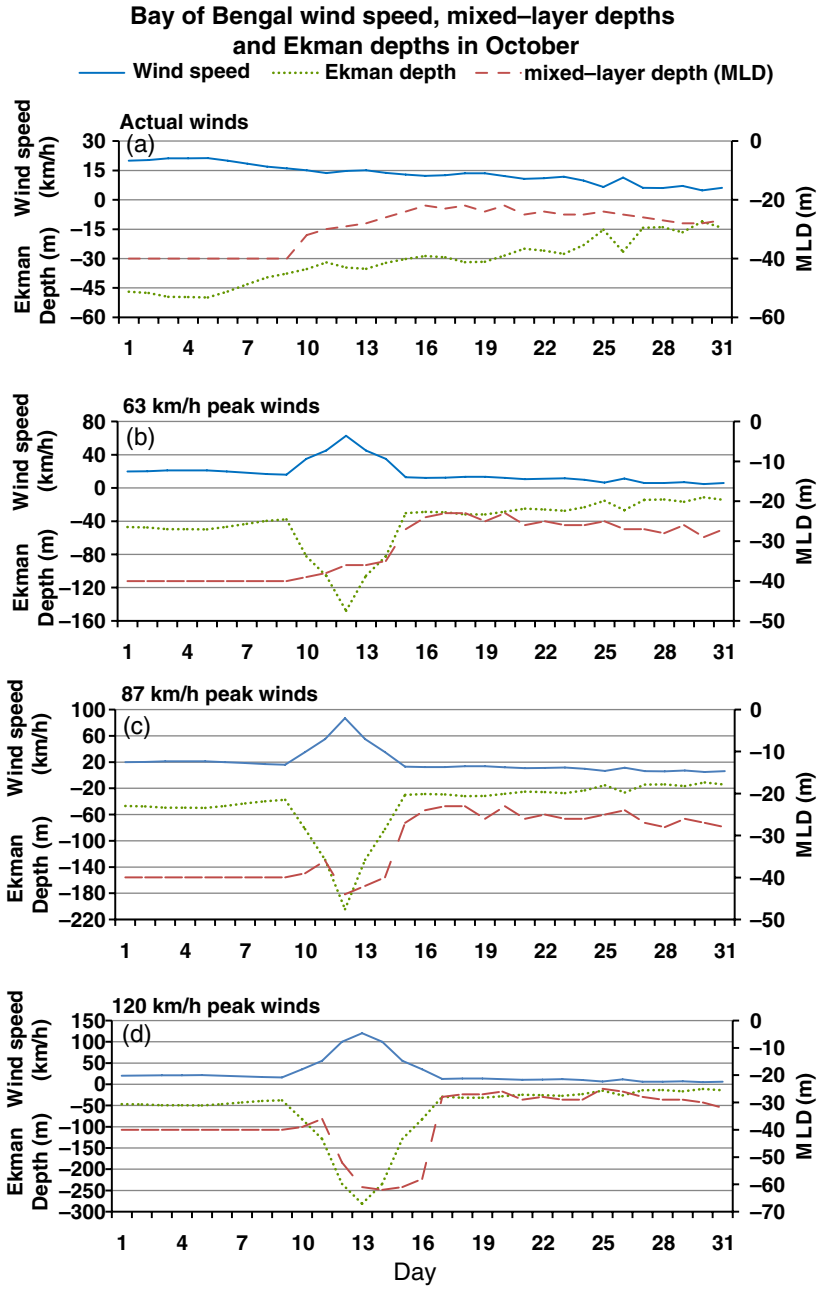

Figure 5. Bay of Bengal wind speeds (km h^{-1}; solid line), Ekman depths (m; dotted line) and mixed-layer depths (m, dashed lines) for actual wind speeds (a), model wind speeds peaking to 63 km h^{-1} (b), model wind speeds peaking to 87 km h^{-1} (c) and model wind speeds peaking to 120 km h^{-1} (d), all in the month of October.

An examination of the 5-year running mean of yearly total number of depressions, cyclones and severe cyclonic storms in the BoB showed an overall decreasing trend from 1960 to 2002 and thereafter it showed a sharp increase (Figure 2).

In order to decipher the relative roles of the above said processes in cooling the upper ocean waters in the BoB we have computed partial correlation of SST with wind speed (WS), net heat flux (NHF), evaporation minus precipitation (E – P) and the total number of DCS. Since the disruption in decadal cycle as well as slowdown in SST warming was noticed after 1995, we computed the partial correlation prior to and after 1995 and presented in Table 1.

The highest correlations of SST prior to 1995 were with NHF and E – P, which indicated that SST was controlled by latent heat loss through evaporative cooling. Note that though the number of DCS was negatively correlated its contribution was very small. In contrast, after 1995 the role of NHF and evaporative cooling diminished considerably, while the influence of number of DCS on SST increased. Thus, an increase in the number of DCS would lead to an enhanced cooling of surface waters through increased occurrence of upward-Ekman-pumping. In addition, mechanical-mixing by the cyclonic winds would also lead to deepening of mixed-layer and thereby cooling of surface waters. In order to explore this, we used PWP

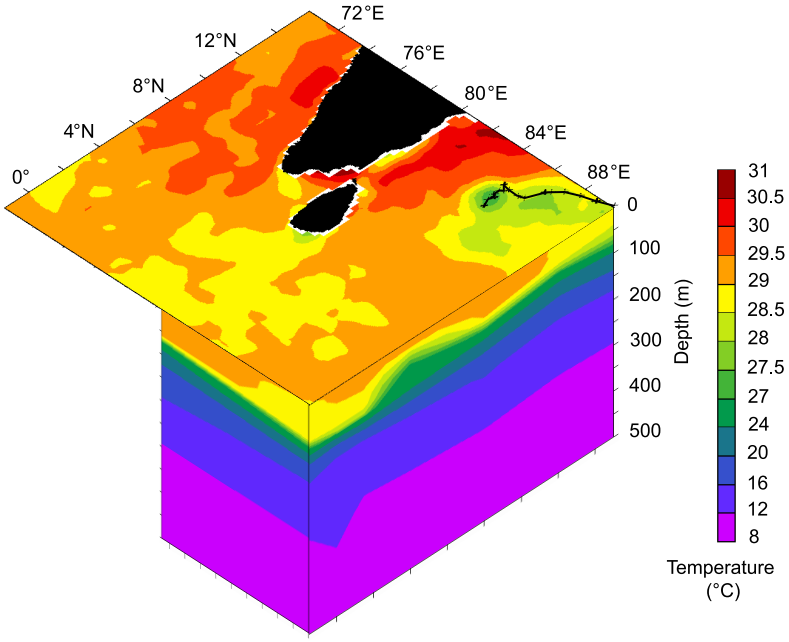

Figure 6. Schematic showing the SST cooling associated with the passage of cyclone Nargis, which occurred during the period from the 27 April to the 3 May 2008. The black solid line is the cyclone track and is plotted from the 27 April to the 1 May 2008, while the 'x' marks denote the 6-hourly positions in this period. The SST data is on the 2 May 2008, from NOAA daily OISST and is obtained from http://www.ncdc.noaa.gov/sst/griddata.php (Reynolds *et al.*, 2007). The vertical temperature data along the 90°E (5-day average centred on the 2 May) and 1.5°S (5-day average centred on the 3 May) sections (http://www.pmel.noaa.gov/tao/disdel/frames/main.html) are from Research moored Array for African-Asian-Australian Monsoon Analysis and prediction (RAMA) moorings. The cyclone track data is from http://weather.unisys.com/hurricane/n_indian/2008H/NARGIS/track.dat

model (Price *et al.*, 1986). This model computes the vertical mixing, with the temperature and salinity profiles taken from World Ocean Atlas (WOA09) as initial conditions and forced by heat (NHF), momentum (wind-stress) and fresh water fluxes. The fresh water flux is computed as the difference of the evaporation from the sum of precipitation and river run-off (E − P − R). Our purpose of using a one-dimensional mixed-layer model is only to diagnose the role of wind-mixing under strong cyclonic conditions, similar to that of a sensitivity analysis approach, for identifying the process.

The model was run with the daily mean climatology for 2 years. The seasonal cycle of wind speed and model mixed-layer depth (MLD) from the second year is presented in Figure 3.

The MLD, in general, co-varied with wind but inversely. The model MLD showed a bimodal distribution with shallow MLD during April and October coinciding with the periods of relatively weaker wind speeds. Note that the shallowest MLD was in April. The seasonal cycle of model MLD was similar to that obtained by Narvekar and Prasanna Kumar (2006) from in situ data, as well as those obtained from the data of Holte *et al.* (2010) and Keerthi *et al.* (2013), which gave us confidence in the model simulation. In order to assess the impact of cyclonic winds on the MLD during spring–summer and fall–winter transitions, the model was forced with wind speeds peaking to 63 km h^{-1} (run 1), 87 km h^{-1} (run 2) and 120 km h^{-1} (run 3) in the second year of the runs (see Appendix S2). We see a deepening of the model MLD, both during spring–summer (Figure 4) and the fall–winter (Figure 5) transitions, which is similar to the Ekman depth calculated using scalar winds. This indicated that the mixed-layer deepening, which occurred under the influence of cyclonic winds, was through wind-mixing.

Thus, it is evident from the model run that strong winds associated with cyclones during both spring–summer as well as fall–winter transitions lead to deep mixed-layer through enhanced mechanical-mixing. This is depicted in the schematic diagram (Figure 6), which shows the SST cooling of approximately 1.5 to 2.5 °C, at (12°N, 86°E) location, associated with the passage of cyclone Nargis during 27 April to 3 May 2008. The SST daily data, at the RAMA mooring location (15°N, 90°E) shows a maximum drop of 1.93 °C, from the 27 April 2008 to the 2 May 2008, and a drop of 0.52 °C, in the period from the 27 April 2008 to the 11 May 2008, showing that the cooling due to the cyclone lasts around 15 days.

We have also examined the actual observational data on MLD prepared by Keerthi *et al.* (2013) from 1969 to 2009. This data base for the Indian Ocean domain was assembled using all the measurements of mechanical bathythermographs (MBT), expendable bathythermographs (XBT), conductivity-temperature-depth (CTD) and profiling floats, besides Argo and RAMA moored buoys data. This MLD data also showed a deepening in the period from 1995 to 2009 (Figure 7).

Finally, to bring out the unique, relative contributions of CO_2 concentration, sunspot numbers and the number of DCS on the SST, a partial correlation analysis was carried out (Table 2).

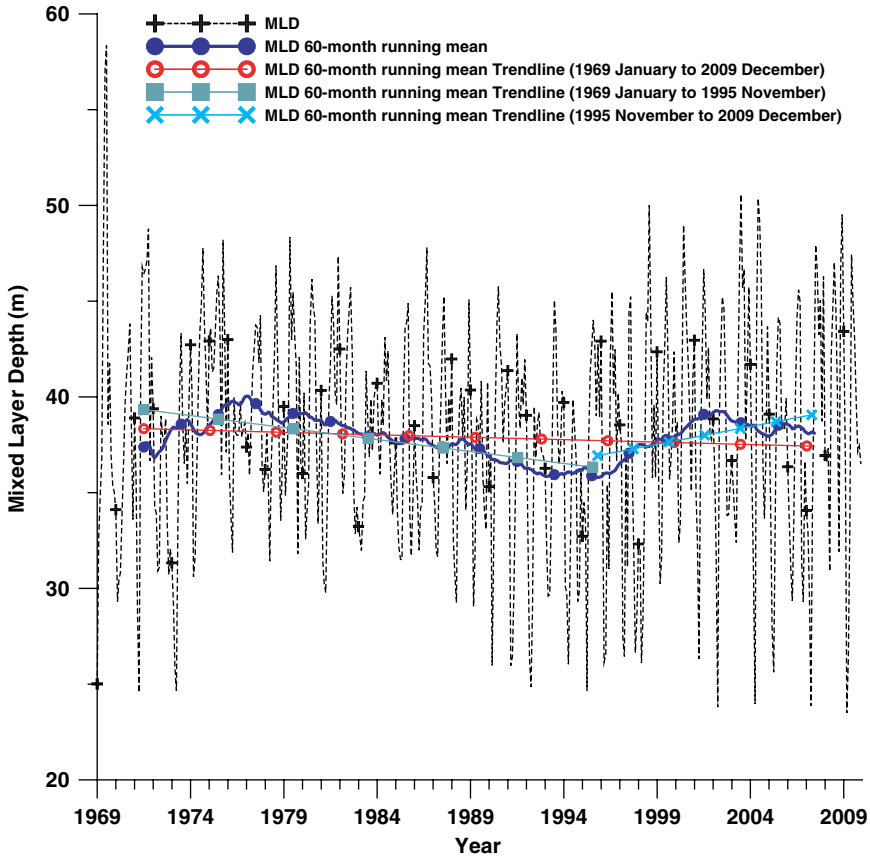

Figure 7. Bay of Bengal (Eq. −25 °N, 80 °E −99 °E) basin-averaged mixed layer depth (MLD) in metres. Data plotted is monthly (dashed line with "+" symbols), 60-month running mean (line with filled circles), and trendlines of the 60-month running mean, in the periods from 1969 January to 2009 December (line with open circles) and from 1969 January to 1995 November (line with filled squares) and from 1995 November to 2009 December (line with "×" symbols).

Table 2. Bay of Bengal (BoB) partial correlation coefficients (r) and significance levels, between the 60-month running mean of SST and 60-month running mean of the international sunspot number, 60-month running mean of the global CO_2 concentration and 60-month running mean of the BoB number of DCS, in different periods.

Partial correlation	Period	Sunspot number		CO_2 concentration		Number of DCS	
		r	Significance level (%)	r	Significance level (%)	r	Significance level (%)
SST	1960–2011	**0.74**	**>99.99**	**0.88**	**>99.99**	**−0.18**	**>99.99**
	1960–1995	**0.76**	**>99.99**	**0.47**	**>99.99**	**−0.26**	**>99.99**
	1995–2011	0.2	99.03	**0.82**	**>99.99**	**−0.43**	**>99.99**

Both partial correlation and significance level values are in bold face, when significance level is greater than 99.99%.

The partial correlation of SST and sunspot number in the pre-1995 and post-1995 periods reduce from 0.76 (significance level > 99.99%) to 0.2 (significance level = 99.03%), respectively. This indicated the decreased post-1995 influence of sunspot number on SST and we attribute this weakening link to be the cause for the disruption of the SST decadal cycle after-1995. In contrast to the sunspot number and SST partial correlation, the partial correlation coefficient of CO_2 concentration with SST increases from 0.47 (significance level >99.99%) to 0.82 (significance level >99.99%). Similarly, the partial correlation of SST and the number of DCS increases from −0.26 (significance level >99.99%) to −0.43 (significance level >99.99%). This shows that the link between the number of DCS and SST is stronger after 1995.

Though the sunspot number reduction can cause some amount of fall in the rate of SST rise, i.e. the SST slowdown, the post-1995 influence of the sunspot number on SST is lesser than the post-1995 influence of the number of DCS on SST, as seen from the partial correlation coefficients (Table 2). Thus, in the BoB during the post-1995 period, the contribution of increased number of DCS in reducing the SST warming overwhelms that due to reduced solar irradiance. Besides this, since the magnitude of the post-1995 partial correlation of CO_2 concentration and SST is greater than that of the number of DCS and SST partial correlation, we conclude that the influence of the CO_2

concentration is greater on the SST, compared to the number of DCS. However, the impact of the CO_2 concentration and number of DCS on SST, being generally opposite, the increase in the number of DCS though leading to enhanced cooling of the upper ocean, cannot completely offset the CO_2 driven warming. Thus, the above situation leads to a slowdown in SST warming in the BoB.

4. Concluding remarks

The present study, based on 52 years of data, brings out three important aspects of SST variability such as (1) decadal cycle in SST riding over a linear warming trend until 1995, (2) disruption in decadal cycle after 1995 and (3) a post-1995 slowdown in SST warming. The reasons for the observed variability was a combination of factors such as weakening of the link between SST and sunspot number after 1995 and the increase in the occurrence of cyclonic systems in the BoB post-1995 leading to an increase in the mixing of cold sub-surface waters with warm surface waters. Although the cyclones are very intense in terms of air–sea interaction, they are temporally short lived. However, the oceanic mixing process triggered by them could impact the SST for a longer time. The cooling in the case of Cyclone Nargis lasted at least a fortnight. Thus, the BoB can cool twice a year during spring–summer and fall–winter periods through episodic occurrence of cyclonic systems. This cyclone-induced cooling of the upper waters of the BoB will increase with enhanced occurrence of the numbers of cyclonic systems, which in turn leads to a slowdown in the rise of the basin-wide SST. However, it is not clear how long will the present trend of slowdown in SST warming continue in the BoB. The greatest challenge lies in the quantification of the observed variability and the uncertainty associated with it. Equally challenging is to decipher how these changes will impact the regional food and water security as most of the agriculture in this part of the world profoundly depends on the monsoon/cyclonic system-driven rainfall.

Acknowledgements

The authors wish to acknowledge Director, CSIR-National Institute of Oceanography (CSIR-NIO), Dona Paula, Goa as well as Council of Scientific and Industrial Research (CSIR), New Delhi for all the support and encouragement. JRD'M acknowledges CSIR for the fellowship. This is NIO contribution number 5764.

Supporting Information

The following supporting information is available as part of the online article:

Appendix S1. The PWP model and the data used to force the model and for the initial conditions and also the MLD data, which is used to compare with the resultant MLD.

Appendix S2. The peaking of the wind speeds and the resultant MLDs obtained.

References

Chen X, Tung K-K. 2014. Varying planetary heat sink led to global-warming slowdown and acceleration. *Science* **345**: 897–903, doi: 10.1126/science.1254937.

Holte J, Talley L. 2009. A new algorithm for finding mixed layer depths with applications to argo data and subantarctic mode water formation. *J. Atmos. Oceanic Technol.* **26**: 1920–1939, doi: 10.1175/2009JTECHO543.1.

Holte J, Gilson J, Talley L, Roemmich D. 2010. *Argo mixed layers, Scripps Institution of Oceanography/UCSD*. http://mixedlayer.ucsd.edu (accessed 15 October 2014).

Kalnay E, Kanamitsu M, Kistler R, Collins W, Deaven D, Gandin L, Iredell M, Saha S, White G, Woolen J, Zhu Y, Leetmaa A, Reynolds R, Chelliah M, Ebisuzaki W, Higgins W, Janowiak J, Mo KC, Ropelewski C, Wang J, Jenne R, Joseph D. 1996. The NCEP/NCAR 40-year reanalysis project. *Bull. Am. Meteorol. Soc.* **77**: 437–470, doi: 10.1175/1520-0477(1996)077<0437:TNYRP>2.0.CO;2.

Keeling CD, Piper SC, Bacastow RB, Wahlen M, Whorf TP, Heimann M, Meijer HA. 2001. Exchanges of atmospheric CO_2 and $^{13}CO_2$ with the terrestrial biosphere and oceans from 1978 to 2000. I. Global aspects, SIO Reference Series No. 01-06. Scripps Institution of Oceanography, San Diego, CA.

Keerthi MG, Lengaigne M, Vialard J, de Boyer Montégut C, Muraleedharan PM. 2013. Interannual variability of the Tropical Indian Ocean mixed layer depth. *Clim. Dyn.* **38**: 1–17, doi: 10.1007/s00382-012-1295-2.

Kosaka Y, Xie S-P. 2013. Recent global-warming hiatus tied to equatorial Pacific surface cooling. *Nature* **501**: 403–407, doi: 10.1038/nature12534.

McCreary JP, Kundu PK, Molinari RL. 1993. A numerical investigation of dynamics, thermodynamics and mixed-layer processes in the Indian Ocean. *Prog. Oceanogr.* **21**: 181–244.

McGregor S, Timmermann A, Stuecker MF, England MH, Merrifield M, Jin F-F, Chikamoto Y. 2014. Recent Walker circulation strengthening and Pacific cooling amplified by Atlantic warming. *Nat. Clim. Change* **4**: 888–892, doi: 10.1038/nclimate2330.

Narvekar J, Prasanna Kumar S. 2006. Seasonal variability of the mixed layer in the central Bay of Bengal and associated changes in nutrients and chlorophyll. *Deep Sea Res., Part I* **53**: 820–835.

Narvekar J, Prasanna Kumar S. 2014. Mixed layer variability and chlorophyll *a* biomass in the Bay of Bengal. *Biogeosciences* **11**: 3819–3843.

Potemra JT, Luther ME, O'Brien JJ. 1991. The seasonal circulation of the upper ocean in the Bay of Bengal. *J. Geophys. Res.* **96**: 12667–12683.

Prasad TG. 1997. Annual and seasonal mean buoyancy fluxes for the tropical Indian Ocean. *Curr. Sci.* **73**: 667–674.

Prasanna Kumar S, Narvekar J. 2005. Seasonal variability of the mixed layer in the central Arabian Sea and its implication on nutrients and primary productivity. *Deep Sea Res., Part II* **52**: 1848–1861.

Prasanna Kumar S, Prasad TG. 1996. Winter cooling in the northern Arabian Sea. *Curr. Sci.* **71**: 834–841.

Prasanna Kumar S, Roshin RP, Narvekar J, Dinesh Kumar PK, Vivekanandan E. 2009. Response of the Arabian Sea to global warming and associated regional climate shift. *Mar. Environ. Res.* **68**: 217–222.

Price JF, Mooers CNK, van Leer JC. 1978. Observation and simulation of storm-induced mixed-layer deepening. *J. Phys. Oceanogr.* **8**: 582–599.

Price JF, Weller RA, Pinkel R. 1986. Diurnal cycling: observations and models of the upper ocean response to diurnal heating, cooling, and wind mixing. *J. Geophys. Res.* **91**: 8411–8427.

Rao RR, Sivakumar R. 2000. Seasonal variability of near-surface thermal structure and heat budget of the mixed layer of the tropical Indian Ocean from a new global ocean temperature climatology. *J. Geophys. Res.* **105**(C1): 995–1015, doi: 10.1029/1999JC900220.

Rao RR, Sivakumar R. 2003. Seasonal variability of sea surface salinity and salt budget of the mixed layer of the north Indian Ocean. *J. Geophys. Res.* **108**(C1): 3009, doi: 10.1029/2001JC000907.

Reynolds RW, Smith TM, Liu C, Chelton DB, Casey KS, Schlax MG. 2007. Daily high-resolution blended analyses for sea surface temperature. *J. Clim.* **20**: 5473–5496, doi: 10.1175/2007JCLI1824.1.

Rupa Kumar K, Krishna Kumar K, Ashrit RG, Patwardhan SK, Pant GB. 2002. Climate change in India: observations and model projections, NATCOM book on climate change. In *Climate Change and India – Issues, Concerns and Opportunities*, Shukla PR, Sharma S, Raman PV (eds). Tata McGraw-Hill Publishing Co. Ltd.: New Delhi.

Schott FA, McCreary JP. 2001. The monsoon circulation of the Indian Ocean. *Prog. Oceanogr.* **51**: 1–123, doi: 10.1016/S0079-6611(01)00083-0.

Shankar D, Vinayachandran PN, Unnikrishnan AS. 2002. The monsoon currents in the north Indian Ocean. *Prog. Oceanogr.* **52**: 63–120.

Shetye SR, Shenoi SSC, Gouveia AD, Michael GS, Sundar DS, Nampoothiri G. 1991. Wind-driven coastal upwelling along the western boundary of the Bay of Bengal during the south-west monsoon. *Cont. Shelf Res.* **11**: 1397–1408.

Shetye SR, Gouveia AD, Shankar D, Shenoi SSC, Vinayachandran PN, Sundar D, Michael GS, Nampoothiri G. 1996. Hydrography and circulation in the western Bay of Bengal during the northeast monsoon. *J. Geophys. Res.* **101**: 14011–14025.

Solar Influences Data analysis Centre (SIDC) team. 2012. Monthly Report on the International Sunspot Number, online catalogue of the sunspot index. '1749–2011'. World Data Center for the Sunspot Index, Royal Observatory of Belgium, Brussels. http://www.sidc.be/sunspot-data/ (accessed 13 January 2012).

Subramanian V. 1993. Sediment load of Indian Rivers. *Curr. Sci.* **64**: 928–930.

Trenberth KE, Fasullo JT. 2013. An apparent hiatus in global warming? *Earth's Future* **1**: 19–32, doi: 10.1002/2013EF000165.

Trenberth KE, Fasullo JT, Branstator G, Phillips AS. 2014. Seasonal aspect of the recent pause in surface warming. *Nat. Clim. Change* **4**: 911–916, doi: 10.1038/nclimate2341.

Varkey MJ, Murty VSN, Suryanarayana A. 1996. Physical oceanography of the Bay of Bengal and Andaman Sea. *Oceanogr. Mar. Biol. Annu. Rev.* **34**: 1–70.

Vinayachandran PN, Yamagata T. 1998. Monsoon response of the sea around Sri Lanka: generation of thermal domes and anticyclonic vortices. *J. Phys. Oceanogr.* **28**: 1946–1960.

Webster PJ, Holland GJ, Curry JA, Chang H-R. 2005. Changes in tropical cyclone number, duration, and intensity in a warming environment. *Science* **309**: 1844–1846.

White WB, Lean J, Cayan DR, Dettinger MD. 1997. Response of global upper ocean temperature to changing solar irradiance. *J. Geophys. Res.* **102**(C2): 3255–3266, doi: 10.1029/96JC03549.

Willson RC, Hudson HS. 1988. Solar luminosity variation in solar cycle 21. *Nature* **332**: 810–812, doi: 10.1038/33281OaO.

Woodruff SD, Diaz HF, Worley SJ, Reynolds RW, Lubker SJ. 2005. Early ship observational data and ICOADS. *Clim. Change* **73**: 169–194, doi: 10.1007/s10584-005-456-3.

Yu L, Jin X, Weller RA. 2008. Multidecade Global Flux Datasets from the Objectively Analyzed Air-sea Fluxes (OAFlux) Project: latent and sensible heat fluxes, ocean evaporation, and related surface meteorological variables. OAFlux Project Technical Report OA-2008-01, Woods Hole Oceanographic Institution, Woods Hole, MA, 64 pp.

Why is the Bay of Bengal experiencing a reduced rate of sea surface warming?

Short Title:

Bay of Bengal Sea Surface Temperature slowdown

Joshua Rosario D'Mello[a] and S. Prasanna Kumar[a,*]

[a] CSIR-National Institute of Oceanography, Dona Paula– 403 004, Goa, India.

*Corresponding author

S. Prasanna Kumar

[a] CSIR-National Institute of Oceanography (CSIR-NIO), Dona Paula– 403 004, Goa, India.

e-mail: prasanna@nio.org

Telephone: 0091-832-2450300

Fax: 0091-832-2450608

Supporting Information

The Sea Surface Temperature (SST) in the Bay of Bengal is analysed in the period from 1960 January to 2011 December, and shows a decadal cycle riding on an increasing trend till 1995. In the post-1995 period, there is a disruption of the decadal cycle and an SST slowdown.

The SST decadal cycle is due to the sunspot number cycle, while the SST rise is due to the increasing CO_2 concentration in the atmosphere. The slowdown in the SST rise, in the post-1995 period, is due to the increase in the number of depressions, cyclones and severe cyclone (DCS). The cyclonic systems can cause mechanical mixing and cause the mixing of the mixed-layer waters with the cooler of the sub-surface waters, there-by reducing the SST.

This process of the deepening of the mixed-layer is shown through the Price Weller Pinkel (PWP) model. The increase in the SST by the atmospheric CO_2 concentration and the SST cooling due to the increasing number of depressions, cyclones and severe cyclones after-1995, are opposing processes. The SST in the Bay of Bengal is observed as a slowdown.

S1

S.1.1 Price-Weller-Pinkel (PWP) Model

The Price-Weller-Pinkel (PWP) model (Price *et al.*, 1986) is a mixed-layer model similar to the dynamic instability model of Price *et al.* (1978), but modified to include mixing in the stratified fluid, below the mixed-layer. The model takes into account mixing processes namely (1) free convection arising due to surface heat loss, (2) mixed-layer entrainment by relaxation and (3) shear flow instability driven mixing. Generally, mixing due to free convection in the BoB is very shallow and mostly confined to the upper few tens of centimetres of the water column. In contrast, the last two are the dominant processes that determine the depth of the mixed-layer and are related to momentum flux by the wind through the Richardson number.

Since the vertical mixing of the water is caused by changes in the density due to the changes in the net heat and fresh water fluxes and momentum flux they were calculated from zonal and meridional wind stress components, shortwave and longwave radiations, latent and sensible heat fluxes, evaporation, precipitation and riverine discharge, riverine runoff and catchment area data. The model was initialized with the climatological temperature and salinity profiles and the daily fluxes were used to force the model. The model was run for 730 days (2 years), with a time step of 86400 seconds (1 day) and with a vertical grid interval of 1 m.

S.1.2 Data for the Model

The daily wind stress components were obtained from http://apdrc.soest.hawaii.edu/dods/public_data/satellite_product/ifremer/daily_flux, while the daily evaporation data was obtained from ftp://ftp.whoi.edu/pub/science/oaflux/data_v3/daily/ evaporation/. The daily rainfall data was obtained from http://apdrc.soest.hawaii.edu/dchart/ index.html?dset=a2c287de3ad7cab9999e50371916fe . The daily riverine discharge, run-off and catchment area data for the rivers Sittang, Irrawaddy, Chindwin, Brahmaputra, Ganges, Damodar, Subarnarekha, Godavari, Krishna, Penner and Cauvery were obtained from http://www.compositerunoff.sr.unh.edu (Fekete *et al.*, 2000). Similarly, for the rivers Mahanadi, Ponnaiyar, Vaigai, Mahaveli Ganga and Gin Ganga the riverine discharge, riverine runoff and catchment area data were obtained from http://www.sage.wisc.edu/riverdata/scripts/ station_table.php?qual=32&filenum=1114. The fore-mentioned website gave data for the riverine discharge and runoff data of the river Brahmani, but the catchment area was taken from Vaithiyanathan *et al.* (1988).

The daily downward solar radiation flux and upward long wave radiation flux were obtained from http://www.esrl.noaa.gov/psd/data/gridded/data.ncep.reanalysis.derived. otherflux.html , while the daily latent heat flux and sensible heat flux data were obtained from http://oaflux.whoi.edu .

Temperature (Locarnini *et al.*, 2010) and salinity (Antonov *et al.*, 2010) profile data were taken from World Ocean Atlas 2009 available at http://www.nodc.noaa.gov/OC5/WOA09/ netcdf_data.html. For comparing the model MLD, the data on the mixed-layer depths were taken from Holte *et al.* (2010) (http://mixedlayer.ucsd.edu/data/monthlyclim.nc) and Keerthi *et al.* (2013) (http://www.ifremer.fr/cerweb/deboyer/mld/Surface_Mixed_Layer_ Depth.php). In Holte *et*

al. (2010) the MLD climatology was computed using Argo profiles and a hybrid method (Holte and Talley, 2009), while in Keerthi *et al.* (2013) the monthly MLD data for the Indian Ocean, during 1969 to 2009 was based on temperature and salinity profiles taken from different sources namely National Oceanographic Data Centre (NODC) World Ocean Database 2009 (WOD 09), World Ocean Circulation Experiment (WOCE) global dataset version 3.0, Argo profile data and Tropical Atmosphere Ocean project Research moored Array for the African-Asian-Australian Monsoon Analysis and prediction (TAO RAMA) buoy daily data. Using this data monthly mean climatology (1969-2009) was computed for comparing with PWP model output.

S2

S2.1 PWP model wind speeds in April (spring- summer transition)

The cyclonic winds were introduced in a stepped manner from the 10th of April so as to attain the peak value on the 12th of April (runs 1 and 2, having peak values of 63 km/hr and 87 km/hr respectively) and the 13th of April (run 3, having a peak value of 120 km/hr). The model output was analyzed and the maximum mixed-layer depths were found to be 41 m (run 1, Panel b in Figure 4), 45 m (run 2, Panel c in Figure 4) and 61 m (run 3, Panel d in Figure 4) respectively (Figure 4). Note that in April the model MLD was 17 m when forced with the actual winds of 11 km/hr (Panel a in Figure 4).

S2.2 PWP model wind speeds in October (fall- winter transition)

The model was forced with increasing winds in a stepped manner from 10th October so as to attain peak value of 63 km/hr (run 1, Panel b in Figure 5) and 87 km/hr (run 2, Panel c in Figure 5) on 12th October and 120 km/hr (run 3, Panel d in Figure 5) on 13th October. The model MLDs were found to be 38 m (run 1), 44 m (run 2) and 62 m (run 3) respectively, while it was 30m when forced with actual winds of 13 km/hr (Panel a in Figure 5).

References

Antonov JI, Seidov D, Boyer TP, Locarnini RA, Mishonov AV, Garcia HE, Baranova OK, Zweng MM, Johnson DR, 2010. World Ocean Atlas 2009, Volume 2: Salinity, in:

Levitus S, *NOAA Atlas NESDIS 69*. U.S. Government Printing Office: Washington, D.C., U.S.A.

Fekete BM, Vorosmarty CJ, Grabs W, 2000. *Global Composite Runoff Fields based on observed river discharge and simulated water balances.* Global Runoff Data Centre, Koblenz, Germany.

Holte J, Talley L, 2009. A New Algorithm for Finding Mixed Layer Depths with Applications to Argo Data and Subantarctic Mode Water Formation. *Journal of Atmospheric and Oceanic Technology* **26:** 1920–1939. doi:10.1175/2009JTECHO543.1.

Holte J, Gilson J, Talley L, Roemmich D, 2010. Argo Mixed Layers, Scripps Institution of Oceanography/UCSD. http://mixedlayer.ucsd.edu, accessed 15th October, 2014.

Keerthi MG, Lengaigne M, Vialard J, de Boyer Montégut C, Muraleedharan PM, 2013. Interannual variability of the Tropical Indian Ocean mixed layer depth. *Climate Dynamics* **38:** 1–17. doi:10.1007/s00382-012-1295-2.

Locarnini RA, Mishonov AV, Antonov JI, Boyer TP, Garcia HE, Baranova OK, Zweng MM, Johnson DR, 2010. World Ocean Atlas 2009, Volume 1: Temperature, in: Levitus, S., *NOAA Atlas NESDIS 68*. U.S. Government Printing Office: Washington, D.C.

Price JF, Mooers CNK, van Leer JC, 1978. Observation and simulation of storm-induced mixed-layer deepening. *Journal of Physical Oceanography* **8:** 582–599.

Price JF, Weller RA, Pinkel R, 1986. Diurnal cycling: Observations and models of the upper ocean response to diurnal heating, cooling, and wind mixing. *Journal of Geophysical Research* **91:** 8411–8427.

Vaithiyanathan P, Ramanathan AL, Subramanian V, 1988. Erosion, Transport and Deposition of sediments by the tropical rivers of India. *Sediment Budgets* **174:** 561–574.

INTERNATIONAL JOURNAL OF CLIMATOLOGY
Int. J. Climatol. (2017)
Published online in Wiley Online Library
(wileyonlinelibrary.com) DOI: 10.1002/joc.5198

RMetS
Royal Meteorological Society

Short Communication

Processes controlling the accelerated warming of the Arabian Sea

Joshua Rosario D'Mello† and S. Prasanna Kumar*

Physical Oceanography Division, CSIR-National Institute of Oceanography, Dona Paula, Ilhas, Goa, India

ABSTRACT: The Arabian Sea (AS) has undergone a regime shift after 1995, manifesting the disruption of its natural decadal cycle over-riding a secular rise in its sea-surface temperature (SST). Using a suite of *in situ* and remote sensing data, we show that the rate of post-1995 accelerated warming is spatially different, due to regionally and seasonally differing oceanographic processes. Along parts of the western boundary, the accelerated warming was mediated by a reduction in the post-1995 linear trend of wind speed during summer monsoon leading to reduced upwelling and also reduced evaporation trend. In the northeast AS, post-1995 increase in specific humidity during late winter, lead to a decrease in the evaporative cooling and subsequent convective mixing resulting in the increased rate of warming. The continued warming seen in the northeast AS until spring inter-monsoon was due to the increasing net heat flux trend into the ocean along with reducing trend in evaporation. The accelerated warming in the central AS was linked to the reduced wind speed trend.

KEY WORDS sea-surface temperature (SST); warming trend; reduced cooling; Arabian Sea; upwelling; winter cooling; decadal cycle

Received 29 February 2016; Revised 6 June 2017; Accepted 6 June 2017

1. Introduction

The Arabian Sea (AS) is a tropical basin situated in the western part of the north Indian Ocean. The distinct feature of this basin is that it is land-locked in the north at approximately 25°N latitude and comes under the monsoon regime. As a result of being blocked by the Eurasian landmass, the basin's waters are not cooled by the polar waters from the north, while the monsoons lead to a strong seasonality in the hydrography and circulation. The semi-annual wind-reversal associated with monsoons, having south-westerly winds during summer monsoon (June to September) and north-easterly winds during winter monsoon (November to February), leads to a reversal in the direction of surface current as well. The winds during spring (March to May) and fall (October) inter-monsoons are weak and variable. The waters of the basin also experiences cooling twice annually in summer and winter monsoons. During summer monsoon upwelling of cold sub-surface waters along Somalia (Smith and Codispoti, 1980), Arabia (Smith and Bottero, 1977) and the southern part of the west coast of India (Sharma, 1966; Varadachari and Sharma, 1967) cools the surface waters. However, in the east-central AS the summer cooling was attributed to the downward transfer of heat due to mixing of warmer surface and the colder sub-surface waters (Ramesh Babu and Sastry, 1984). In addition, the open-ocean upwelling driven by positive wind-stress curl (Bauer *et al.*, 1991) north of the Findlater Jet (Findlater, 1969) as well as wind-mixing contributes to the cooling of various regions in the AS during summer monsoon (Prasanna Kumar *et al.*, 2001). In winter, the upper layers of the northern AS are cooled by the radiative heat loss combined with evaporative cooling and subsequent convective mixing (Prasanna Kumar and Prasad, 1996). Based on mooring data Weller *et al.* (2002) showed that during the winter, in the period from October 1994 to October 1995, under the influence of dry and moderate winds and clear skies when the SST dropped by around 3 °C, the ocean lost 19.7 W m^{-2} and the mixed-layer deepened by 100 m in the central AS. Meso-scale eddies and heat budgets were studied by Fischer *et al.* (2002), while the influences of the diurnal and intra-seasonal forcing on the mixed layer and biological variability in the central AS were studied by McCreary *et al.* (2001).

On an inter-annual timescale, De Boyer Montégut *et al.* (2007) showed that the eastern AS SST is strongly controlled by winds, through variation in the latent heat fluxes, while the western AS SST is controlled by vertical processes and horizontal advection.

Recent studies on the AS SST are indicating a secular warming trend. It was Rupa Kumar *et al.* (2002) who first

* Correspondence to: S. Prasanna Kumar, Physical Oceanography Division, CSIR-National Institute of Oceanography, Dona Paula - 403 004, Ilhas, Goa, India. E-mail: prasanna@nio.org

†Current address: Rosary College of Commerce and Arts, Navelim - 403 707, Salcete, Goa, India.

Table 1. Sources of data and their specifications.

Name of the data set	Parameters	Period	Temporal and spatial interval	URL	References/Source
International Comprehensive Ocean–Atmosphere Data Set (ICOADS)	SST, specific humidity, wind components	1960–2011	Monthly; $1^\circ \times 1^\circ$	www.esrl.noaa.gov/psd/data/gridded/data.coads.1deg.html	Woodruff *et al.*, 2011
Objectively Analysed Air-Sea Fluxes (OAFlux)	Evaporation rate	1960–2011	Monthly; $1^\circ \times 1^\circ$	Now available at http://rda.ucar.edu/datasets/ds260.1/	Yu *et al.*, 2008
CDC Derived NCEP Reanalysis Products Surface Flux	Precipitation	1960–2011	Monthly; $\sim 1.875^\circ \times 1.875^\circ$	ftp://ftp.cdc.noaa.gov/Datasets/ncep.reanalysis.derived/surface_gauss/prate.sfc.mon.mean.nc	Kalnay *et al.*, 1996
NCEP/NCAR reanalysis monthly means and other derived variables data	Shortwave radiation (SWR), longwave radiation (LWR), LHF and SHF	1960–2011	Monthly; T62 Gaussian grid (192×94)	http://www.esrl.noaa.gov/psd/data/gridded/data.ncep.reanalysis.derived.surfaceflux.html	Kalnay *et al.*, 1996
WDC-SILSO, Royal Observatory of Belgium, Brussels Sunspot Number data	International sunspot number	1960–2011	Monthly; Global	Now available at www.sidc.be/silso/datafiles	WDC-SILSO, Royal Observatory of Belgium, Brussels
Keeling Carbon Dioxide Concentration Data	Carbon dioxide atmospheric concentration	1960–2011	Monthly; Mauna Loa (January 1960–December 1979); Global (January 1980–December 2011)	ftp://ftp.cmdl.noaa.gov/ccg/co2/trends/co2_mm_mlo.txt (Mauna Loa); ftp://ftp.cmdl.noaa.gov/ccg/co2/trends/co2_mm_gl.txt (Global)	Keeling *et al.*, 2001; Keeling *et al.*, 2005
Simple Ocean Data Assimilation (SODA) data v2.2.4	Temperature section	1960–2010	Monthly; $0.5^\circ \times 0.5^\circ$; 40 vertical levels	http://apdrc.soest.hawaii.edu/las/v6/constrain?var=3076	Carton *et al.*, 2000; Carton and Giese, 2008

documented the rise in sea-surface temperature (SST) of the AS, during the period from 1904 to 1994, which was 0.5 °C. Subsequently, the study by Alory *et al.* (2007), based on 1960 to 1999 thermal data from Indian Ocean, showed a warming of around 1 °C over large regions in the AS. Prasanna Kumar *et al.* (2009) noted that the AS is experiencing secular warming and undergoing a regime shift after 1995 as seen from the disruption in the natural decadal cycle of the SST. The heat content of the upper ocean, in the Indian Ocean, shows a warming trend and the Hadley Centre Sea Ice and SST show that the tropical Indian Ocean regions warmed faster than most of the tropical Pacific and Atlantic, since the 1950s (see Han *et al.*, 2014 and references therein). Roxy *et al.* (2014) showed that the western tropical Indian Ocean is warming faster than the rest of the tropical oceans, while Dinesh Kumar *et al.* (2016) reported an increasing SST of 0.12 °C per decade in the AS for the period from 1960 to 2009. Han *et al.* (2014) reviewed the decadal variability and the long-term trends in the Indian Ocean. Although it is unequivocally evident from the above that the AS is indeed undergoing a secular warming, it is not known whether the reported warming trends will be similar in all parts of the AS. Hence, the present study attempts to understand the nature and characteristics of this warming in different parts of the AS and at understanding the processes that controls such warming.

2. Data and methodology

The data pertaining to SST, specific humidity and surface wind components were obtained from the International Comprehensive Ocean–Atmosphere Data Set (ICOADS) (Woodruff *et al.*, 2011). To our best knowledge, ICOADS is the most complete and heterogeneous collection of surface marine data. There are some data-coverage issues though, a cause being no addition of delayed-mode ship data in recent years. The ship-recorded data dominate until 1970s; thereafter contribution of buoys and other automated platforms has rapidly increased. Ship-recorded data are mainly in the shipping lanes. Drifting buoys data have near ubiquitous coverage, but as they are generally not recovered, the recording sensors may drift which results in a reduced accuracy. Some other problems of ICOADS data are the change in observation practices, i.e. bucket intake and engine intake. This was sorted out to some extent in HADSST (Rayner *et al.*, 2003, 2006; Kennedy *et al.*, 2011a, 2011b). The sampling of ICOADS is another issue. However, this was addressed for all ICOADS variables (Gulev *et al.*, 2007a, 2007b).

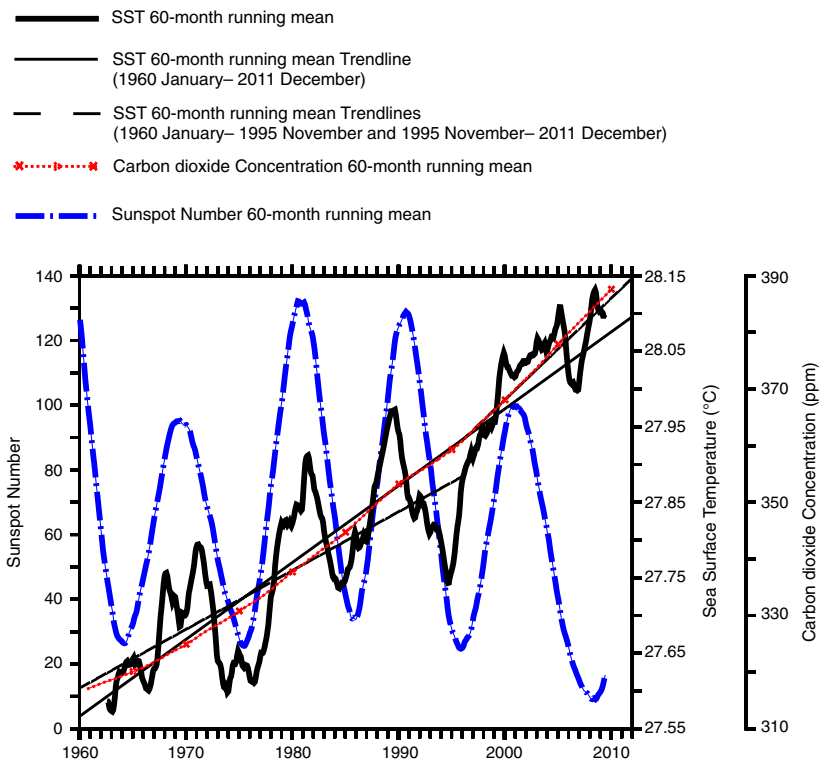

Figure 1. Arabian Sea (equator to 25°N, 45°–80°E) SST 60-month running mean (thick solid-line) from January 1960 to December 2011, with trend lines for the entire period (thin solid-line) and in the pre-1995 and post-1995 November periods (thin dashed-lines), Sunspot number 60-month running mean (thick dashed and dotted line) and carbon dioxide concentration 60-month running mean (thin dotted-line with cross-marks). [Colour figure can be viewed at wileyonlinelibrary.com].

Figures S1–S3, Supporting Information, are given to show more information on the quality of the ICOADS SST data. Despite a number of drawbacks, due to the widely differing data source, ICOADS data are used as the basis for many derived products and is regarded as the long-term marine-surface reference data set (Woodruff *et al.*, 2011). In order to examine the robustness of the ICOADS data in the AS, we have plotted the basin-averaged 60-month running mean ICOADS SST, NOAA Optimally Interpolated SST (https://www.esrl.noaa.gov/psd/data/gridded/data.noaa.oisst.v2.html) and Kaplan SSTA (https://www.esrl.noaa.gov/psd/data/gridded/data.kaplan_sst.html) in the Figure S4. From the figure, it is evident that though there are differences between data sets, all of them showed similar trends. Hence, for the present study we principally relied upon the ICOADS and the values were extracted for the AS in the domain equator to 25°N and 45°–80°E. The evaporation rate was taken from Objectively Analysed Air-Sea Fluxes (OAFlux). The OAFlux data use optimal blending of satellite retrievals and three atmospheric re-analyses (Yu *et al.*, 2008). The precipitation data are the CDC-Derived NCEP Reanalysis Products Surface Flux. The evaporation and precipitation difference ($E-P$) were then computed, using the above-mentioned data sets. The AS as a whole is generally dominated by evaporation; but in order to better represent the freshwater flux, $E-P$ is taken. The monthly gridded data of the shortwave radiation, longwave radiation (LWR), latent heat flux (LHF) and sensible heat flux (SHF) are from the NCEP/NCAR reanalysis monthly means and other derived variables data (Kalnay *et al.*, 1996). The NCEP/NCAR reanalysis data are classified into four types, based on the influence of observations and the model. The variables of class 'A' are influenced strongly by the observations and are more reliable. The flux data are of class 'C' which are variables not directly affected by observations. Although the classification is somewhat subjective, a little caution is required in interpreting the results of the re-analysis variables of class 'C' (Kalnay *et al.*, 1996). There have been some studies showing the over-estimation or underestimation of fluxes in the NCEP/NCAR data as seen by the studies of Josey (2001) in the Atlantic Ocean and Moore and Renfrew (2002), Kubota *et al.* (2008) in the Pacific Ocean. The NCEP/NCAR large SHF and LHF overestimation compared to World Ocean Circulation Experiment (WOCE) ships was studied by Smith *et al.* (2001). However, in the absence of large continuously observed flux data, this reanalysis data are probably the best alternative, and besides this the Tropflux and OAFlux data are of shorter periods. The NCEP/NCAR flux data were used to compute the net heat flux (NHF). All fluxes are considered positive into the ocean. The TropFlux data, which is not used in this analysis, is a project aimed giving heat and momentum flux data at daily interval, in the region from 30°N to 30°S. The data are available only in the period from 1979 to 2013 March. The international sunspot number data are produced by the Solar Influences Data Analysis Center (SIDC), World Data Center for the Sunspot Index,

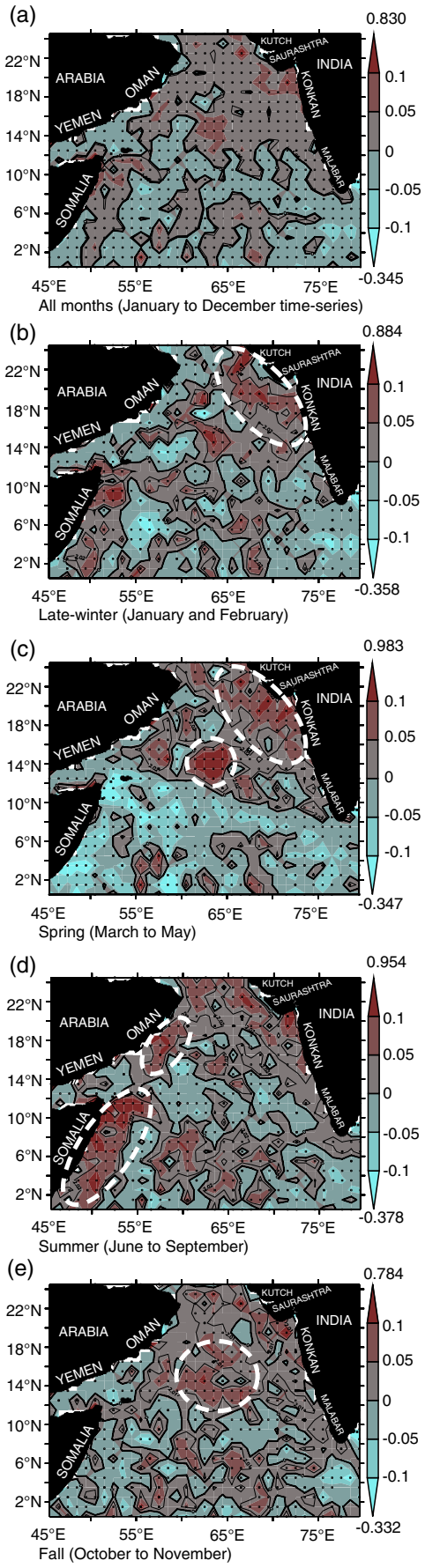

Figure 2. Legend on next column.

at the Royal Observatory of Belgium. The Carbon dioxide concentration values, on Mauna Loa, from 1958 March to 2012 September and globally from 1980 January to 2012 August annually, are obtained from ftp://ftp.cmdl.noaa.gov/ccg/co2/trends/co2_mm_mlo.txt and ftp://ftp.cmdl.noaa.gov/ccg/co2/trends/co2_mm_gl.txt respectively. The carbon dioxide concentrations at Mauna Loa are merged to the global carbon dioxide concentration data to extend the time series before 1980 January (Keeling *et al.*, 2001, 2005).

The temperature section is plotted using from Simple Ocean Data Assimilation (SODA) data v2.2.4. The data used and its characteristics are mentioned in Table 1.

All the data were analysed and plotted using ferret software, in the time period from January 1960 to December 2011, wherever available. The data period was divided at 1995 November as it is the minimum of a sunspot-number cycle period and there are differences in SST decadal cycle and slopes across this period. The 60-month running means were computed for the parameters, besides computing the slopes of the trend lines and their correlation coefficients with SST, both the fore-mentioned at 95% significance levels, in the pre-1995 November and post-1995 November periods. The non-zero slopes of the trend lines were computed (http://stattrek.com/regression/slope-test.aspx?Tutorial=AP). The basin-averaged 60-month running mean SST slopes were found to be significant with p-value of <0.0001.

3. Results and discussion

We first examined the trend in the basin-averaged SST in the context of sunspot-number cycle and the atmospheric carbon dioxide concentrations during 1960–2011, in order to study the differential rate of warming across 1995. Subsequently, we explored how the warming rate seen in the SST differs regionally and the parameters responsible for it. Finally, we investigated the processes that led to the observed differential-warming in the AS.

3.1. Basin-averaged SST, sunspot number cycle and atmospheric CO_2 concentration

The sunspot number 60-month running mean shows the 11-year cycle (Figure 1), first discovered by Schwabe and Schwabe Herrn (1844). This 11-year solar cycle is also seen in its luminosity (Willson and Hudson,

Figure 2. Arabian Sea slope difference (°C year^{-1}) between the periods from November 1995 to December 2011 and January 1960 to November 1995, of SST 60-month running mean (a) and of SST 5-year running means in late-winter (January to February) (b), spring season (March to May) (c), summer (June to September) (d) and fall season (October to November) (e). The regions are dotted if significant at the 95% level. The regions are shaded above and contoured at $|t\text{-value}| > 1.964$, number of points (N) = 560 (a); $|t\text{-value}| > 2.015$, $N = 44$ (b–d) and $|t\text{-value}| > 2.014$, $N = 45$ (e). The approximate region of highest accelerated SST warming is indicated by a dashed ellipse or circle. [Colour figure can be viewed at wileyonlinelibrary.com].

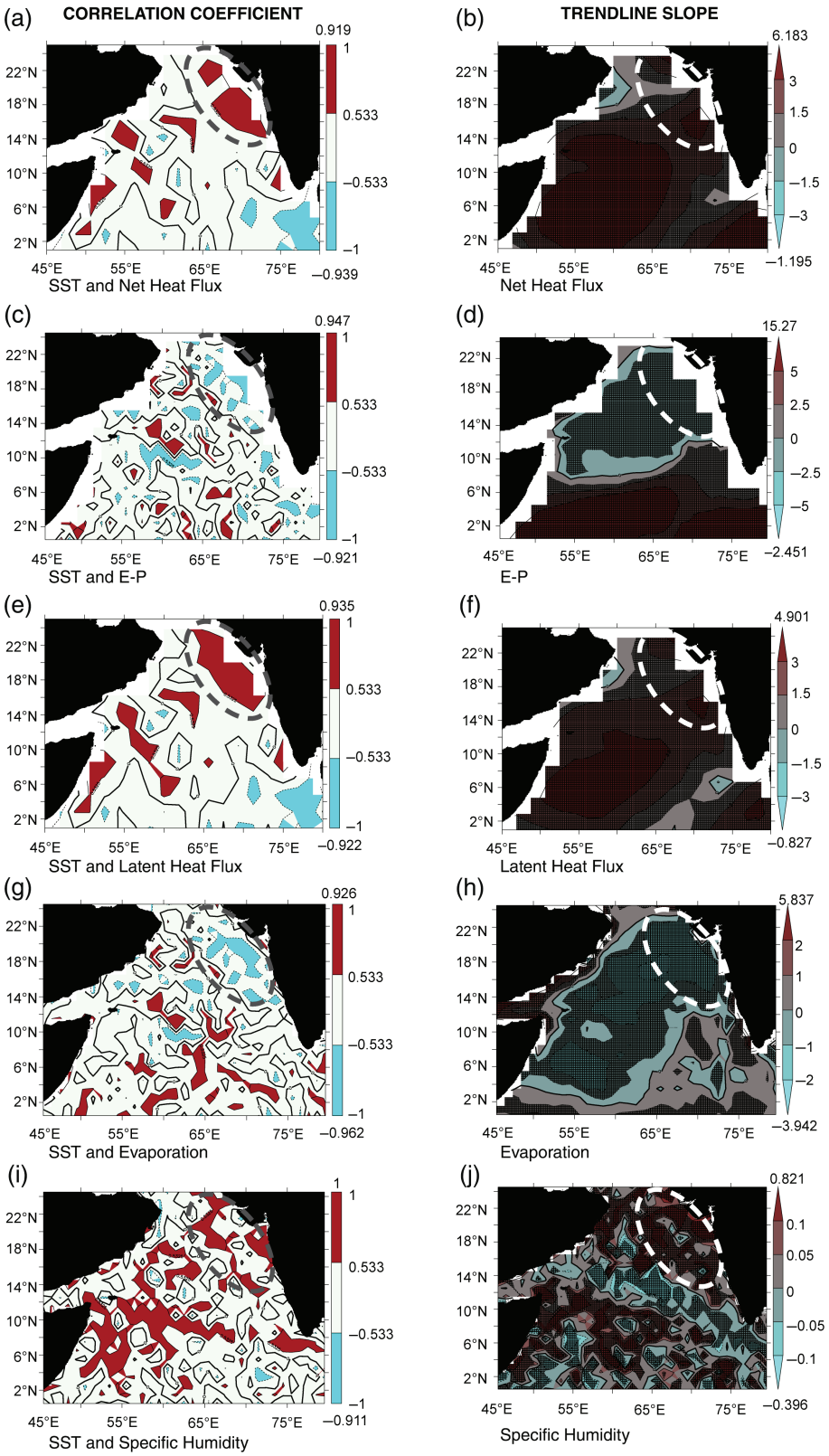

Figure 3. Arabian Sea late-winter season (January to February) averaged, correlation coefficients of SST with NHF (a), $E-P$ (c), LHF (e), evaporation (g) and specific humidity (i), shaded for regions having 95% and above significance level ($r > |\pm 0.5325|$, $N = 14$). Late-winter season averaged slopes of NHF ((W m^{-2}) year^{-1}) (b), $E-P$ ((cm year^{-1}) year^{-1}) (d), LHF ((W m^{-2}) year^{-1}) (f), evaporation ((cm year^{-1}) year^{-1}) (h) and specific humidity ((g kg^{-1}) year^{-1}) (j), are cross-hatched for regions having 95% and above significance level (two-tailed t-statistic GE $|\pm 2.18|$, $N = 14$). Both NHF and LHF are considered positive into the ocean. The approximate region of highest accelerated SST warming is indicated by a dashed ellipse. [Colour figure can be viewed at wileyonlinelibrary.com].

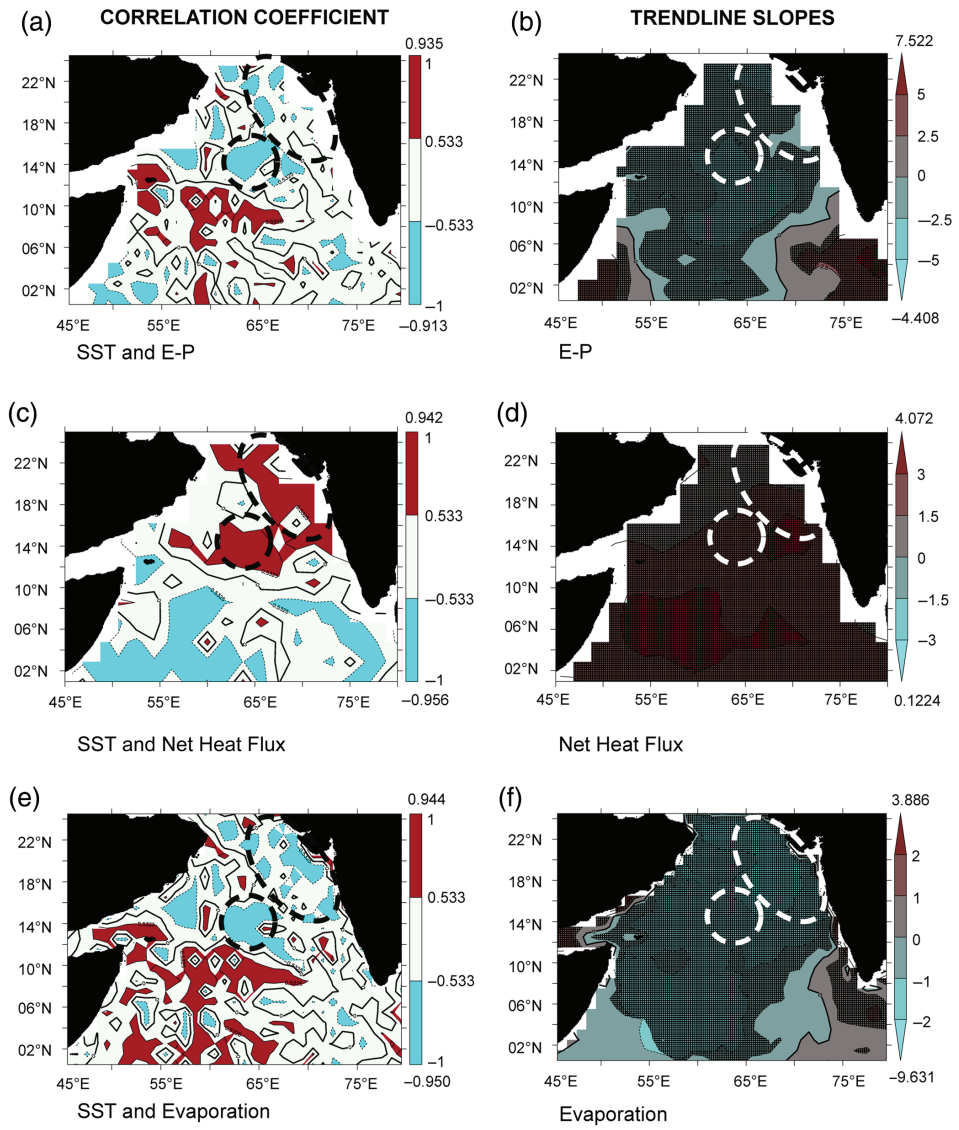

Figure 4. Arabian Sea spring season (March to May) averaged, correlation coefficients of SST with $E-P$ (a), NHF (c) and evaporation (e), shaded for regions having 95% and above significance level ($r > |\pm 0.5325|$, $N = 14$). Spring season averaged slopes of $E-P$ ((cm year^{-1}) year^{-1}) (b), NHF ((W m^{-2}) year^{-1}) (d) and evaporation ((cm year^{-1}) year^{-1}) (f), are cross-hatched for regions having 95% and above significance level (two-tailed t-statistic GE $|\pm 2.18|$, $N = 14$). NHF is considered positive into the ocean. The approximate regions of highest accelerated SST warming are indicated by a dashed ellipse or circle. [Colour figure can be viewed at wileyonlinelibrary.com].

1991). Variations in the solar luminosity (total energy output) are caused by the changing sunspot numbers, during the 11-year cycle (Foukal *et al.*, 2006). The solar irradiance affects the climate (Haigh *et al.*, 2010) and sunspot number is taken as a proxy for the solar irradiance. The basin-averaged 60-month running mean SST in the AS, in the period from January 1960 to December 2011, showed a gradual increasing trend, at the rate of 0.010 °C year^{-1}, which was over-riding the dominant decadal cycle (Figure 1). White *et al.* (1997) showed that the natural decadal cycle is closely linked to the solar activity. A noteworthy feature was the co-variation of AS SST and sunspot number cycle until 1995 demonstrating the dominant decadal cyclicity, a result consistent with Prasanna Kumar *et al.* (2009). Such a link between the decadal cycle and SST is also seen in the eastern part of the North Indian Ocean, i.e. the Bay of Bengal, from 1960 to 1995 (D'Mello and Prasanna Kumar, 2016). However, this decadal relation between AS SST and sunspot number cycle is disrupted post-1995, as can be seen in Figure 1. As November 1995 is the minimum of the sunspot number, it is chosen as the time to divide the time series into two periods. The rate of warming, as inferred from the slope of the SST, increased from 0.008 °C year^{-1} in the pre-1995 period to 0.014 °C year^{-1} in the post-1995 period, a result not reported by Prasanna Kumar *et al.* (2009). However, the changes in the total energy output of the sun is unlikely to have any significant impact on the global warming since the 17th century (Foukal *et al.*, 2006). The increasing SST trend is due to the increasing CO_2 concentration, through greenhouse effect (Arrhenius, 1896). However, the CO_2 concentration does not show an accelerated post-1995 rise like the SSTs. Therefore, other processes should contribute to this acceleration in SST rise.

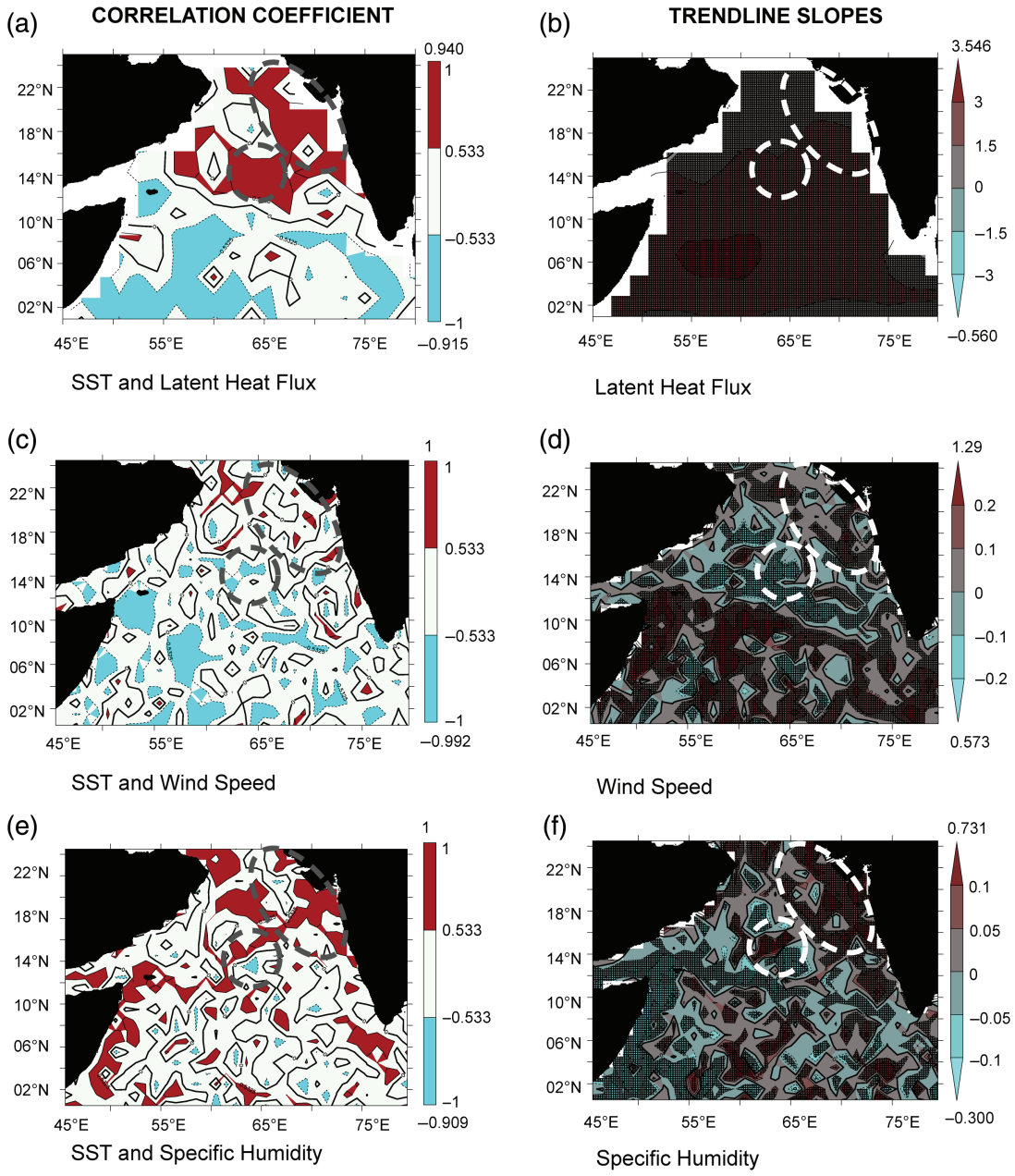

Figure 5. Arabian Sea spring season (March to May) averaged, correlation coefficients of SST with LHF (a), wind speed (c) and specific humidity (e), shaded for regions having 95% and above significance level ($r > |\pm 0.5325|$, $N = 14$). Spring season averaged slopes of LHF ((W m^{-2}) year^{-1}) (b), wind speed ((m s^{-1}) year^{-1}) (d) and specific humidity ((g kg^{-1}) year^{-1}) (f), are cross-hatched for regions having 95% and above significance level (two-tailed t-statistic GE $|\pm 2.18|$, $N = 14$). LHF is considered positive into the ocean. The approximate regions of highest accelerated SST warming are indicated by a dashed ellipse or circle. [Colour figure can be viewed at wileyonlinelibrary.com].

3.2. Regionally differentiated post-1995 SST accelerated warming

A pertinent question is whether the above observed accelerated rate of warming is spatially similar in the entire AS. In order to address this, we computed difference of the 60-month running mean SST trend line slopes between the post-1995 and the pre-1995 periods (Figure 2(a)). The result showed that the highest accelerated warming is spatially-segregated and occurred along the north-eastern AS (off the Konkan, Saurashtra, Kutch and Makran coasts), off Oman, off northern-Somalia, central AS and parts of the southern AS. In order to study the temporal occurrence of the post-1995 accelerated warming, the post-1995 SST slopes were computed for each month, but presented seasonally or sub-seasonally for brevity (Figures 2(b)–(e)). The seasons or sub-season presented were based on the monthly accelerated SST rise. Accordingly, the average values for the months of January to February is designated as late winter and the whole winter season, which includes the month of December, is not considered as the accelerated SST-rise was lesser. Other seasons include March to May as spring, June to September as summer (as this includes the period of the southwest monsoon) and October to November as fall.

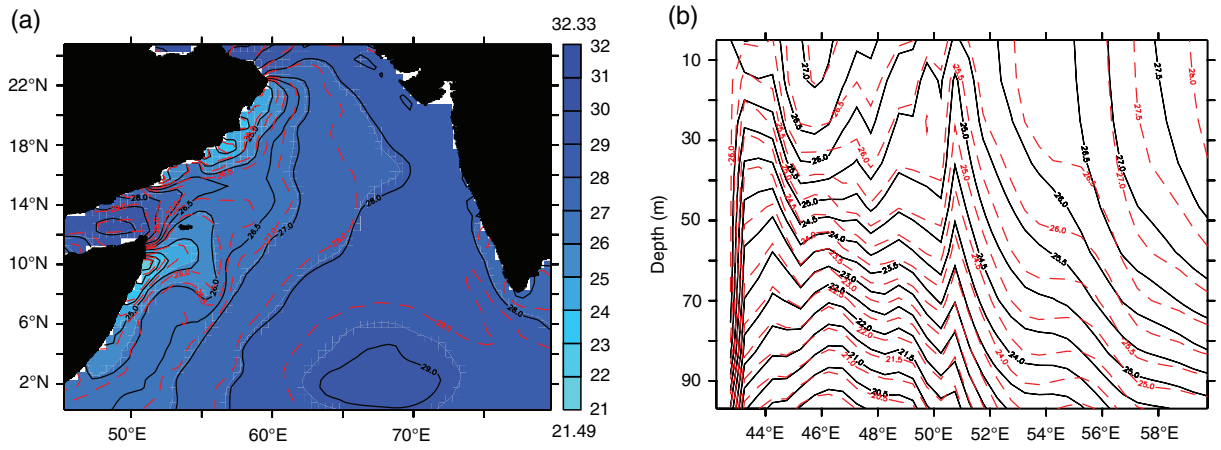

Figure 6. Arabian Sea averaged June to September, SODA: (a) surface temperature (°C), at 5 m depth, shaded in the period averaged from January 1960 to December 2011, contoured in the period from January 1960 to November 1995 (solid-line) and from November 1995 to December 2011 (dashed-line); and (b) temperature (°C) section till 100 m depth, averaged off the Somali coast (equator to 12°N) in the period from January 1960 to November 1995 (solid-line) and November 1995 to December 2011 (dashed-line). [Colour figure can be viewed at wileyonlinelibrary.com].

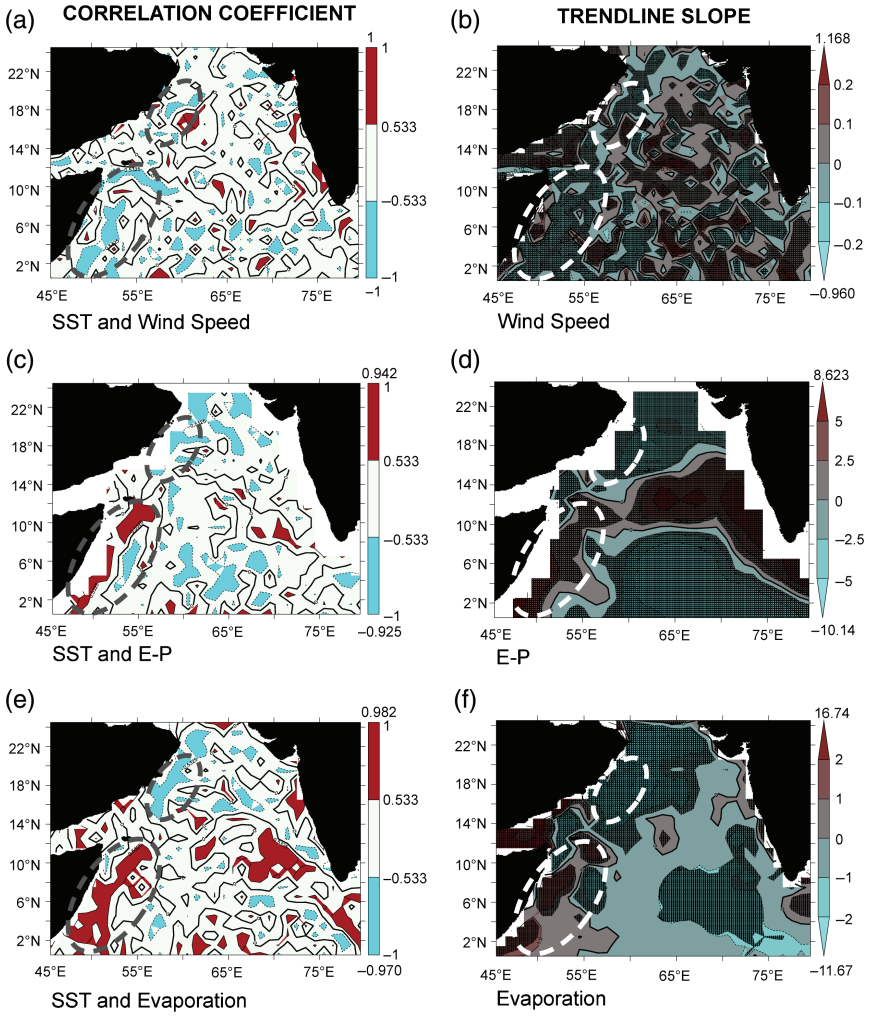

Figure 7. Arabian Sea summer season (June to September) averaged, correlation coefficients of SST with wind speed (a), $E-P$ (c) and evaporation (e), shaded for regions having 95% and above significance level ($r > |\pm 0.5325|$, $N = 14$). Summer season averaged slopes of wind speed ((m s^{-1}) year^{-1}) (b), $E-P$ ((cm year^{-1}) year^{-1}) (d) and evaporation ((cm year^{-1}) year^{-1}) (f) are cross-hatched for regions having 95% and above significance level (two-tailed t-statistic GE $|\pm 2.18|$, $N = 14|$). The approximate regions of highest accelerated SST warming are indicated by dashed ellipses. [Colour figure can be viewed at wileyonlinelibrary.com].

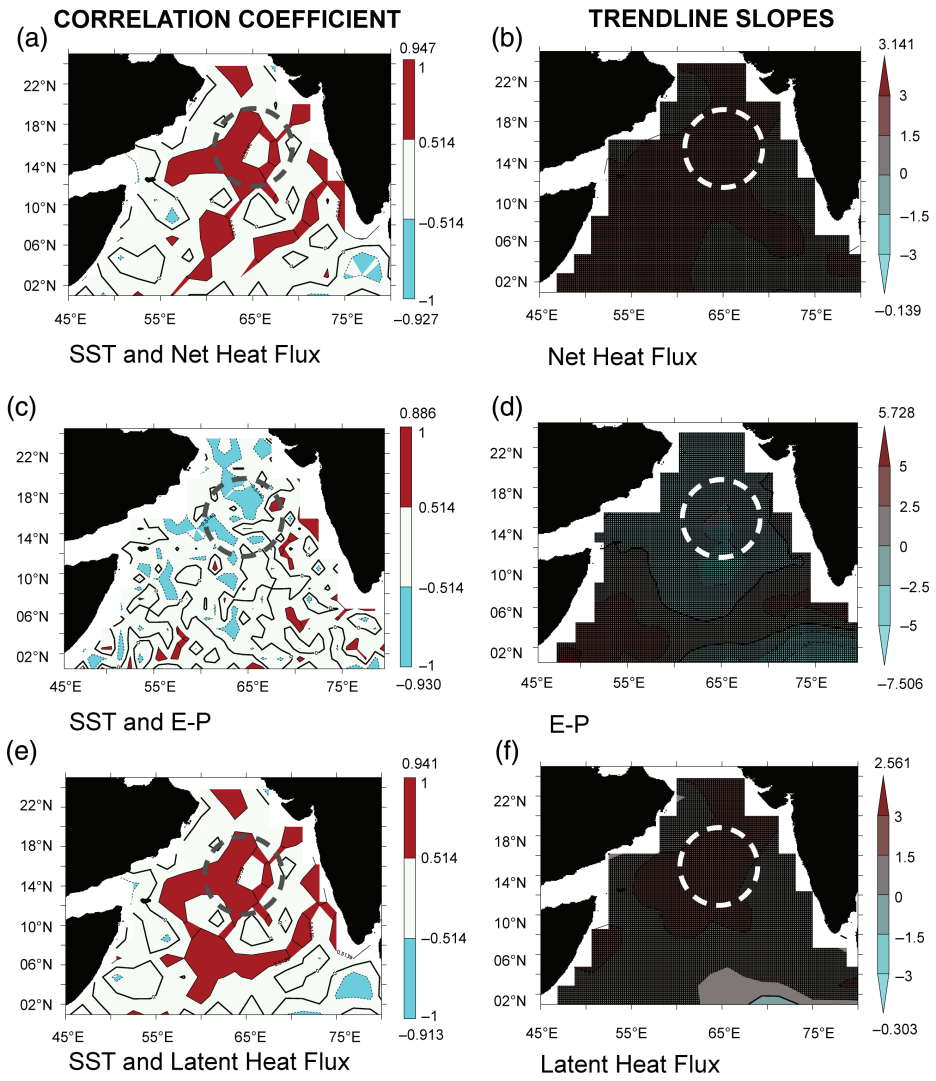

Figure 8. Arabian Sea fall season (October to November) averaged, correlation coefficients of SST with NHF (a), $E-P$ (c) and LHF (e), shaded for regions having 95% and above significance level ($r > |\pm 0.514|$, $N = 15$). Spring season averaged slopes of NHF ((W m^{-2}) year^{-1}) (b), $E-P$ ((cm year^{-1}) year^{-1}) (d) and LHF ((W m^{-2}) year^{-1}) (f), are cross-hatched for regions having 95% and above significance level (two-tailed t-statistic GE $|\pm 2.160|$, $N = 15$). NHF and LHF are considered positive into the ocean. The approximate region of highest accelerated SST warming is indicated by a dashed circle. [Colour figure can be viewed at wileyonlinelibrary.com].

The highest accelerated warming occurred seasonally in the late winter in the north-eastern AS (see Figure 2(b)), in spring season in the central and north-eastern AS (see Figure 2(c)), summer along the western boundary of the AS (see Figure 2(d)) and in fall in the central AS (see Figure 2(e)). Having delineated the regions of highest accelerated warming both spatially and temporally, we now focus on the processes that are responsible for the observed changes.

3.3. Processes controlling the accelerated warming

In order to decipher the factors leading to the observed spatial and temporal pattern of the highest accelerated warming of SST, we have examined the slopes of the post-1995 wind, $E-P$ (freshwater flux) and NHF, and their correlation coefficients with SST, all parameters being 5-year running mean. To further understand which parameter dominantly controlled the above-mentioned fluxes, we have analysed their components, but presented only the ones which significantly influenced SST, besides the specific humidity. We present below the season-wise processes responsible for the highest accelerated warming.

3.3.1. *Late winter*

The post-1995 accelerated warming that occurred in the north-eastern AS during late winter was significantly correlated with NHF and $E-P$ at 95% confidence level (Figures 3(a) and (c) respectively). The slopes of the NHF (Figure 3(b)) showed an increasing trend, while the $E-P$ showed a decreasing trend (Figure 3(d)). As could be inferred from Figure 3(b), the NHF increasing trend into the ocean is due to the decreasing trend of the LHF release to the atmosphere (Figure 3(f)). Similarly, an increasing trend in the specific humidity (Figure 3(j)) leads to a decreasing-trend in the evaporation (Figure 3(h)) resulting

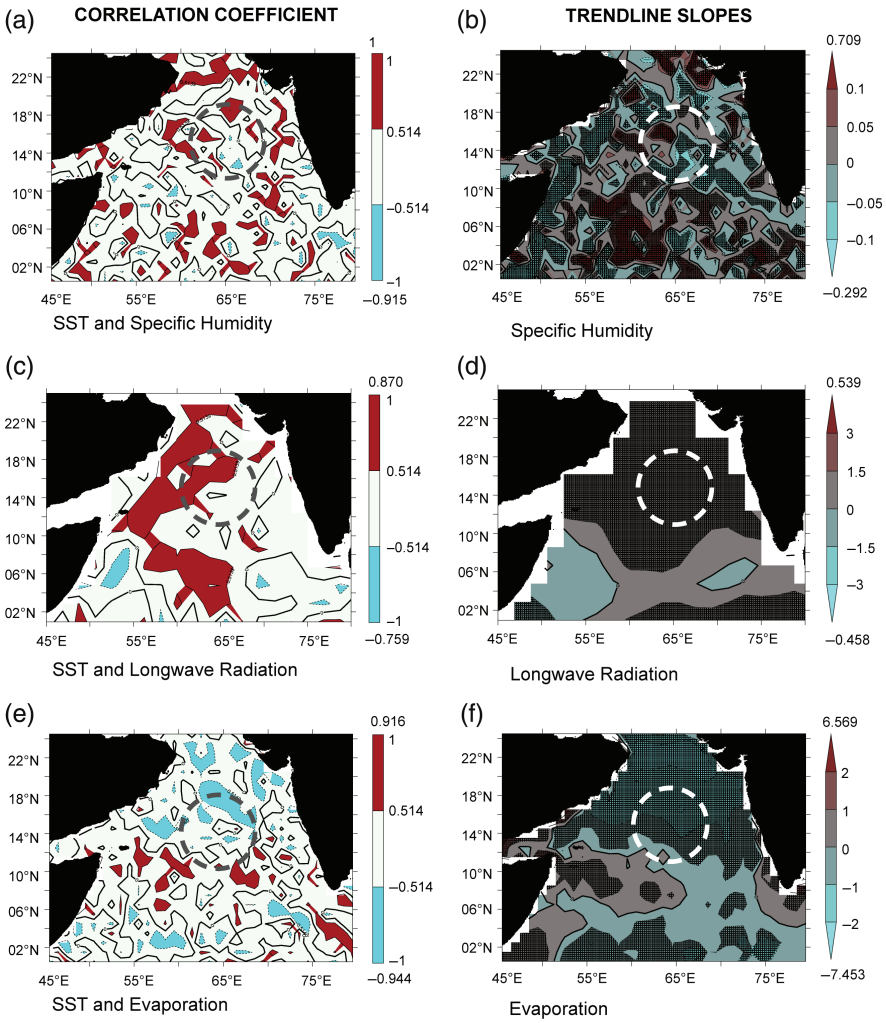

Figure 9. Arabian Sea fall season (October to November) averaged, correlation coefficients of SST with specific humidity (a), LWR (c) and evaporation (e), shaded for regions having 95% and above significance level ($r > |\pm 0.514|$, $N = 15$). Spring season averaged slopes of specific humidity ((g kg^{-1}) year^{-1}) (b), LWR ((W m^{-2}) year^{-1}) (d) and evaporation ((cm year^{-1}) year^{-1}) (f), are cross-hatched for regions having 95% and above significance level (two-tailed t-statistic GE $|\pm 2.160|$, $N = 15$). LWR is considered positive into the ocean. The approximate region of highest accelerated SST warming is indicated by a dashed circle. [Colour figure can be viewed at wileyonlinelibrary.com].

in reduced cooling. Thus, the combined effect of both processes favoured an accelerated warming. Recall that during winter the northern AS undergoes evaporative cooling causing surface densification. Subsequent convective mixing leads to the mixed-layer deepening (Prasanna Kumar and Prasad, 1996; Wiggert *et al.*, 2000). The observed reducing trend in post-1995 evaporation will thus lead to a lesser cooling through the above-mentioned process in the north-eastern AS.

3.3.2. *Spring*

During spring, the post-1995 accelerated warming occurred in the north-eastern and central AS (Figure 2(c)). The central AS accelerated SST rise was caused by the decreasing $E - P$ trends (Figure 4(b)) and NHF increasing trend into the ocean (Figure 4(d)), both of which occurred due to the decreasing trends in evaporation (Figure 4(f)) and LHF (Figure 5(b)) release from the ocean to the atmosphere. Although the wind (Figure 5(c)) did not show any significant direct correlation with the spring warming in the central AS, the wind speed decreasing trend (Figure 5(d)) in the central AS, from March to May was responsible for the decreasing trends of the evaporation and LHF release. Note that a small region of increasing specific humidity trend is also seen (Figure 5(f)), which can decrease evaporation leading to rise in SST. In the north-eastern AS, the increasing trend of NHF into the ocean, due to decreasing trend of the LHF release to the atmosphere, occurred as a consequence of the specific humidity increasing trend (Figure 5(f)). Significant negative correlation coefficients of SST with $E - P$ (Figure 4(a)) and evaporation (Figure 4(e)) as well as positive correlation coefficients of SST with NHF (Figure 4(c)), LHF (Figure 5(a)) and specific humidity (Figure 5(e)) respectively, indicated the contributing factors that led to the accelerated warming in spring.

3.3.3. *Summer monsoon*

The post-1995 accelerated SST rise, in the summer monsoon season (from June to September), occurred at two

Table 2. Variance between 60-month running means of the SST and the various fluxes, in the Arabian Sea.

	Net heat flux	Evaporation precipitation difference	Wind speed
July 1962 to November 1995	0.05	0.28	0.35
November 1995 to June 2009	0.34	0.13	0.51

distinct regions along the western boundary of the AS namely the Somali and the Arabian coasts. The averaged SST difference, in the two periods, is shown using SODA SST data (Figure 6(a)). Along the Somalia coast the correlation coefficient between SST and wind speed was significant at 95% level (Figure 7(a)), while off the Arabian coast the SST was significantly correlated with $E-P$ at 95% level (Figure 7(c)). Note that along the Somali and Arabian coasts, the wind speed showed a reducing-trend in the post-1995 period (Figure 7(b)). The intensity of reduction, however, was more along the Somali coast. The $E-P$, however, showed a reducing trend only along the Arabian coast (Figure 7(d)). Here again, the mechanism that brought about the accelerated warming in SST was different for both regions as would be shown below. An examination of the zonally averaged (equator to 12°N) mean thermal structure during June to September in the upper 100 m of the water column across the Somalia coast, derived from SODA, showed that the colder isotherms during post-1995 surfaces closer to the coast than that during pre-1995 period (Figure 6(b)). For example, the 26 °C isotherm surfaced at 51°E during post-1995 (dashed-line), which was beyond 52°E during pre-1995 (solid-line). Similarly, in the vertical, the 25 °C isotherm was at 15 m depth during pre-1995 period, which was at 25 m depth during post-1995, indicating the reduction in upwelling intensity as well as its spatial extent. This is also corroborated from Figure 6(a) depicting the spatial pattern of June to September averaged pre- and post-1995 SST. Thus, the above results demonstrated the role of ocean dynamics in controlling the accelerated SST warming in the Somali region. However, a similar analysis across the Arabian coast did not yield a similar result (figure not presented) indicating the role of processes other than reduced upwelling contributing to the accelerated warming too. Further analysis showed a significant correlation of evaporation with SST at 95% level along the Arabian coast (Figure 7(e)) and the observed reducing trend in evaporation during the post-1995 period (Figure 7(f)) was linked to the reducing trend in the wind speed implying the role of thermodynamic processes controlling the accelerated SST warming.

3.3.4. Fall

The post-1995 accelerated SST rise occurred in the months averaged from October to November in the central AS (Figure 2(e)). Correlation coefficients significant at 95% levels were seen between SST and NHF (Figure 8(a)) and also between SST and $E-P$ (Figure 8(c)). The NHF into the ocean showed an increasing trend (Figure 8(b)), while the $E-P$ showed a decreasing trend (Figure 8(d)).

The increasing trend of the NHF into the ocean was due to a decreasing trend LHF release from the ocean to the atmosphere (Figure 8(f)), which in turn was due to the increasing trend in the specific humidity (Figure 9(b)). Besides the LHF, the reducing trend in the release of LWR to the atmosphere (Figure 9(d)) also contributed to the increasing trend of NHF into the ocean. The decreasing trend of $E-P$ (Figure 8(d)) was due to the reducing evaporation trend (Figure 9(f)). Thus, the increasing NHF trend into the ocean and decreasing trend in the evaporation lead to higher SSTs.

4. Summary and concluding remark

We examined the regions, seasons and reasons for the post-1995 highest accelerated warming seen in the AS using a suite of *in situ* as well as remotely sensed ocean and atmospheric data. The accelerated warming did not occur uniformly throughout the AS. The regions of highest accelerated warming were in the north-eastern AS during late-winter and spring, central AS in spring and fall and along the Somali and Arabian coasts during summer. In the north-eastern AS during late winter, a post-1995 reduced rate of evaporation resulted from an increasing trend in the specific humidity, led to the accelerated warming. However, the continued warming-trend exhibited by this region well into spring resulted from a reducing trend in the LHF release to the atmosphere, due to an increasing trend in the specific humidity. In the central AS, the accelerated warming during spring was brought about by a combination of processes. A reducing trend in the post-1995 winds caused reducing trends in the evaporation and reducing trends in the LHF release to the atmosphere, leading to an increasing NHF trend into the ocean. In addition to this an increasing specific humidity trend in some parts in the central AS also leads to the same effect. During fall, an increasing trend in the NHF into the ocean contributed by the decreasing trends of the LHF and LWR release to the atmosphere lead to the accelerated warming. Besides this, reducing trends in evaporation in other part of the central AS also contributed to the accelerated post-1995 rise. In summer, the reducing trend in the post-1995 winds caused a reduction in the upwelling intensity as well as its spatial extent along the Somali coast. In contrast, along the Arabian coast a reducing trend in wind speeds lead to lesser evaporation, in turn causing an accelerated warming. Although north-eastern AS shows an accelerated warming in summer and fall too, the mechanisms that cause the warming in these seasons are not the same.

Some of the principal mechanisms by which the accelerated SST rise in the AS can occur are due to an increasing trend in the specific humidity causing a decrease in the evaporation and hence the decrease in $E-P$. Another mechanism is the increasing trend in the specific humidity causing a decreasing trend in the LHF release to the

atmosphere, leading to a decreasing trend in the NHF release to the atmosphere, thus causing an increasing SST trend. Similarly, a decreasing wind speed can proceed a SST warming through reduced evaporation and $E - P$. The decreasing wind speeds can also reduce the upwelling off the Somali and Omani coasts in the summer causing a reduced cooling of SST. A reduction of the LWR release to the atmosphere can also cause a reduction in the NHF release to the atmosphere, thereby increasing the SST. The relative contributions of the heat, freshwater and momentum fluxes on the SST across-1995 are shown in Table 2. The different air–sea processes and reduced upwelling along the Somali coast add to the rise caused by the increase in the carbon dioxide concentrations causing acceleration in the post-1995 SST rise in the AS.

An increased rate of warming in the AS, a region of very high phytoplankton and fish production, can have serious implications to the structure and functioning of ecosystem. It can also impact the mid-depth oxygen minimum zone (OMZ) and seasonal hypoxia experienced along the eastern boundary. A lot of future work has to be vested in understanding and quantifying the full impact of accelerated warming on ecosystem as it will alter the hydrological cycle as well as food-web dynamics of this region.

Acknowledgements

The authors thank Director CSIR-National Institute of Oceanography, Dona Paula, Goa and Council of Scientific and Industrial Research (CSIR), New Delhi for all the support and encouragement for this research. They also thank Mr. Shamkant Akerkar, Mr. Udayakumar Javali and Mrs. Sujal Bandodkar for help with the figures. Joshua Rosario D'Mello would like to thank the CSIR for granting a fellowship and also the Principal and management of the Rosary College of Commerce and Arts, Navelim, Salcete, Goa. This is NIO contribution number 6064.

Supporting information

The following supporting information is available as part of the online article:

Figure S1. Arabian Sea basin-averaged number of ICOADS SST observations 60-month running mean.

Figure S2. Arabian Sea average number of monthly observations of SST, in the period from January 1960 to December 2011.

Figure S3. Arabian Sea ICOADS average SST 60-month running mean (thick black line) and the envelope of standard error (dashed lines), in the period from January 1960 to December 2011.

Figure S4. Arabian Sea 60-month running means of ICOADS SST (black), NOAA Optimally Interpolated SST (green) and Kaplan SSTA + 27.65 (red).

References

Alory G, Wijffels S, Meyers G. 2007. Observed temperature trends in the Indian Ocean over 1960–1999 and associated mechanisms. *Geophys. Res. Lett.* **34**: L02606. https://doi.org/10.1029/2006GL028044.

Arrhenius S. 1896. On the influence of carbonic acid in the air upon the temperature of the ground. *Lond. Edinb. Dubl. Philos.Mag. J. Sci. Ser. 5* **41**: 237–276. https://doi.org/10.1080/14786449608620846.

Bauer S, Hitchcock GL, Olson DB. 1991. Influence of monsoonally-forced Ekman dynamics upon the surface layer depth and plankton biomass distribution in the Arabian Sea. *Deep-Sea Res. I Oceanogr. Res. Pap* **38**: 531–553. https://doi.org/10.1016/0198-0149(91)90062-K.

Carton JA, Giese BS. 2008. A reanalysis of ocean climate using Simple Ocean Data Assimilation (SODA). *Mon. Weather Rev.* **136**: 2999–3017. https://doi.org/10.1175/2007MWR1978.1.

Carton JA, Chepurin G, Cao X, Giese BS. 2000. A simple ocean data assimilation analysis of the global upper ocean 1950–95, part I: methodology. *J. Phys. Oceanogr.* **30**: 294–309. https://doi.org/10.1175/1520-0485(2000)030<0294:ASODAA>2.0.CO;2.

D'Mello JR, Prasanna Kumar S. 2016. Why is the Bay of Bengal experiencing a reduced rate of sea surface warming. *Int. J. Climatol.* **36**: 1539–1548. https://doi.org/10.1002/joc.4414.

De Boyer Montégut C, Vilard J, Shenoi SSC, Shankar D, Durand F, Ethé C, Madec G. 2007. Simulated seasonal and interannual variability of the mixed layer budget in the northern Indian Ocean. *J. Clim.* **20**: 3249–3268. https://doi.org/10.1175/JCLI4148.1.

Dinesh Kumar PK, Steeven Paul Y, Muraleedharan KR, Murthy VSN, Preenu PR. 2016. Comparison of the long-term variability of sea surface temperature in the Arabian Sea and Bay of Bengal. *Reg. Stud. Mar. Sci.* **3**: 67–75. https://doi.org/10.1016/j.rsma.2015.05.004.

Findlater J. 1969. A major low-level air current near the Indian Ocean during the northern summer. *Q. J. Roy. Meteorol. Soc.* **95**: 362–380. https://doi.org/10.1002/qj.49709540409.

Fischer AS, Weller RA, Rudnick DL, Eriksen CC, Lee CM, Brink KH, Fox CA, Leben RR. 2002. Mesoscale eddies, coastal upwelling, and the upper-ocean heat budget in the Arabian Sea. *Deep-Sea Res. II Topic. Stud. Oceanogr.* **49**: 2231–2264. https://doi.org/10.1016/s0967-0645(02)00036-x.

Foukal P, Fröhlich C, Spruit H, Wigley TML. 2006. Variations in solar luminosity and their effect on the Earth's climate. *Nature* **443**: 161–1666. https://doi.org/10.1038/nature05072.

Gulev S, Jung T, Ruprecht E. 2007a. Estimation of the impact of sampling errors in the VOS observations on air–sea fluxes. Part I: uncertainties in climate means. *J. Clim.* **20**: 279–301. https://doi.org/10.1175/JCLI4010.1.

Gulev S, Jung T, Ruprecht E. 2007b. Estimation of the impact of sampling errors in the VOS observations on air–sea fluxes. Part II: impact on trends and interannual variabilty. *J. Clim.* **20**: 302–315. https://doi.org/10.1175/JCLI4008.1.

Haigh JD, Winning AR, Toumi R, Harder JW. 2010. An influence of solar spectral variations on radiative forcing of climate. *Nature* **467**: 696–699. https://doi.org/10.1038/nature09426.

Han W, Vialard J, McPhaden MJ, Lee T, Masumoto Y, Feng M, de Ruijter WPM. 2014. Indian Ocean decadal variability: a review. *Bull. Am. Meteorol. Soc.* **95**: 1679–1703. https://doi.org/10.1175/BAMS-D-13-00028.1.

Josey SA. 2001. A comparison of ECMWF, NCEP-NCAR, and SOC surface heat fluxes with moored buoy measurements in the subduction region of the northeast Atlantic. *J. Clim.* **14**: 1780–1789. https://doi.org/10.1175/1520-0442(2001)014<1780:ACOENN>2.0.CO;2.

Kalnay E, Kanamitsu M, Kistler R, Collins W, Deaven D, Gandin L, Iredell M, Saha S, White G, Woollen J, Zhu Y, Leetmaa A, Reynolds R, Chelliah M, Ebisuzaki W, Higgins W, Janowiak J, Mo KC, Ropelewski C, Wang J, Jenne R, Joseph D. 1996. The NCEP/NCAR 40-year reanalysis project. *Bull. Am. Meteorol. Soc.* **77**: 437–470. https://doi.org/10.1175/1520-0477(1996)077<0437:TNYRP>2.0.CO;2.

Keeling CD, Piper SC, Bacastow RB, Wahlen M, Whorf TP, Heimann M, Meijer HA. 2001. Exchanges of atmospheric CO_2 and $^{13}CO_2$ with the terrestrial biosphere and oceans from 1978 to 2000. I. Global aspects. SIO Reference Series No. 01-06, Scripps Institution of Oceanography, San Diego, CA, 88 pp.

Keeling CD, Piper SC, Bacastow RB, Wahlen M, Whorf TP, Heimann M, Meijer HA. 2005. Atmospheric CO_2 and $^{13}CO_2$ exchange with the terrestrial biosphere and oceans from 1978 to 2000: observations and carbon cycle implications. In *A History of Atmospheric CO_2 and Its Effects on Plants, Animals, and Ecosystems*, Ehleringer JR, Cerling TE, Dearing MD (eds). Springer Verlag: New York, 83–133.

Kennedy JJ, Rayner NA, Smith RO, Saunby M, Parker DE. 2011a. Reassessing biases and other uncertainties in sea-surface temperature observations since 1850, part 1: measurement and sampling errors. *J. Geophys. Res.* **116**: D14103. https://doi.org/10.1029/2010JD015218.

Kennedy JJ, Rayner NA, Smith RO, Saunby M, Parker DE. 2011b. Reassessing biases and other uncertainties in sea-surface temperature observations since 1850, part 2: biases and homogenisation. *J. Geophys. Res.* **116**: D14104. https://doi.org/10.1029/2010JD015220.

Kubota M, Iwabe N, Cronin MF, Tomita H. 2008. Surface heat fluxes from the NCEP/NCAR and NCEP/DOE reanalyses at the Kuroshio Extension Observatory buoy site. *J. Geophys. Res.* **113**: C02009. https://doi.org/10.1029/2007JC004338.

McCreary JP Jr, Kohler KE, Hood RR, Smith S, Kindle J, Fischer A, Weller RA. 2001. Influences of diurnal and intraseasonal forcing on mixed-layer and biological variability in the central Arabian Sea. *J. Geophys. Res.* **106**(C4): 7139–7155. https://doi.org/10.1029/2000JC900156.

Moore GWK, Renfrew IA. 2002. An assessment of the surface turbulent heat fluxes from the NCEP-NCAR reanalysis over the western boundary currents. *J. Clim.* **15**: 2020–2037. https://doi.org/10.1175/1520-0442(2002)015<2020:AAOTST>2.0.CO;2.

Prasanna Kumar S, Prasad TG. 1996. Winter cooling in the northern Arabian Sea. *Curr. Sci.* **71**: 834–841.

Prasanna Kumar S, Madhupratap M, Dileep Kumar M, Muraleedharan PM, de Sousa SN, Sawant S, Gauns M, Sarma VVSS. 2001. High biological productivity in the central Arabian Sea during the summer monsoon driven by Ekman pumping and lateral advection. *Curr. Sci.* **81**: 1633–1638.

Prasanna Kumar S, Roshin RP, Narvekar J, Dinesh Kumar PK, Vivekanandan E. 2009. Response of the Arabian Sea to global warming and associated regional climate shift. *Mar. Environ. Res.* **68**: 217–222. https://doi.org/10.1016/j.marenvres.2009.06.010.

Ramesh Babu V, Sastry JS. 1984. Summer cooling in the east central Arabian Sea: a process of dynamic response to the southwest monsoon. *Mausam* **35**: 17–26.

Rayner NA, Parker DE, Horton EB, Folland CK, Alexander LV, Rowell DP, Kent EC, Kaplan A. 2003. Global analyses of sea surface temperature, sea ice, and night marine air temperature since the late nineteenth century. *J. Geophys. Res.* **108**(D14): 4407. https://doi.org/10.1029/2002JD002670.

Rayner NA, Brohan P, Parker DE, Folland CK, Kennedy JJ, Vanicek M, Ansell TJ, Tett SFB. 2006. Improved analyses of changes and uncertainties in sea surface temperature measured in situ since mid-nineteenth century: the HadSST2 Dataset. *J. Clim.* **19**: 446–469. https://doi.org/10.1175/JCLI3637.1.

Roxy MK, Ritika K, Terray P, Masson S. 2014. The curious case of Indian Ocean warming. *J. Clim.* **27**: 8501–8509. https://doi.org/10.1175/JCLI-D-14-00471.1.

Rupa Kumar S, Krishna Kumar K, Ashrit RG, Patwardhan SK, Pant GB. 2002. Climate change in India: observations and model projections. In *Climate Change and India: Issues Concerns and Opportunities*, Shukla PR, Sharma SK, Ramana PV (eds). Tata McGraw-Hill Publishing Company Limited: New Delhi, 24–75.

Schwabe H, Schwabe Herrn H. 1844. Sonnen-Beobachtungen im Jahre 1843. *Astron. Nachr.* **21**: 234–235. https://doi.org/10.1002/asna.18440211505.

Sharma GS. 1966. Thermocline as an indicator of upwelling. *J. Mar. Biol. Assoc. India* **8**: 8–19.

Smith RL, Bottero JS. 1977. *On Upwelling in the Arabian Sea: A Voyage of Discovery*. Pergamon Press: New York.

Smith SL, Codispoti LA. 1980. Southwest monsoon of 1979: chemical and biological response of Somali coastal waters. *Science* **209**: 597–600. https://doi.org/10.1126/science.209.4456.597.

Smith SR, Legler DM, Verzone KV. 2001. Quantifying uncertainties in NCEP reanalyses using high-quality research vessel observations. *J. Clim.* **14**: 4062–4072. https://doi.org/10.1175/1520-0442(2001)014<4062:QUINRU>2.0.CO;2.

Varadachari VVR, Sharma GS. 1967. Circulation of the surface waters in the North Indian Ocean. *J. Indian Geophys. Union* **4**: 61–73.

Weller RA, Fischer AS, Rudnick DL, Eriksen CC, Dickey TD, Marra J, Fox C, Leben R. 2002. Moored observations of upper-ocean response to the monsoons in the Arabian Sea in 1994–1995. *Deep-Sea Res. II Topic. Stud. Oceanogr.* **49**: 2195–2230. https://doi.org/10.1016/S0967-0645(02)00035-8.

White WB, Lean J, Cayan DR, Dettinger MD. 1997. Response of global upper ocean temperature to changing solar irradiance. *J. Geophys. Res.* **102**: 3255–3266. https://doi.org/10.1029/96JC03549.

Wiggert JD, Jones BH, Dickey TD, Brink KH, Weller RA, Marra J, Codispoti LA. 2000. The Northeast Monsoons's impact on mixing, phytoplankton biomass and nutrient cycling in the Arabian Sea. *Deep-Sea Res. II Topic. Stud. Oceanogr.* **47**: 1353–1385. https://doi.org/10.1016/S0967-0645(99)00147-2.

Willson RC, Hudson HS. 1991. The Sun's luminosity over a complete solar cycle. *Nature* **351**: 42–44. https://doi.org/10.1038/351042a0.

Woodruff SD, Worley SJ, Lubker SJ, Ji Z, Freeman JE, Berry DI, Brohan P, Kent EC, Reynolds RW, Smith SR, Wilkinson C. 2011. ICOADS Release 2.5: Extensions and enhancements to the surface marine meteorological archive. *Int. J. Climatol.* **31**: 951–967. https://doi.org/10.1002/joc.2103.

Yu L, Jin X, Weller RA. 2008. Multidecade global flux datasets from the objectively analyzed air-sea fluxes (OAFlux) project: latent and sensible heat fluxes, ocean evaporation, and related surface meteorological variables. OAFlux Project Technical Report No. OA-2008-01, Woods Hole Oceanographic Institution , Woods Hole, MA, 64pp.

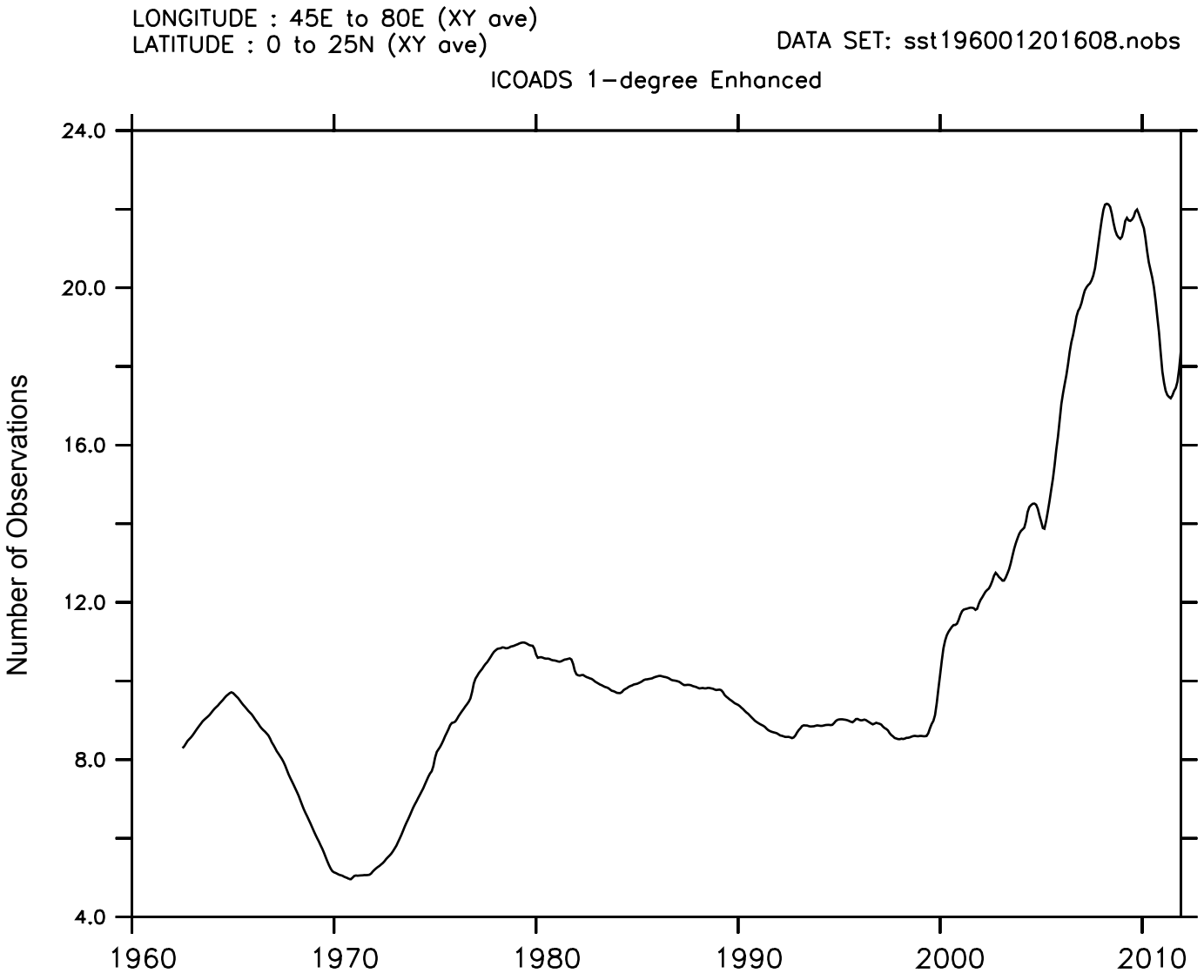

Supplementary Figure 1.
Arabian Sea basin-averaged number of ICOADS SST observations 60-month running-mean

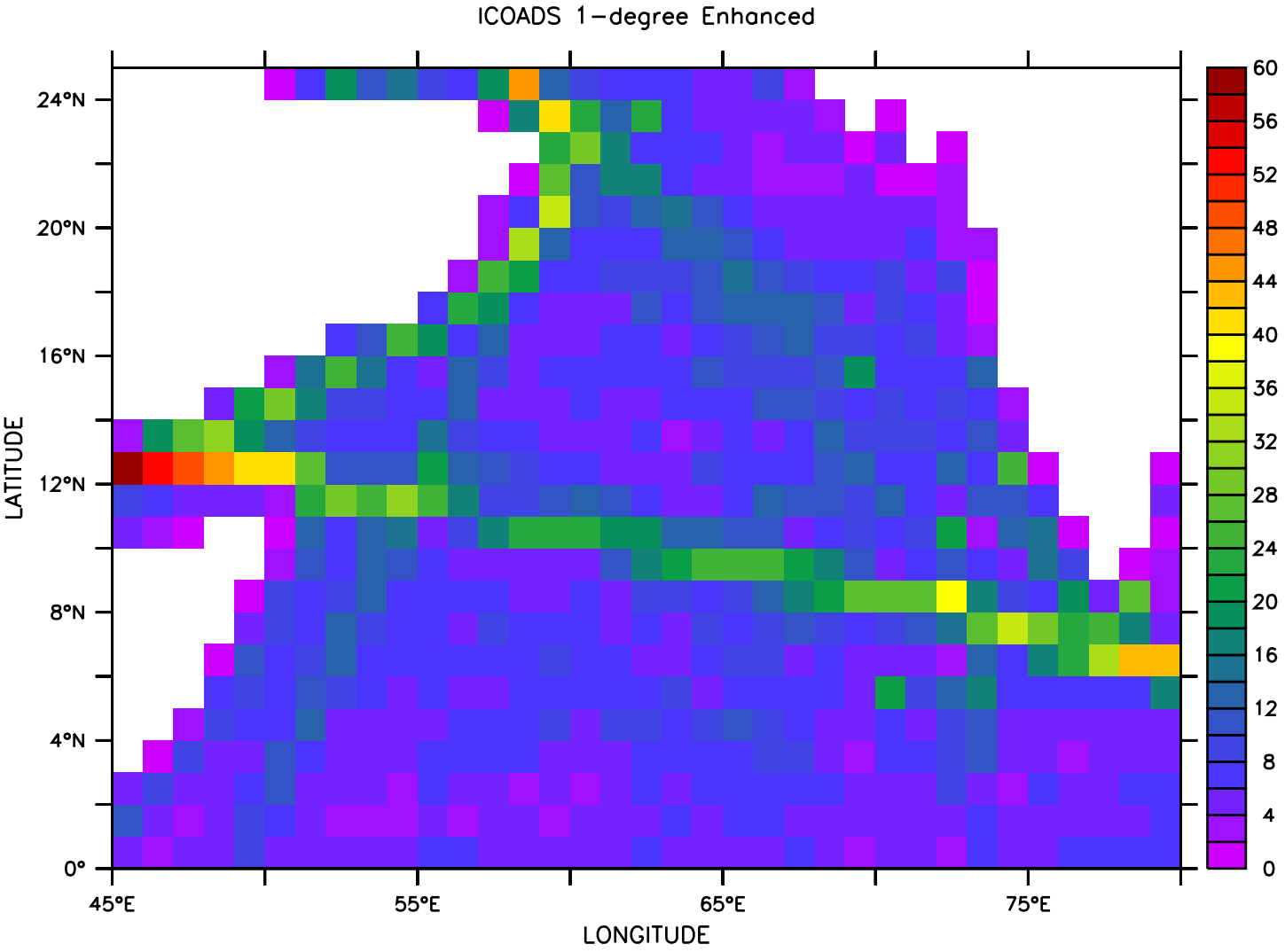

Supplementary Figure 2.
Arabian Sea average number of monthly observations of SST, in the period from 1960 January to 2011 December

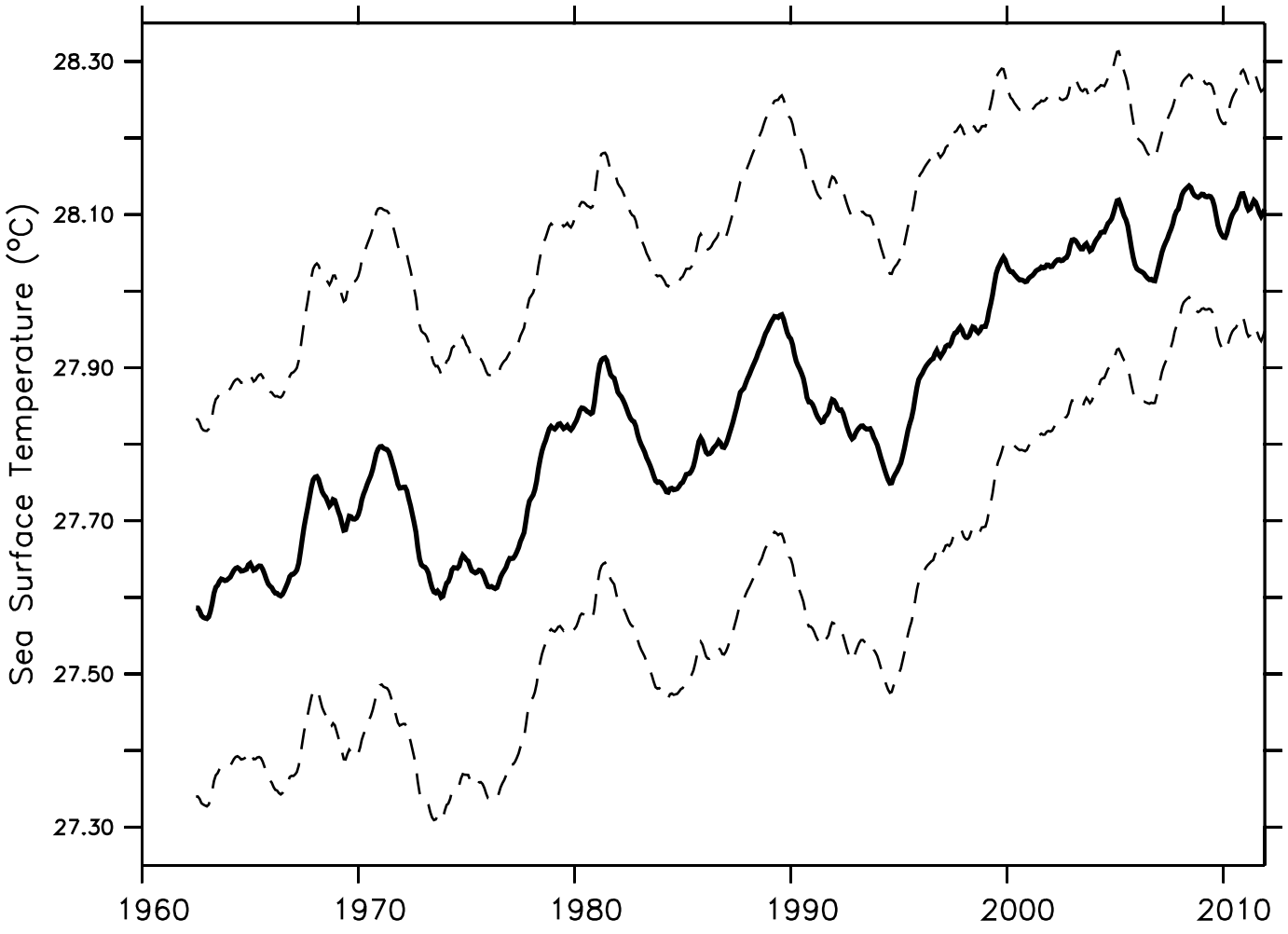

Supplementary Figure 3.
Arabian Sea ICOADS average SST 60-month running mean (thick black line) and the envelope of standard error (dashed lines), in the period from 1960 January to 2011 December

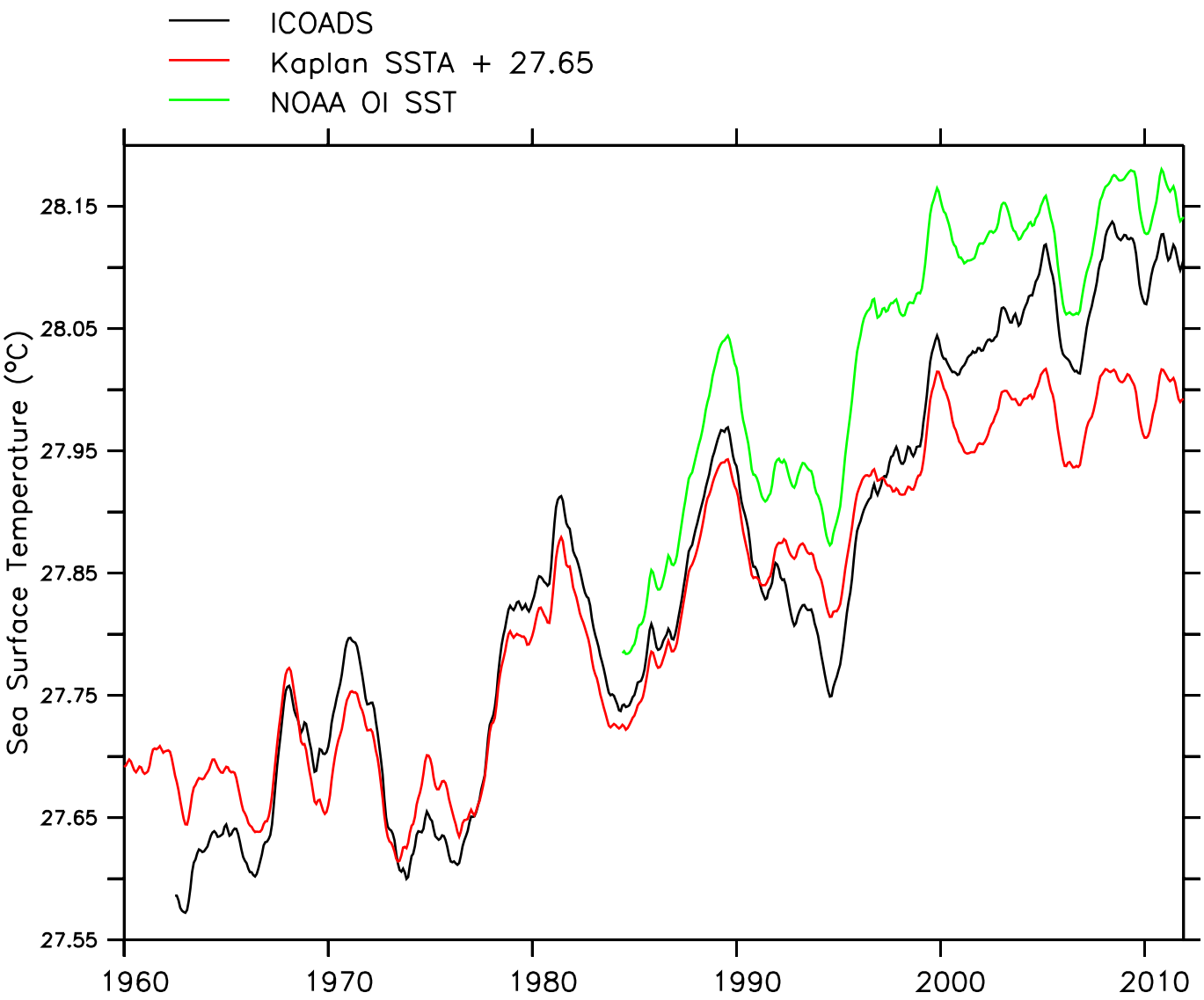

Supplementary Figure 4.
Arabian Sea 60-month running means of ICOADS SST (black), NOAA Optimally Interpolated SST (green) and Kaplan SSTA + 27.65 (red)